pmd*CRC

Project A3 Final Report 2008

Geophysical signatures of alteration

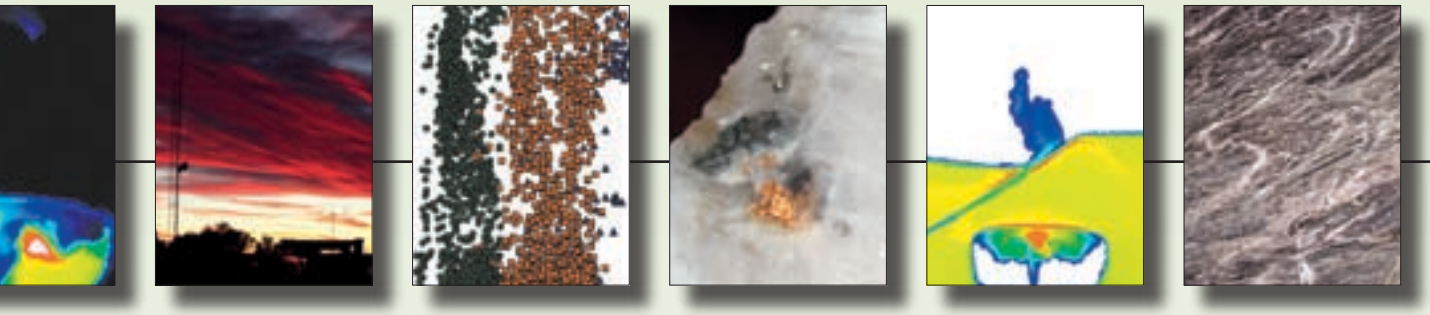

Richard Chopping

pmd*CRC

CRC AUSTRALIA

pmd*CRC

Project A3 Final Report 2008

Geophysical signatures of alteration

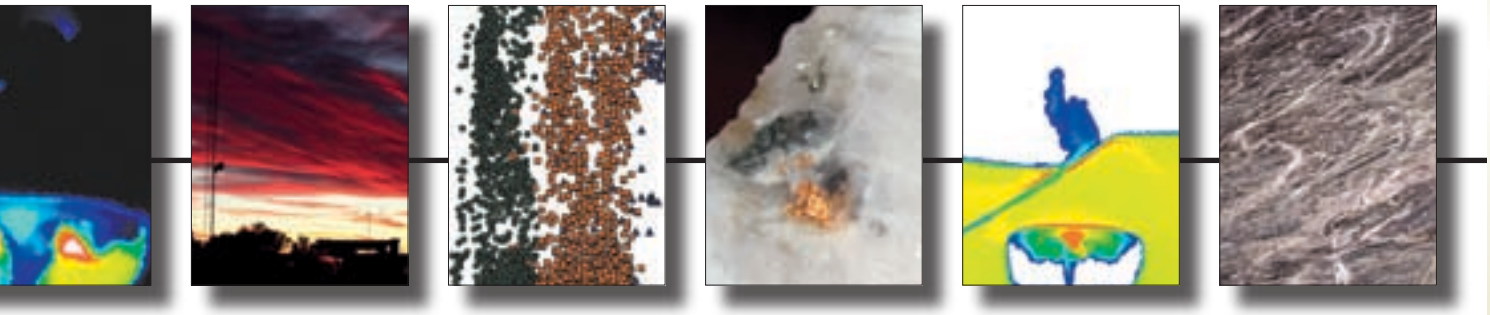

Richard Chopping

pmd*CRC

CRC AUSTRALIA

Core Partners

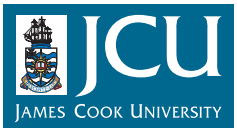

Sponsors

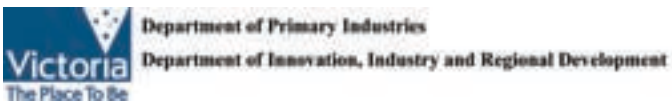

ACKNOWLEDGEMENTS

The work of ***pmd*CRC*** Project A3 was made possible due to the generous support and interest of the ***pmd*CRC*** sponsors. Of these sponsors, AngloGold Ashanti, Barrick Gold and Gold Fields International provided significant support to the project. The following staff, in no particular order, from these companies are thanked for their assistance in the many facets of the project:

AngloGold Ashanti: Mike Nugus, Mark Doyle

Barrick Gold: Yvonne Wallace, Karen Prittard, Barry Bourne, Mark Pirlo.

Gold Fields International: Ned Stolz, Tony Roache.

Other staff from these companies are thanked for their assistance in many matters, from data compilation to organising the freight of samples.

Russell Korsch acted as the main project mentor and manager; other project mentors who shaped the project were Andy Barnicoat, Bruce Goleby and Evgeniy Bastrakov. Barry Drummond provided the initial inspiration for the project. Russell Korsch also provided the excellent editorial support for the project. The quality of this final report is a result of his tireless effort.

The project would not have been possible without collaboration with a number of other ***pmd*CRC*** projects, in particular Project Y4 and Project M9. Section 6 was produced with input from P.A. Henson, I.G. Roy (Project Y4) and J.S. Cleverley (Project M9).

Richard Chopping, January 2008
richard.chopping@ga.gov.au

Sunrise at Sunrise Dam

CONTENTS

EXECUTIVE SUMMARY

What were the aims and objectives of the project?

The aim of Project A3 was to examine the geophysical signatures of fluid alteration that was caused by mineralising fluids, with a view to showing how to detect the footprint of mineral systems in geophysical data. To achieve this, three objectives were formulated:

- To examine available datasets (gravity, total intensity magnetics and seismic reflection data) for geophysical signatures which may be attributed to alteration
- To examine physical property measurements (density, magnetic susceptibility and seismic velocity) on selected suites of rocks to establish the physical property contrasts created by chemical alteration
- To establish a method to predict physical properties and hence also predict geophysical response for alteration models.

What physical property changes result from alteration in mineral systems?

- Increases in density are observed for a number of alteration types (Sections 3.2 and 5.2). Sulphide alteration, in particular, will markedly increase the density of a host lithology (for example, Section 3.2.3)
- Decreases in density are observed for some mineralised rocks (Sections 4.2 and 5.2.1.1). Mineralised rocks may also exhibit no density contrast with respect to their host lithology (Sections 3.2, 5.2.1.2 and 5.2.2)
- Increases in magnetic susceptibility are created for both proximal (magnetite) and distal (magnetic pyrrhotite) alteration to gold deposits (Sections 3.2, 4.2, 4.3 and 5.2). The nature of the magnetic susceptibility-density relationship these two alteration types to be delineated
- Subtle variations in seismic velocity can occur due to alteration, with alteration containing pyrite or magnetite increasing the seismic velocity of a host lithology, and alteration predominantly containing micas and/or pyrrhotite decreasing the seismic velocity of a host lithology (Section 3.2, 4.3 and 5.2). Quartz and carbonate alteration generally maintains seismic velocity of a host lithology (for example, Section 5.2.1).

What geophysical signatures may result from alteration?

Alteration around a gold system produces (Sections 3.2, 4.3 and 5.2):

- An increase in gravity response, with respect to the unaltered gravity response, as a result of the increase in density caused by alteration (predominantly an increase in epidote and sulphides and a decrease in quartz). Directly above the deposit, however, the gravity response is reduced with respect to the unaltered gravity response due to the low-density outflow alteration associated with the deposit
- A variable magnetic response around a deposit, controlled predominantly by the magnetite and pyrrhotite distribution. Temperature effects can result in either magnetic (monoclinic crystal symmetry) or nonmagnetic (hexagonal crystal symmetry) pyrrhotite, changing the magnetic response markedly
- A magnetic 'spike' occurs directly above a buried deposit
- Variable seismic reflectivity along the faults which have acted as fluid conduits and thus have been altered. This type of reflectivity is predicted by numerical models, is consistent with hand-specimen and downhole physical property measurements, and is very likely to have been observed in regional seismic data from a known world-class mineral system (Section 2).

Can we predict the physical properties that will result from alteration?

- Using established techniques described in the literature, there are many methods that we can use to predict the physical properties that result from alteration (Section 4.1.1)
- Applying these methods to coupled fluid-flow and chemical reaction models (reactive transport models) allows us to predict of the geophysical signatures of alteration (Section 4.3.2)

Can we use physical property information to estimate alteration?

- For any given set of physical properties of a sample, and assuming we know the expected unaltered physical properties, we can predict the alteration that may have resulted in the observed physical properties. At a minimum, two properties are required to define alteration – the more properties that are utilised, the more specific the alteration assemblage can be defined (Section 3.2)
- Physical properties used for this process need not be measurements from hand-specimens or downhole probes: the result of a geophysical inversion is generally some model of physical properties of the subsurface. If we have a model with two or more collocated properties, then we can use these results to interpret alteration (Section 7.1).

What are the implications of the project results?

- Understanding the physical properties for a deposit, or even just the physical properties of unaltered rocks in a region, is vitally important to understanding probable geophysical responses. Physical property studies can be performed simply and cheaply on existing data (Sections 3.2 and 5.2.1) or through the acquisition of new data (Section 5.2.2). For acquisition of new data, it may be best to combine the results of a hand-specimen survey and a downhole geophysical survey to both calibrate the downhole measurements and to adequately sample both unaltered and altered material
- Numerical simulations can be used to produce geophysical responses due to alteration (Section 4)
- Regional data, such as seismic data (Section 2) or gravity data (Section 6) may very well contain subtle signatures of alteration
- Using inversion results we may be able to detect alteration footprints (Section 7.1).

Banded Iron Formation, Laverton lookout

1. INTRODUCTION

A geophysical response, such as gravity, magnetic intensity or seismic reflection results from a contrast of a physical property (density, magnetic susceptibility, acoustic impedance) beneath the point of geophysical observation. In crystalline terranes, such as are typical for many mineral provinces, the physical properties of any given rock are largely determined by the mineralogy of the rock (Guéguen and Palciauskas, 1994). Other factors, such as structural defects, the shape and size of constituent minerals and the porosity and permeability of the rock may vary these physical properties, but, primarily the assumption that the mineralogy controls the physical property of the rock holds (Carmichael, 1989b). Chemical alteration, by definition, alters the mineralogy of a rock. This change in mineralogy will also change the physical properties of the rock. Understanding these changes in physical properties is a fundamental step in gaining an understanding of the potential changes in the geophysical response over a mineral system.

Physical property changes have been reported for a variety of alteration styles within mineral systems, and for many physical properties, such as density and magnetic susceptibility changes in iron oxide-copper-gold systems (Williams and Dipple, 2006) or seismic velocity (P- and S-wave) and density changes for nickel sulphide systems (Salisbury and Snyder, 2004).

Some studies have also linked physical properties to alteration mineralogy in an attempt to understand the geophysical signatures of alteration. Sulphide alteration at a copper-oxide deposit in Arizona is reported to have a strong geophysical response (Nelson and Johnston, 1994). Alteration proximal to the polymetallic mineral system at Mt Isa has also been detected in gravity and magnetic datasets (Leaman, 1991). Sulphide alteration was detected by seismic data and confirmed by physical property studies and modelling at the Bell Allard sulphide orebody in Canada (Adam et al., 2002). Density and magnetic susceptibilities as a result of serpentinisation reactions have been calculated and compared to real samples that have undergone serpentinization (Toft et al., 1990).

Within the Abitibi greenstone belt, chemical alteration producing magnetite and resetting remanent magnetism for some intrusions produces a distinct magnetic signature that is recognisable in regional datasets (Schwarz, 1991). Alteration of portions of an ophiolite complex to magnetite and titanomaghemite has produced an observable change in the magnetic susceptibility of samples (Beske-Diehl and Banerjee, 1979). Hydrothermal alteration around black smokers is also noted to produce changes in the magnetic susceptibility of samples (Rona, 1978). Finally, the magnetic susceptibility response of pyrrhotite in altered host rocks has been studied in the 9.1 km deep KTB drillhole in Germany (Berkhemer et al., 1997).

Thus, it is very likely that the chemical alteration of a rock to form new minerals with respect to those in the host will cause physical property contrasts with respect to the unaltered rock.

1.1 Symbols

Symbol	Definition
m	Mass, given in kg.
M	Molar mass, given in $kg.mol^{-1}$.
ρ	Density, given in tm^{-3}, equivalent to gcm^{-3}.
V	Volumetric proportion. V_i indicates the volumetric proportion of the i^{th} constituent of a subject. Uppercase is used so as not to confuse seismic velocity and proportions.
k	Magnetic susceptibility, given in SI units. Although magnetic susceptibility is dimensionless, the value varies according to the units of magnetism used.
v_p	P-wave seismic velocity, given in ms^{-1}. v_{pi} is the P-wave velocity of the i^{th} constituent of a subject.
v_s	S-wave seismic velocity, given in ms^{-1}. v_{si} is the S-wave velocity of the ith constituent of a subject.
Z	Acoustic impedance, the product of seismic velocity and density.
R	Reflection coefficient, which, for two acoustic impedances Z_1 and Z_0, is defined as $R = (Z_1 - Z_0) / (Z_1 + Z_0)$. See below for further details.
`filename`	Text in a monospaced font indicates the filename of computer software, or software variables or methods.

Table 1: Symbols and terms used throughout this report.

1.2 Abbreviations

Abbreviation	Term
Bt	Biotite
Calc	Calcite
Carb	Carbonate
Chl	Chlorite
Epd	Epidote
Fuchs	Fuchsite
Hem	Hematite
Mag	Magnetite
Ms	Muscovite
Po	Pyrrhotite
Py	Pyrite
Qtz	Silica
Ser	Sericite
+ve	Positive
-ve	Negative

Table 2: Abbreviations used throughout this report.

1.2.1 A note on the seismic reflection coefficient

As noted above the seismic reflection coefficient is a term which provides information on the amplitude and sign of reflections from geological interfaces. For two units a and b with corresponding acoustic impedances Z_a and Z_b the reflection coefficient is defined as:

$$R = \frac{Z_b - Z_a}{Z_b + Z_a} \quad \text{(Equation 1)}$$

A commonly quoted 'minimum' reflection coefficient required for a strong seismic reflection is R = ±0.06 (Salisbury et al., 2000).

Seismic velocity-density scatter plots within this report show contours of isoimpedance. These contours are selected such that the reflection coefficient between one contour and the adjacent contour are approximately equivalent to a reflection coefficient of 0.06. The reflection coefficient of a contour to the right of another is +0.06, and the contour to the left has a reflection coefficient of -0.06. This relationship is depicted in Figure 1.

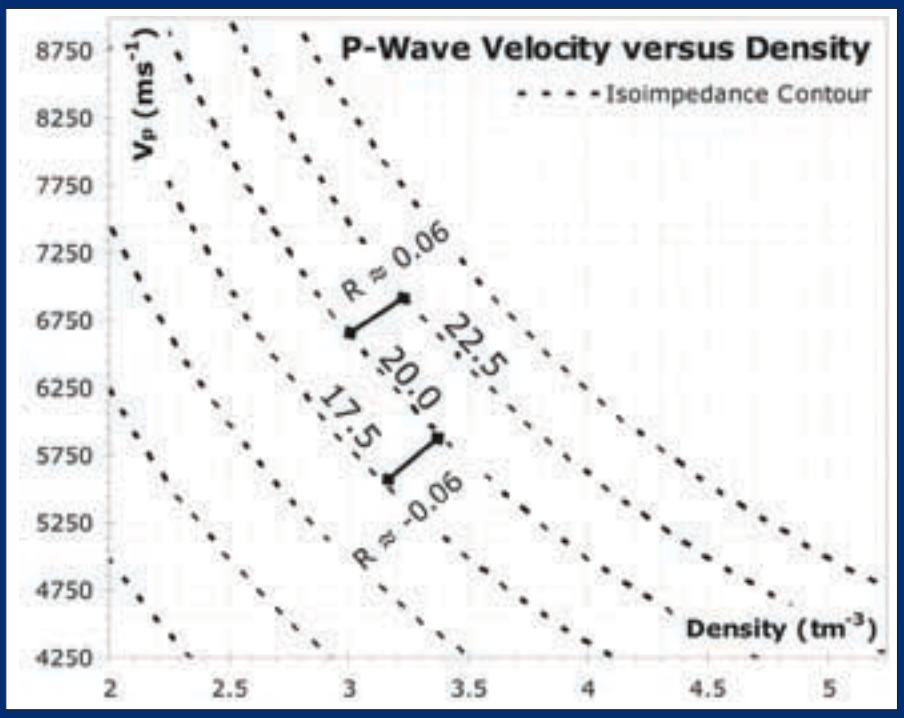

Figure 1: Reflection coefficient relationship between adjacent isoimpedance contours. The number parallel to an isoimpedance contour is the value of the acoustic impedance along the contour. The reflection coefficient is defined with respect to the initial contour, and utilising the following acoustic impedances:

Z_a is the initial impedance, and

Z_b is the impedance of the adjacent contour.

The reflection coefficient is calculated using these impedances in the equation for calculating the reflection coefficient (Equation 1).

2. SEISMIC 'MAPPING' OF FLUID PATHWAYS FOR THE WORLD-CLASS GOLD MINERAL SYSTEM AT LAVERTON

Executive Summary

Seismic data are often used to define geometries of structures at depth in 3D maps. Seismic data can also be used to understand generalised palaeo-fluid flow in the volume of interest of the 3D map. In the Laverton region, regional and mine-scale seismic data have been used to map out potential palaeo-fluid flow systems and provide details on the distribution of mineralisation in the Laverton region.

2.1 Introduction

The Laverton region in the Eastern Goldfields, Yilgarn Craton, is an area rich in gold mineralisation with considerable resources, including world-class deposits and other minor deposits (Groves et al., 1998; Jaques et al., 2002). The region is also rich in seismic data, with both regional and mine-scale seismic data available (Figure 2).

These seismic traverses have been used to construct a 3D map, with the seismic data providing information on the geometry of structures (Henson et al., 2006).

More information about the nature of the structures in the map, however, may be obtained by examining the character of seismic reflections around structures to predict those which may represent palaeo fluid-flow pathways. Drummond et al. (2004a) examined such mapping of potential fluid flow zones in the Kalgoorlie region.

Based on first principles of seismic reflection (Telford et al., 1990b), the seismic character of structures will be influenced by the following factors:

- Processing or acquisition artefacts.
- If the material is anisotropic, a change in dip
- Change in thickness of the structure.
- 3D topography due to the effect of acquiring 2D seismic over 3D geometries (Drummond et al., 2004c).
- Change in lithology (± alteration) of the structure and/or surrounding crust (Salisbury et al., 2000).

2.2 Seismic Characteristics

The three regional seismic lines studied in the Laverton region are 01AGS-NY1, 01AGS-NY2 and 01AGS-NY4; these will be referred to as NY1, NY2 and NY4 respectively. These seismic lines, and the processing applied, are described in Goleby et al. (2003). Although all three lines were examined, the details of only part of line NY1 are pictured in this report (Figure 3A). The trace of the intersection of the faults from the Laverton 3D map (Henson et al., 2006) and the seismic line is also shown (Figure 3B). Note that although the faults and surfaces in Henson et al.'s model were created in part from the seismic data, these data were used only to constrain the fault geometry.

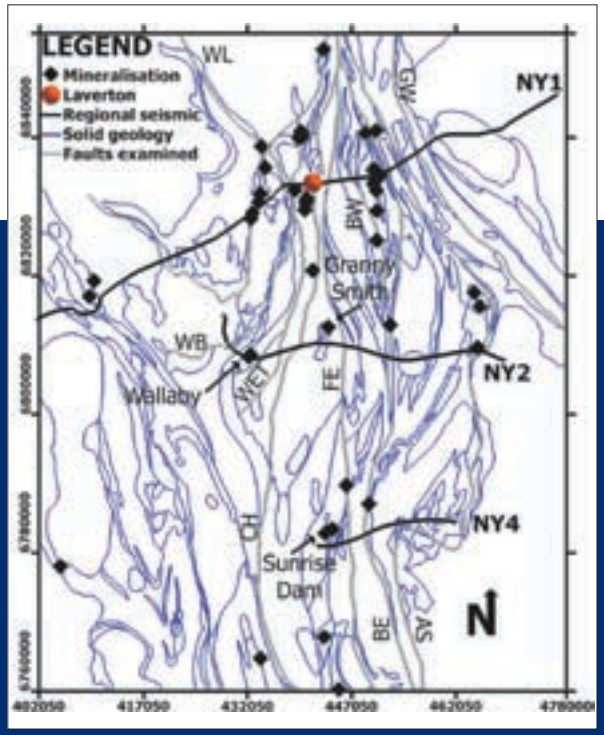

Figure 2: Solid geology, mineralisation and regional seismic traverses in the Laverton region. Solid geology after Henson et al. (2006). Mineral deposit locations (points) derived from the MINLOC database (Ewers and Evans, 2001). A full discussion of the seismic data is in Goleby et al. (2003). Seismic traverses are 01AGS-NY1, 01AGS-NY2 and 01AGS-NY4, labelled NY1, NY2 and NY4 respectively. Map coordinates are GDA94, zone 51. Faults and surfaces from Henson et al.'s (2006) 3D model and are named as follows: WL – Wallaby low-angle shear zone (LASH); WB – Wallaby Basin; WET – Wallaby East Thrust; CH – Childe Harold Fault; FE – Far East Fault; BW – Barnicoat (West) Fault; BE – Barnicoat (East) Fault; AS – Apollo Shear; GW – Granite Well Fault.

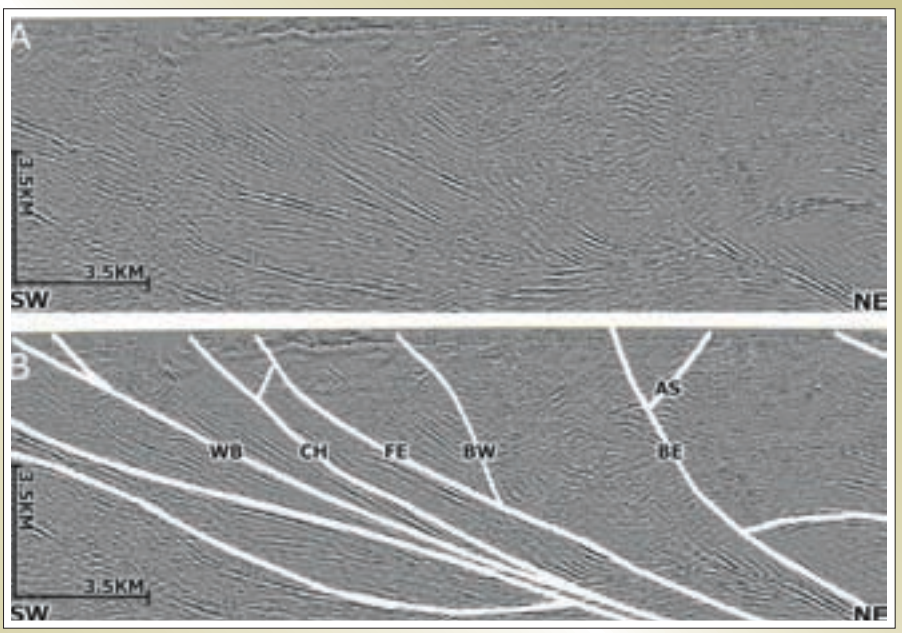

Figure 3: (A) Uninterpreted part of seismic traverse NY1. (B) Interpretation of part of seismic traverse NY1. Faults and surfaces named as per Figure 2, derived from Henson et al.'s (2006) model of the Laverton architecture.

Two faults which are proximal to each other, such as the Childe Harold and Far East Faults, will often differ in seismic response. The Childe Harold and Far East Faults differ most significantly in the amount and length of linear reflections around, or at a low angle to, the inferred structures. The largest package of reflections occurs below and to the west of the Childe Harold Fault. Some reflections occur within the block between the Childe Harold and the Far East Faults, although these terminate against the Far East Fault. These reflections are not those used by Henson et al. to constrain the geometries of the fault.

These linear reflections appear to be of two types (Figure 4). The first type of reflection features a relatively low frequency response with high amplitudes. This second type also is more variable in amplitude, ranging from mid to high amplitudes. There are also some regions where interference between the two types of reflections results in both high and low frequency reflections.

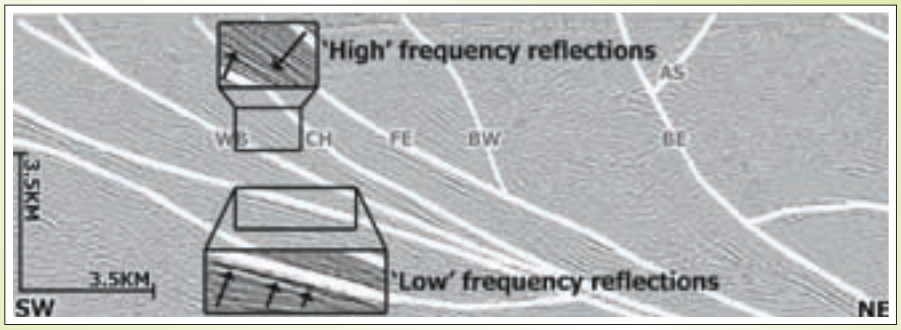

Figure 4: Examples of the two types of reflections near to, but not directly associated with, faults or surfaces. Faults and surfaces named as per Figure 2. Arrows in each inset highlight a typical reflection for that type.

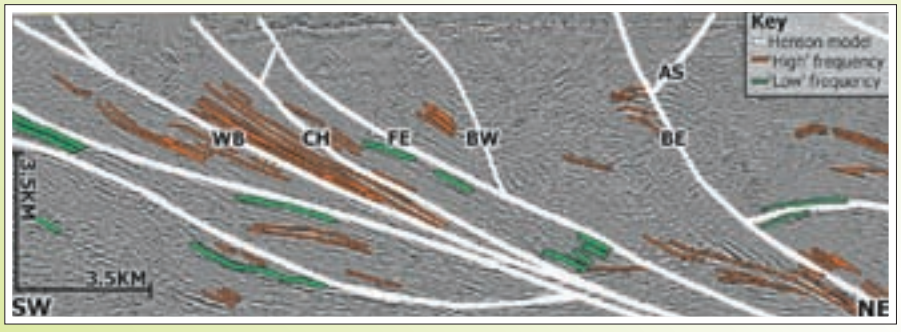

Figure 5: Summary of reflections around the major faults and surfaces imaged in NY1. Flow interpretation after Drummond et al. (2004b).

There also appears to be some high-frequency reflections subparallel to the Wallaby Basin which mirrors the amplitudes and other characteristics (such as frequency) of reflections around the Childe Harold Fault (Figure 5).

2.3 Interpretation

In the context of this research, the term 'fluid pathway' refers to a volume of higher permeability material (e.g. a shear zone) within the crust. This zone acts as a conduit for fluids which may chemically alter the material within the shear zone and the surrounding crust.

The two reflection types, discussed above (and shown in Figure 5), may result from two different phenomena. The lower frequency type of reflections most likely represents out-of-plane seismic energy, an artefact of acquiring 2D seismic traverses over a three-dimensional structure. Hobbs et al. (2006) studied such phenomena and noted that the effects of out-of-plane energy, due to tuning of seismic waves and interference (constructive and destructive) of seismic energy results in broader or low-frequency responses as well as multiple reflections from a single structure.

The high-frequency reflections appear to be similar to the palaeo-fluid flow hypothesis proposed by Drummond et al. (2004a), with high frequency and high amplitude reflections subparallel and in close proximity to faults. These faults were hypothesised to have acted as fluid pathways and had also altered by the fluids. These reflections could also occur around aquacludes where altering fluids could pond or where aquacludes are breached. The largest package of reflections to the west of the Childe Harold Fault, and partly enclosed by the Far East Fault, would therefore represent an area of highly altered material due to palaeo-fluid flow.

The Childe Harold and Far East faults have similar dips, similar strikes, and occur in a similar area of the seismic traverse. They also have broadly similar 3D geometries

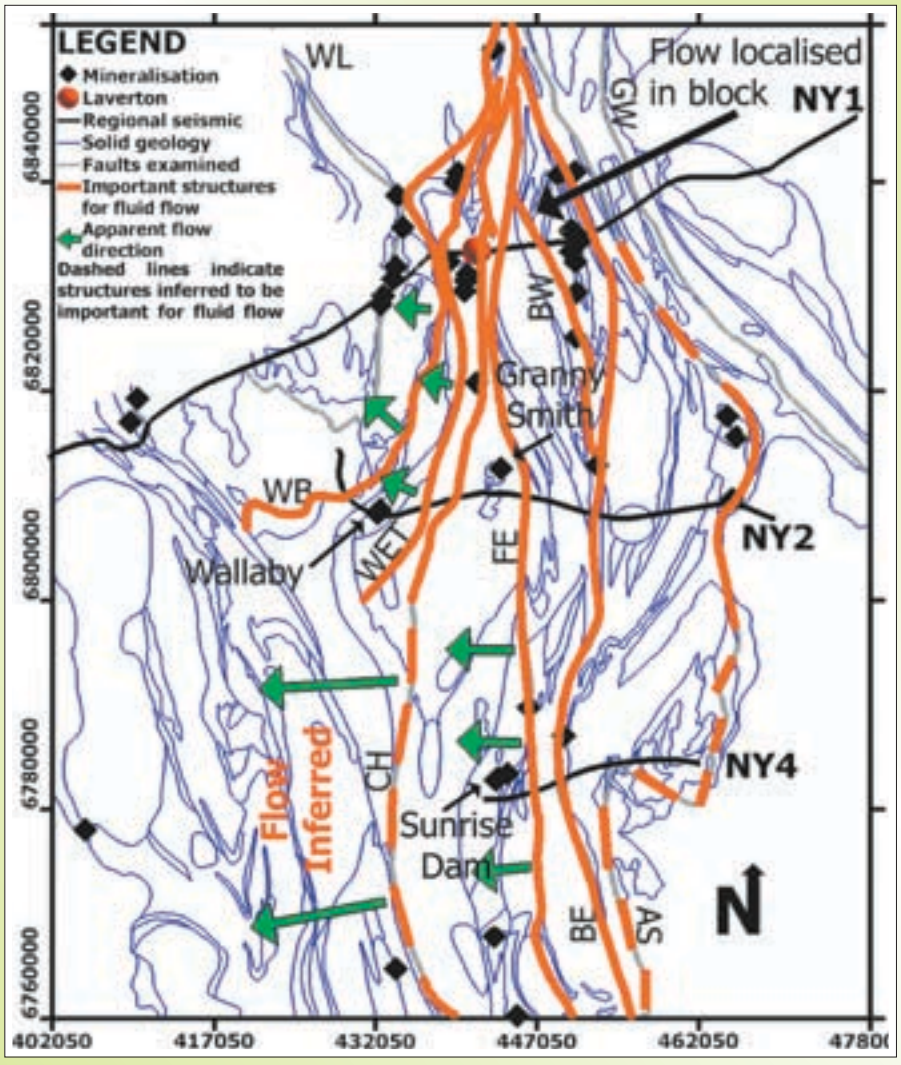

Figure 6: Simplified map view of palaeo-fluid flow in the Laverton region. Arrows indicate fluid flow directions inferred from regional and mine-scale seismic data.

Faults and surfaces from Henson et al's (2006) 3D model and are named as follows: WL – Wallaby low angle shear zone (LASH); WB – Wallaby Basin; WET – Wallaby East Thrust; CH – Childe Harold Fault; FE – Far East fault; BW – Barnicoat (West) Fault; BE – Barnicoat (East) Fault; AS – Apollo Shear; GW – Granite Well Fault. Dashed lines indicate uncertainty in importance of structures in the palaeo fluid flow regime in the Laverton region.

around the seismic traverse. Where small-scale 3D topography has affected the seismic data it may be imaged as low-frequency reflectors. Thus the reflection character differences are unlikely to be due to processing or acquisition artefacts, or dip or strike changes. Thickness differences are unable to account for the large package of high-frequency reflectors to the west of the Childe Harold Fault (Widess, 1973). Thus the most likely cause of the high-frequency reflections to the West of the Childe Harold Fault represents alteration by palaeo-fluid flow, streaming off from the area the Wallaby Basin connects with the Childe Harold Fault.

2.4 Conclusions

Assuming the high-frequency reflections (Figure 5) represent signatures of altering palaeo-fluid flow, it appears that in the region around NY1 the Childe Harold Fault and structures below it are acting as a fluid pathway, focussing fluids up and to the west. The spatial distribution of mineralisation (Figure 2) indicates that there are a large number of areas of reported mineralisation around where the Childe Harold Fault, and faults to the west of it, reaches the surface or near-surface. These faults could represent a control on the focussing of mineralising fluid. This is also consistent with observed occurrences of mineralisation in the western part of the region.

An example of this consistency with reported mineralisation is that the Far East Fault appears to act as an aquaclude, which results in lower fluid flow through the block between the Far East Fault and the Barnicoat West Fault, and there is minimal alteration signatures recorded in the seismic data within this block. The Barnicoat West Fault does not display the same reflectivity variability as the Childe Harold and Far East Faults; the steeper dip on the structure means that the seismic will be unable to resolve the subparallel features as seen around the Childe Harold and Far East Faults. Evidence supporting the Barnicoat West Fault focusing some mineralising fluids is that there are several occurrences of mineralisation along the fault (Figure 2).

The large amount of high-frequency reflections to the west of the Childe Harold Fault would indicate this would be an area most favourable for alteration and thus the most prospective. High-frequency reflections also rarely appear to the east of the Far East Fault, and in the regional around NY1 it may be possible that the Far East Fault acts as an aquaclude. More high-frequency reflections are noted near the Barnicoat East Fault, and fluid flow may have been locked in the block between the Barnicoat West and Barnicoat East Faults.

Application of these principles developed on NY1 to NY2 and NY4 and incorporating knowledge from mine-scale seismic around Granny Smith, Sunrise Dam and Wallaby allows a simplified map of possible fluid-flow zones and directions to be developed (Figure 6). Although there is no seismic data in the southwest of the Laverton region, we can infer, from this study that the region would have been subject to a large volume of palaeo-fluid flow and hence is a prospective area within the Laverton region. Furthermore, this area is under a salt lake (Lake Carey) and is underexplored.

Further refinement in the understanding of the mineral systems in the Laverton region may be achieved by integration of these results with computational simulations, such as the numerical fluid flow modelling of Sheldon et al. (2006). The refinement of this understanding will greatly assist in predicting prospective areas within the Laverton region and other similar systems.

3. RELATIONSHIP BETWEEN PHYSICAL PROPERTIES AND ALTERATION AT THE ST IVES GOLD MINE, WESTERN AUSTRALIA

Executive Summary

Case studies of mineral systems have shown that alteration can produce geophysical signatures in datasets such as magnetics and gravity, and potentially in seismic data. These geophysical signatures are the result of alteration causing physical property contrasts with respect to the host (unaltered) rocks. By using a simple rock physics model, we can predict the physical properties of altered rocks. This model uses linear combinations of the physical properties of the host rock and alteration assemblage.

The majority of samples at St Ives, Eastern Goldfields, Western Australia, plot within a limited field when viewed on a scatter plot of physical properties. We infer this field to reflect unaltered host samples, although it may include weakly altered samples, or samples altered to minerals with physical properties similar to those of the host rock. Samples plotting outside this field of expected properties are inferred to have undergone alteration.

As there are limits on the physical properties of the host rock, there are limits on the paths (alteration trajectories) that progressively altered samples follow. These limited alteration trajectories define a field which is cone shaped. The open end of the cone encompasses the expected physical properties of unaltered samples, and the focus of the cone lies on the physical properties of the alteration assemblage. This field is termed the alteration cone. Our model can also be used to predict the properties of an alteration assemblage of an arbitrary composition. Samples plotting inside an alteration cone can be inferred to be the result of alteration of a host lithology to that alteration assemblage.

The distance a sample occurs along an alteration cone from the host is proportional to the amount of alteration the sample has undergone. By considering the possible range of host rocks, we can quantify the range of alteration required to explain the physical properties of the sample.

The model accounts for physical properties of samples with known alteration. These samples are known to be altered by comparison with external datasets, such as the HyLogger core logging system and alteration defined in the St Ives drillhole database.

3.1 Introduction

3.1.1 Visualising and identifying alteration trends

Mineralogy is one of the main controls of the physical properties of rocks (Carmichael, 1989b; Guéguen and Palciauskas, 1994) . Thus, it would be expected that samples that are altered, that is, they have undergone a change in their constituent minerals, would also show differing physical properties from the original host, assuming that there is a net physical property difference between the host and the alteration assemblage.

Most host lithologies in mineral systems show variations within their physical properties (Guéguen and Palciauskas, 1994), whereas alteration minerals show significantly less variability (Christensen, 1989). This variability of the host rock property will also change the net physical property responses for alteration.

If we imagine physical properties plotted on a scatter (bivariate) plot, most lithologies tend to plot within a limited field rather than as a point (Salisbury et al., 2000). Samples from the upper extreme of a field will tend toward the physical properties of the end-member alteration assemblage along a certain trajectory; likewise samples from the lower extreme of a field will tend towards the same end-member alteration along a different alteration trajectory. For examples of these alteration trajectories see Figures 7 and 8. These alteration trajectories mark a boundary of a zone termed the alteration cone. The alteration cone is a region on a scatter plot of physical properties within which samples are inferred to be altered versions of a given host rock; thus these rocks are a mixture of the host and the alteration assemblage located at the focus of the alteration cone.

In order to correctly identify these alteration trends we need to know the physical properties of end-member alteration minerals. A compilation of properties is Appendix A1.

It is likely that some host and alteration combinations can have overlapping alteration cones with other host and alteration combinations. An example of this is the pyrite and magnetite alteration cones shown in Figure 7. For a single lithology, samples plotting within both the pyrite

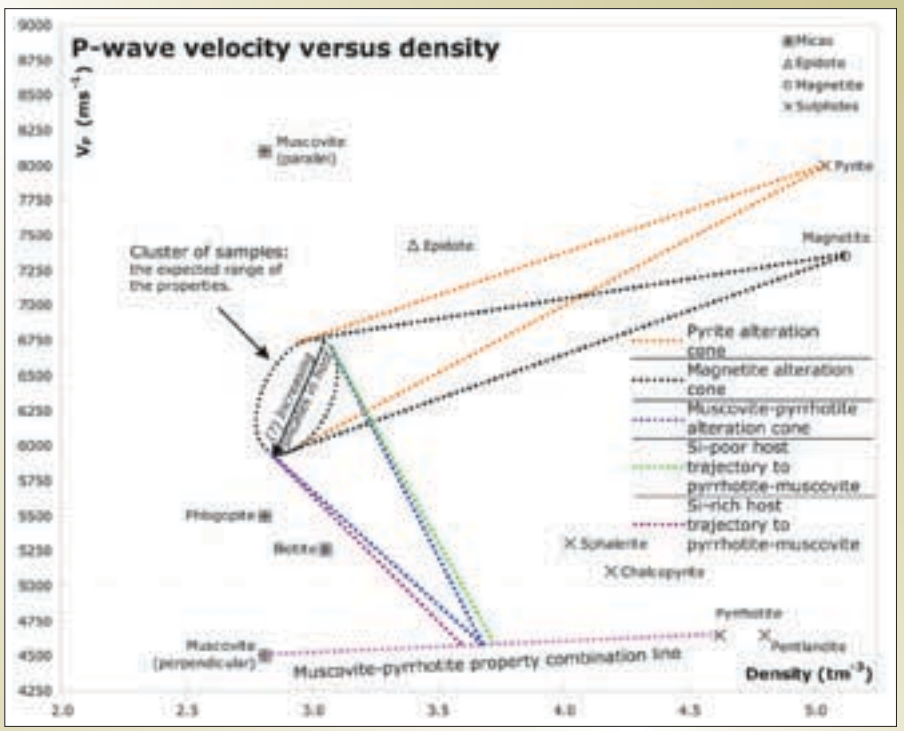

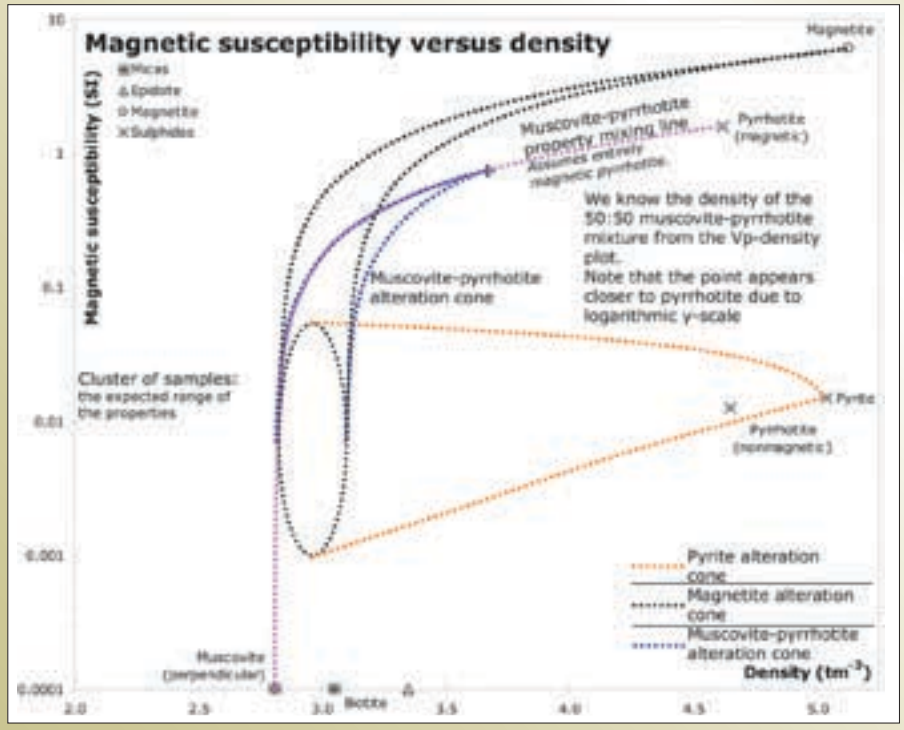

Figure 7: Seismic velocity versus density plot, showing the range of expected properties for a hypothetical host rock (oval) and the properties of some alteration minerals. Three alteration cones are shown. These cones are the expected alteration fields of the host rock to progressively greater amounts of pyrite (orange), magnetite (black) and a combination of muscovite and pyrrhotite (blue). The variation in the physical properties of the main cluster of samples may result from differing silicate content. Differing host chemistry may result in differing alteration assemblages; for example, SiO2-rich hosts may yield more muscovite if altered to a muscovite-pyrrhotite assemblage. Trajectories for these SiO2-rich and SiO2-poor hosts are shown (dashed violet and green lines).

Figure 8: Magnetic susceptibility versus density plot showing the same alteration cones as Figure 7. Note the sides of the alteration cone appear curved as they are plotted logarithmically (y-scale). For this example, the combination of muscovite and pyrrhotite is assumed to be entirely a combination with the magnetic form of pyrrhotite. Real alteration systems may create magnetic and non-magnetic pyrrhotite.

and magnetite alteration cones cannot be unequivocally assigned to one style of alteration or another.

In order to resolve the ambiguity, we need to examine as many physical properties as possible and attempt to ensure that the properties we examine have the most spread between probable types of alteration. Although the alteration cones for pyrite and magnetite showed significant overlap in Figure 7, Figure 8 shows there is no overlap on a magnetic susceptibility-density plot. This means we can be more certain of the type of alteration that has affected various samples, and can accurately predict the type of alteration. Plotting samples on a magnetic susceptibility-density plot allowed for the discrimination of magnetite and pyrrhotite alteration in samples from the 9.1 km deep KTB drillhole (Rauen et al., 2000).

Alteration assemblages may not necessarily be a single alteration mineral – they can be a combination of several alteration minerals. For the purposes of this report we assume that the physical properties of a combination of two alteration minerals combine in a linear fashion. This assumption suggests that the physical properties of an alteration phase combining 50% muscovite and 50% pyrrhotite would have a density halfway between that of muscovite and pyrrhotite, and similarly for other physical properties. The focus of an alteration cone for an alteration assemblage of several minerals lies on the physical properties of that combination of minerals. An example of this is shown for a 50:50 combination of muscovite and pyrrhotite in Figures 7 and 8.

It is not guaranteed that the alteration cone will have a well-defined focus. This is the result of differing host chemistry which may dictate the alteration assemblage. For example, a more silicate-rich host may produce more silicates in a mixed alteration assemblage of pyrrhotite and muscovite. Possible alteration trajectories for this scenario are depicted in Figure 7.

Once we consider the possibilities of combining alteration minerals it is also important to realise that some alteration combinations provide no or little net physical property change with respect to the original host lithology. In such cases, identification of alteration using physical property methods would not be possible.

3.1.2 Quantifying alteration and physical property variations

For our simple rock model, imagine a rock and alteration assemblage with properties:

Property	Host	Alteration assemblage
Density	ρ_h	ρ_a
Magnetic susceptibility	k_{a_h}	k_{a_a}
Seismic velocity (P-wave)	V^p	V^p

If we have a sample which we would classify as being 15% altered, that is, alteration assemblage is 15% by volume of the sample, then the calculation for the density of the sample would be $\rho_{sample} = 0.85\rho_{host} + 0.15\rho_{alteration}$, and similarly for the other physical properties.

Although this is a useful concept to predict the physical properties of altered samples, and is a concept we can exploit for modelling the effect of alteration, we can also quantify the amount of alteration, assuming we can characterise the host and the alteration phase and know some physical properties for a sample.

To quantify the proportion of alteration, given the physical properties of a sample, we use:

$$Proportion\ of\ alteration = \frac{sample - host}{alteration - host}$$

Equation 2: Proportion of alteration calculated as the ratio of the differences between the sample and host, and the alteration end-member and host physical properties.

In more specific terms, the calculation for the alteration proportion based on the density of a sample is as follows:

$$proportion\ of\ alteration = (\rho_{sample} - \rho_{host})/(\rho_{alteration} - \rho_{host}).$$

This can be applied for any physical property we desire to calculate a proportion of alteration for.

The technique of linear mixing ratios to calculate the properties has differing validity depending on the property that is being calculated. For the purposes of this report we are concerned mainly with three physical properties: density, magnetic susceptibility and seismic (P-wave) velocity.

Linear mixing ratios are valid for density calculations, assuming the ratio of minerals to pore space does not change markedly with the addition of alteration to a host (Olhoeft and Johnson, 1989).

Linearity of magnetic susceptibility with respect to proportion of magnetite can be assumed for small proportions of magnetite for magnetic susceptibility. The concentration of magnetite, below which the increase in magnetic susceptibility is linear with respect to the volume of magnetite is reported to be at least 6% (Williams and Dipple, 2006). Other studies have experimentally confirmed the concentration of magnetite above which where linear mixing ratios are not acceptable and report a range between 13% (Fannin et al., 1990) and 20% (Shandley and Bacon, 1966). Above this concentration level, the magnetic susceptibility increases more rapidly than the density of the sample. This is thought to be due to the combination of small magnetic domains of magnetite to create larger magnetic domains (Stacey, 1962; Hargraves and Banerjee, 1973; Dunlop, 1995). This relationship may also apply to the more weakly magnetic mineral pyrrhotite.

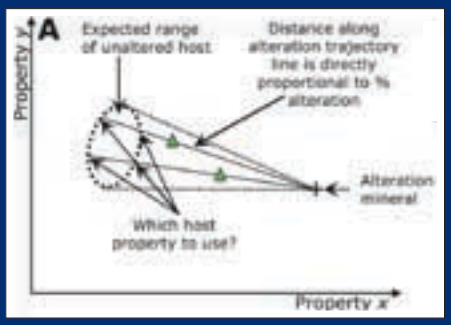

Figure 9(A): Theoretical example showing different alteration trajectory lines (solid black lines) for a single type of alteration and for two different samples. The different positions of the samples within the alteration cone indicate that these samples may result from alteration of hosts with differing physical properties.

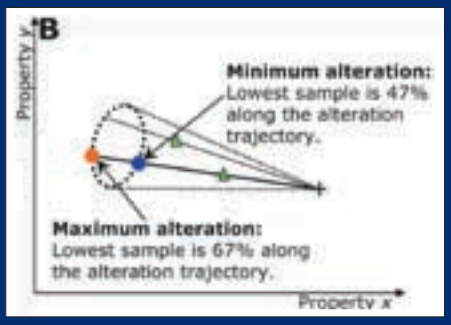

(B): Illustration, using the lowest sample, of how the choice of the properties of the host lithology determines the proportion of alteration. If we choose the host as having the properties of the red circle, we have maximised the distance the sample is from the host, and the sample is 67% altered. Alternatively, we can choose a host closest to the sample, minimising the proportion of alteration. For this case, the sample is 47% altered.

Linear mixing ratios are applicable for seismic velocity although they are not regarded as the most accurate method (Ji et al., 2002). A more accurate method of calculating seismic velocities for an arbitrary concentration of minerals is to use either the Voight or Reuss' methods or a combination of both (Hill's method). All three methods are discussed in Christensen (1989). Both Voight and Reuss' methods are linear combinations of strain or stress along crystallographic axes, and the most common method (Hill's method) is often relatively similar to velocities calculated by linear mixing ratios. The errors between using Voight, Reuss or Hill methods and linear mixing ratios is most likely within the order of 5-10% (Christensen, 1989).

We must also consider the effect of disparity of laboratory measurements and downhole geophysical logging. Differences of up to ±10% are reported for in-situ versus laboratory measurements (Berkhemer et al., 1997).

Once the alteration properties relevant to the alteration are identified (through the use of the alteration cone concept shown in Figures 7 and 8) we require an estimate of the original host property. This choice of a representative figure for host property has the potential to greatly affect the calculation of the proportion of alteration.

Consider a situation where we know some samples are altered towards a certain alteration mineral, that is, they sit within one alteration cone, but these samples sit along different alteration trajectories. The positions of samples within the alteration cone are determined by two parameters – the amount of alteration and the original host material they are altered from. Although they are still from the same host lithology, the variability in this host lithology means that the samples follow different alteration trajectories. This situation and an illustration of how much this variability can affect physical property calculations of the proportion of alteration are shown in Figures 9A and B.

By defining an acceptable range of physical properties for a given lithology (depicted by the oval in Figure 9) and by using our linear relationship to predict likely hosts, we can provide limits on the range of alteration proportion for a given sample. The method to provide this range is as follows:

1. Construct a straight line between the sample and the focus of the alteration cone. Based upon our assumptions, the host material that this sample is altered from will also need to lie along this line.

2. Extend this line from the sample to the furthest edge of the field that defines our unaltered sample field.

3. The distance from the sample to the furthest edge of the unaltered field is directly proportional to the maximum alteration proportion. The minimum alteration proportion is also calculated similarly; however the distance is from the closest edge of the unaltered field to the sample (see Figure 9B).

By understanding the probable distribution of samples along the alteration trajectory within the unaltered field we are also able to understand the relative likelihood of different alteration proportions. If we were dealing with a single property or were parallel to the axis of a property we could simply use a single dimension frequency histogram for this purpose. Most alteration trajectories, however, are expected to be oblique to an axis or deal with multiple properties; hence we need to understand the physical property distribution within a multidimensional space.

3.1.3 Summary

- Use of the alteration cone concept allows us to identify alteration of a host rock. The focus of the alteration cone is typically the physical properties of what we refer to as the alteration assemblage. Host chemistry may influence the alteration cone such that it may lack a truly well-defined focus.
- Once an alteration trend has been identified, individual samples can be quantified in terms of alteration proportion by use of Equation 2.
- Identification of the range of possible host lithology physical properties allows us to measure the uncertainty within the process of quantifying the amount of alteration for any altered sample.

3.2 Case studies of lithologies at the St Ives Gold Mine

3.2.1 Introduction to the St Ives Gold Mine

The St Ives Gold Mine is located approximately 80km south-southeast of Kalgoorlie, Western Australia, and is hosted within the Norseman-Wiluna greenstone belt of the Archaean Yilgarn craton (Watchorn, 1998). The camp consists of many deposits, aligned northwest-southeast for a strike length of approximately 30km. The locations of the gold camp within the Yilgarn craton and major gold deposits of the St Ives camp are depicted in Figure 10.

Typical host rocks for gold mineralisation are mafic to ultramafic rocks (Connors et al., 2003) and felsic to intermediate porphyry intrusions (Neumayr et al., 2004). Mineralisation is proximal to shear-zone systems (Cox and Ruming, 2004) and the St Ives gold mine is regarded as a typical Archaean lode-gold system. Stratigraphy at St Ives is depicted in Figure 11.

The Victory-Defiance mine area at St Ives represents an excellent study area for the physical properties of alteration. The area shows a well-developed alteration system of multiple types (Neumayr et al., 2003), and the major host lithologies of St Ives are present. There are a number of relatively deep (>500m) drillholes in the vicinity, with some holes being geophysically logged. The positions of the drillholes studied for this report are shown in Figure 12.

For each drillhole, physical properties were logged utilising downhole geophysical probes. The properties recorded were density, magnetic susceptibility, natural gamma radiation, seismic velocity (P- and S-wave) and resistivity. Drillhole CD10662 was also logged by CSIRO's HyLogger system to map the downhole distribution of alteration minerals. Results of this survey are reported in Yang (2006).

Figure 10: Locations of the St Ives gold camp within the Yilgarn Craton and the major gold deposits of the camp (Watchorn, 1998).

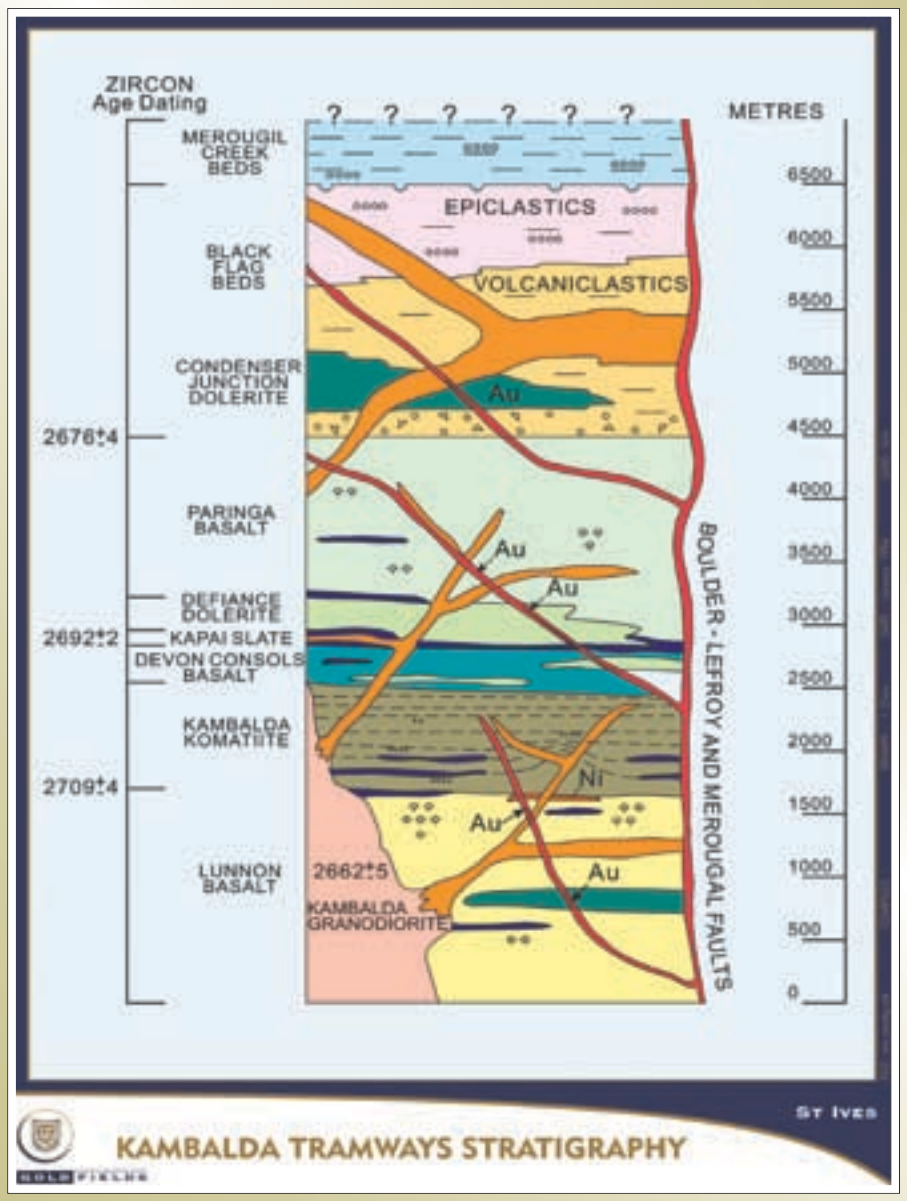

Figure 11: Generalised stratigraphy of the St Ives gold camp. Note that the 'Condenser Junction Dolerite' is regarded as two separate units – the Junction Dolerite and the Condenser Dolerite. Stratigraphy courtesy of Gold Fields (Connors et al., 2003).

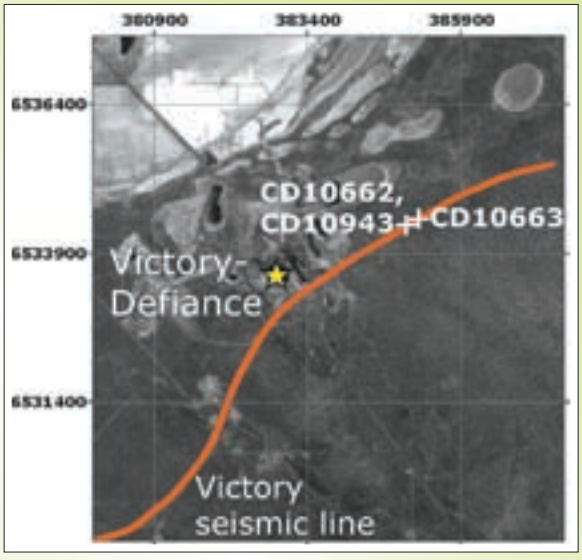

Figure 12: The location of the three drillholes studied for this report with respect to the Victory-Defiance complex and the Victory seismic line. Base map is the Landsat ETM+ Band 8 panchromatic image (courtesy Australian Centre for Remote Sensing). Drillholes are denoted by the cross symbols. Drillholes CD10662 and CD10663 dip to the west, with drillhole CD10943 dipping to the east. Note that all three drillholes are positioned directly on the Victory seismic line. These drillholes are within the Greater Nelson's Fleet prospect of St Ives.

The drillholes studied are all proximal to the Victory seismic line, a seismic line acquired in 2002. This seismic line has been used along with other mine-scale seismic experiments to assist in the definition of the architecture of the St Ives region (Stolz et al., 2004; Urosevic et al., 2006). The spatial relationship of drillholes and seismic data may allow for testing of hypothesis of the signatures of alteration in seismic data.

The drillholes studied are relatively poorly mineralised, with gold intersections of:

- CD10662 – 3 m grading 0.4 ppm gold.
- CD10663 – 4 m grading 1.9 ppm gold.
- CD10943 – 1 m grading 2.5 ppm gold.

Despite this low level of mineralisation, the drillholes represent an excellent dataset to study alteration and geophysical response. Within these holes it may be possible to detect alteration styles typical distal to mineralisation. The minor intersections of gold mineralisation suggest we may also detect alteration styles typical proximal to mineralisation. Understanding both proximal and distal alteration types is the key to characterise the geophysical signatures of alteration for this type of gold deposit.

3.2.2 Intermediate and Mafic (Unclassified) Unit

The samples examined for this case study were all logged in drillhole CD10662 (location illustrated in Figure 12). The samples studied occur from 480 m to 815 m downhole depth, with 7 m of this interval (510 m to 517 m) geologically logged as the mafic (unclassified) unit. A 3 m wide interval of intermediate (unclassified) unit is also intersected at approximately 915 m downhole depth, but this is regarded as alteration of the Devon Consols Basalt it intrudes (A. Roache, *pers. comm.*).

Hole CD10662 is poorly mineralised, with the highest gold intersection of 0.4 gt^{-1} over 3 m. This gold mineralisation occurs at 514-517 m downhole depth, entirely within the mafic (unclassified) unit.

The intermediate and mafic units occur above the Devon Consols Basalt within the CD10662, and below the Condenser Dolerite. From the regional stratigraphy (Figure 11), the intermediate unit most likely correlates with intermediate units within the Black Flag Group. The intermediate unit has also been postulated to be silicified Paringa Basalt, which also correlates with the regional stratigraphy (K. Connors, *pers. comm.*)

Less likely, the intermediate unit may represent an intermediate intrusion approximately 350 m thick (A. Roache, *pers. comm.*). The mafic (unclassified) unit may either represent a 7 m thick mafic intrusion into this intermediate unit or it may represent an alteration of the intermediate unit. For the purposes of this report, we regard the intermediate unit to be a primary lithology, although we note it may be a thick and regionally altered package.

3.2.2.1 Relationship between the intermediate and mafic (unclassified) units

The samples geologically logged as the mafic (unclassified) unit occurs as a 7 m wide zone within the intermediate (unclassified) unit in drillhole CD10662. Furthermore, the mafic unit contains the only gold mineralisation within this drillhole. This spatial association with the gold mineralisation may suggest that the mafic unit may represent an altered product of the intermediate unit. Due to the spatial associate with mineralisation, we would expect that the possible alteration assemblages would reflect common alteration types found near to gold mineralisation at St Ives.

Figure 13 depicts common alteration surrounding gold mineralization at St Ives. Neumayr et al. (2003) observe similar alteration assemblages.

If the mafic unit represents alteration of the intermediate unit and the alteration assemblages from Figure 13 also apply to this lithology, then we would expect to be able to use our concept of alteration cones (Section 3.1.1) to explain physical property differences in terms of alteration to different minerals. We must first establish the expected range of physical properties for the intermediate unit, and the physical properties of the mafic unit to allow interpretation of potential alteration assemblages. As per Section 3.1.1, we will examine these properties on scatter plots. Seismic velocity-density and magnetic susceptibility-density plots for the intermediate unit is shown in Figures 14 and 15; Figures 16 and 17 show the corresponding plots for the mafic unit. Interpreted alteration cones for the common alteration types are shown in Figures 18 and 19.

In Figure 19, not all mafic unit samples plot within the pyrrhotite alteration cone. Thus we are unable to explain the mafic unit purely in terms of pyrrhotite alteration of the intermediate unit. This is expected, as pyrrhotite generally occurs distal to gold mineralisation, and almost half the thickness of the mafic unit is mineralised. Based on our understanding of probable alteration assemblages (Figure 13), we can test the hypothesis that we can explain

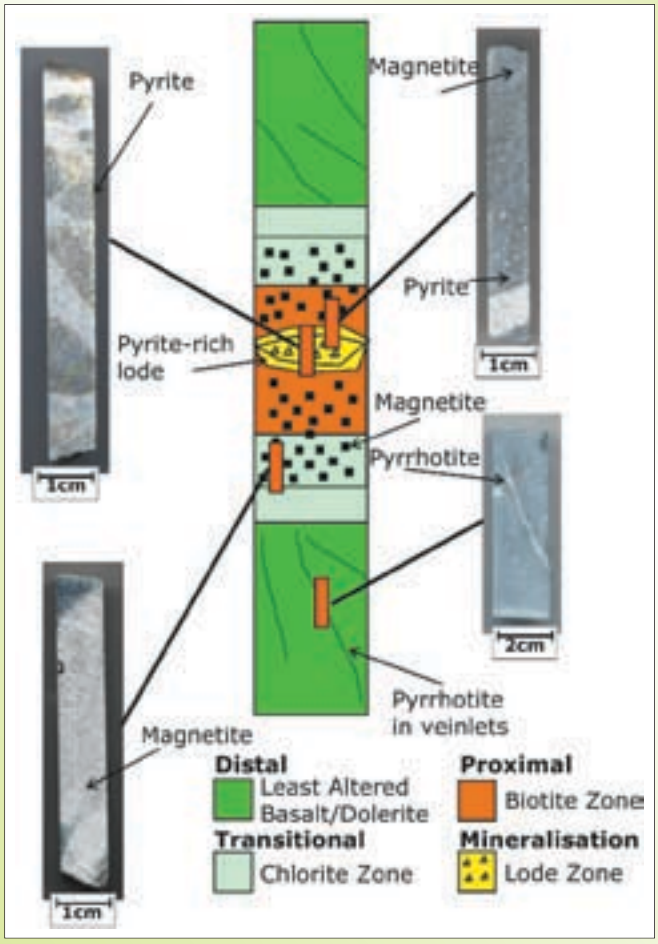

Figure 13: Common alteration assemblages and their relationship to gold mineralisation at St Ives (Figure after Ruming, 2006).

These assemblages are:

- *Distal – pyrrhotite (in veinlets), possible minor pyrite (Neumayr et al., 2003).*
- *Transitional – chlorite ± magnetite with possible pyrite (Neumayr et al., 2003).*
- *Proximal – biotite, magnetite ± pyrite.*
- *Mineralisation – gold, pyrite.*

Note that these are the major alteration minerals, and that other alteration minerals may be present but in minor concentrations (Neumayr et al., 2004). These minerals also have physical properties that vary significantly from the common host physical properties at St Ives. Therefore they represent minerals we potentially can detect by physical property means.

the physical properties of the mafic unit by alteration to any of these assemblages. In this regard Figure 18 is inconclusive, as the samples of the mafic unit plot within alteration cones for magnetite, pyrite, and a combination of equal parts of magnetite, biotite and pyrite. Note, for comparison, chlorite has approximately similar seismic velocity to muscovite and biotite (Connolly and Kerrick, 2002), although it has a density closer to biotite than muscovite, so alteration to chlorite-magnetite-pyrite would show broadly similar trends to that seen for biotite-magnetite-pyrite alteration.

To resolve the ambiguity in our interpretation of the alteration type, we can refer to a plot of magnetic susceptibility and density (Figure 19). We can now see some separation between the alteration cones for magnetic, pyrite and biotite-magnetite-pyrite alteration. We observe that only one mafic sample plots within the magnetite alteration cone and thus we cannot explain the mafic unit by purely magnetite alteration of the intermediate unit. The samples with magnetic susceptibilities above approximately 0.2 SI are most likely explained by alteration towards an assemblage containing biotite, magnetite and pyrite. Although we have an understanding of likely alteration minerals, we have little information on the relative proportions of these minerals within the end-member alteration assemblage. For this reason we have assumed equal proportions of the minerals in order to explain the broad alteration trend. There is some freedom on the placement of the focus of the alteration cone and thus the exact composition of the alteration assemblage.

There are some samples that do not plot within the biotite-magnetic-pyrite alteration cone (Figure 18). These samples plot within the nonmagnetic pyrrhotite alteration cone and also within the pyrite alteration cone. Although some samples plot within the alteration cone for pyrrhotite in Figure 18, creation of purely nonmagnetic pyrrhotite is relatively unlikely (Clark, 1984). Thus we can conclude that the samples not altered to biotite-magnetite-pyrite are most likely altered to almost entirely pyrite.

These physical property observations lead us to conclude that 10 within the intermediate unit. The alteration is most likely due to alteration of the intermediate unit to biotite,

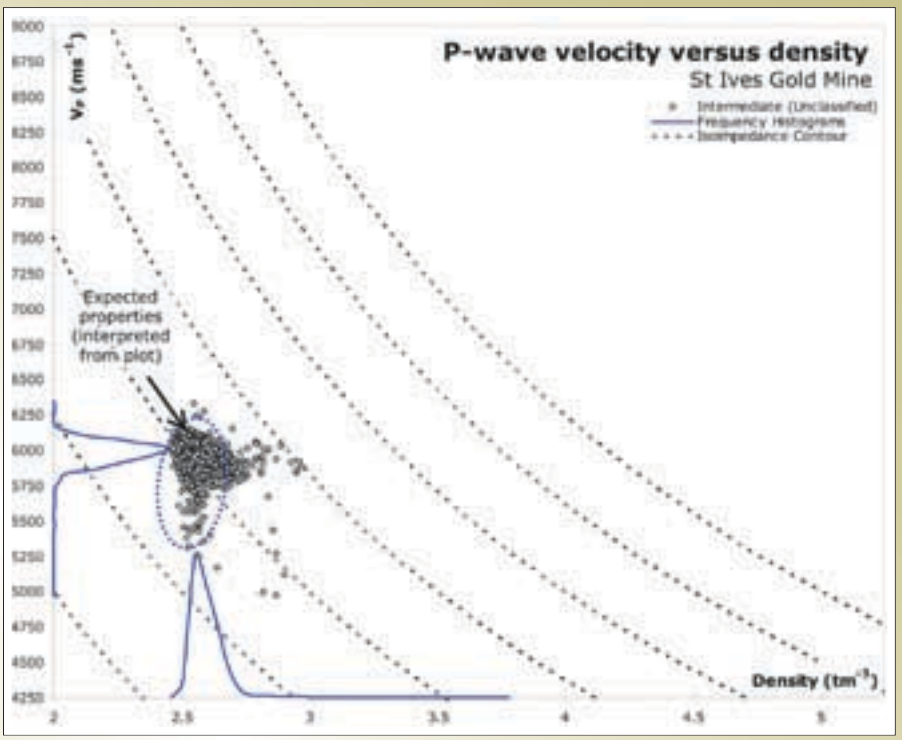

Figure 14: Seismic velocity-density plot for the intermediate (unclassified) unit, CD10662 drillhole. The samples occur from 475m to 815m downhole depth. The dotted oval depicts the expected range of physical properties. Also shown on this plot are frequency histograms for both density and seismic velocity.

Note the intermediate unit samples which appear to be heading towards marginally higher seismic velocities and densities – these samples may represent alteration.

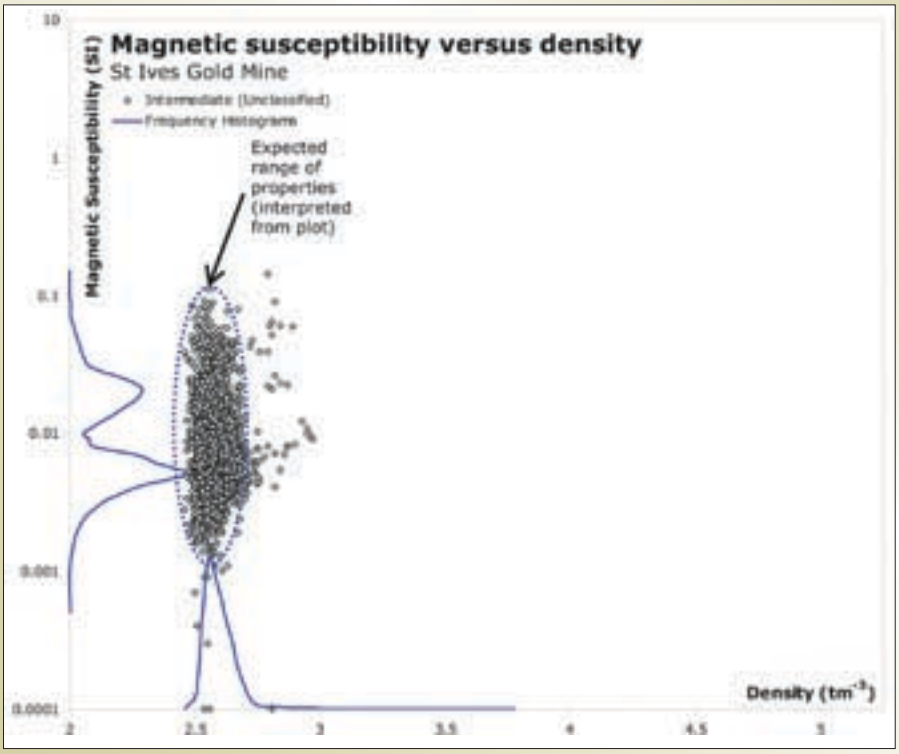

Figure 15: Magnetic susceptibility-density plot for the intermediate (unclassified) unit. Expected range of magnetic susceptibility and density is shown as the dotted oval. Frequency histograms for each physical property are also shown. Note the bimodal distribution of magnetic susceptibility.

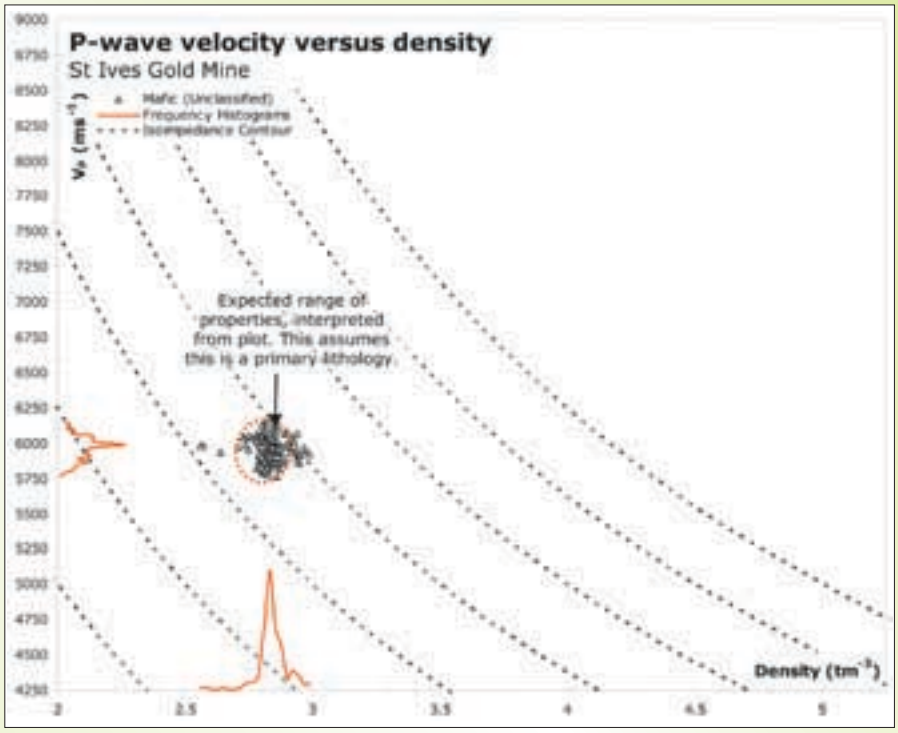

Figure 16: Seismic velocity-density plot for the intermediate (unclassified) unit, CD10662 drillhole. The samples occur from 510 m to 517 m downhole depth. The dotted oval depicts the expected range of physical properties. Also shown on the plot are frequency histograms for both density and seismic velocity.

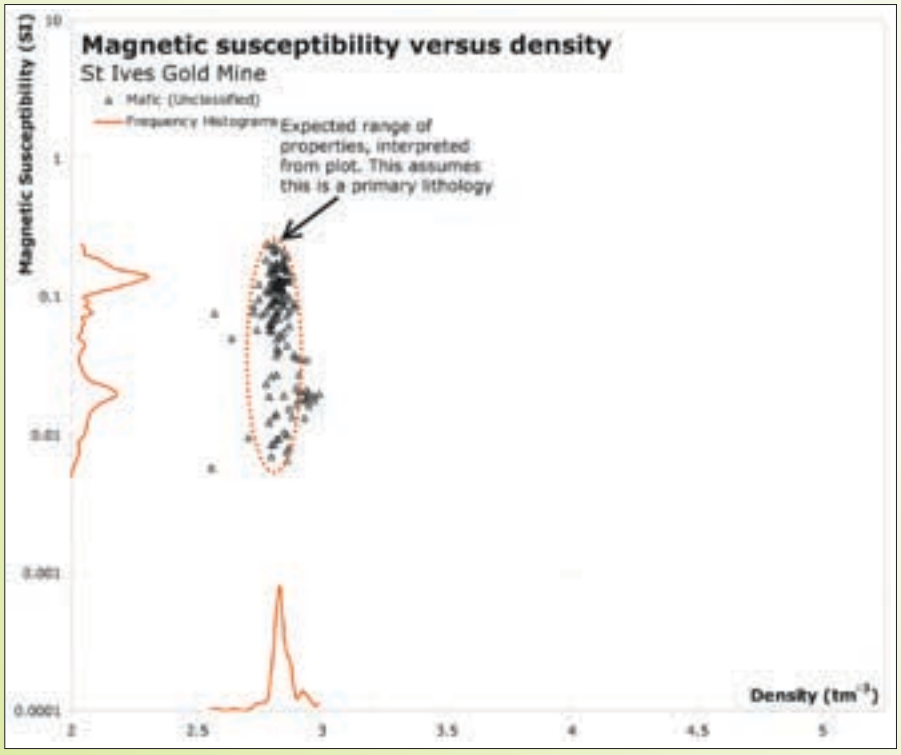

Figure 17: Magnetic susceptibility-density plot for the intermediate (unclassified) unit. Note the bimodal distribution of magnetic susceptibility. Comparison with the magnetic susceptibility frequency histogram of the intermediate unit (Figure 15) we note that there is a shared mode at 0.02 SI. The mafic unit has a second mode at 0.15 SI, and the intermediate unit has a second mode of 0.005 SI.

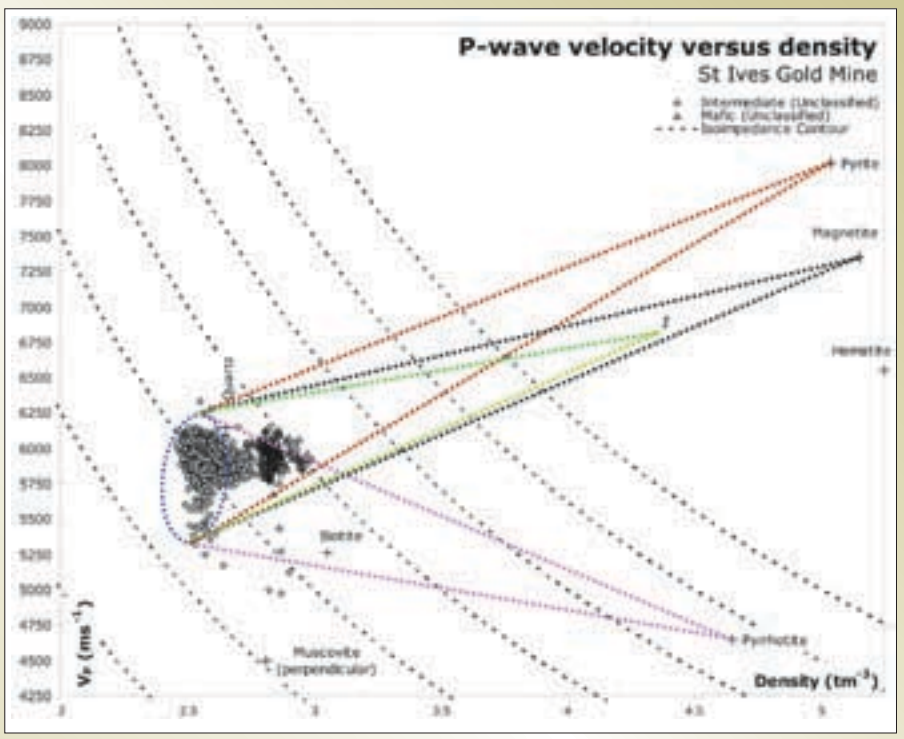

Figure 18: Alteration cones for different alteration assemblages that may affect the intermediate unit to result in the mafic (unclassified) unit. The green alteration cone with its focus at point 1 is an alteration cone defined by an assemblage containing equal proportions of biotite, magnetite and pyrite. Although arbitrary this combination allows us to identify if the mafic unit may result from alteration of the intermediate unit to some mixture of biotite, pyrite and magnetite.

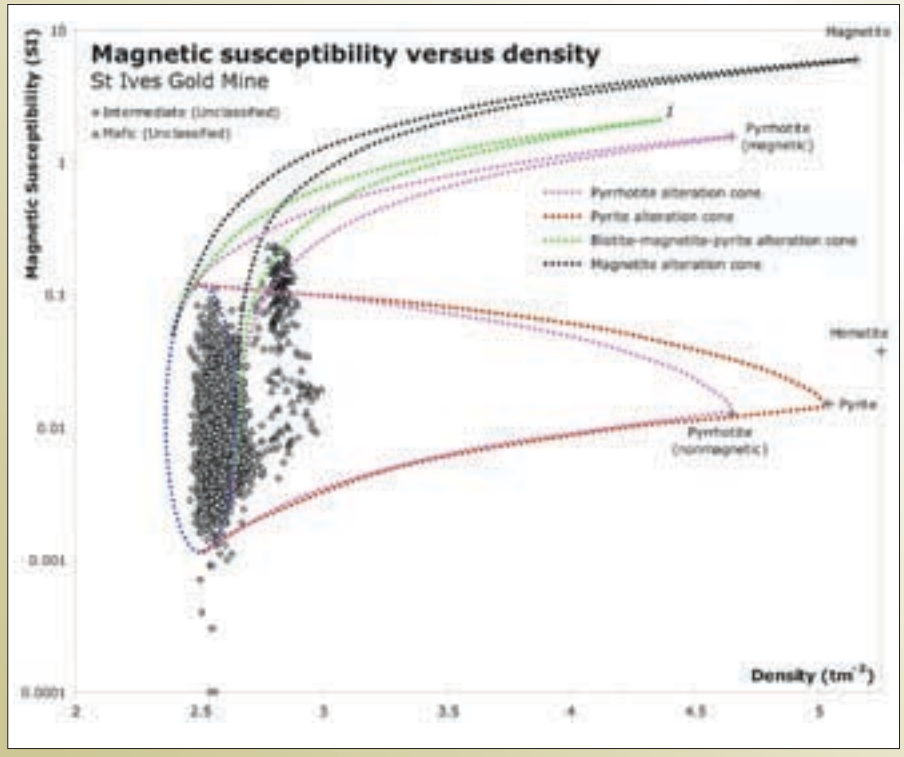

Figure 19: Alteration cones from this unit for common alteration types at St Ives. Point 1 is defined as per Figure 18 and is a mixture of biotite, magnetite and pyrite. Note that alteration to pyrrhotite may be to the magnetic or non-magnetic pyrrhotite, or may even be to a mixture of the two types.

magnetite and pyrite, although the exact proportions of these minerals in the alteration assemblage is unable to be determined from physical properties. Based on these observations, we can use the physical properties of the mafic unit as the expected physical properties of proximal alteration of silicified Paringa Basalt, or an intermediate member of the Black Flag Group.

3.2.2.2 Comparison with logged alteration

Studies of hydrothermal alteration mineral assemblages have previously been undertaken at St Ives by Neumayr et al. (2005). These studies have examined the exploration drillhole database and paper geological logging (P. Neumayr, pers. comm.) for possible mineral assemblages, for example, pyrite and pyrrhotite alteration types have been mapped. These studies were purely based on capturing prior logging information and did not directly relate alteration assemblage to the cores. They represent a dataset, however, that we can compare to alteration assemblages obtained from physical property measurements.

As we have previously established the expected range of physical properties for the intermediate and mafic unit (Figures 14 though 17), we can examine the samples reported to be altered to pyrrhotite and pyrite, as obtained from the St Ives Gold Mine exploration database and reported by Neumayr et al. (2005). The seismic velocity-density plot for the intermediate and mafic units with highlighted alteration assemblages is shown in Figure 20, and magnetic susceptibility-density plot for the same units and alteration assemblages is shown in Figure 21.

Examining the seismic velocity-density plot (Figure 20) we note that many of the samples identified by Neumayr et al. (2005) to be altered to pyrite or pyrrhotite plot outside the expected range of physical properties for the intermediate unit but within alteration cones for pyrite or pyrrhotite. Furthermore, a number of samples identified to be altered by Neumayr et al. plot within the field for the expected range of properties. This is not surprising, as the dataset from Neumayr et al. does not contain information regarding the proportion of alteration but simply presence or absence of an alteration assemblage. Pyrite, in particular, is identified in many samples. This is most likely the result of pyrite being a common mineral and readily identified, even in small concentrations, within drillcore. Although the field of expected range of properties represents largely unaltered samples, it may represent some samples with minor alteration.

There are also several samples that are identified to be the result of pyrite or pyrrhotite alteration. These show a decreasing seismic velocity with respect to density. This is most likely the effect of microfractures of samples – downhole geophysical logging of seismic velocity is sensitive to fracturing, however density measurements are generally more reliable for fractured samples (Dolan et al., 1998).

Approximately 10 samples identified as pyrite altered by Neumayr et al. (2005) do not plot within either the pyrite alteration cone, and most of these 10 samples do not plot within the pyrrhotite cone. These samples are noted as being anomalous samples in Figure 20. These samples may be the result of the combination of minerals within the alteration assemblage.

The interpretation of the magnetic susceptibility-density plot (Figure 21) is more complex. As two different types of pyrrhotite may be generated, each with different magnetic properties, we need to consider alteration cones for both these end-members. The intermediate and mafic units also vary in their magnetic properties, significantly more than the seismic velocity differences between the two units.

Although we have presented evidence that the mafic unit is an altered product of the intermediate unit, for the purposes of this comparison we can consider it to be a separate lithology. If we consider the mafic unit to be the product of biotite-magnetite-pyrite alteration, as interpreted above, an alteration cone between pyrite and the mafic unit is essentially the addition of more pyrite to the alteration assemblage of biotite-magnetite-pyrite.

Due to the positions of the non-magnetic type of pyrrhotite and pyrite, the interpretation of Figure 21 is more ambiguous. We cannot clearly identify where samples lie within, say, a pyrrhotite alteration and not within a pyrite alteration cone. For this reason, we must consider the general trends of the samples.

We can identify three different trends within Figure 21, with two trends evident in the samples identified to be altered to pyrrhotite, and one trend in the samples identified to be altered to pyrite. One trend within the pyrrhotite samples is to relatively high magnetic susceptibility for a small increase in density. This is consistent with alteration towards almost solely magnetic pyrrhotite (Peters and Thompson, 1998; Rauen et al., 2000). The second trend is a lower increase in magnetic susceptibility with respect to density. This is consistent with a trend towards either to non-magnetic pyrrhotite, or, more likely, a trend towards a combination of

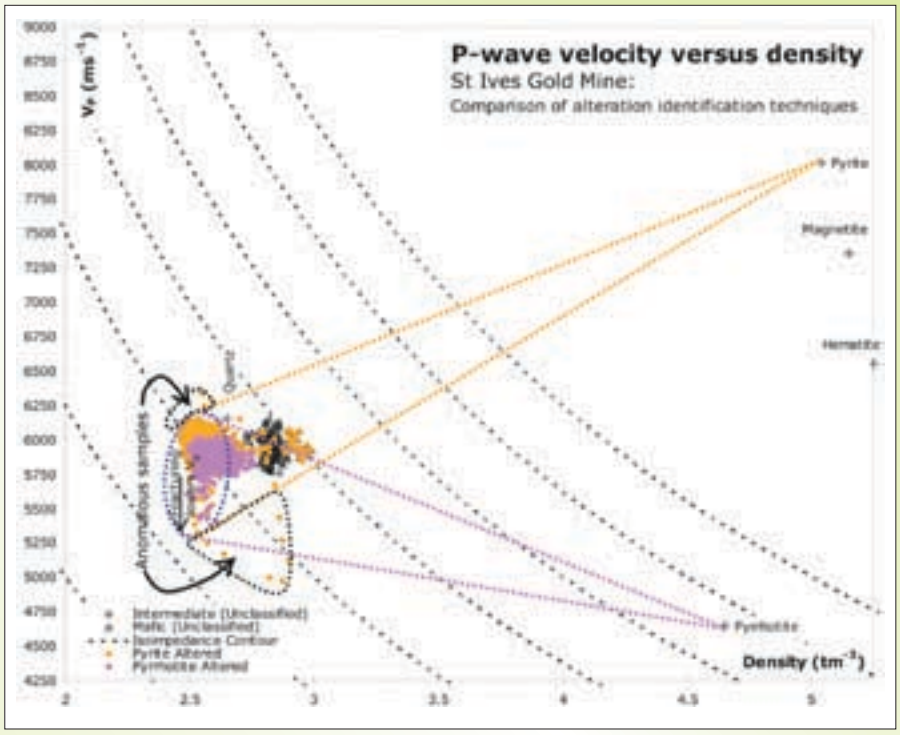

Figure 20: Seismic velocity-density plot for the intermediate and mafic (unclassified) units, CD10662 drillhole. Samples reported to be altered to pyrite and pyrrhotite are highlighted. Anomalous samples, which cannot be explained by pyrite or pyrrhotite alteration, are also highlighted.

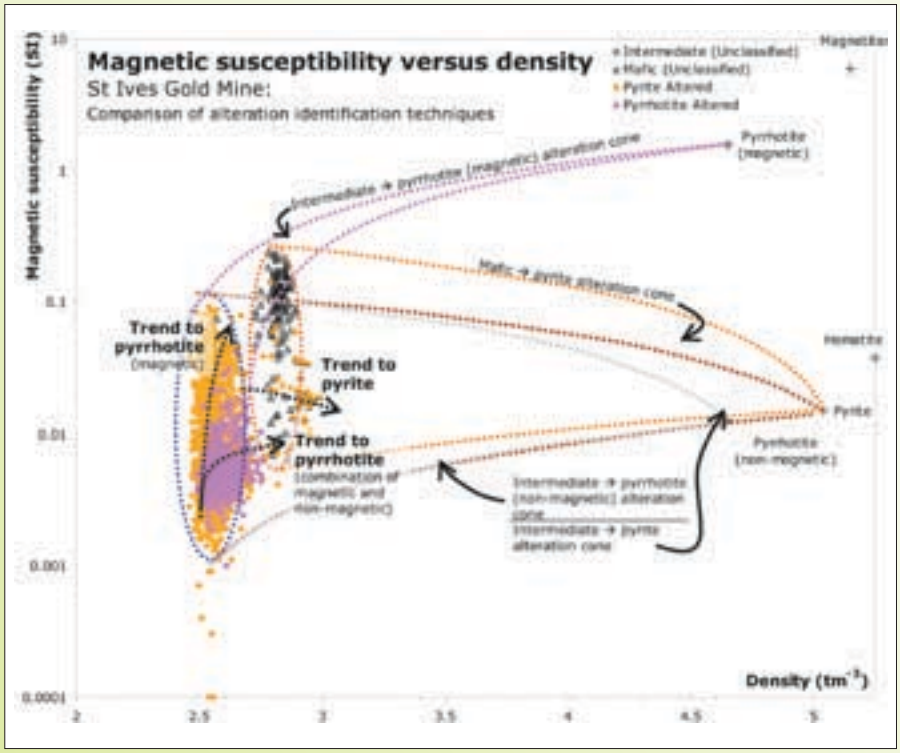

Figure 21: Magnetic susceptibility-density plot for the intermediate and mafic (unclassified) units, CD10662 drillhole. Highlighted samples are as per Figure 20. Alteration cones for pyrite and pyrrhotite are also shown. The interpretation of trends is discussed within the text.

magnetic and non-magnetic pyrrhotite. The proportions of magnetic and non-magnetic pyrrhotite produced may relate to the amount of iron available during alteration (Putnis, 1975) or other physical conditions such as temperature during alteration (Konty et al., 1997; O'Reilly et al., 2000).

The trend interpreted to be towards pyrite is a trend to lower magnetic susceptibilities with respect to density. This is consistent with alteration towards pyrite, especially given the seismic velocity of samples exhibiting this trend.

By considering seismic velocity, density and magnetic susceptibility generally we find good agreement between the alteration assemblages identified by Neumayr et al. (2005) and samples we can recognise via physical property considerations.

3.2.2.3 Comparison with the HyLogger technique

One of the most prominent features observed in the HyLogger results (Yang, 2006) from drillhole CD10662 is a rapid change in white mica AlOH feature wavelength at approximately 640 m downhole depth (Figure 22). This change in AlOH feature wavelength corresponds to a switch from phengitic to muscovitic mica composition (Herrmann et al., 2001). At this same location, there is an increase in relative mica abundance (Figure 22), with an AlOH feature depth of ~45%. This feature depth is a measure of the depth of the AlOH absorption feature in the spectral results, with more absorption implying more abundant white mica, with a composition indicated by the wavelength of the spectral feature. As the feature depth at 640 m is one of the deepest observed for this drillhole, we infer that considerable amounts of muscovite are present at this location.

As the physical properties of muscovite vary from those of the host rock, the intermediate unit, muscovite should be able to be detected by physical property measurements. A seismic velocity-density plot highlighting samples noted to be altered in the HyLogger results is shown in Figure 23, and Figure 24 shows a magnetic susceptibility-density plot for the same samples.

The maximum density of the samples inferred from the HyLogger to show anomalous mica compositions is 2.9 tm-3. This is a higher density than that of muscovite (2.81 tm-3). Even 100% alteration purely to muscovite would, therefore, not account for this density. Furthermore, the magnetic susceptibility is greater than that expected for alteration to nearly pure muscovite. The magnetic susceptibility of the samples is similar to that of the host rock (see Figure 24). The magnetic susceptibility of the intermediate unit is maintained during alteration, despite the addition of significant amounts of muscovite.

To explain the magnetic susceptibility of the altered samples, the alteration assemblage must contain some magnetic material. For lode-gold systems, such as St Ives, the only common magnetic minerals are magnetite and pyrrhotite. These minerals would also account for the density of the altered samples. Assuming an alteration assemblage that is a combination of either muscovite and

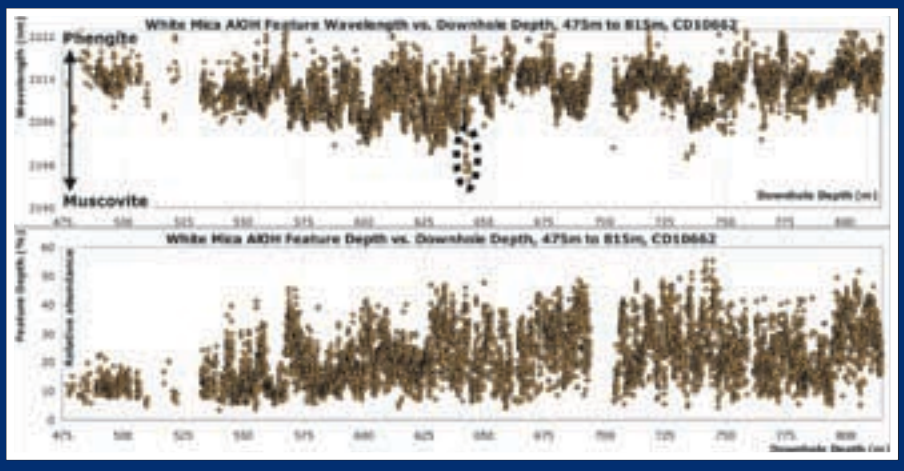

Figure 22: White mica composition (top) and relative abundance (bottom) for the intermediate unit, drillhole CD10662. The change, at ~640m, from phengite to muscovite composition is highlighted by the dashed oval. The feature depth (bottom) measures the depth of the absorption feature of AlOH as detected by the HyLogger, and is a measure of the relative abundance of white mica at a particular drillhole depth (Yang, 2006).

magnetite or muscovite and pyrrhotite, according to our rock property model (Section 3.1.1) the focus of the alteration cone must lie somewhere upon a combination line between either muscovite and magnetite or muscovite and pyrrhotite.

The seismic velocity of muscovite is highly anisotropic, that is, the seismic velocity varies according to the angle of measurement of the seismic velocity. We have little knowledge of the orientation of the drillhole relative to the cleavage plane of muscovite, although the decrease in seismic velocity (Figure 23) in the altered samples suggests that we are more likely to be observing muscovite oriented approximately perpendicular to the drillhole. If we constrain the seismic velocity of the muscovite in the alteration assemblage to 4500 ms-1 then we can draw combination lines for alteration assemblages including muscovite and pyrrhotite. The focus of the alteration cone for each alteration assemblage should lie somewhere along this line (Section 3.1.1). As the combination lines are different, we can only satisfy this requirement if we infer slightly different alteration cones for each alteration assemblage.

From Figure 23 we know the density of end-member alteration assemblage for each type (the density at the focus of the alteration cone), and can use this information to establish if the alteration assemblage is muscovite-magnetite or muscovite-pyrrhotite.

The magnetic susceptibility-density plot (Figure 24) shows that the altered samples do not plot within the muscovite-magnetite alteration cone. Furthermore, the samples do not plot within an alteration cone that is muscovite-magnetic pyrrhotite. The samples do plot entirely within a muscovite-non-magnetic pyrrhotite alteration cone. From studies at the KTB borehole, however, in Germany, alteration systems generally create both magnetic and non-magnetic pyrrhotite (Berkhemer et al., 1997).

We have successfully established that, in broad terms, the physical properties of muscovite altered rock, as determined by the HyLogger study, tend towards the physical properties of muscovite. In order to fully explain the physical properties of the altered samples we have observed, we must also introduce magnetic material to the alteration assemblage. By examining the velocity, density and magnetic properties we are able to establish that the most likely composition of the alteration assemblage is muscovite-pyrrhotite, with both magnetic and non-magnetic pyrrhotite included in the alteration assemblage.

3.2.2.4 Broad alteration trends within the Intermediate-Mafic Unclassified Units

By examination of the entire downhole logging for the intermediate and mafic units we can also establish more broad alteration trends within the data. The physical property character of the intermediate unit changes significantly down the drillhole. This character has allowed us to split the intermediate unit into 6 separate regions, each showing different physical property character. These regions are illustrated on downhole geophysical and HyLogger logs in Figure 25.

Region 1

This region includes the mafic (unclassified) unit which we have previously inferred to be proximal alteration. This region is typified with an increased density and slightly elevated magnetic susceptibility with respect to the host we infer to be typical of the intermediate unit (Region 6). The alteration assemblages to explain these properties are pyrrhotite alteration, occurring distal to the mineralisation and biotite-magnetite-pyrite or pyrite alteration, occurring proximal to the mineralisation. Seismic velocity is increased with respect to other regions, again supporting the inclusion of sulphide alteration. Although the white mica composition is approximately phengitic, there are only low relative white mica abundances.

Region 2

Region 2 shows a gradient in density, from the high density observed in Region 1 to the low density of Region 3. The magnetic susceptibility is less variable than Region 1. The natural gamma radiation increases on that of Region 1, corresponding to an increase in white mica relative abundance. White mica composition is broadly phengitic. The properties of this region most likely reflect the properties expected for the edge of distal alteration (pyrrhotite), potentially with slightly increasing white micas.

Region 3

Region 3 is characterised by consistently low magnetic susceptibility and an increasing downwards gradient in natural gamma. This gradient corresponds to an increase in white mica abundance, although the composition of the white micas is broadly tending towards muscovite rather than phengite. This unit is characterised by a natural gamma spike approximately 10 m from its base, and is bounded by the rapid change from phengite to muscovite white micas, as discussed above. We can

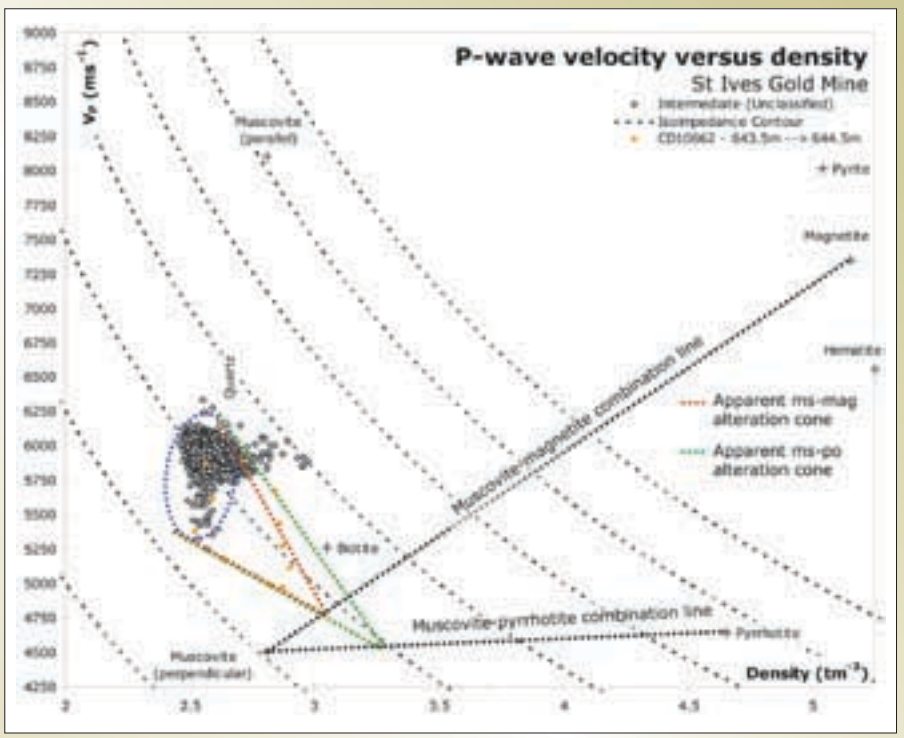

Figure 23: Seismic velocity-density plot for the intermediate unit. Highlighted samples (orange) are samples inferred from the HyLogger study that show a switch from phengitic to muscovitic mica composition.

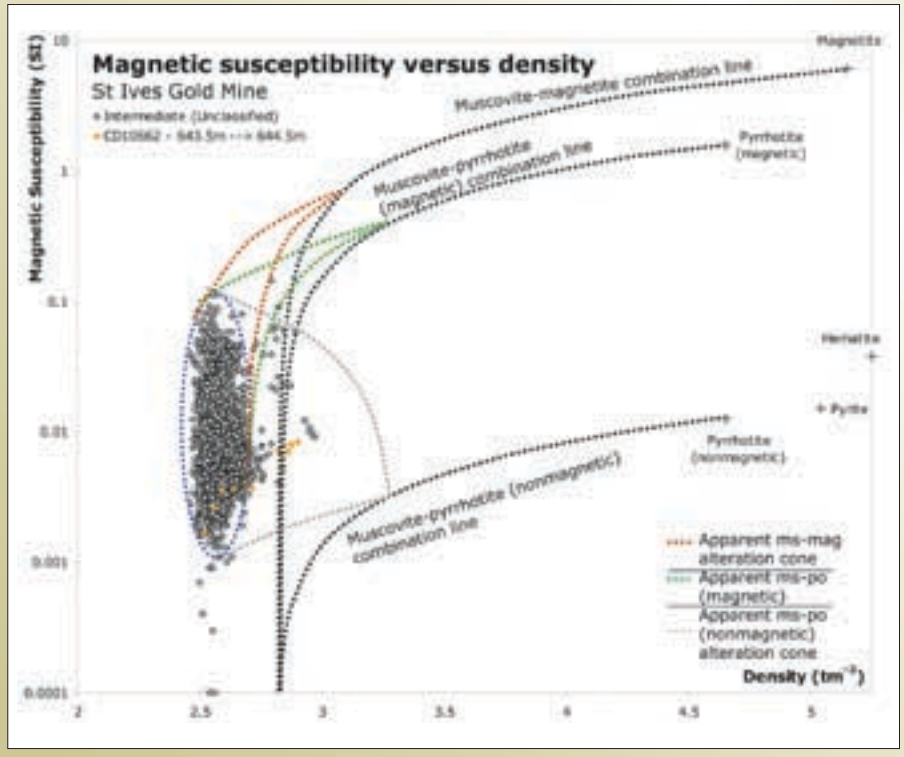

Figure 24: Magnetic susceptibility-density plot for the intermediate unit.

Figure 25: Downhole geophysical logs for drillhole CD10662, 475m to 815m downhole depth. The AlOH feature wavelength (measure of mica composition) and feature depth (measure of mica abundance) are derived from the HyLogger results; the other physical parameters are derived from downhole geophysical logging performed by Gold Fields at St Ives. Six main regions of physical property character are recognised for this interval in drillhole CD10662. Inferred alteration types are shown to the left of the density log, abbreviations as per Section 1.2. Lithology codes shown on these logs: Iu – Intermediate (unclassified), Iz – Monzodiorite, Md – Dolerite, Mu – Mafic (unclassified), Vn – zone of significant veining.

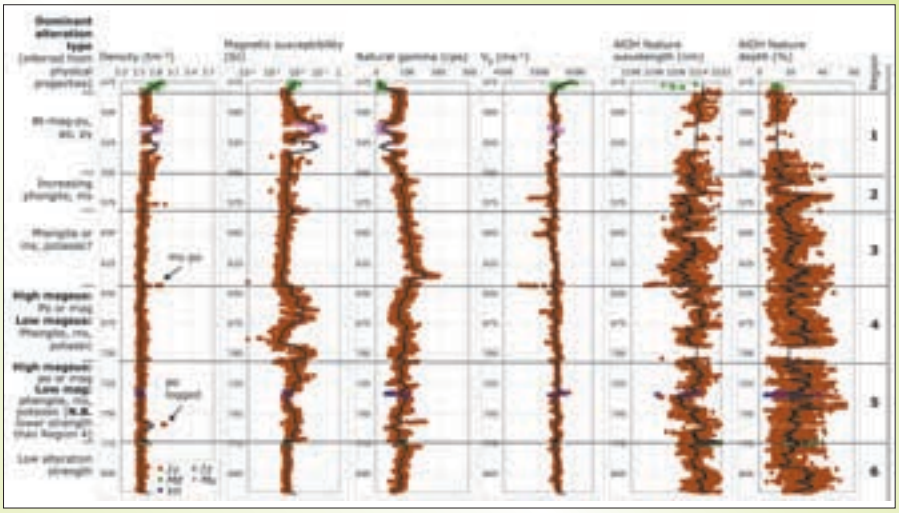

therefore expect this region to be one whose properties are influenced by increasing white micas.

Region 4

Region 4 is characterised by highly variable magnetic susceptibility. Magnetic susceptibility shows an inverse correlation with natural gamma, suggesting a switch between iron-rich (high magnetic regions, pyrrhotite or magnetite) and potassic-rich (low magnetic regions, muscovite or phengite) regions. The natural gamma radiation response broadly correlates with white mica relative abundance. On a broad scale, seismic velocity is slightly higher than within Regions 2 and 3. This slight velocity increase correlates with the more magnetic regions and suggests inclusion of some magnetite.

Region 5

Region 5 shows magnetic variability similar to that observed in Region 4, although with lower maximum and minimum susceptibilities. The dominant alteration type is inferred to be approximately similar to that in Region 4. Region 5 contains a 1 m wide vein system, and also has a small interval logged as monzodiorite. This monzodiorite may represent alteration rather than a primary lithology, but the physical properties are broadly similar to that of the intermediate unit and the exact nature of this interval is difficult to determine.

Region 6

Region 6 has the weakest signature of alteration, with a consistent magnetic susceptibility and density. The seismic velocity is slightly increased to that of Regions 4 and 5, although this may be due to depression of the velocity within these regions by alteration to white micas. The natural gamma radiation of this unit also decreases, suggesting less white mica. There is an increase in white mica abundance in the HyLogger results at approximately 795 m. This increase does not correlate with any changes in physical properties.

3.2.2.5 Summary

- The mafic unit is most likely the result of pyrite or biotite-muscovite-pyrite alteration of the intermediate unit, and thus represents the signature of alteration proximal to gold mineralisation within hosts of generally silicified Paringa Basalt, or a lower volcaniclastic member of the Black Flag Group.
- Comparison of samples inferred geologically to correlate to pyrite and pyrrhotite alteration show alteration trends predicted by the physical property model as described in Section 3.1.1.
- Samples inferred to be highly altered to muscovite by the HyLogger study indicates that highly altered samples to muscovite may be detected by physical

property means. Other zones of white mica alteration are less apparent in physical property data, although comparison of downhole log physical property character shows broad correlation with physical properties and the expected properties of muscovite.

3.2.3 Basalt

The samples of basalt examined for this study are from the CD10662 drillhole. Within this drillhole, the basalts are termed the Devon Consols Basalt.

Scatter plots of seismic velocity versus density and magnetic susceptibility versus density for the basalts for this study are shown in Figures 26 and 27. Shown on these plots is the interpreted range of physical properties expected for the samples of basalts which we regard as unaltered.

Highlighted in Figure 26 is a field we consider to be representative of the unaltered samples. This field includes some samples of significantly lower density than the main cluster of basalt samples. These samples are interpreted to be the product of fracturing, as fracturing affects the seismic velocity significantly more than the density measurements for downhole physical measurements (Dolan et al., 1998). This is the same interpretation for similar samples of the intermediate (unclassified) unit.

After inclusion of the fractured samples within the unaltered host field, there remain several points, from two different drillhole intervals, which lie outside the unaltered host field for both the seismic velocity-density and magnetic susceptibility-density plots. These points appear to show a trend to higher densities, lower seismic velocities and higher magnetic susceptibilities.

One alteration mineral that would account for the physical property changes is pyrrhotite. Basalt-pyrrhotite alteration cones for seismic velocity-density and magnetic susceptibility-density are shown in Figures 28 and 29. Both Figures 28 and 29 highlight some drillhole intervals – some of these intervals are representative of fractured zones, and two intersections contain the samples that lie outside the unaltered host field.

All the anomalous samples plot within the pyrrhotite alteration cone for the seismic velocity-density diagram but not all samples plot within the magnetic pyrrhotite alteration cone for the magnetic susceptibility-density diagram. The three samples that lie outside of the alteration cone may do so due to the influence of a combination of magnetic and non-magnetic pyrrhotite, or possibly a combination of pyrrhotite and a dense and non-magnetic alteration mineral, for example, pyrite.

There is no evidence to support one alteration scenario over the other. The only samples to plot outside the magnetic pyrrhotite alteration cone are the most altered samples. These may be altered significantly enough to include some other alteration minerals, or to produce more non-magnetic pyrrhotite.

Note that the more altered samples appear to plot with higher velocities than expected in the alteration cone as depicted on seismic velocity-density plot (Figure 28). This may suggest the most altered samples have an influence of an alteration mineral that has higher velocity than pyrrhotite, for example, pyrite. This is far from conclusive evidence to support the hypothesis that the most altered samples are a combination of pyrrhotite and pyrite.

For the purposes of quantifying the proportion of alteration we assume that the anomalous samples are entirely altered to pyrrhotite. To simplify the calculation, we will only consider proportion of alteration calculated from the seismic velocity and density. We will also attempt to provide limits on the possible values of alteration, with an illustration quantifying the possible ranges of alteration proportion for the most altered sample.

One of the keys to utilising our proportion of alteration calculation (Equation 2) is an estimate of the original host property. Remember, we are also dealing with alteration that affects the physical properties linearly, so we expect the direction a sample will head from its host is along a straight line (the alteration trajectory, as per Section 3.1.1) to the physical properties of the alteration end-member.

If we consider the most altered sample apparent in the basalts studied, we can construct the alteration trajectory such that we can obtain an estimate of the host rock that this sample is altered from. This technique is illustrated in Figure 30. Our methods imply that the host this sample is altered from lies somewhere along the alteration trajectory. By definition, we know that the host for this sample must lie within the unaltered field. We can use this information to provide boundaries on the possible range of properties of the unaltered host for this sample. This range gives us a limit on the minimum and maximum amount of alteration to pyrrhotite that the sample we are investigating represents.

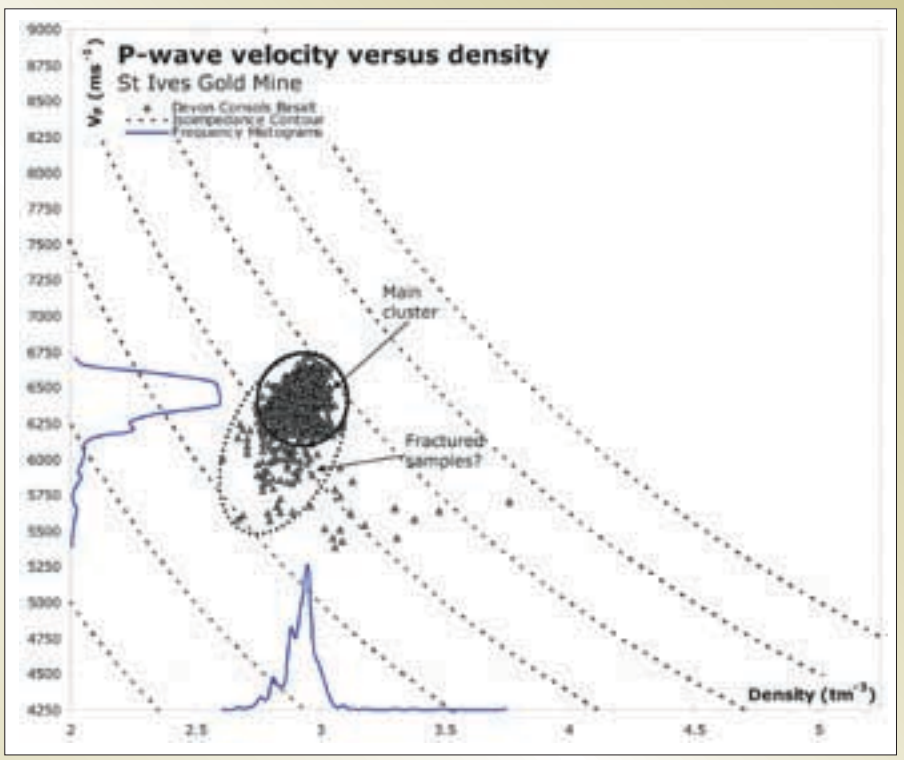

Figure 26: Seismic velocity-density plot for the Devon Consols Basalt, drillhole CD10662. The main cluster represents samples which are inferred to be representative of the host rock; the fractured sample field includes samples inferred to result from fracturing of the host rock. Fracturing is known to decrease the seismic velocity of samples in downhole logging (Dolan et al., 1998).

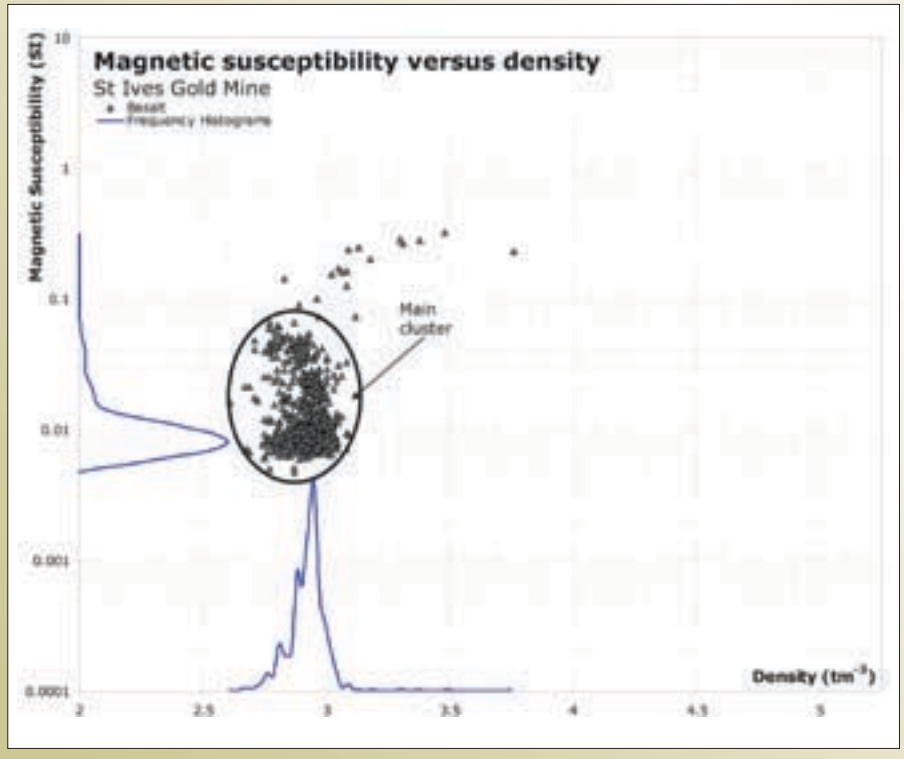

Figure 27: Magnetic susceptibility-density plot for the Devon Consols Basalt, drillhole CD10662. The solid oval depicts the expected range of physical properties for this unit.

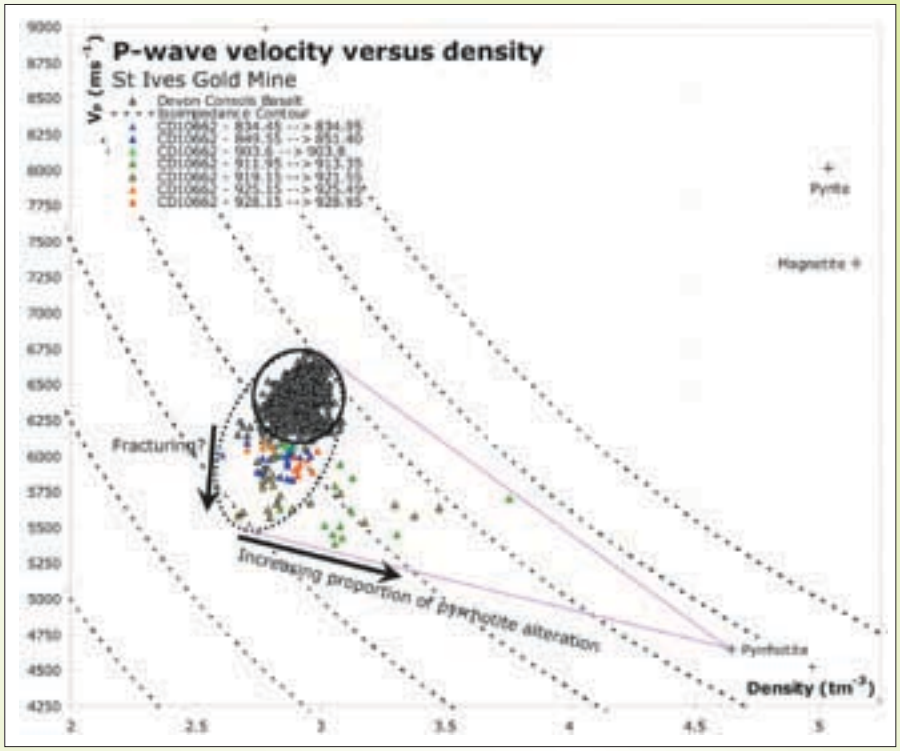

Figure 28: Seismic velocity-density plot showing key intersections and a basalt-pyrrhotite alteration cone. The two intersections inferred to contain pyrrhotite alteration are both in the CD10662 drillhole. The first intersection is 911.95 to 9.13.35m downhole length, and the second intersection is 919.15 to 921.55m downhole length. The most altered sample (contained within the 911.95 to 913.35m intersection) is approximately 50% along the alteration cone to pyrrhotite, indicating it is approximately 50% altered to pyrrhotite.

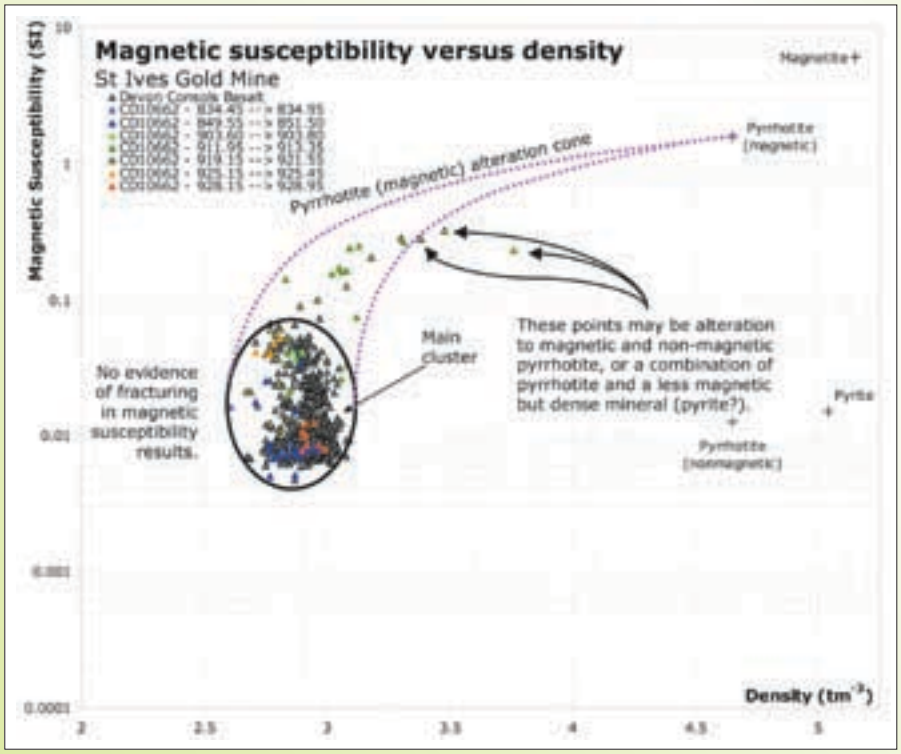

Figure 29: Seismic velocity-density plot showing intervals inferred to be altered to pyrrhotite and a basalt-pyrrhotite alteration cone. The first intersection is 911.95 to 913.35m downhole length, and the second intersection is 919.15 to 921.55m downhole length. The most altered sample is approximately 50% between the density of the main cluster of basalt samples and pyrrhotite, indicating it is likely to be 50% altered to pyrrhotite.

Figure 30: Seismic velocity-density plot showing key intersections and a basalt-pyrrhotite alteration cone with the alteration trajectory for the most altered sample drawn as the yellow-black dashed line. Lying somewhere along this alteration trajectory and within the unaltered sample field is the original host that the sample under inspection is altered from. Because we cannot know which sample represents the original host, we can use the probability of different physical property combinations to understand the relative likelihood of different hosts. From this scatter plot we can immediately recognise the properties that will give rise to the minimum and maximum amounts of alteration that would explain the physical properties of the most altered sample. These properties are those at the intersection of the alteration trajectory and the unaltered host field. The point closest to the alteration end-member (blue octagon) gives rise to the minimum alteration proportion, and the point farthest from the alteration end-member (red octagon) gives rise to the maximum alteration proportion.

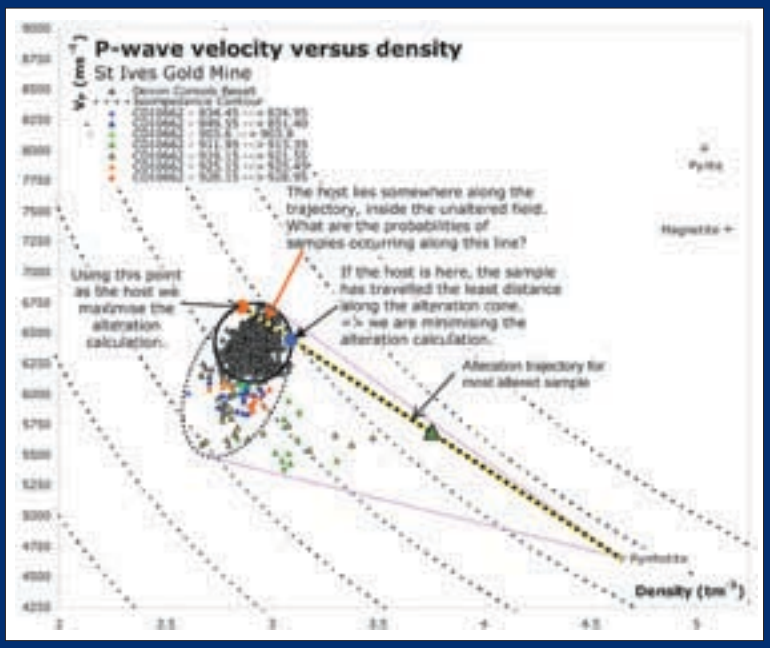

We do not know the likely distribution of possible hosts along this alteration trajectory and thus the relative probabilities of various hosts. The choice of host determines the quantity of alteration and thus by understanding the likelihood of various hosts we also gain an understanding of the most likely amount of alteration that the sample under investigation contains.

We can examine this distribution by constructing a 2D histogram. Like a 1D histogram we begin by binning the data – but instead of binning the data according to ranges of a single property, we bin the data according to ranges of two properties. A simple 2D histogram would be to look at the distribution of points that fit into the following categories: low velocity and low density; high velocity and low density; low velocity and high density; and high velocity and high density. The 2D histogram (density and velocity) for all the samples of basalt studied is shown in Figure 31.

This 2D histogram can be sliced along any arbitrary direction. A slice for the alteration trajectory shown in Figures 30 and 31 is shown in Figure 32. Figure 32 illustrates the probabilities of obtaining particular physical property combinations along the alteration trajectory. Assuming that the most likely host for the sample we are investigating is also the most commonly occurring sample, taking the modal point gives us the most likely properties of the host.

We can also convert these positions into values for percentage alteration. The proportion of alteration calculation depends upon the value for a host so for a single altered sample the proportion of alteration is influenced by the choice of host. Transforming of the points along the alteration trajectory into possible alteration percentages for the sample at 912.95 m is shown in Figure 33. From this analysis we can conclude that the most likely host represents a proportion of alteration of approximately 45%.

Unless the host is the one which yields the minimum alteration proportion, some of the samples with minor amounts of alteration will plot within the unaltered host field. Thus the unaltered host field does not represent only unaltered samples but is a mixture of some minor altered products and unaltered samples. Despite this, without further evidence we can only be confident about a sample being altered if a sample plots outside the unaltered field.

This inclusion of some altered samples will tend to bias the estimates of most likely proportion of alteration, assuming that many minor-altered samples occur within the unaltered field. This bias can affect the most likely alteration amount and depends on the distribution of

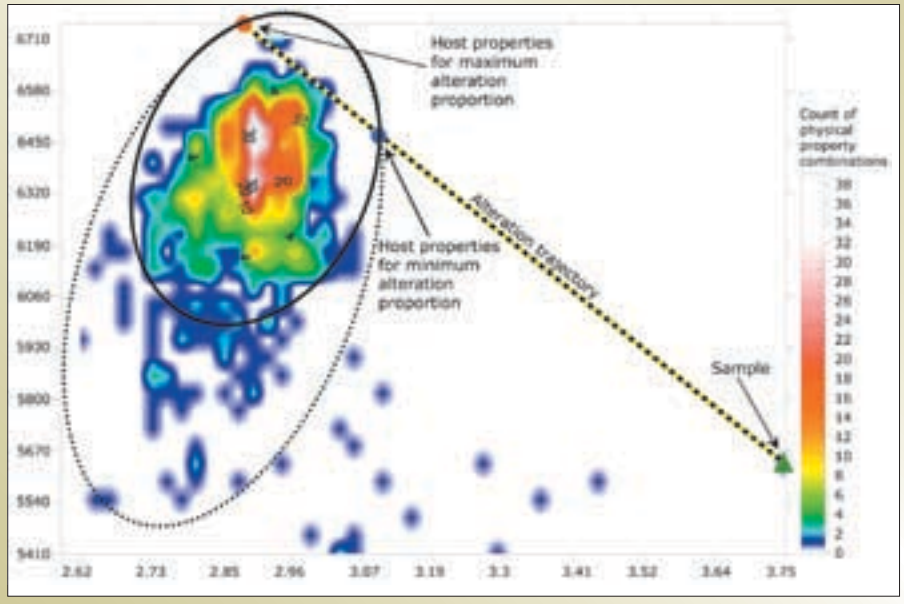

Figure 31: 2D histogram for seismic velocity and density of the samples of the Devon Consols Basalt studied. Note that the aspect ratio is slightly different to the plot shown in Figure 26, and the histogram does not have the same data extents as Figure 26. The unaltered host fields and alteration trajectory are at the same positions as Figure 30. We can use this 2D histogram to understand the probability of different physical property combinations occurring between the blue and the red octagons (hosts that yield the minimum and maximum alteration proportions). These differing combinations of physical properties result in differing alteration proportions, and thus we can understand the likelihood of various amounts of alteration.

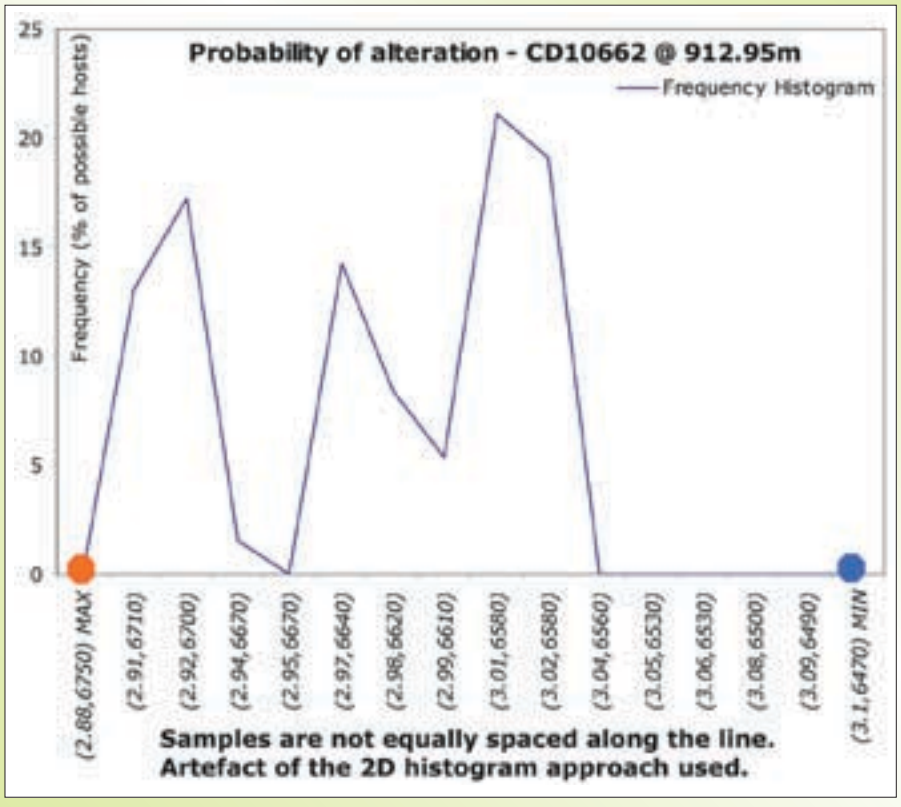

Figure 32: Frequency histogram for points along the alteration trajectory. Frequency is a count for a particular point normalised by the number of samples occurring along the alteration trajectory. Points relating to the minimum and maximum amount of alteration are shown as the blue and red octagons (as per Figures 30 and 31).

N.B. The points are not equally spaced along the alteration trajectory so the shape of the histogram is distorted.

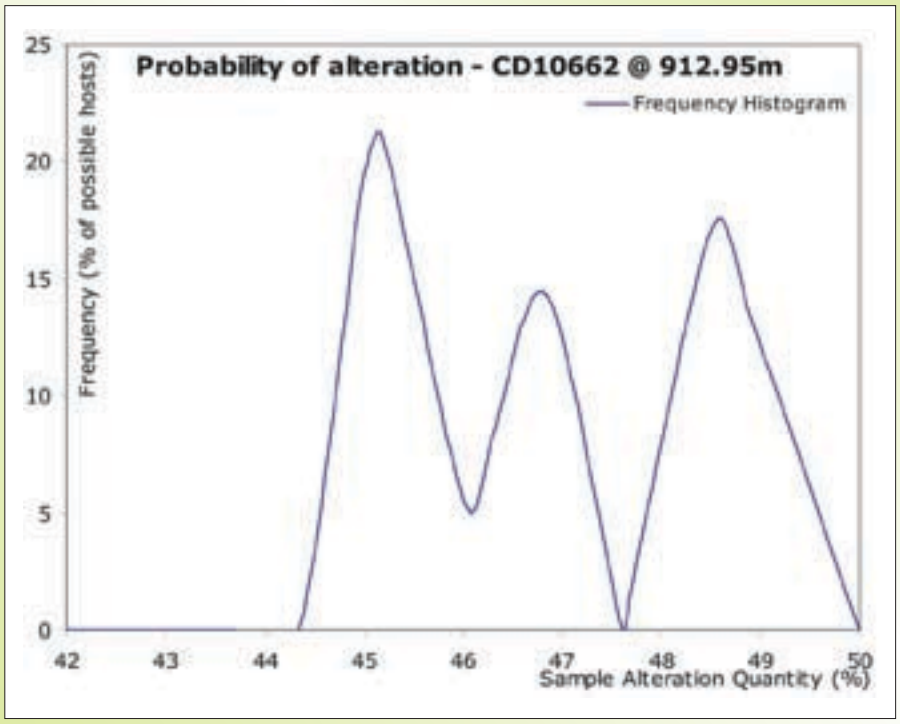

Figure 33: Frequency histogram (probability of hosts) plotted against the sample alteration quantity as calculated from the positions of the points from Figure 32. This figure shows us the probabilities of certain amounts of alteration. The most likely (highest peak, or the modal amount) alteration proportion for this sample is approximately 45%. Note that this graph is effectively reversed on the x-axis with respect to Figure 32.

samples showing very minor alteration. These samples are difficult to detect and remove and so we assume, for the purposes of a relatively simple calculation, that we are dealing with more unaltered than altered samples along any alteration trajectory within the unaltered field.

As we only identify samples as being altered if they plot outside the unaltered field, there is a threshold of alteration that a sample must cross in order to be identified as altered. This depends on the net physical property changes to the alteration end-member and the width of the unaltered field with respect to the alteration trajectory and thus is difficult to quantify. This threshold may work to our advantage, as we will only detect more significant zones of alteration.

We performed the analysis for proportion of alteration for every sample identified as altered in Figures 28 and 29 and determined the minimum, maximum and most likely proportion of pyrrhotite alteration that explains the physical properties observed. These results are most appropriately examined spatially. A display of these results with respect to depth is shown in Figure 34.

One result from this analysis of proportion of alteration is that the majority (with the exception of the most altered sample) of the apparent hosts for altered samples appear to be from the more fractured samples. This is a geologically plausible scenario – we would expect fracturing to occur, and then some fractured sites to be more favourable to access alteration fluids than others.

The physical property method of identifying alteration identified two intervals of pyrrhotite alteration. The first is from approximately 911.85 m to 913.15 m and shows a general increase from low levels of alteration to a maximum close to the base of the alteration zone. The second is from 919.75 m to 920.85 m, although there is a 0.3 m gap between a narrow (20 cm) and more zone of alteration at the top and a higher proportion and thicker (0.6 m) zone.

Both of the alteration intervals show a trend from low to high proportion of alteration and a relatively sharp boundary where the samples tend back to negligible alteration amounts. This gradient in alteration amount may have an influence on the possibility of certain geophysical signatures, for example, the signature of pyrrhotite alteration within seismic reflection surveys.

3.2.3.1 Summary

- From the physical properties of basalts studied, we infer that anomalous samples of basalt are the result of pyrrhotite alteration.
- This pyrrhotite alteration appears to be concentrated within the space of ~10 m within the drillhole, with two major bands of pyrrhotite alteration.

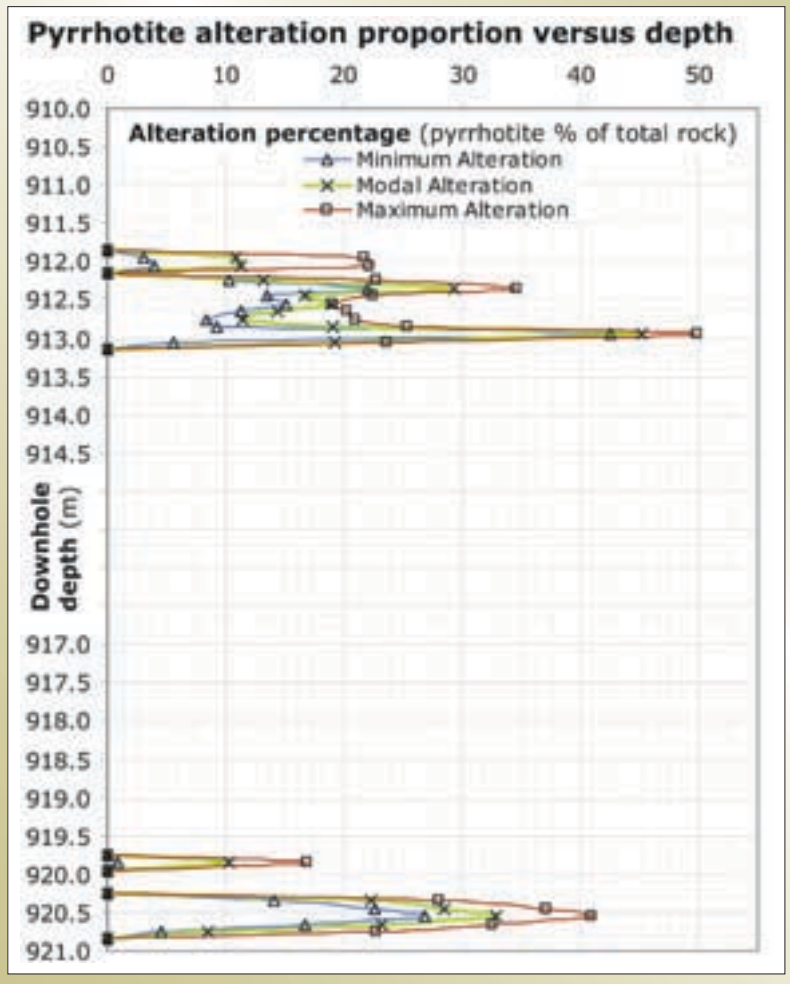

Figure 34: Proportion of pyrrhotite alteration (as a volume percentage of total rock) vs. downhole depth for basalts studied from the CD10662 drillhole. The minimum, maximum and modal (most likely) alteration proportions are shown. Note the variation where the modal property lies with respect to the minimum and maximum. For some intersections (for example, ~912.0 m) the modal proportion is approximately halfway between the minimum and maximum. It is sometimes skewed to be closer to the minimum (such as for 912.75 m), and sometimes skewed to be closer to the maximum (such as for 912.55 m).

- The pyrrhotite alteration bands appear to show a trend from low amounts of alteration at the top and reach the maximum amount of alteration close to or at the base of the alteration band.
- We have an understanding of the possible ranges of alteration amounts that may represent the same physical properties. These results must be utilised with modelling geophysical responses of alteration to truly capture the nature of the alteration.
- Modelling the affect of pyrrhotite alteration on magnetic susceptibility may be problematic due to the difficulty in understanding the proportion of magnetic and non-magnetic pyrrhotite in the alteration phase. More altered samples may include more non-magnetic pyrrhotite.

3.2.4 Dolerite

Physical properties of samples of dolerite from three drillholes, CD10662, CD10663 and CD10943 are analysed here. The dolerites were all logged at St Ives as the Condenser Dolerite (see regional stratigraphy, Figure 11).

The positions of the drillholes are shown in Figure 12. Holes CD10662 and CD10663 were drilled perpendicular to major structures in the region. CD10943 was drilled orthogonal to CD10662 and CD10663. We examined these samples using bivariate plots of seismic velocity and density (Figure 35) and magnetic susceptibility and density (Figure 36).

The magnetic susceptibility data from the three drillholes shows a very similar distribution, but the seismic velocity and density observed in CD10943 are both significantly lower than drillhole CD10662 and CD10663. The most likely cause of this is calibration differences between downhole logging surveys. The seismic velocity difference may result from anisotropy of materials, but this interpretation is unlikely for density. These differences may result in incorrect interpretation of alteration affecting samples, so we should discount one population. The density and seismic velocity observed in drillholes CD10662 and CD10663 are similar to that in previous physical property studies at St Ives, such

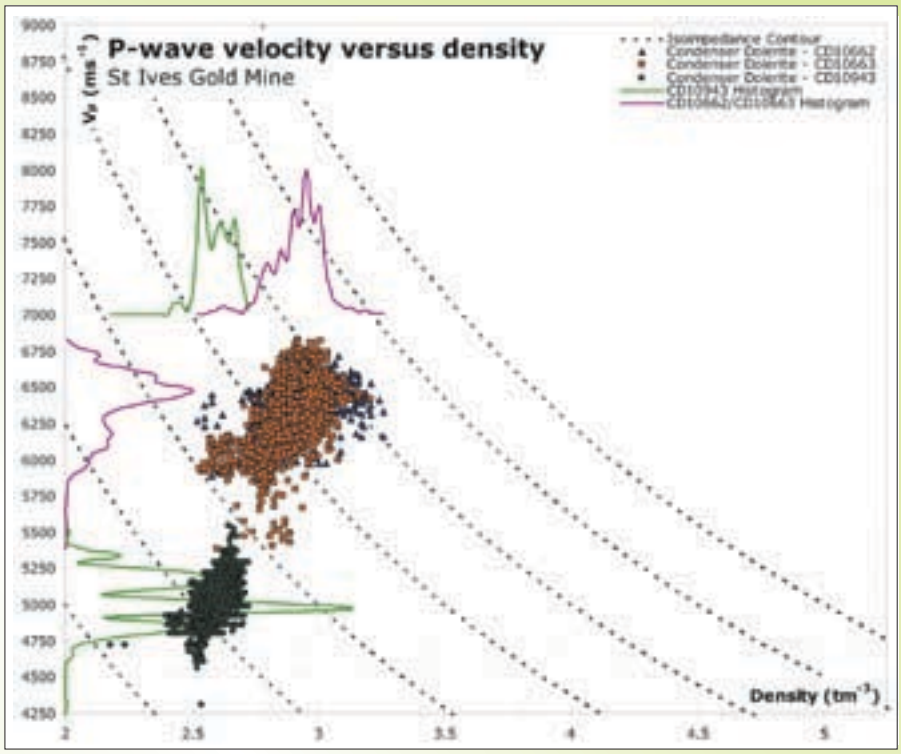

Figure 35: Seismic velocity-density plot for the Condenser Dolerite, drillholes CD10662, CD10663 and CD10943. Note the positions of the samples from the three drillholes. The offset between samples from CD10943 and the other drillholes is probably due to a calibration issue between the two surveys.

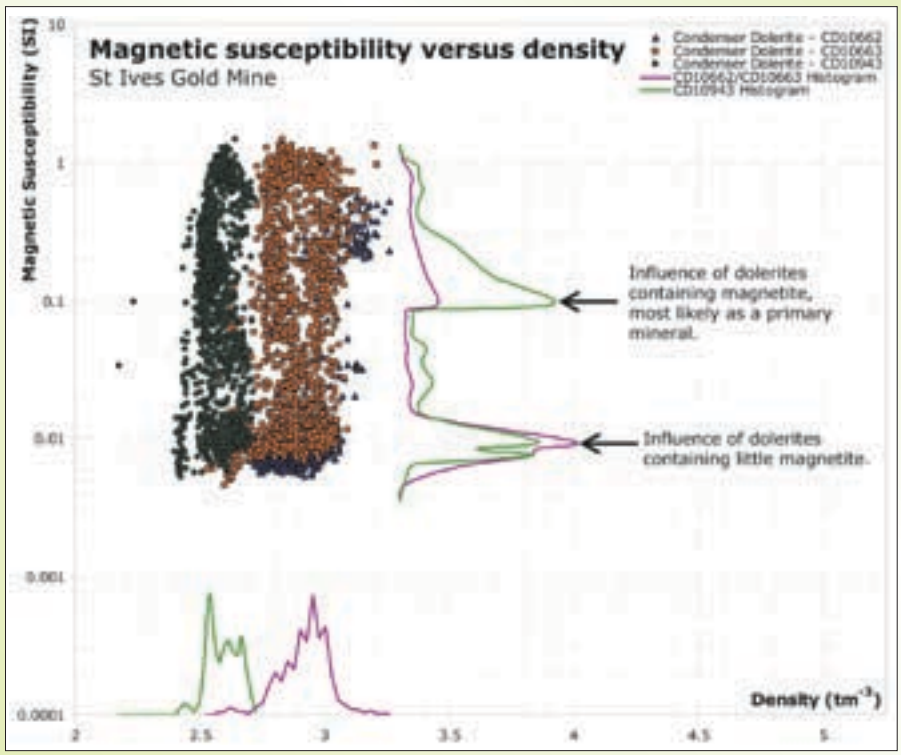

Figure 36: Magnetic susceptibility-density plot for the Condenser Dolerite, drillholes CD10662, CD10663 and CD10943. There are two populations within the magnetic susceptibility – those which are non-magnetic and those which appear to be magnetic. The magnetic dolerites may either be due to primary magnetite, or the result of large-scale alteration.

as Emerson (1997). For this reason, the results of downhole logging drillhole CD10943 are not used in this study.

Magnetite can occur as a primary mineral within dolerites at St Ives (Connors et al., 2003). Our physical property model infers that dolerites containing magnetite (either primary or alteration related) would show high magnetic susceptibilities. The majority of samples of Condenser Dolerite studied do not show high magnetic susceptibilities; 70% of the samples from CD10662 and CD10663 have a magnetic susceptibility less than 0.02 SI (see magnetic susceptibility frequency histogram, Figure 36). These samples most likely do not contain any magnetite. Some dolerites do show a trend to increasing magnetic susceptibilities with only minor density increases. Although it is unlikely we can distinguish between alteration and primary magnetite from physical properties, we infer that samples showing an increasing magnetic susceptibility with only a minor increase in density reflect primary magnetite within the dolerite, yielding the second magnetic susceptibility mode at 0.15 SI.

As we expected it to be difficult to distinguish between alteration and primary magnetite within the dolerites, we can examine the physical properties of non-magnetic dolerites to understand the likely distribution of properties for unaltered dolerites. After accounting for dolerite samples in drillhole CD10943, we can utilise magnetic susceptibility-density information to examine alteration trends (Figure 37).

Shown in Figure 37 are fields showing the expected properties for samples of non-magnetic dolerites (black oval) and samples containing low proportions of magnetite (orange ovoid). We defined the expected range of properties for the non-magnetic dolerites by examining the distribution of physical properties on the plot (see Figure 36 for frequency histograms), and only include samples showing low magnetic susceptibilities. Samples showing very low density (< 2.65 tm^{-3}) were not included in the expected properties of the non-magnetic samples as we interpret these to be due to alteration to a low-density material.

Also shown in Figure 37 is an alteration cone to a highly magnetic material (grey dotted lines). Many samples show high magnetic susceptibilities, such as the samples depicted by the yellow-black triangles. The magnetic susceptibilities for these samples exceed the magnetic susceptibilities we

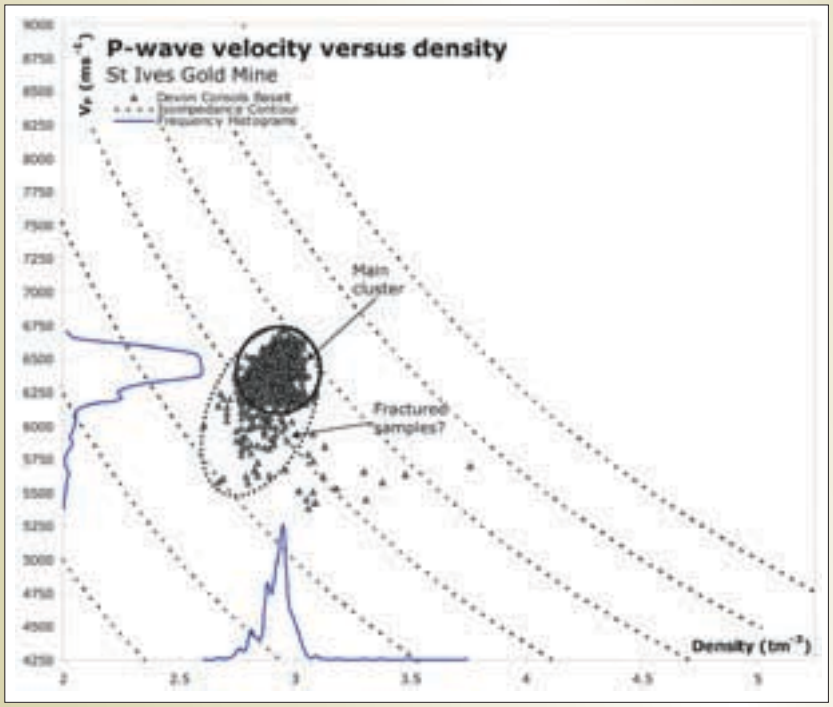

Figure 37: Magnetic susceptibility-density plot for Condenser Dolerites in drillholes CD10662 and CD10663. Highlighted on the plot are five populations of dolerites:

- *Grey-black triangles, all Condenser Dolerite samples. Samples are also further categorised, as described below.*
- *Black triangles, samples with magnetic susceptibilities below 0.02 SI. These are non-magnetic dolerites and therefore expected to contain minimal magnetite.*
- *Yellow- black triangles, samples with magnetic susceptibilities above 1 SI. These are highly magnetic dolerites, most likely dolerites containing primary magnetite and altered to contain more magnetite*
- *Red-black triangles, samples with densities above 3.12 tm^{-3} and magnetic susceptibilities below 0.4 SI. These samples are most likely dolerites altered to pyrrhotite, although some could be altered to magnetite.*
- *Blue-black triangles, samples with densities above 3.12 tm^{-3} and magnetic susceptibilities exceeding 0.4 SI. These samples are most likely dolerites altered to magnetite.*

would expect for alteration of dolerite to magnetite.
As we expect that magnetite is the most magnetic material we would encounter at St Ives, to explain the magnetic susceptibilities of these samples we can infer either of the following scenarios:

- Variability in the magnetic susceptibility of magnetite.
- Non-linearity of the rock physics model.

On average, magnetite shows the magnetic susceptibility that we have utilised on our plots (Carmichael, 1989b); other workers, however, note that magnetite may be up to 20 times more magnetic than monoclinic pyrrhotite (Milsom, 2003b). As we cite pyrrhotite as having a magnetic susceptibility of ~1.5 SI, we may expect magnetite to show a magnetic susceptibility of up to 30 SI. This magnetic susceptibility is approximately the position of the focus of the apparent alteration cone show in grey in Figure 37.

The samples may also show anomalous magnetic susceptibilities with respect to their densities, as our rock physics model assumes linearity with respect to magnetic susceptibility and densities. As discussed in Section 3.1.2, concentrations of magnetite above approximately 20% may show magnetic susceptibility increases above that predicted by linear methods. The non-linearity may also affect the physical properties of an alteration assemblage. A 50:50 combination of quartz and magnetite will have the density of 50% of each mineral, but have a magnetic susceptibility much closer to magnetite than quartz.

To confirm our inferences of possible alteration types, we can examine the populations from Figure 37 in terms of their seismic velocity and density (Figure 38).

The samples of non-magnetic dolerite show a similar distribution to the dolerites as a whole. We cannot distinguish between dolerites that potentially contain primary magnetite or do not contain magnetite on the seismic velocity-density relationships alone.

Figure 38 also shows that the most magnetic samples (the yellow-black triangles) do not plot outside the field we have defined as the expected properties of the non-magnetic dolerite. According to our rock physics model, these samples must contain significant proportions of magnetite to explain their magnetic susceptibilities.

The samples may all have hosts with properties close to the low-density edge of the unaltered field and altered to low amounts of magnetite, or they may be the product of alteration to an assemblage containing a low density material. As magnetite often occurs within or proximal to quartz veins within dolerites at St Ives (Roache, 2005), we can expect that the alteration to magnetite may contain some quartz. Figure 38 also shows a combination line for quartz and magnetite, and a possible alteration cone for this scenario is shown. Note that any alteration cone to quartz and magnetite will plot within the magnetite alteration cone, and thus we cannot distinguish between this alteration type and purely magnetite alteration.

If the alteration of the most magnetic samples is to quartz and magnetite, the alteration assemblage must remain highly magnetic to explain the magnetic susceptibility of samples we infer to have undergone this type of alteration. This suggests our assumption of linearity of physical properties with respect to proportions of minerals has been violated.

Some dolerite samples show anomalously low densities (less than 2.65 tm^{-3}). These samples are highlighted in terms of their seismic velocity and density relationships (Figure 39) and their magnetic susceptibility and density relationships (Figure 40).

The likely low-density alteration materials at St Ives are feldspars or quartz (Roache, 2005). The net physical property changes between any of the potential alteration minerals and the unaltered samples are relatively small. This means it is more difficult to identify and quantify the particular alteration type with respect to end-member minerals.

Some of the samples plot very close to the position of quartz, and so these samples may represent areas of considerable quartz addition or major siliceous alteration. Other samples, however, plot with considerably higher velocity than that of quartz, and others plot with lower density and velocity than that of quartz.

The samples showing higher velocities than quartz and densities below 2.65 tm^{-3} may represent samples altered to some proportion of k-feldspar and quartz. An alternate hypothesis is that the samples are the product of alteration to quartz but with differing orientations of the quartz crystals. As quartz is approximately 15% anisotropic with respect to seismic velocity (that is, the velocity of quartz differs by 7.5% above and below the velocity of quartz indicated in Figure 39).

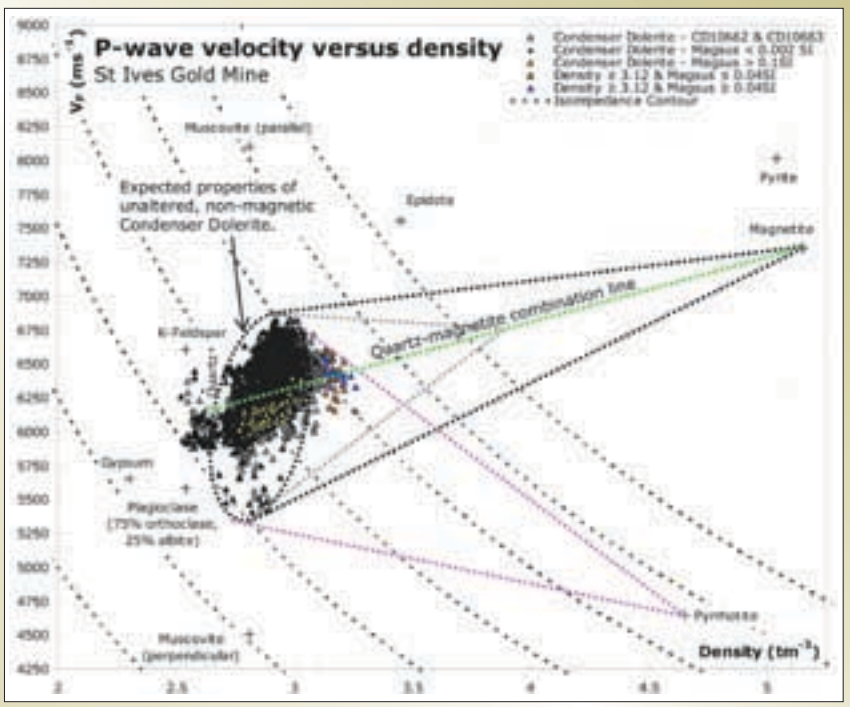

Figure 38: Seismic velocity-density plot for Condenser Dolerite samples, showing a number of sample distributions defined from magnetic susceptibility-density relationships. Key populations and definitions are the same as Figure 37. Note that the non-magnetic dolerites (black triangles) plot in similar positions to dolerites showing magnetic susceptibilities greater than 0.02 SI (grey and other coloured triangles). The unaltered field was defined to encompass the majority of dolerite samples (as per Figure 37), with samples showing densities lower than 2.65 tm^{-3} not included in the field as we interpret these to be the product of alteration of dolerites to lower-density material. We infer samples showing low seismic velocity (below 5850 ms^{-1}) with no corresponding decrease in density to be the result of fracturing of the samples.

Note that samples showing high magnetic susceptibilities (yellow triangles) plot entirely within the field of unaltered samples. Due to their magnetic susceptibility, these samples must be altered to contain magnetite or be dolerites containing significant proportions of primary magnetite. If these samples are the result of alteration, the alteration phase must contain some low-density material such as quartz. As the combination line for a quartz-magnetite (green dashed line) lies wholly within the magnetite alteration cone, an alteration cone to quartz-magnetite would have a broadly similar shape and position to the alteration cone for magnetite. The grey dashed cone depicts one possible scenario for this alteration type, with a 50:50 proportion of the two minerals.

This alteration style also shows magnetic susceptibilities up to approximately 0.10 SI (Figure 40). The maintaining of the magnetic susceptibility, even when the density and seismic velocity suggests alteration to large proportions of alteration minerals which are non-magnetic, indicates that there is at least some magnetic minerals in the alteration phase. For common alteration styles at St Ives, these magnetic minerals are either magnetite or pyrrhotite, and make the determination of the alteration assemblage more difficult.

3.2.4.1 Summary

- Both pyrrhotite and magnetite alteration appears to have affected the dolerites. Some highly magnetic dolerites exceed the magnetic susceptibilities predicted by our rock physics model. They may contain so much magnetite that they violate our assumption of linearity of physical properties with respect to proportion of alteration. Alternatively, magnetite may show a variable magnetic susceptibility which would also account for the magnetic susceptibility-density relationships observed.

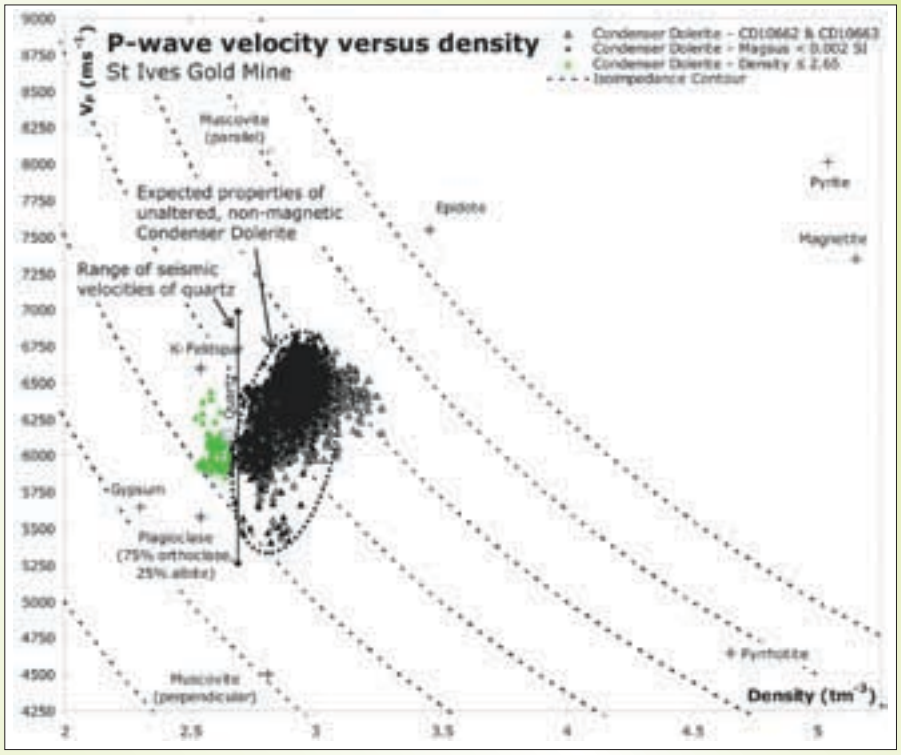

Figure 39: Seismic velocity-density plot for the Condenser Dolerite, drillholes CD10662, CD10663. The black samples represent samples observed to be non-magnetic (magnetic susceptibility less than 0.02 SI), and the green samples are samples of dolerites showing anomalously low susceptibilities. The most likely alteration minerals for this type of alteration at St Ives (feldspars or quartz) have minimal physical property contrasts to the expected properties of dolerite, and thus it is difficult to quantify or identify the alteration type. As the seismic velocity of quartz is approximately 15% anisotropic, the possible range of quartz velocities (Ji et al., 2002) are shown.

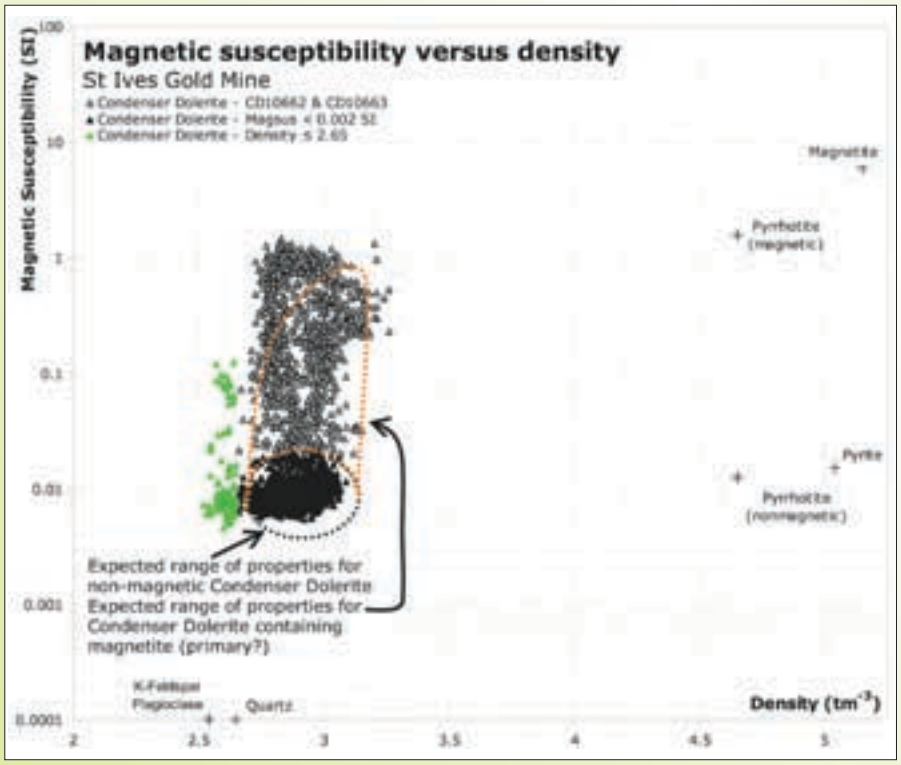

Figure 40: Magnetic susceptibility-density plot for the Condenser Dolerite, drillholes CD10662, CD10663. The black samples represent samples observed to be non-magnetic (magnetic susceptibility < 0.02 SI), and the green samples are samples of dolerites showing anomalously low densities. Note the magnetic susceptibilities for the low-density alteration – the alteration assemblage must contain a small proportion of magnetic material (magnetite or pyrrhotite). The likely alteration minerals within the low-density alteration at St Ives (feldspars or quartz) have low physical property contrasts with the dolerite, and thus we cannot identify the alteration type.

- An alteration type is identified which lowers the density and slightly lowers the seismic velocity. This alteration type has unknown end-member minerals. End member physical properties are difficult to determine due to low physical property contrasts, but are approximately that of quartz ± k-feldspar, with the exception of magnetic susceptibility, which is very similar to that of the host dolerite. Alteration of this type maintains its magnetic susceptibility and so contains a small proportion of magnetite or pyrrhotite.

3.2.5 Volcaniclastic Sedimentary Unit

The samples logged as the volcaniclastic sedimentary unit represent one member of the Black Flag beds (St Ives Gold Mine, geological logging).

This unit is intersected in two drillholes studied, drillholes CD10662 and CD10943. Figure 41 shows the seismic velocity-density and magnetic susceptibility-density relationships were studied for the same group of samples is depicted in Figure 42.

The samples from different drillholes show different physical properties, with the samples from drillhole CD10943 showing consistently lower densities and velocities than the samples from drillhole CD10662. We observe this relationship for the samples of dolerite from the same drillholes (Section 3.2.4). This relationship may be the result of calibration issues between downhole geophysical surveys. As the results appear to be unreliable for drillhole CD10943 (as per Section 3.2.4), we will only study samples of the volcaniclastic sedimentary unit from drillhole CD10662.

The physical properties of these samples imply that we can define two types of alteration. We define these alteration types by their seismic velocity-density (Figures 43) and magnetic susceptibility-density (Figure 44) relationships.

The first type of alteration is a trend to rapidly increasing magnetic susceptibility with respect to density (Figure 44), which we would infer to be alteration to magnetite. This is consistent with observations of alteration to magnetite in other lithologies in this region (Sections 3.2.2 through 3.2.4).

The second type of alteration appears to be an increase in density with a minor increase in magnetic susceptibility (Figure 44). This type of physical property response is typical of alteration to pyrrhotite, such as that we observed for the Devon Consols Basalt (Section 3.2.3). This physical property response is observed for other alteration systems, such as alteration to pyrrhotite in the 9.1 km deep KTB borehole (Rauen et al., 2000). The alteration of the second type, however, cannot be explained purely by alteration to pyrrhotite, as many of the samples of this alteration type do not plot within the pyrrhotite alteration cone on the seismic velocity-density plot (Figure 43).

Typically, samples we have assigned to the second type of alteration show an increase in density, a moderate increase in magnetic susceptibility with respect to density, and a slight increase in seismic velocity with respect to density.

Possible alteration assemblages that would result in the physical properties observed for the second type of alteration are:

- Muscovite (parallel) – pyrrhotite
- Epidote – pyrrhotite
- Pyrite – pyrrhotite
- Quartz – magnetite

Of these possibilities, we feel that muscovite (parallel) and pyrrhotite is the least likely alteration assemblage. At St Ives most muscovite is oriented with its cleavage plane parallel to structures (A. Roache, *pers. comm.*); drillhole CD10662 was drilled to be perpendicular to these structures. We have also observed physical property evidence for muscovite's cleavage plane oriented perpendicular to the CD10662 drillhole within the intermediate (unclassified) unit (Section 3.2.2).

For each alteration assemblage, alteration cones were inferred on the seismic velocity-density plot (Figure 45). We constructed these alteration cones by creating an alteration cone that had its focus on the combination line of the minerals of the alteration assemblage, and was the closest fit to the observed physical properties of samples of this alteration type. The density and seismic velocities of the focus of the alteration cones allowed calculation of the magnetic susceptibility of the alteration assemblage. We used this magnetic susceptibility to create alteration cones for magnetic susceptibility-density (Figure 46).

All of the alteration cones created for the seismic velocity-density for the second type of alteration also lie within the magnetite alteration cone shown in Figure 43. As the alteration cones entirely overlap with each other, we cannot use the seismic velocity and density to resolve the ambiguity regarding the composition of the second type of alteration.

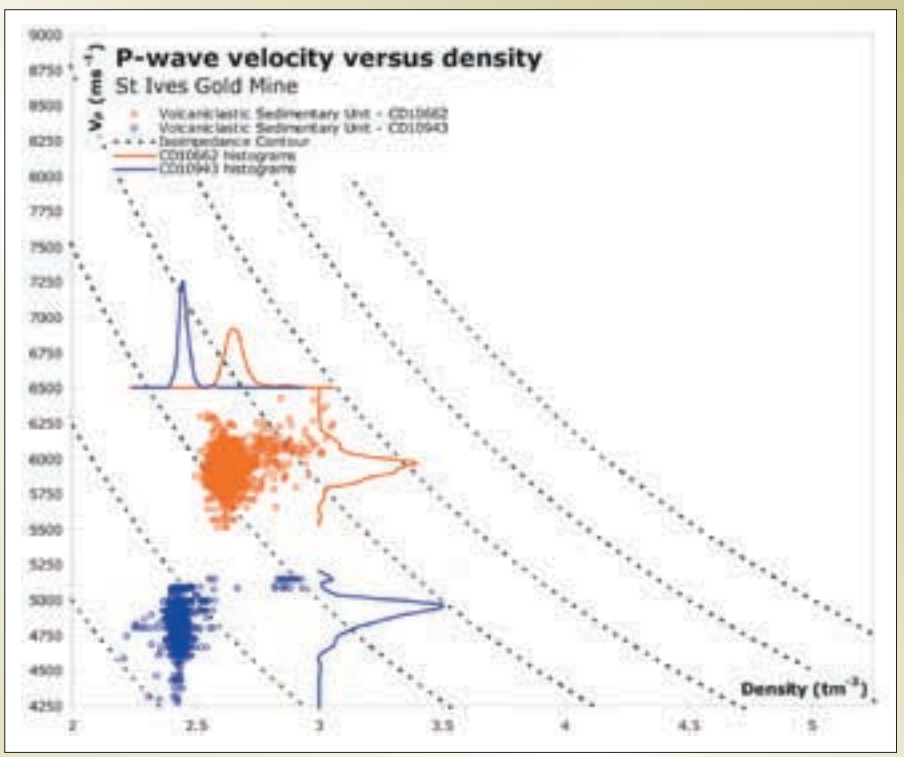

Figure 41: Seismic velocity-density plot for the volcaniclastic sedimentary unit, drillholes CD10662 (red) and CD10943 (blue). Note the different positions of the sample populations which reflect the drillholes the samples were obtained from. The differences in velocity and density between the two populations appear to be similar to that observed for the dolerites (Figure 35) and most likely result from calibration differences between the two drillhole surveys.

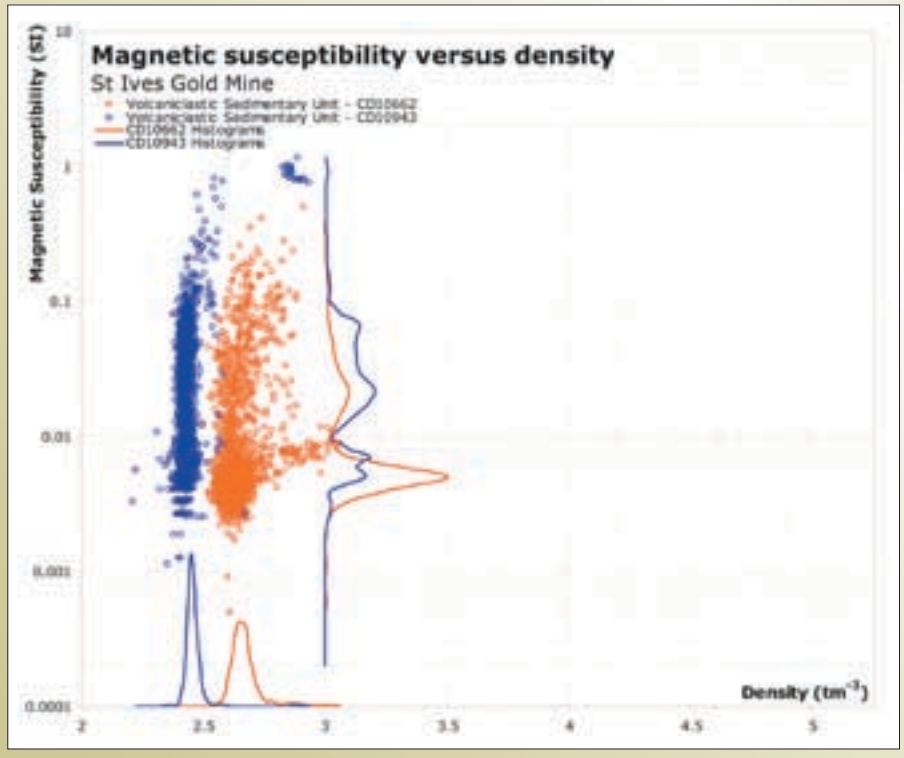

Figure 42: Magnetic susceptibility-density plot for the volcaniclastic sedimentary unit, drillholes CD10662 (red) and CD10943 (blue). Note the different positions of the sample populations which reflect the drillholes the samples were obtained from. The differences in density between the properties appear to be similar to that observed for the dolerites (Figure 36) and most likely result from calibration differences between the two drillhole surveys.

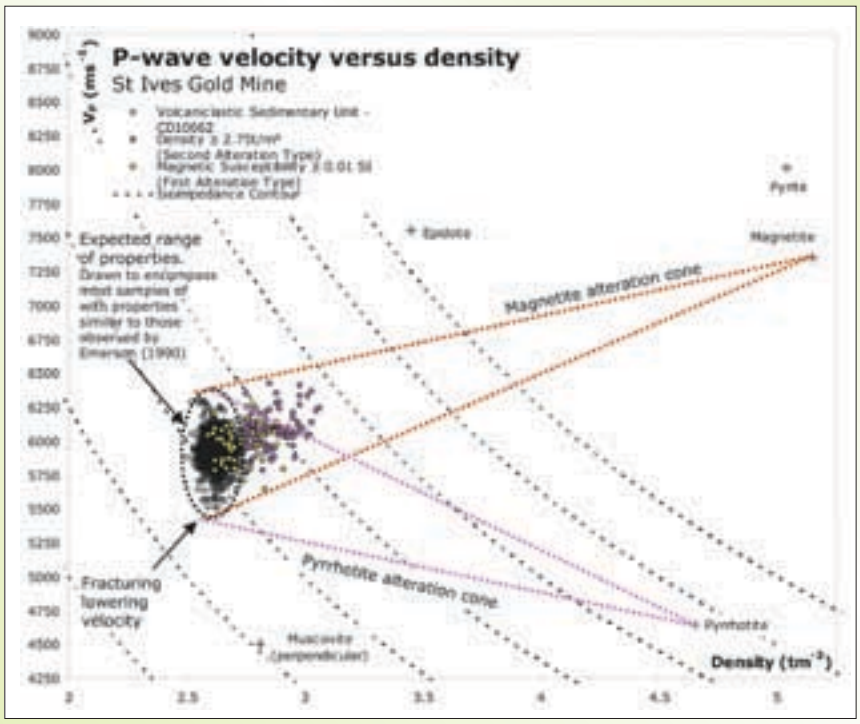

Figure 43: Seismic velocity-density plot for the volcaniclastic sedimentary unit with alteration cones for different alteration types shown. The expected range of properties is interpreted to include the majority of the points that do not show anomalously high densities for this lithology, with expected densities supported by previous studies of physical properties at St Ives (such as Emerson, 1997). Depicted are two alteration types.

We infer the first alteration type (yellow-black symbols) to be alteration to magnetite. All the samples plot within the alteration cone shown here for magnetite, and also plot within the magnetite alteration cone for magnetic susceptibility-density (Figure 44).

The second alteration type (purple-black symbols) also plots within the magnetite alteration cone for this diagram, but shows significantly lower magnetic susceptibility with respect to density than we would expect for alteration to magnetite (Figure 44). The magnetic susceptibility-density relationship is similar to that which we would expect for pyrrhotite alteration. To explain the physical properties of the second alteration type samples, we must either reduce the magnetic susceptibility of an alteration assemblage containing magnetite, or we must increase the seismic velocity of an alteration assemblage containing pyrrhotite. The likely alteration types at St Ives to explain these physical properties are:

- *Muscovite (parallel) and pyrrhotite*
- *Epidote and pyrrhotite*
- *Pyrite and pyrrhotite*
- *Quartz and magnetite*

Of these, muscovite (parallel) and pyrrhotite alteration is the least likely. We expect that, as drillhole CD10662 was drilled perpendicular to the structures within the region, muscovite is most likely to occur with its cleavage plane oriented perpendicular to the drillhole. This orientation of muscovite was observed in the intermediate (unclassified) unit discussed in Section 3.2.2, with the samples occurring within the same drillhole.

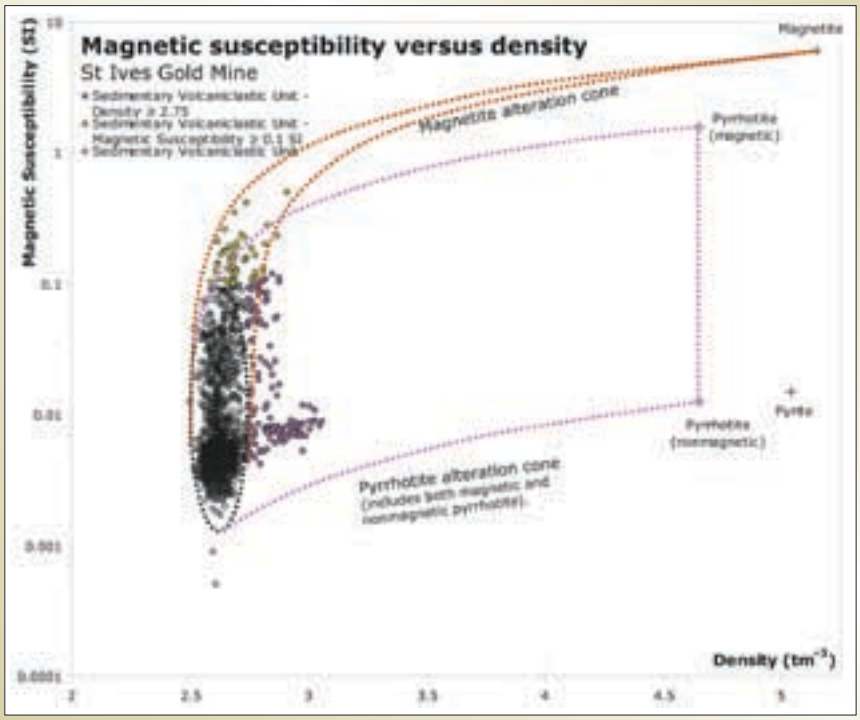

Figure 44: Magnetic susceptibility-density plot for the volcaniclastic sedimentary unit, with alteration cones for different alteration types shown. The expected range of properties is interpreted to include the majority of the points that do not show anomalously high densities for this lithology Expected densities supported by previous studies of physical properties at St Ives (such as Emerson, 1997). Two alteration types are inferred.

We infer the first alteration type (yellow-black symbols) to be alteration to magnetite. All the samples plot within the alteration cone shown here for magnetite, and also plot within the magnetite alteration cone for seismic velocity-density (Figure 43).

The second alteration type (purple-black symbols) plots within the pyrrhotite alteration cone for this diagram, but shows significantly higher seismic velocity with respect to density than we would expect for alteration to magnetite (Figure 43). The seismic velocity-density relationship is similar to that which we would expect for magnetite alteration. To explain the physical properties of samples we have inferred to be the result of the second alteration type, we must either reduce the magnetic susceptibility of an alteration assemblage containing magnetite, or we must increase the seismic velocity of an alteration assemblage containing pyrrhotite. The likely alteration types at St Ives to explain these physical properties are:

- *Muscovite (parallel) and pyrrhotite*
- *Epidote and pyrrhotite*
- *Pyrite and pyrrhotite*
- *Quartz and magnetite*

Of these, muscovite (parallel) and pyrrhotite alteration is the least likely. We expect that, as drillhole CD10662 was drilled perpendicular to the structures within the region, muscovite is most likely to occur with its cleavage plane oriented perpendicular to the drillhole. We have observed muscovite oriented approximately parallel to the drillhole for CD10662, within alteration in the intermediate (unclassified) unit (Section 3.2.2).

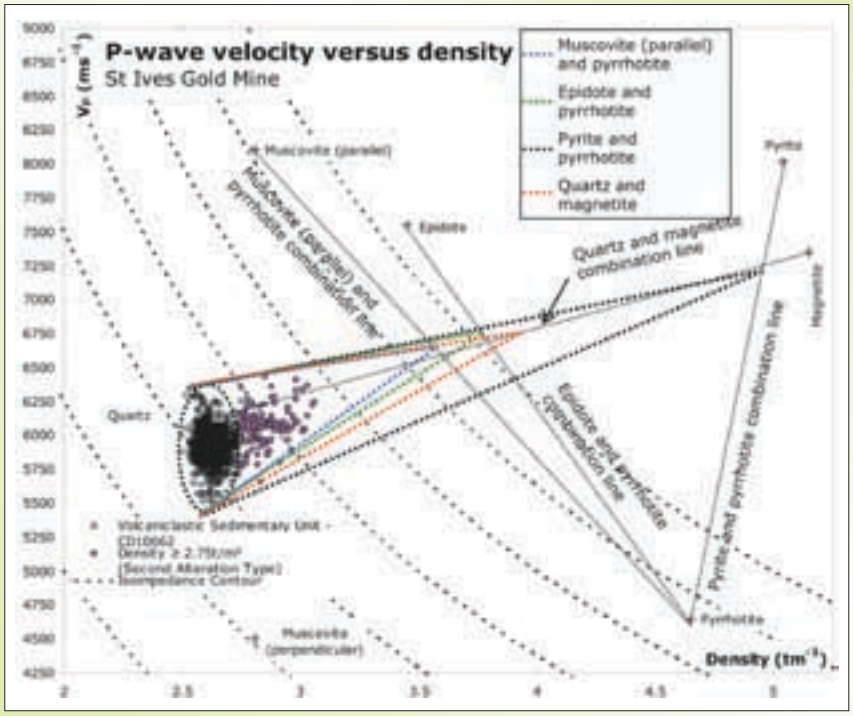

Figure 45: Seismic velocity-density plot for the volcaniclastic sedimentary unit with alteration cones for different alteration types shown. Four alteration cones are defined:

- *Muscovite (parallel) and pyrrhotite*
- *Epidote and pyrrhotite*
- *Pyrite and pyrrhotite*
- *Quartz and magnetite*

The alteration cones are defined to encompass the smallest area while still encompassing all samples inferred to be altered to this alteration type. A further constraint on the position of the alteration cone is that the focus of the alteration cone must lie on the appropriate combination line of end-member alteration minerals.

All of the alteration cones lie within the magnetite alteration cone for this lithology (as shown in Figure 43). There is significant overlap with each alteration cone, and thus it is difficult to distinguish between the alteration types using the seismic velocity and density relationships.

We used the density of the focus of each alteration cone to define the magnetic susceptibility of the alteration assemblage. Alteration cones were defined from this information and plotted on a magnetic susceptibility-density plot to attempt to discriminate between the alteration types (Figure 46).

The magnetic susceptibility-density plot (Figure 46) shows that the second alteration type is very unlikely to be quartz-magnetite. Only 12 samples lie within the alteration cone for quartz-magnetite on this magnetic susceptibility-density plot. As stated above, we also believe that the alteration assemblage is unlikely to be muscovite (parallel) and pyrrhotite. Based on the physical properties, our best estimate of the alteration resulting in the physical properties of the anomalous samples is that it is alteration pyrite and pyrrhotite, or epidote and pyrrhotite.

The HyLogger results for this lithology (Yang, 2006) suggests that the lower half of the volcaniclastic sedimentary unit features high counts of epidote. Yang interprets these as alteration to epidote. For this reason, epidote is likely to be one of the minerals within our alteration assemblage. The samples we have inferred to result from alteration to the second type (Figures 43 to 46) occur within the interval that Yang notes to contain considerable proportions of epidote.

3.2.5.1 Summary

Two main types of alteration appear to have affected the volcaniclastic sedimentary unit:

- The first type of alteration is that to a pure magnetite end-member.
- The second type of alteration is an alteration to higher densities, moderately higher magnetic susceptibilities, and a slight increase in seismic velocity. Based solely on the physical properties, the alteration is either to muscovite (parallel)-pyrrhotite, pyrite-pyrrhotite or epidote-pyrrhotite. Alteration containing muscovite

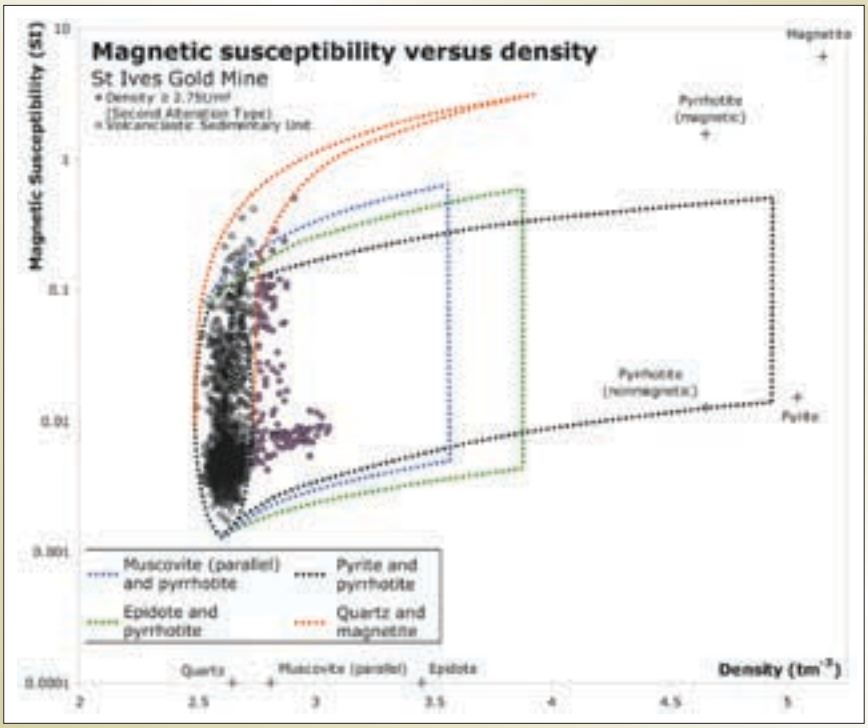

Figure 46: Magnetic susceptibility-density plot for the volcaniclastic sedimentary unit with alteration cones for different alteration types shown. Four alteration cones are defined:

- *Muscovite (parallel) and pyrrhotite*
- *Epidote and pyrrhotite*
- *Pyrite and pyrrhotite*
- *Quartz and magnetite*

Alteration assemblages containing pyrrhotite may involve both magnetic and nonmagnetic pyrrhotite. For this reason, both the magnetic and nonmagnetic pyrrhotite types are included in the alteration assemblage. This yields a broad alteration field rather than a cone with a defined focus.

Combination lines of end-member minerals are not shown for clarity, but the alteration end of each alteration cone or field lies upon the combination line of the alteration minerals in the assemblage.

The magnetic susceptibility of the end-member assemblage of the alteration was calculated using the density of the alteration cone focus in Figure 45. We defined the alteration cones for Figure 45 using a best-fit relationship to the samples observed to exhibit physical properties indicative of the second alteration type, that is, we created alteration cones which encompassed the smallest area but still contained all anomalous samples.

Of the four alteration types depicted, only 12 samples lie within the quartz and magnetite alteration cone. Based on the magnetic susceptibility-density relationships depicted here, we regard alteration to quartz and magnetite as unlikely. We also expect that alteration to muscovite (parallel) and pyrrhotite alteration is the unlikely. Drillhole CD10662 was drilled perpendicular to structures within the Victory-Defiance region. Furthermore, at St Ives, muscovite is most likely to occur with its cleavage plane oriented perpendicular to the drillhole. We have observed muscovite oriented approximately parallel to the drillhole for CD10662, within alteration in the intermediate (unclassified) unit (Section 3.2.2).

(parallel) is expected to be unlikely at St Ives for the drillholes studied, and the HyLogger results support alteration to an assemblage containing epidote.

3.3 Summary

Through the use of a simple rock physics model we are able to make predictions regarding the physical properties of altered samples. This rock physics model uses linear combinations of physical properties with respect to proportions of alteration assemblages and the unaltered host rock. The linear model is applicable for determination of density, is applicable for low (less than 20%) concentrations of magnetite and is a reasonable estimate for seismic velocities of altered materials. The model can be applied to predict the properties of an arbitrary alteration assemblage, although this has not been experimentally verified.

For a physical property contrast between host lithologies and alteration assemblage, this model is able to allow us to confirm our hypothesis regarding alteration type. To detect changes in physical properties, even with a moderate physical property contrast, the model requires a proportion of alteration such that samples will exceed the range of physical properties that we infer to represent unaltered samples.

The model compares favourably with observed sulphide alteration to pyrrhotite and pyrite at St Ives, and complements results from the HyLogger system. Of the lithologies studied, all results from the HyLogger were able to be explained in terms of physical property changes of the samples, as per our rock physics model. The majority of alteration that this technique is able to detect is sulphide and oxide alteration, due to the physical property contrasts of these minerals to the host lithologies present at St Ives.

As the majority of samples studied were from unmineralised drill holes, this technique requires further testing against drill holes containing significant amounts of mineralisation. Study of the technique against known mineralogy of samples, including mineralogy of least-altered or unaltered samples will allow for testing of both our hypothesis regarding the physical properties of alteration, and the physical properties we expect from unaltered host lithologies. Knowledge of the expected range of physical properties is important to allow quantification of theoretical alteration types, such as those predicted by Neumayr et al. (2005) or Ruming (2006).

3.3.1 Implications for geophysical signatures of alteration

The key to predicting the geophysical signatures of alteration systems is the knowledge of how alteration and physical properties are related. An example of this would be the prediction of the physical property response of chemical numerical models. The rock physics model utilised in this study is broadly supported by external datasets such as geological logging of alteration or other physical property techniques such as the HyLogger system. As there is support from external evidence that our rock physics model explains broad alteration trends and their physical property responses, we can apply this model to predict the physical property response of numerical models or alteration assemblages predicted by other researchers.

Broadly, the physical property response to alteration at St Ives is:

- To denser materials
- To more magnetic material
- To increasing acoustic impedances

We mainly observe only increase in density rather than both increase and decrease of density. This is because common alteration minerals at St Ives such as chlorite, muscovite, quartz or albite (Roache, 2005) have similar densities to the majority of host lithologies. For example, muscovite alteration within the Devon Consols Basalt will change in density from around 2.9 tm^{-3} to 2.8 tm^{-3}, assuming we have 100% alteration. This proportion of alteration is unlikely. On the other hand, an increase in density to 3.0 tm^{-3} would only require approximately 10% alteration to magnetite. This proportion of alteration is common proximal to gold mineralisation. A corresponding 10% alteration to muscovite of the basalt would change the density from 2.9 tm^{-3} to 2.89 tm^{-3}. This density change is unlikely to be detected in a gravity survey.

The alteration at St Ives shows rapid increases in magnetic susceptibility without significant increases in density (magnetite alteration), or shows moderate increases in magnetic susceptibility with respect to density (pyrrhotite alteration). The magnetic susceptibility response of pyrrhotite alteration is more variable due to the inclusion of non-magnetic (hexagonal crystal symmetry) pyrrhotite, which may produce a distinct character within a magnetic map, such as the mottled texture hypothesised to be the signature of pyrrhotite alteration halos proximal to the Wallaby and Kanowna Belle deposits (Neumayr et al., 2006).

The majority of alteration detected shows limited to moderate acoustic impedance contrasts. Pyrrhotite alteration, although decreasing the velocity of altered samples, also increases the density, and it is likely to maintain or slightly increase the acoustic impedance of the altered samples. An example of this is the alteration of the Devon Consols Basalt to pyrrhotite (Figure 28). Fracturing of the rock lowers the seismic velocity with no decrease in density (a negative acoustic impedance to the host rock), and alteration to pyrrhotite increases the acoustic impedance, resulting in a moderate positive acoustic impedance contrast for the most altered samples. This acoustic impedance contrast would yield a reflection coefficient to unfractured, unaltered host rock of approximately 0.03 (using Equation 1). This reflection coefficient is half that suggested to be the minimum for a strong seismic reflection (Salisbury et al., 2000).

Fracturing of the rocks would yield a reflection coefficient, with respect to the host rock, of -0.06. This reflection coefficient would yield a strong negative reflection. The contrast between the fractured samples and altered samples would also yield a strong but positive seismic reflection.

For all alteration types, geophysical signatures must consider the geometries of the alteration packages. Study of more mineralised holes and geological mapping may provide more information regarding possible thicknesses and dips of alteration packages. Understanding the geometry and positions of alteration packages, incorporating the mineralogy of these packages, and using the methods within this report to calculate probable physical properties for these packages, will allow us to define the expected geophysical signatures of these alteration packages.

Lake Lefroy (location of St Ives Gold Mine) near sunset, from Kambalda lookout

4. PREDICTIVE GEOPHYSICS: TURNING GEOCHEMICAL MODELS INTO GEOPHYSICAL TARGETS

Executive Summary

Predictive geophysics, in the context of this report, is defined as the prediction of geophysical responses in gravity, magnetic and seismic data that result from chemical alteration. These predictions are based on geochemical and geological simulations of this alteration. Predictive geophysics is our link from the Five Questions, developed by the AGCRC and the ***pmd****CRC*, to observable geophysical responses.

We apply predictive geophysics to a 1D conceptual alteration model, and to a 2D reactive transport geochemical model. From these applications, the following geophysical signatures are detectable:

- An average increase in gravity response in an altered region of crust
- A decrease in gravity response directly above a deposit
- A small amplitude magnetic spike directly above the contact between a deposit and a fault which was used as a fluid conduit
- Two zones of variable seismic reflectivity along a fault which was a fluid conduit

These geophysical signatures of alteration are derived from our understanding of alteration and physical properties, and represent a new concept of geophysical targeting: targeting directly from alteration models, rather than empirical criteria derived by comparisons with previous ore deposits.

4.1 Introduction

The purpose of this report is to establish a methodology to turn any arbitrary geochemical model into a set of geophysical responses. This process is termed *predictive geophysics*, and it is defined as the method where predictive ore-forming chemical alteration models are transformed into geophysical targets. Traditional geophysical surveying has involved defining an anomaly and then attempting to explain this anomaly geologically, that is, through structure, lithology and/or alteration. Predictive geophysics is the reverse case of this scenario – predicting the structure, lithology and alteration around an ore body, and using this to define the geophysical anomalies we might expect. Ultimately, if ore-forming processes are simulated with enough detail, and using realistic architectures and deformation, we will have a method to predict mineralogical targets through their geophysical expressions. A suitably complex simulation of a mineral system will encapsulate the answers to the five questions (Barnicoat, 2006), and so predictive geophysics links the five questions to the results of geophysical survey.

The use of predictive geophysics requires a method to obtain physical properties from estimates of mineralogy or alteration. There exist a number of methods to calculate physical properties from a given arbitrary mineralogy. Of these available methods, some are more suited to predictive geophysics than others. To illustrate the use of these methods, probable physical properties for a simple 1D alteration model, from non ***pmd****CRC* references in the literature, are calculated. This will illustrate how physical property contrasts arise from chemical alteration.

Physical property distributions are also calculated for a 2D reactive transport model, using it to define physical property distributions and then to calculate geophysical signatures for these distributions. The potential field responses of this model are examined in detail, and probable sources for seismic reflections within altered regions of the crust are established. Commonalities in the predicted geophysical responses for the 1D and 2D models are also explored.

4.1.1 Theory

The source of geophysical responses is simple: geophysical responses result from a volume of rock with certain of physical properties, which are different to the properties of the background medium in which the volume is located. Any geological feature is capable of being detected, assuming the volume is of appropriate size, and the physical property has sufficient contrast to the host material. Detectability also relates to the property resolution of the technique, and the noise of any instrument used. The calculation of a theoretical geophysical response of an arbitrary geological scenario requires the creation of a physical property model.

Different minerals have different physical properties, such as their density, how magnetic they are, and the speed of sound within that mineral. Using this knowledge, we can create a physical property model from geochemical models by applying the principles of mixture theory (Berryman, 1995), where we are combining the properties of minerals for a geochemical model.

Mixture theory states that we can calculate a property for a subject, such as a rock sample or a cell within a geochemical model, if we know the following:

- What are the constituents of the subject?
- What are the proportions of the constituents of the subject?
- What are the physical properties of the constituents?

The physical properties of the subject are simply a weighted sum of all of the physical properties of the constituents of the subject (the primary properties). The weights for this calculation relate to the proportions of the constituents of the subject.

4.1.1.1 Density

Density combines linearly if we express proportions per unit volume, by definition. If we consider a subject containing ⅓ quartz, ⅓ plagioclase and ⅓ k-feldspar, linear mixing theory states that the density of this subject would be:

$$\rho_{subject} = ⅓ \times \rho_{quartz} + ⅓ \times \rho_{plagioclase} + ⅓ \times \rho_{k\text{-}feldspar}$$
$$= ⅓ \times 2.65\ tm^{-3} + ⅓ \times 2.615\ tm^{-3} + ⅓ \times 2.54\ tm^{-3}$$
$$= 2.60\ tm^{-3}.$$

Density can also be calculated from chemical properties. For any given species, we know the molar mass and volume. As an example, this is required for any models computed using using the reactive transport code pmd*RT, developed by the ***pmd****CRC*. For a subject expressed as a molar amount of minerals, each with a corresponding molar volume and mass, we can calculate the mass and volume of each mineral as:

$$mass_{mineral} = \text{Molar mass}_{mineral} \times \text{number of molecules}_{mineral}$$

$$volume_{mineral} = \text{Molar volume}_{mineral} \times \text{number of moleucules}_{mineral}$$

We can then sum the masses and volumes of all constituent minerals, to create a total mass and volume for the subject, then divide these quantities to provide the density.

4.1.1.2 Magnetic susceptibility

Most minerals are weakly to non-magnetic, and a few magnetic minerals principally control the magnetic susceptibility of bulk rocks. These minerals are (Carmichael, 1989a), approximately arranged in order of strongest to weakest magnetic susceptibility:

- magnetite
- pyrrhotite
- pyrite (and marcasite)
- siderite
- ilmenite
- hematite, maghemite (and martite)

Magnetic susceptibility can be assumed to be linear for concentrations of magnetite lower than approximately 20% by volume (Shandley and Bacon, 1966; Fannin et al., 1990), although above this volume the change in magnetic susceptibility is no longer linear with respect to the proportions of magnetite or pyrrhotite, due to the effect of increasing the effective magnetic domain size (Hargraves and Banerjee, 1973).

Other schemes to calculate magnetic susceptibility for constituent minerals include:

- Linear averaging of magnetic susceptibility in log (magnetic susceptibility)-log(magnetite content) space, rather than in linear-linear space (Mooney and Bleifuss, 1953).
- Werner (1945), which relates magnetic susceptibility of a subject to the volumetric proportions of the magnetic susceptibilities of magnetic material:

$$k_{subject} = \sum_{i=1}^{N} \left(\frac{V_i\, k_i}{1 + \frac{4}{3}\pi(1 - v_i^{\frac{1}{6}})} \right)$$

  Empirically derived methods relating only to the magnetite content.
  - Mooney and Bleifuss (1953), who define magnetic susceptibility as $k_{subject} = 0.289(v_{magnette})^{1.01}$
  - Grant and West (1965), $k_{subject} = 0.26(v_{magnette})^{1.11}$
  - Parasnis (1973), $k_{subject} = 0.116(v_{magnette})^{1.39}$

These schemes only relate magnetic susceptibility to magnetite content, but they could be applied using concentrations of other materials. To apply them,

we invoke the use of magnetite-equivalent proportion (Shandley and Bacon, 1966) to express concentrations of other materials. A magnetite-equivalent proportion is the equivalent volume that would yield the same magnetitc susceptibility ($k_{equiv} = V_{mineral} \times [k_{mineral} \div k_{magnetite}]$). Pyrrhotite, for example, is tenfold less magnetically susceptibile than magnetite, and hence 30% pyrrhotite by volume represents a magnetite-equivalent proportion of 3%.

All of the schemes presented for calculating magnetic susceptibility have been implemented in a Python library, `property_calcs.py` (Appendix A2). The schemes that relate only to magnetite content, that is, Mooney and Bleifuss (1953), Grant and West (1965) and Parasnis (1973), could be utilised using magnetite-equivalent proportions.

4.1.1.3 Seismic velocity

Linear mixing methods can also be used as an approximate method to determine seismic velocity from mineralogy, and produce results that are often within error of measurements, such as those from downhole geophysics (Christensen, 1989; Ji et al., 2002). The linear mixing method only requires knowledge of the properties of the minerals that you wish to calculate, for example, if you wish to calculate P-wave velocity, then you only require the P-wave velocities of the constituent minerals.

Another method to determine seismic velocities is the time-averaging method (Wyllie et al., 1956; Dvorkin and Nur, 1998). The time-averaged method is calculated using the following formula:

$$\frac{1}{v_{subject}} = \sum_{i=1}^{N} \frac{V_i}{v_i}$$

We can apply this method equally to P- and S-wave velocities. As per the linear mixing method, the time-average method only requires the properties of the minerals you wish to calculate for.

The Voigt-Reuss-Hill (Berryman, 1995) or Hashin-Shtrikman (Watt, 1988) methods are regarded as more accurate methods of predicting seismic velocity for subjects where the exact mineralogy is known. Both of these methods require knowledge of the tensor of elastic moduli to describe the constituent minerals. For many of the minerals studied for this report, these moduli are not known, and for simplicity, this report calculates seismic velocity by linear averaging.

4.2 1D Alteration Model

4.2.1 Introduction

In this section, we explore the creation of physical property distributions from a simple 1D alteration model, and infer possible geophysical signatures of this alteration model. As per our introduction, we can calculate the physical properties for this alteration model, assuming we know:

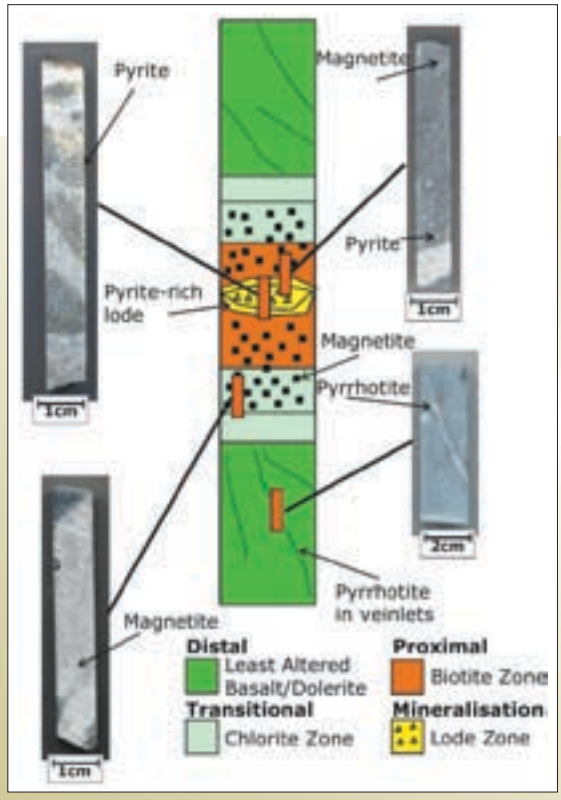

Figure 47: 1D model of hydrothermal alteration at the St Ives Gold Mine, Western Australia (Ruming, 2006). This alteration model generalises alteration within the basalt units at St Ives. Similar alteration assemblages are observed for other common host rocks in the region (Hagemann and Cassidy, 2001). Entire alteration assemblages for each zone (distal, transitional, proximal and mineralisation) are defined for this model (Table 3).

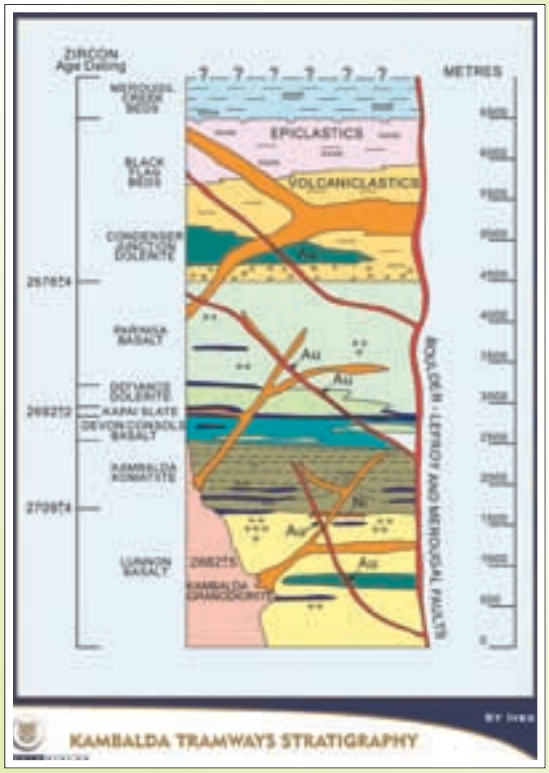

Figure 48: Regional stratigraphy at the St Ives Gold Mine (Connors et al., 2003). For this section, we consider three host rocks in the region: the Devon Consols Basalt, the Defiance Dolerite, and the Black Flag beds.

- The components of the alteration and the host rock
- The relative proportion of alteration and the host rock
- The properties of each alteration mineral and those of the host rock

For this exercise, we examine an alteration model (Figure 47 and Table 3) for the St Ives Gold Mine, an Archaean orogenic gold deposit in the Yilgarn Craton, Western Australia (Ruming, 2006). This alteration model has very similar alteration mineralogy to other studies at St Ives and more widely in the Yilgarn (Hagemann and Cassidy, 2001; Neumayr et al., 2005; Neumayr et al., 2006). St Ives also has a stratigraphy similar to other Yilgarn orogenic gold deposits (Figure 48).

4.2.2 Methodology

Mixture theory requires that in order to calculate the properties of an altered package of rock, we need to know relative proportions of alteration and host minerals and the fundamental properties of these materials. The alteration model only states the alteration assemblages (Table 3). As a diagnostic mineral is going to occur at least as often as any other mineral in the alteration assemblage, and indeed is more likely to occur than any other, we assume that the diagnostic mineral occurs approximately[1] twice as often as any other mineral within the assemblage, and calculate a set of median alteration assemblage properties (Table 4) using a Monte Carlo method (Appendix A3). We define the host properties using the downhole geophysical results from stratigraphic drilling at St Ives (Table 5).

Upon establishing the properties of the host and alteration, we require an estimate of the relative proportions of each. For our alteration model, these are not explicitly defined. One hypothesis of these proportions is that a mineralised zone will most likely have very large amounts of alteration, and distal to the deposit there are more likely to be smaller amounts of alteration (Neumayr et al., 2003, summarised in Figure 49).

Zone	Mineralogy (diagnostic mineral listed first)
Distal	Disseminated pyrrhotite
Transitional	Chlorite, quartz, albite, carbonate, magnetite
Proximal	Biotite, albite, magnetite, Ca-plagioclase, quartz, carbonate, amphibole
Mineralisation	Quartz, carbonate, albite, pyrite, magnetite, biotite, chlorite

Table 3: Alteration assemblages at St Ives (Ruming, 2006).

1 As the method used to calculate alteration assemblage mineralogy is probabilistic we can only approximately ensure that the diagnostic mineral will occur twice as often as any other in the mineralogy.

Alteration zone	ρ (tm^{-3})	k (SI)	v_p (ms^{-1})
Distal	4.62	0.15	4645
Transitional	2.93	0.048	5777
Proximal	3.56	0.42	6244
Mineralisation	2.78	0.10	6088

Table 4: Median physical properties of alteration assemblages of our alteration model (Table 3). Assemblage properties calculated using a Monte Carlo method (Appendix A3), and are the physical properties we would expect for total alteration of a rock in each alteration zone.

Host	ρ (tm^{-3})	k (SI)	v_p (ms^{-1})
Devon Consols Basalt	2.95	0.79 × 10-3	6480
Defiance Dolerite (containing primary magnetite)	2.96	9.5 × 10-3	6450
Black Flag beds	2.64	0.5 × 10-3	5965

Table 5: Median host rock physical properties at St Ives (summarises Section 3.2).

4.2.3 Results and Discussion

Assuming a linear relationship between the proportion of alteration and density, magnetic susceptibility and seismic velocity, we can use mixture theory to predict a likely physical property regime for this 1D alteration model (Figure 49). These predictions allow us to understand what diagnostic geophysical criteria these alteration zones will provide using three geophysical data sets.

For all lithologies studied, alteration generally has increased their density, and hence an altered region would be imaged as a broad gravity high. If we undertake a more detailed gravity survey, mineralisation is in an area flanked by gravity highs; nevertheless, mineralisation itself represents a lower density, and thus gravity response decrease. This decrease is due to the dominant quartz-carbonate alteration of mineralisation, and would only be apparent during geophysical surveying if the station spacings were in the order of the width of the zone of mineralisation, or closer. To observe these signals, we also may need to remove as much lithological effect as we can. As an example, a dolerite is usually imaged as a gravity high and thus we may mistakenly interpret a gravity high that results as a dolerite instead of the result of alteration.

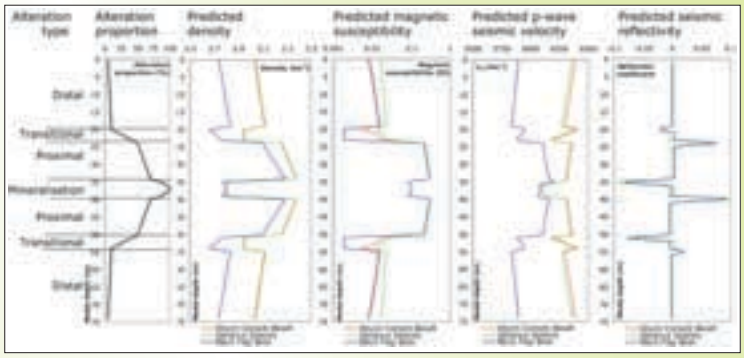

Figure 49: Prediction of three physical properties (density, magnetic susceptibility and p-wave seismic velocity) and a derived parameter (seismic reflection coefficient) using a 1D physical model. Depths are used only to indicate the possible scale of various alteration zones. The predicted properties broadly agree with observed physical properties for alteration at the St Ives Gold Mine (Section 3.2). These physical properties allow us to infer some geophysical signatures. For a gravity survey, the zone of mineralisation would occur within a gravity high, due to the high-density proximal alteration, but the zone of mineralisation itself will be marked by a zone of lower density, due to the carbonate-quartz zone. The zone of mineralisation would also occur within a magnetic intensity high, although the zone itself would be marked by a slightly lower magnetic intensity. Note that seismic reflectivity is determined by the spatial derivative of the acoustic impedance (the product of seismic velocity and density), the reflection coefficient (Figure 1). The reflection coefficient distribution, for this example, indicates that the top and base of the proximal mineralisation could be imaged. The transition from proximal alteration to mineralisation also would result in a reflection, but the zone of mineralisation is likely to be so narrow (5 m or less) that destructive interference of the seismic waveform would result in no apparent reflection (Widess, 1973).

For a magnetic survey, mineralisation is surrounded by very high magnetic response, but, the mineralisation zone itself does not need to be strongly magnetic. Inclusion of only a very small proportion of magnetite in the zone of mineralisation will, however, greatly increase the magnetic susceptibility of this zone.

To understand the likelihood of seismic reflections arising from alteration, we need to examine the acoustic impedance contrast between adjacent portions of rocks. The principle of reflection seismology is that reflections arise from contrasts in acoustic impedances. The strength of the reflection is measured by the spatial derivative of acoustic impedance divided by the total acoustic impedance, known as the reflection coefficient *R* (Figure 1). A reflection coefficient that is greater than 0.06 yields a very strong positive reflection and one less than -0.06 yields a strong negative reflection.

Our predicted physical properties (Figure 49) indicate there are four regions that would provide strong reflections: the top of the upper proximal zone, the transition from the upper proximal to the mineralisation zone, the transition from the mineralisation zone to the top of the lower proximal zone, and the base of the lower proximal zone. The transition from proximal to mineralisation and back to proximal alteration is generally of the order of 5 m (Neumayr et al., 2003; Ruming, 2006), which would result in constructive interference of the reflections (Widess, 1973). The enveloping proximal alteration, however, is able to be imaged. The total thickness of this halo is only in the order of 25 m (Neumayr et al., 2003; Ruming, 2006), which is just less than ¼ of the seismic wavelength for typical hard-rock reflection surveys in Australia (Drummond et al., 2000; Goleby et al., 2003), meaning that we would image this package as a single reflection, rather than imaging both the top and the bottom of the package.

4.2.4 Conclusions

Based on our alteration model and predicting physical properties using simple techniques, gold mineralisation of this type will occur:

- Within broad gravity highs (regional survey), marked by a moderate to low gravity response (detailed survey) directly at the site of mineralisation.
- Within broad magnetic high (regional survey), marked by a moderate magnetic response (detailed survey) directly at the site of mineralisation.
- Seismic reflections from the top and bottom of the enveloping proximal alteration. If this proximal alteration halo is thicker than ¼ of the seismic wavelength, we may detect both the top and the bottom of the proximal alteration halo.

In the next section, we will undertake the same process for a 2D alteration model, producing direct 2D signatures of the geophysical responses we expect for alteration. We will also compare the predicted 2D signatures to those we have predicted for this 1D case, showing commonalities between the two predictions. These commonalities allow us to draw some generic conclusions about the overall expected geophysical signatures.

4.3 2D Alteration Model

4.3.1 Introduction

The creation of 2D geophysical signatures of an orebody requires a reliable estimate of mineralogy for that orebody and the surrounding lithologies and alteration. For this section, we will examine a generic model of the formation of a gold orebody, namely the listric fault model (LFM) of Cleverley et al. (2006).

The LFM (Figure 50; see Appendix A4 for modelled mineralogy) is a generic simulation of the formation of gold orebodies similar to those of the Eastern Goldfields, Yilgarn Craton. The simulations of fluid flow and chemistry were performed with the pmd*RT reactive transport modelling system. The original model is 15 km deep and 30 km in length, with the top of the model just below the surface of the Earth, at the simulated time of ore formation.

The LFM simulates ~1.2 Ma of geological history, and as the model is a simulation of processes in the Yilgarn Craton, we have ~2.5 Ga of geological processes (Swager, 1997) that are not simulated but we can approximate. These processes are those of mineralogical change, permeability change, erosion and deposition of transported cover.

No changes in mineralogy post-mineralisation are assumed in order to simplify the geophysical response modelling of the LFM. Although the Yilgarn has undergone deformation post mineralisation (Swager, 1997), the overall mineralogy (lithology and alteration) was determined during mineralisation (Neumayr et al., 2005).

The permeability structure of the LFM does not represent the present-day permeability structure surrounding

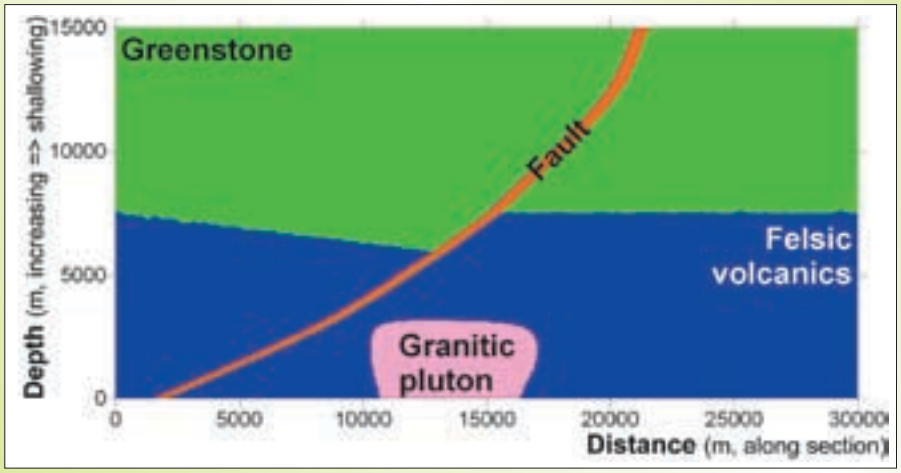

Figure 50: Geology of the listric fault model (LFM). The LFM is described in Cleverley et al. (2006), and the mineralogy of the model is depicted in Appendix A4.

deposits in the Yilgarn. The majority of the Archaean rocks in the Yilgarn have low permeability, except for small-scale structures, such as minor shears (Stolz, 2003). Thus, to simulate the change in permeability, we calculate physical properties just using mineralogy.

The Yilgarn Craton has undergone significant uplift and erosion since the cessation of gold mineralisation in the late Archaean. The simplest method to simulate this process is to remove material from the top of the model (Figure 51).

Gold deposits in the Eastern Goldfields of the Yilgarn Craton are situated within rocks of greenschist metamorphic facies (Groves et al., 2003), indicating that 7 to 10 km of material has been removed from above the deposits (Goleby et al., 2002). Weathering estimates also indicate that 8 and 10 km of material has been removed from the Yilgarn since the cessation of mineralisation (Anand and Paine, 2002).

Regolith also covers present-day gold deposits of the Yilgarn, so we must simulate a realistic thickness of regolith to add to the top of the model. Estimates of regolith depth in the Yilgarn vary: at the Victory-Defiance complex at the St Ives Gold Mine, regolith depth varies between 30 m and 100 m, depending if the depth of regolith is measured from the surface to saprolite, or to bedrock (Whitford, 2004); other localities within the Yilgarn support up to 100 m of regolith covering the Archaean rocks (Anand and Paine, 2002).

Erosion will not have occurred to the same level for all ore bodies. For example, in the case of lower erosional depths, an orebody may not crop out but be covered by some

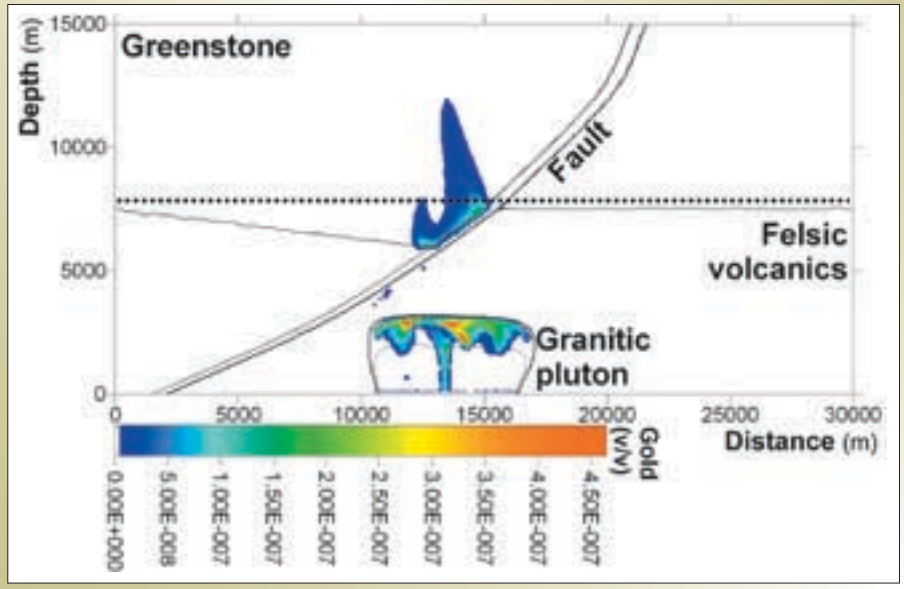

Figure 51: Gold distribution (as volumetric proportion) within the LFM after ~1.2 Ma of reactive fluid flow. For the top of the zone of high gold concentration (> 0.1 ppm by volume) to be close to (or at) the surface, the model would need to be eroded to the dashed line, removing approximately 7.5km of material from the top of the model. This level of erosion is consistent with that observed for the Yilgarn Craton.

regolith and altered but unmineralised rocks. To account for these cases, we will model the geophysical response of geochemical models with progressively less material removed from the top of the model – we consider where the main body of gold in the fault (Figure 50) lies not at the surface, but 500 m, 1 km or 1.5 km below the surface. Erosion may also have partially or entirely removed an ore body; we will also simulate these scenarios.

4.3.1.1 Creation of the physical property model

The output from the pmd*RT modelling software is a variably spaced mesh in the vtk format, version 3 (Kitware, Inc., 2007). Each node of the mesh contains the number of particles of each minerals (as mols). The pmd*RT software also requires the thermodynamic properties of the chemical system being modelled (the chemical system file), to be specified in the UT2K format (Shvarov and Bastrakov, 2003).

A Python script was created (`add_phys_props.py`, Appendix A5) to calculate physical properties for each cell. Three properties are calculated by `add_phys_props.py`: density, magnetic susceptibility, and seismic velocity. These properties are all calculated using the `property_calcs.py` program (Appendix A2), whose methods of calculating physical properties is described above and summarised below (Table 6).

Property	Method
Density (ρ)	Directly from chemistry.
Magnetic susceptibility (k)	Linear averaging of magnetic susceptibility of constituent minerals.
Seismic velocity (v_p)	Linear averaging of seismic velocity of constituent minerals.

Table 6: Methods used to calculate each property for the 2D reactive transport model.

Physical properties are calculated for both the initial and final models, as created by the pmd*RT code (Figures 52–54). These physical properties are imported into Gocad to be converted to pseudo-3D physical property models (Appendix A6).

The physical property models (Appendix A7) are used to calculate the gravity and magnetics response using the forward modelling components of the UBC-GIF GRAV3D (Li and Oldenburg, 1998) and MAG3D (Li and Oldenburg, 1996) packages (Figures 55–60). As the seismic velocity field is highly irregular and therefore very difficult to use to compute synthetic seismograms, we will simply examine the vertical derivatives of acoustic impedance to highlight possible reflectors (Figure 61).

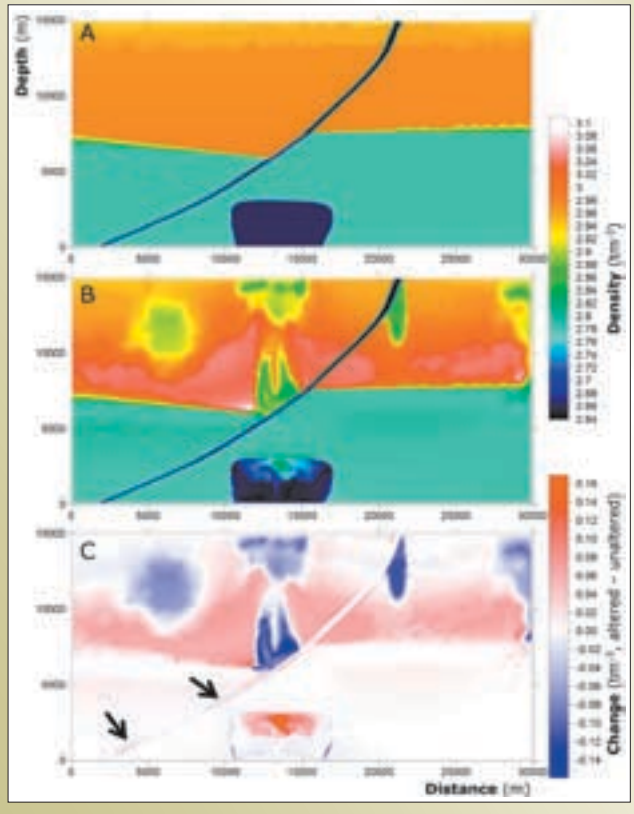

Figure 52: Density models for the unaltered (A) and altered (B) cases. The change in density, from the unaltered to the altered model, is also shown (C). The gold deposit occurs within the region of decreased density, with the top at 7.5 km depth. Alteration further from the deposit is generally to higher density, with the exception of two elongate zones within the lower half of the fault (highlighted by arrows), and some regions within the higher-density greenstone package. The largest increase in density is observed in the greenstone package, with a very moderate increase in density in the felsic volcanics. The density at the top of the granite pluton is also elevated when we compare the altered to the unaltered model. When simulating the geophysical response of this model, we will also consider various erosional scenarios (Appendix A7).

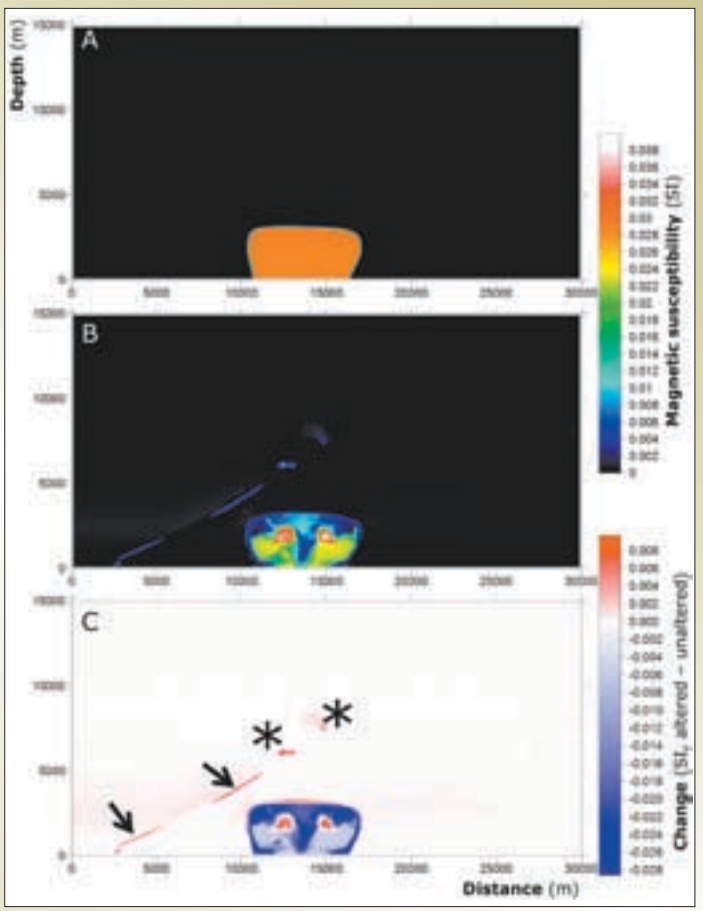

Figure 53: Magnetic susceptibility models for the unaltered (A) and altered (B) cases. The change in magnetic susceptibility, from the unaltered to the altered model, is also shown (C). The gold deposit occurs directly above the centre of the granite pluton, at approximately 7.5 km model depth. Proximal to the deposit are two small zones of increased magnetic susceptibility (highlighted by asterisks). Two elongate zones of increased magnetic susceptibility occur within the lower half of the fault (highlighted by arrows), representing pyrrhotite alteration distal to the alteration. Note that when we consider the geophysical signatures of these models we will examine a number of erosional scenarios (Appendix A7).

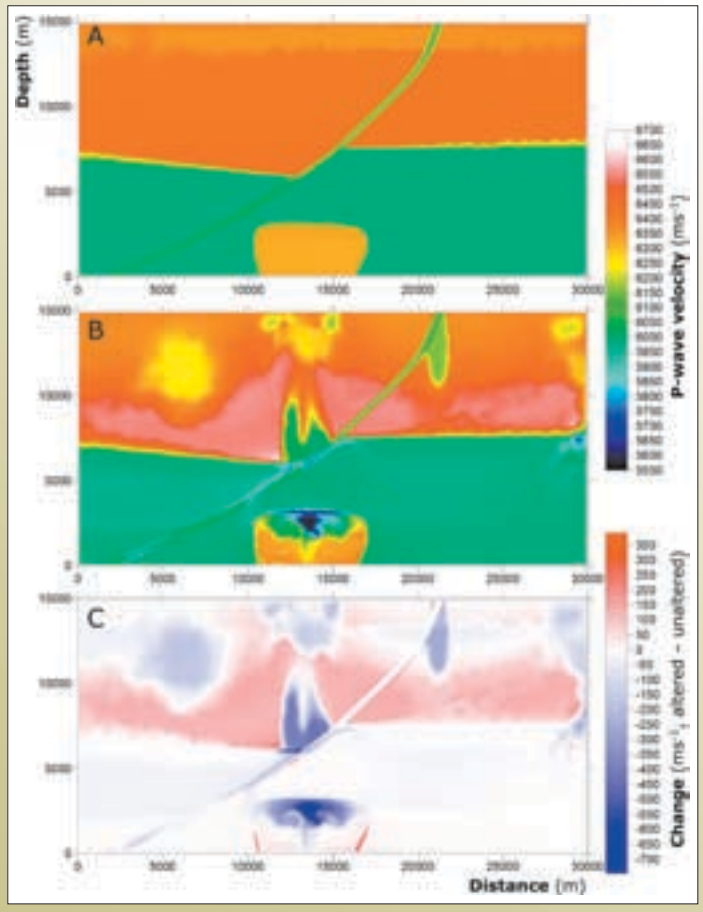

Figure 54: P-wave seismic velocity models for the unaltered (A) and altered (B) cases. The change in seismic velocity, from the unaltered to the altered model, is also shown (C). The gold deposit occurs within the region of reduced seismic velocity. There is also reduced seismic velocity in the granite pluton, and two zones of reduced velocity within the fault.

4.3.2 Results

N.B. Appendix A7 shows the physical property models used to produce these results.

4.3.2.1 Gravity

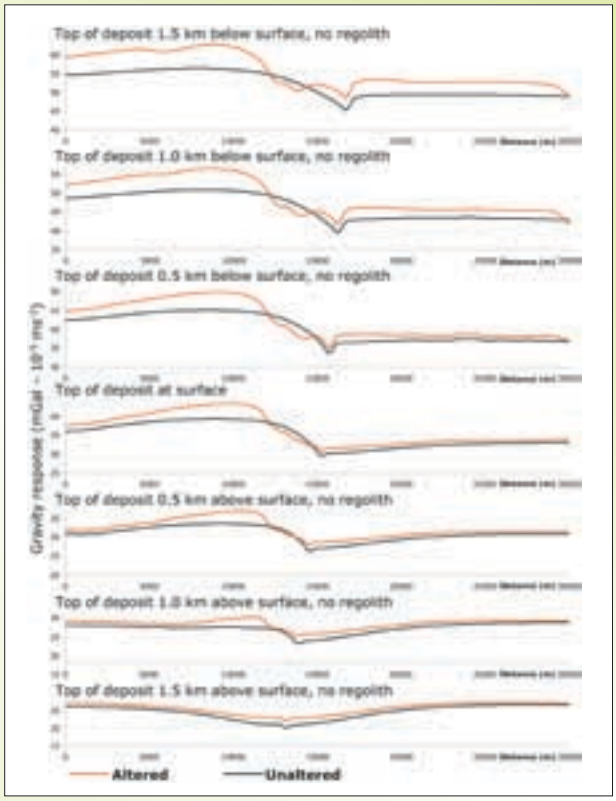

Figure 55: Gravity response, no regolith. The deposit sits between 12.5 km and 14.8 km along the profile, dipping at 30° to the left.

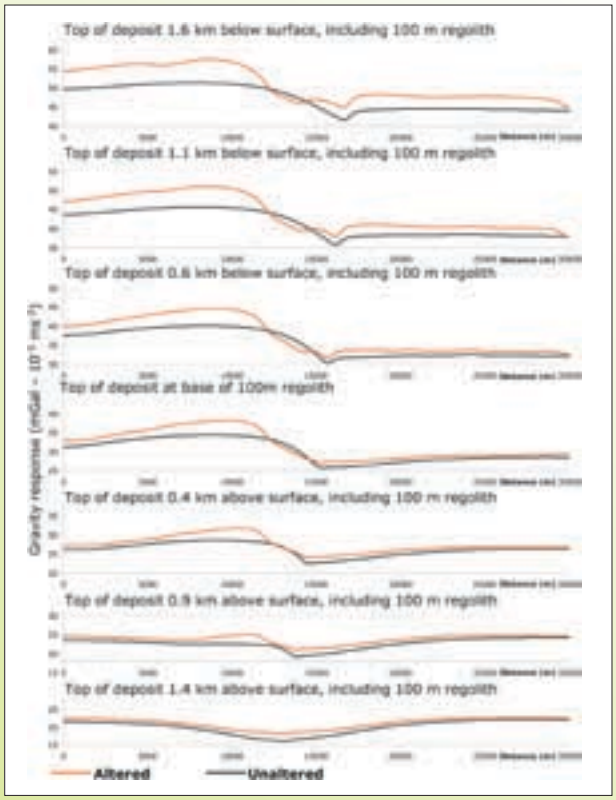

Figure 56: Gravity response, with regolith. The deposit sits between 12.5 km and 14.8 km along the profile, dipping at 30° to the left.

4.3.2.2 Ground magnetic survey

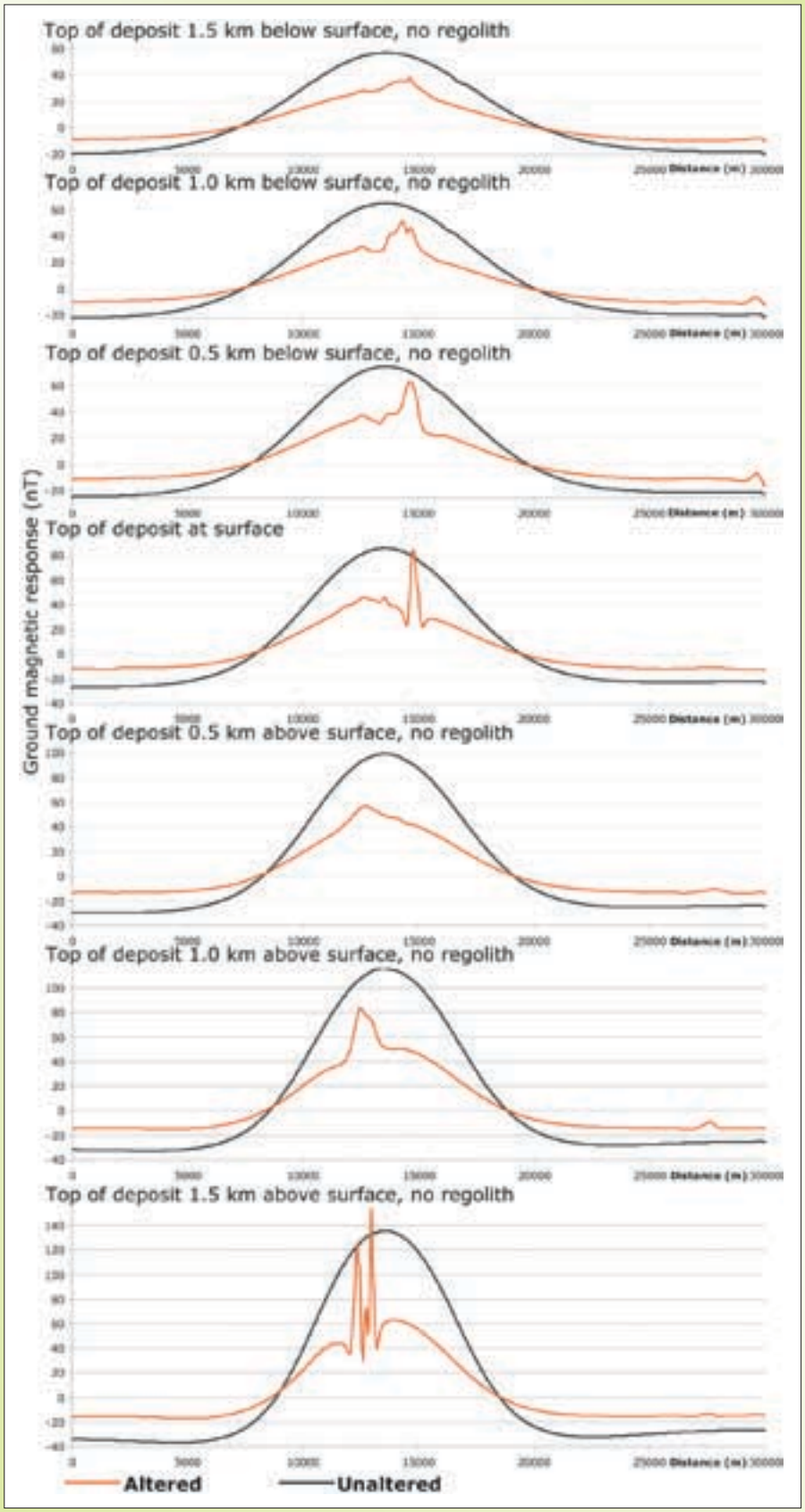

Figure 57: Ground magnetic response, no regolith. The deposit sits between 12.5 km and 15 km along the profile, dipping at 30° to the left..

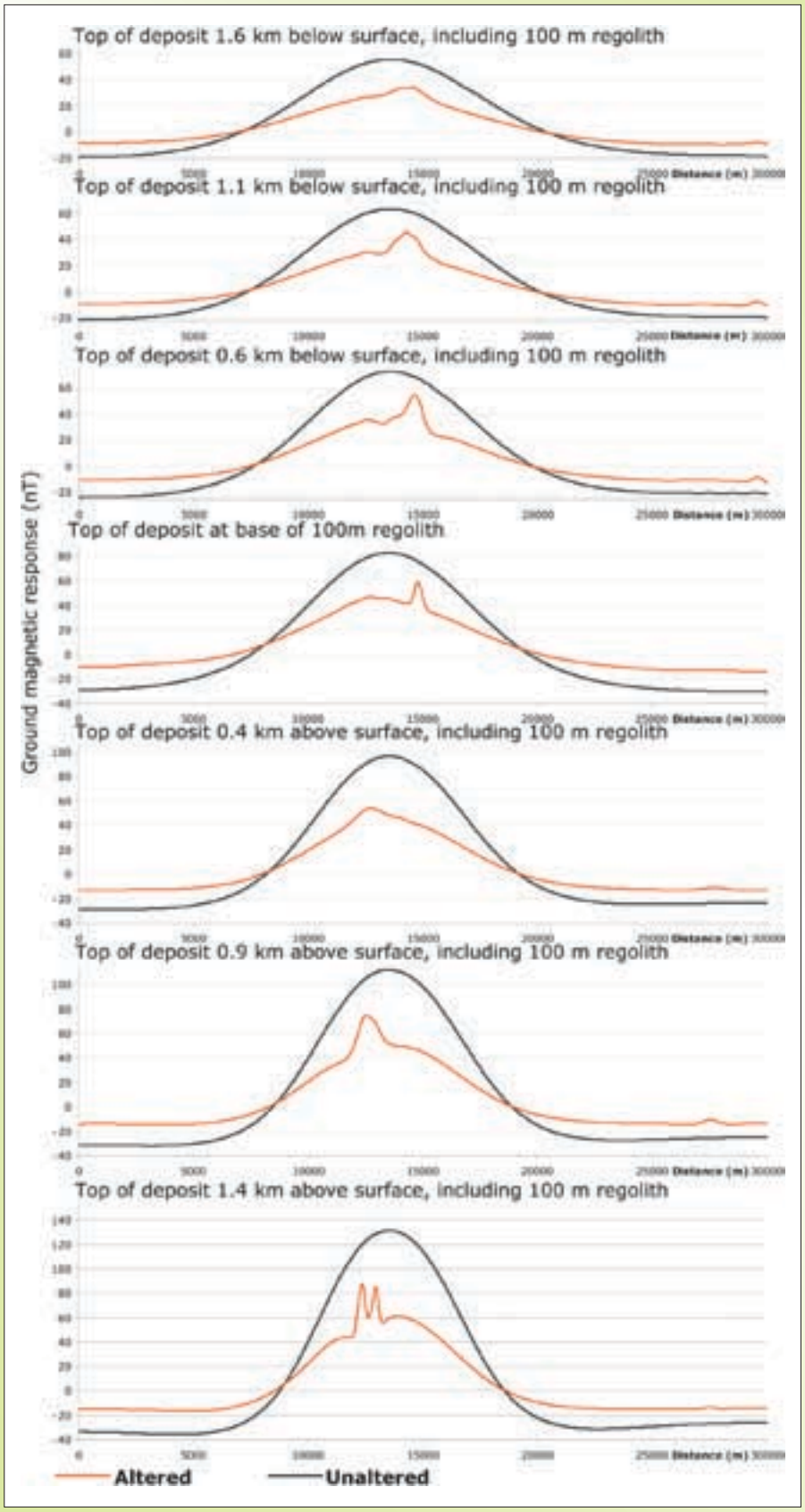

Figure 58: Ground magnetic response, with regolith. The deposit sits between 12.5 km and 14.8 km along the profile, dipping at 30° to the left.

4.3.2.3 Aeromagnetic survey

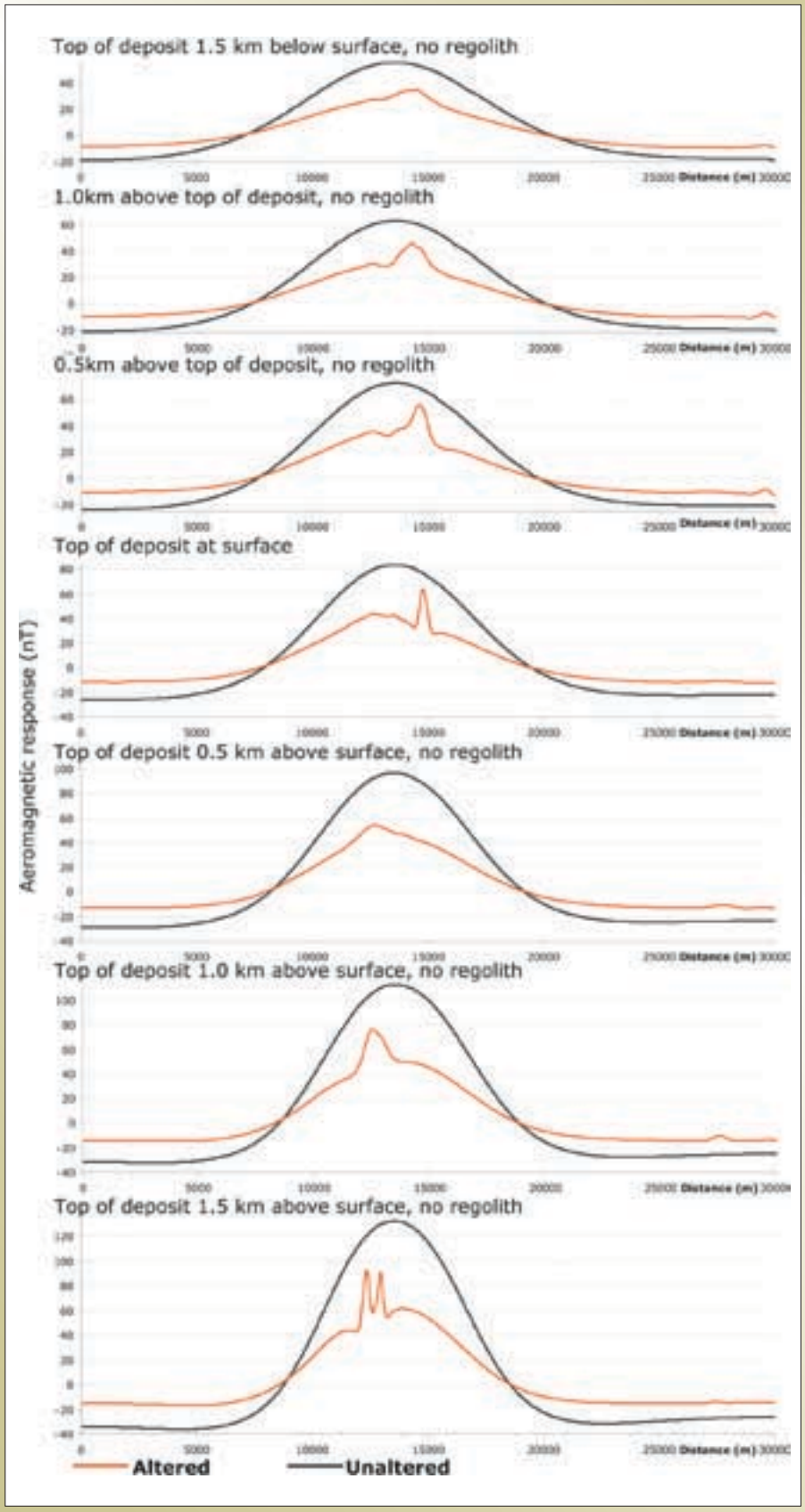

Figure 59: Aeromagnetic survey response, 80 m flight height, no regolith. The deposit sits between 12.5 km and 14.8 km along the profile, dipping at 30° to the left.

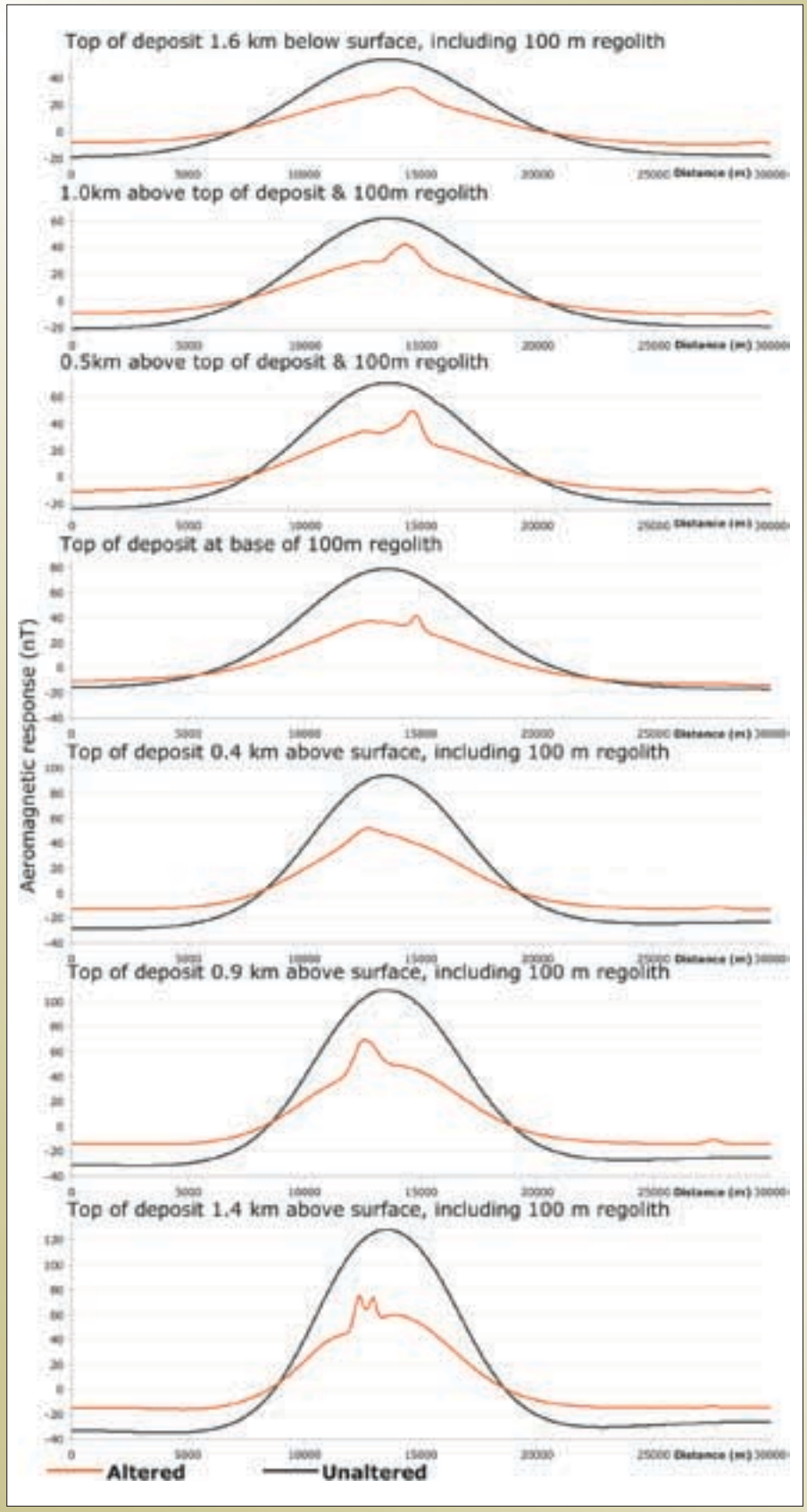

Figure 60: Aeromagnetic survey response, 80 m flight height, with regolith. The deposit sits between 12.5 km and 14.8 km along the profile, dipping at 30° to the left.

4.3.2.4 Seismic (acoustic impedance) results

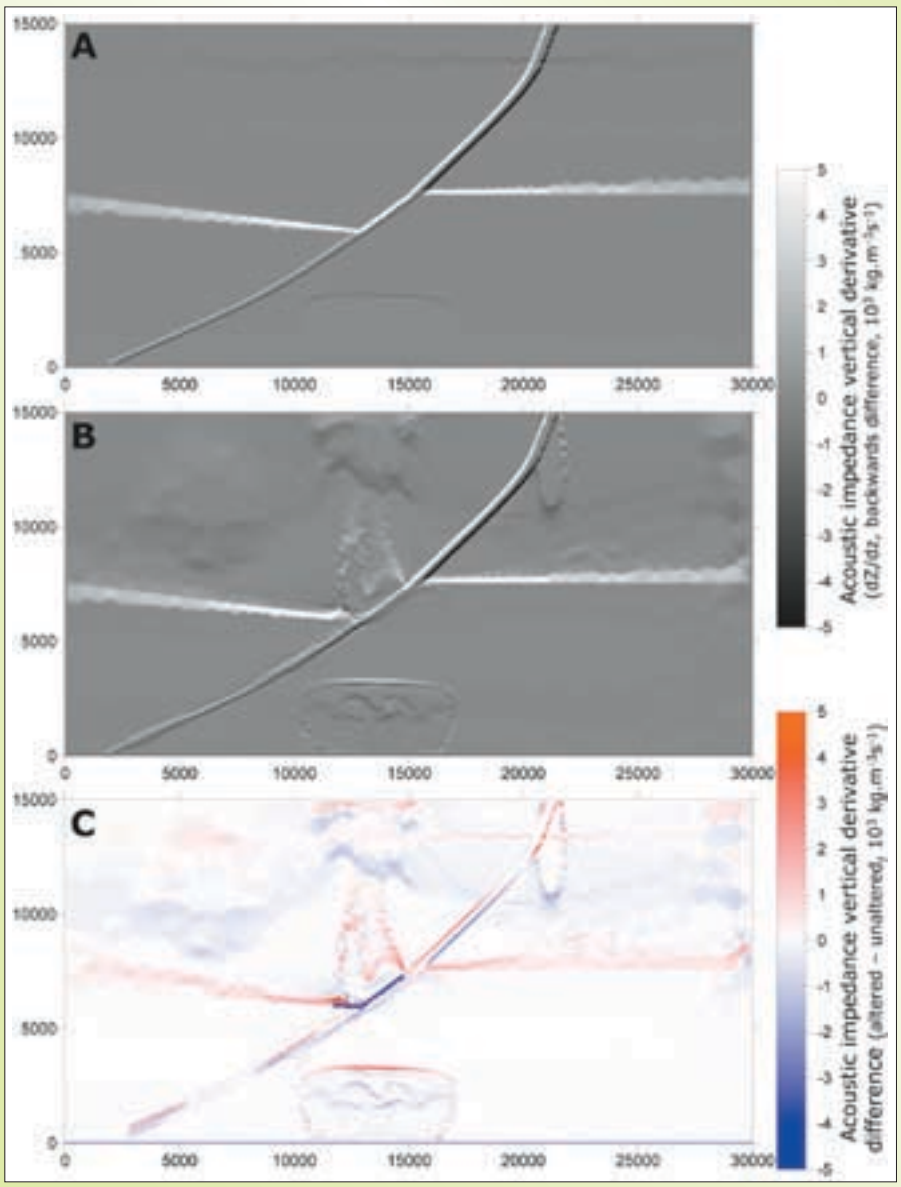

Figure 61: Acoustic impedance vertical derivative for the (A) unaltered and (B) altered LFM. The deposit sits between 12.5 km and 14.8 km along the section, dipping at 30° to the left. Change in the vertical derivative of acoustic impedance (C) indicates where positive (red) and negative (blue) reflections would occur for an altered section with respect to an unaltered section/ For both the unaltered and altered models, strong reflections will occur at the greenstone-felsic volcanic boundary, along the fault, and around the granite body. When the model is altered, the reflectivity of the fault will increase in some areas, for example, the thicker packages in the lower half of the fault in the altered model. This style of reflectivity has been observed in regional seismic data and this thickened and 'patchy' reflectivity have been interpreted as related to fluid flow (Section 2; also Drummond et al., 2004b). If the outflow zone has not been eroded, diffractions will occur, due to the steep sides.

4.3.3 Discussion

4.3.3.1 Gravity

In this section we consider the gravity responses that allow us to identify altered crust and the indirect detection of a deposit.

The effect of regolith, as we have simulated it, is to reduce the amplitude of the profiles, and to slightly smooth out the features. Signatures discussed here relate to both the regolith and uncovered cases. The reduction in amplitude is due to effectively increasing the separation between simulated gravity stations and the density contrasts. In general, this effect is also the cause of the decrease in gravity response for the progressively more eroded models: less mass is present in the more eroded models, reducing their gravity response.

There are two main signatures of alteration within the gravity datasets, when compared to that of unaltered models (Figures 55 and 56):

- Decrease in gravity response directly above the deposit. This is observed for all deposits which are buried, either by regolith or by insufficient erosion. This feature is diagnostic of a buried ore deposit, and is caused by the lower density outflow zone, related to quartz and carbonate alteration.
- Increase in gravity response outboard from the deposit. This feature is observed for all altered scenarios, even when the mineralisation has been eroded,. This feature is due to the alteration of all the lithologies present; it is diagnostic of a region of altered crust but it is not evidence which is diagnostic for the presence of a buried deposit.

Thus, the signature which is diagnostic of an exploitable (potentially able to be found and mined) deposit is the lower gravity response directly above the deposit, with respect to the response expected for an unaltered model. This response is only evident for deposits at surface, buried by only a regolith blanket, or buried by the body's outflow zone (with or without blanketing regolith).

There are some significant differences in the geometry of this reduced gravity response in the various scenarios. For example, the largest amount of decrease below the unaltered response is for the deposit buried by 500 m of outflow altered rocks. The horizontal extent of the zone of decreased response is the same as the horizontal extent of the deposit for the deposit at surface, or buried by 500 m of the outflow zone. As the deposit is eroded further, the low-density alteration of the outflow zone of the deposit becomes thinner, and so the extent of the reduced response becomes narrower. This has implications for the spatial resolution required for the detection of this signature: as the deposit is buried further, the distance between gravity stations must decrease to detect the decreased gravity response. For a deposit buried by 1.0 km of outflow zone, the signature is ~2 km wide; sampling theory dictates that gravity stations no more than 1 km apart would be required to detect this decrease (Telford et al., 1990a).

Detection of a signature also depends on the amplitude of the feature, and if it is able to exceed noise within any survey. The increase in density response is between 5 and 30% of the unaltered gravity response, which is well in excess of typical gravity surveying noise, which is in the order of 5% of the measurement amount (Milsom, 2003a). The decrease in gravity response directly over the deposit is of the order of 7-11% of the unaltered response at the same location, which is nominally able to be detected by a typical gravity survey. The addition of regolith slightly decreases the amplitude of the signals; nevertheless, even for this scenario the signatures still exceed the noise level of gravity surveys.

4.3.3.2 Magnetic surveys

The major response of the magnetic surveys (Figures 57 to 60) is that the magnetic granite body dominates the magnetic response of the LFM. The decrease in the average magnetic response as we bury the deposit is because we are increasing the separation between the height of the magnetic survey and the most magnetic material of the model, the granite body.

Alteration for the LFM produces packages of magnetic material within the fault, as well as some magnetic material proximal to the deposit itself. If alteration has occurred in a manner similar to that simulated by the LFM, then the first sign of alteration is a variable magnetic response along the fault.

These packages of magnetic material within the fault produce different signatures. For example, consider the case of the deposit fully eroded, that is, the profile where the top of deposit is 1.5 km above profile. For this case, there are two high magnetic spikes at 12 and 13 km along the profile, resulting from the magnetic profile intersecting the package of magnetic material surrounding the fault. These spikes are apparent even in the aeromagnetic profiles (Figures 59 and 60), although the amplitudes are decreased

due to the increased separation between the magnetic material and the simulated sensor.

The cases where the deposit is at surface, covered by regolith, or buried by the outflow zone, all indicate that these deposits have an associated magnetic spike. These magnetic spikes all occur at 14.8 km, which is also the distance along the profile that the highest point of the deposit sits. This magnetic spike becomes very subtle for highly buried deposits, especially for aeromagnetic surveys; nevertheless, it is the diagnostic magnetic signature apparent for exploitable deposits.

4.3.3.3 Potential seismic responses

As we have not computed synthetic seismic profiles, we can simply consider where potential reflections will arise from our acoustic impedance model (the product of Figures 52 and 54), by examining the vertical acoustic impedance derivative (Figure 61), remembering that reflections arise from a strong acoustic impedance contrast in an effectively vertical direction.

The apparent reflections differ quite considerably between the unaltered and altered models. In the case of the unaltered model, strong reflections will occur from the greenstone-felsic volcanic contacts, the fault, and the top of the granite body. For the altered model, strong reflections will occur from the greenstone-felsic volcanic contacts, the fault, the top of the granite body, and the outflow zone above the deposit. The fault will be imaged as being variably reflective, due to the packages of higher acoustic impedance along the fault within the felsic volcanic succession. Some minor reflections may also emanate from the alteration-related geometries within the greenstones (assuming they have not been eroded), and also within the granite body.

The key diagnostic criteria for mineralisation, simulated by the LFM, are the zones of variable reflections along the fault within the felsic volcanic succession. These zones would give rise to reflections of slightly higher apparent frequency, due to tuning of the waveforms (Widess, 1973). The geometry of reflections would be similar to those predicted by Drummond et al. (2004b) as well as those interpreted in Section 2.

4.3.4 Conclusions

The construction of potential geophysical responses to a 2D simulation of ore-forming processes has allowed us to draw a number of generic exploration conclusions. In summary, we would detect mineralisation by the following geophysical criteria:

a. an overall increase in gravity response of the crust, compared to that we would expect for an unaltered region of crust
b. a decrease in gravity response directly above a buried target, when compared to the same unaltered architecture
c. a magnetic spike, proximal to a fault that has been a conduit for fluids, and one not associated with a primary magnetic lithology
d. a zone of variable reflectivity, occurring as linear reflections, subparallel to the main reflective feature (a fault, which has been a fluid conduit).

These signatures are very similar to those we interpreted for the 1D case (Section 4.2).

Detecting these signatures may well prove to be difficult; nevertheless, the key finding of this section is that these signatures are of a size such that there is potential to detect them, using three different geophysical surveying techniques.

We will first consider the potential field (gravity and magnetic) signatures. An infinite number of sources can explain a potential field response (Telford et al., 1990a), so the signatures are equivocal. For example, an increase in gravity response for an entire region is evidence for alteration; but it may also be evidence that we underestimated the unaltered density of a rock. The decrease in gravity response directly above a deposit is evidence for a buried deposit; but it is equally evidence for a thicker granite body. Successfully identifying a deposit from signatures requires confidence in the expected architecture of the region. If we do not know the unaltered architecture in a region, and its geophysical response, it is more difficult to detect a signature such as "a reduced gravity response with respect to that of the unaltered rock".

In this case, we need to combine interpretations of datasets, rather than treating them separately. If we have a zone of anomalous potential field response, as well as seismically detecting a fault, with variable reflectivity, leading to this zone then we can be confident that we have correctly identified a zone of mineralisation, as long as our simulation of the ore-forming processes are valid.

4.4 Conclusions

This report has defined the term *predictive geophysics* to be the method by which geophysical responses can be calculated from alteration models. Both 1D and 2D cases have been examined. Although the alteration models were

completely independent, the geophysical signatures that are calculated are very similar. The signatures that provide evidence for a gold deposit are:

- An average increase in gravity response in an altered region of crust
- A decrease in gravity response directly above a deposit
- A small amplitude magnetic spike directly above the contact between a deposit and a fault which was used as a fluid conduit
- Two zones of variable reflectivity along a fault which was a fluid conduit

Identifying these signatures may prove to be difficult in real data, as other effects such as that of lithology need to be accounted for prior to interrogation of the data for evidence of alteration, or they need to be interpreted simultaneously.

We must be wary of interpreting (or discounting) alteration using techniques such as potential field forward modelling. The general approach to potential field forward modelling generally involves manipulation of architectures and rock properties to fit the calculated and observed responses more closely (Telford et al., 1990a). Over-fitting the data will mask the effect of alteration, if it is not identified. The simplest trap may be increasing the overall density of an entire block of rocks to fit observed and calculated responses more closely – this report establishes that such density increases may well be primary evidence for an altered region of crust; we cannot simply discount them as one of the processes of forward modelling.

Although the 1D and 2D signatures are grossly similar, the extra detail provided by the 2D simulations allows for significantly more reliable geophysical signatures to be identified. Should 3D realistic chemical models be created, fully 3D geophysical signatures should also provide even more detail than the 2D signatures derived in this report.

It is very important to note that the use of 2D simulations of ore-forming processes allows for establishing further hypotheses to test our interpretations. As these models contain information regarding the mineralogy, we can also establish likely geochemical regimes in areas such as that directly above the deposit.

With the advent of realistic geochemical simulations, and using these to calculate physical properties, we now have the ability to define geophysical responses with respect to our expected processes of mineralisation, and this represents a different method to interpret geophysical datasets.

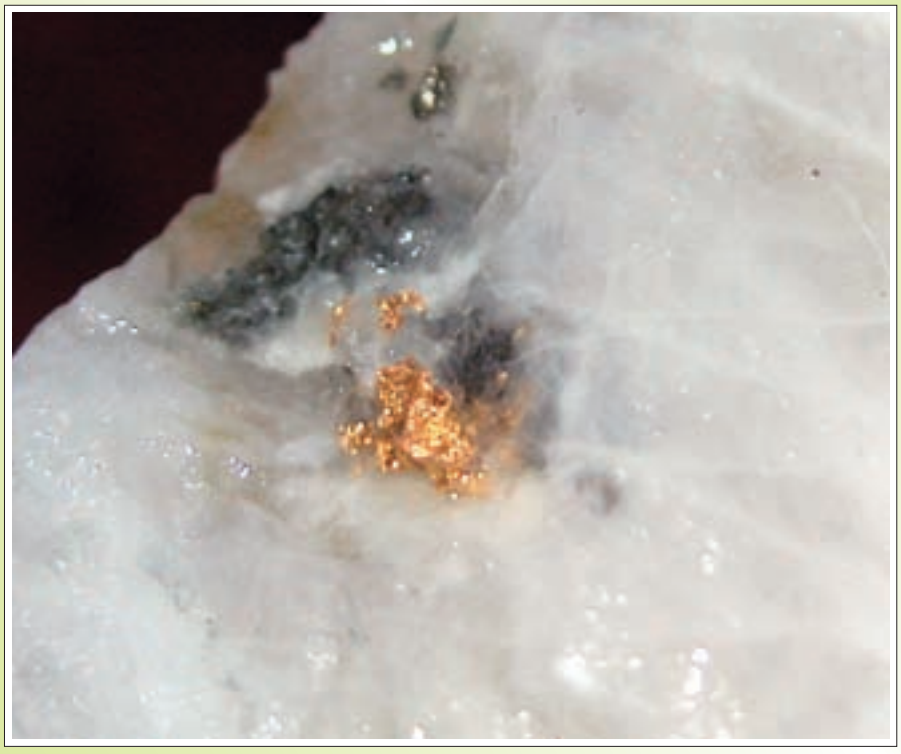

Gold from Mars pit, St Ives

5. RELATIONSHIP BETWEEN ALTERATION AND PHYSICAL PROPERTIES IN THE LAVERTON REGION

Executive Summary

Hand-specimen and downhole geophysical studies of rocks at two deposits, Wallaby and Sunrise Dam, in the Laverton region, Yilgarn Craton have been used to examine the trends of density and seismic velocity that are the result of alteration. In general, unmineralised alteration will increase the density of a given lithology, and alteration associated with mineralisation can either increase the density of a lithology, or marginally reduce it. Unmineralised alteration tends to moderately increase the seismic velocity of a lithology, although this depends on the exact alteration assemblage involved. Alteration associated with mineralisation generally maintains the seismic velocity of the unaltered rocks.

Rocks of the Yilgarn Craton are seismically anisotropic, usually up to approximately 15% anisotropic. The fabric that causes this anisotropy is not organised even at the deposit scale, with the most significantly organised fabrics directly associated with structures such as shear zones. Within these zones, anisotropy is very important, as the coherence of these structures means that seismic velocity varies with the dip of the structure. This variation in velocity controls the seismic reflectivity of a structure, although the strongest reflections are more likely to occur from density changes rather than large variations in seismic velocity.

Hand-specimen measurements of samples can provide very detailed and accurate measurements of seismic velocities but they are expensive and slow to perform. In order to obtain sufficient sampling to delineate alteration trends, it is recommended that a downhole geophysical survey be calibrated to a number of accurate hand-specimen measurements. In this case, the increased sampling of the downhole geophysical survey would augment the accuracy of the hand-specimens.

5.1 Introduction

As noted in Section 1, chemical alteration (by definition) alters the mineralogy of a rock. This change in mineralogy will also change the physical properties of the rocks. Understanding these changes in physical properties is a fundamental step in gaining an understanding of the potential changes in geophysical response over a mineral system.

The Laverton region is a world-class gold province (Huleatt and Jaques, 2005). Three major deposits (Wallaby, Granny Smith and Sunrise Dam) contain nearly 20 MOz of gold (Barrick Gold Corporation, 2006; Sung et al., 2007). There is probably potential in the region, with a vast prospective area underneath a large salt lake, Lake Carey (Figure 62). The Laverton region has a relatively large amount of seismic data2, both at the regional and mine scales. These data, along with geological mapping at many scales and potential-field data, have been used to constrain a regional architecture (Henson et al., 2006). There is also a need to understand some of the other features of the available seismic data, such as the possibility of imaging fluid pathways with seismic data. This has been hypothesised previously, both in the Laverton region (Section 2) and other localities in the Eastern Goldfields (Drummond et al., 2004b).

5.1.1 Wallaby

The Wallaby region, which contains the Wallaby and Granny Smith gold mines, is located approximately 25 km southwest of the town of Laverton and is situated within the Eastern Goldfields Province of the Yilgarn Craton (Drieberg et al., 2004). Total contained gold within the deposits is 7 MOz at Wallaby and 2.5 MOz at Granny Smith (Barrick Gold Corporation, 2006). Both the Wallaby and Granny Smith deposits are located within polymictic conglomerates (Salier et al., 2004), termed "late basins" (Champion and Cassidy, 2002).

Inferred from aeromagnetic data over the Wallaby mine is a magnetite-pyrite alteration phase within a pipe-like body and alteration to pyrite-pyrrhotite along mine-scale structures such as Thets Fault (Walshe et al., 2006). This magnetite pipe also contains considerable actinolite alteration; the overall alteration assemblage is actinolite-magnetite-epidote-carbonate (AMEC) in this pipe-like body. Alteration which is predominantly pyrrhotitic is inferred to be distal alteration of the ore-forming system at Wallaby.

2 Regional seismic data acquired by ANSIR, the National Research Facility for Earth Sounding; mine-scale seismic data acquired by ANSIR for the Minerals and Energy Research Institute of Western Australia (MERIWA) Project M363: *Feasibility of seismic methods for exploration of gold deposits in Western Australia.*

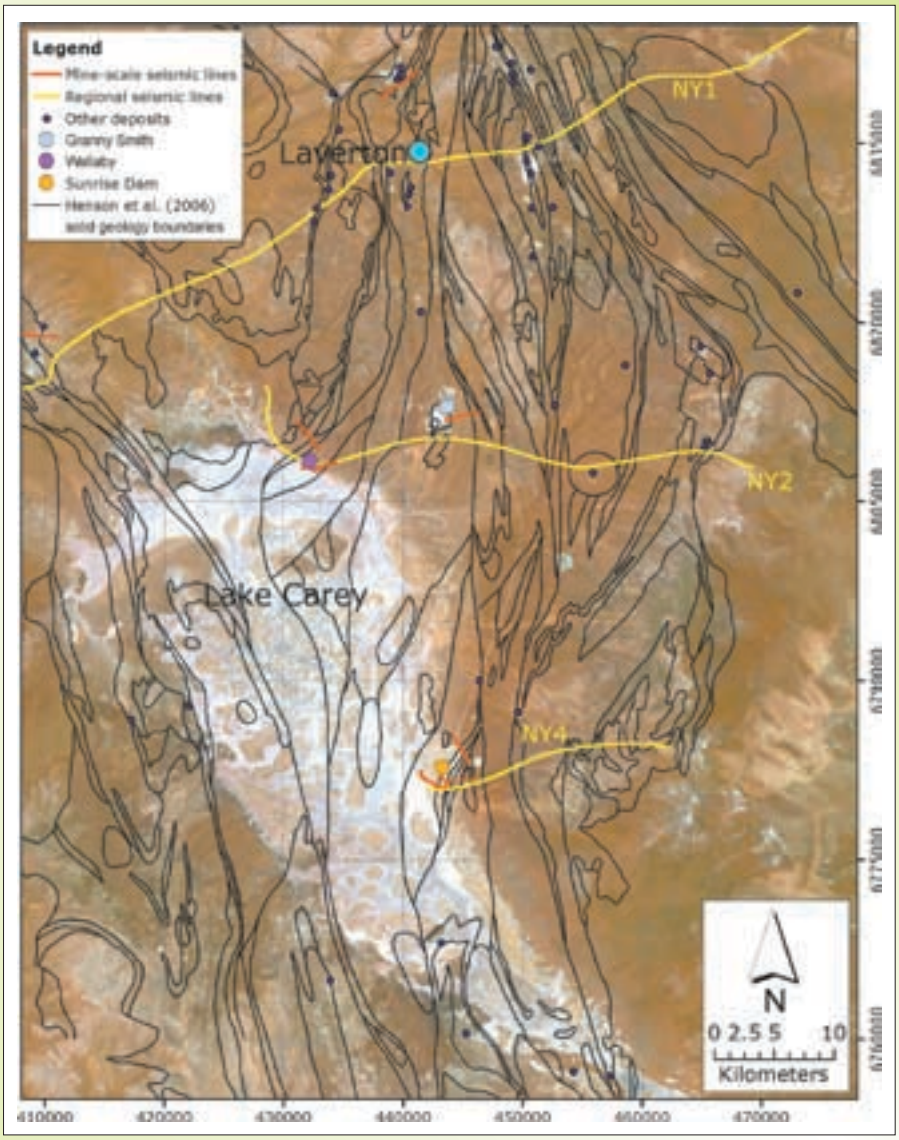

*Figure 62: Laverton region solid geology boundaries (from the **pmd***CRC Y4 project – Henson et al., 2006), regional seismic lines, mine-scale seismic lines and mineral deposits, draped over a Landsat visible-light image. The three major deposits in the region (Wallaby, Granny Smith and Sunrise Dam) are denoted by the three large coloured circles. The region to the west of Wallaby and Sunrise Dam is dominated by the salt-covered Lake Carey, which hinders exploration in this region.*

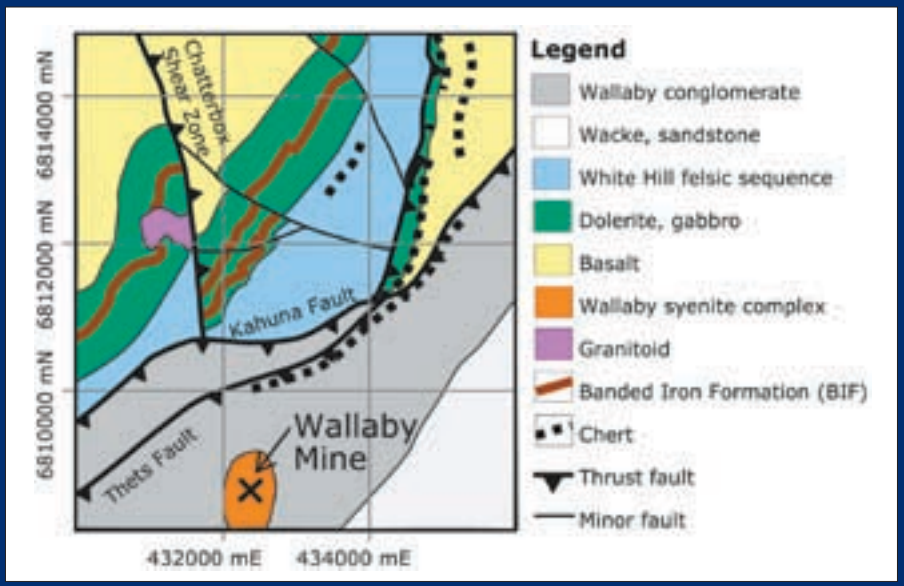

Figure 63: Solid mine-scale geology of the Wallaby mine (Standing, 2007).

5.1.2 Sunrise Dam

Sunrise Dam is the richest gold deposit in the Laverton region, with resources in the order of 10 MOz (Sung et al., 2007). The deposit is hosted in intermediate to felsic volcanic and sedimentary rocks (Newton et al., 1998). There are also magnetic shales, which historically were referred to as a banded iron formation (BIF). There is significant structural control at the deposit, with mineralisation associated with the shallow-to-moderately dipping Sunrise Shear Zone, and other shears parallel to it. The highest grades of mineralisation occur within zones of intersection of the steep-dipping high-strain shear zone structures and the more shallowly-dipping sericite shear zones (Miller and Nugus, 2006). The shears generally contain a shear-parallel fabric, and the multiply deformed host rock contains a fabric with no preferential orientation over the whole deposit (different host rocks and regions of the deposit retain features of various deformational events).

There are structural and stratigraphic differences within the deposit from north to south (Figures 65 and 66). In the northern region of the deposit, the main shear zones (such as the Sunrise Shear Zone) are shallowly dipping (25–35°) and dominate the mine-scale structures; in the southern portions these shears are complimented by more of the high-strain shear zones which are also steeper (60–90°). Stratigraphically, the northern portion of the deposit is dominated by a package which consists of basalt, diorite, andesite and magnetic shale. To the south, there are more intrusive bodies and andesite, and less basalt and magnetic shale (M. Doyle, pers. comm.). The greater number of the small-scale high-strain shear zones, as well as minor late faults, disrupts the stratigraphy and alteration zones in the southern region of the deposit.

5.2 Results

5.2.1 Wallaby

The two types of data for the Wallaby region are hand-specimen measurements and downhole geophysical logs. As there are different errors and calibration levels between the two types of measurements, the two types will be examined separately.

5.2.1.1 Hand-specimen results

Hand-specimen measurements for this region were obtained by two earlier studies, prior to ***pmd****CRC* Project A3. Both studies examined seismic velocity and density in selected drillholes from the Wallaby mine, and are unpublished results provided to PlacerDome. The first of these studies were measurements of 12 samples by Evans (1999), with the majority of the samples being from the Wallaby conglomerate, the major ore-hosting unit (Salier et al., 2004). The second study (Harrison, 2005) used the same

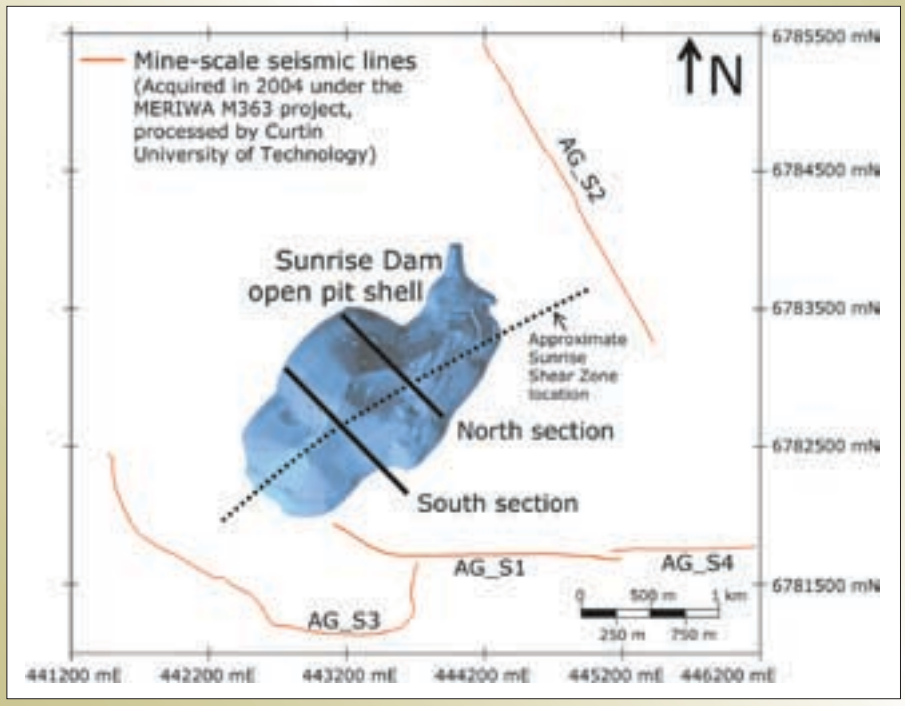

Figure 64: Map of Sunrise Dam showing the location of the mine-scale seismic lines and two schematic cross sections, for both the northern (Figure 65) and southern (Figure 66) regions of the deposit.

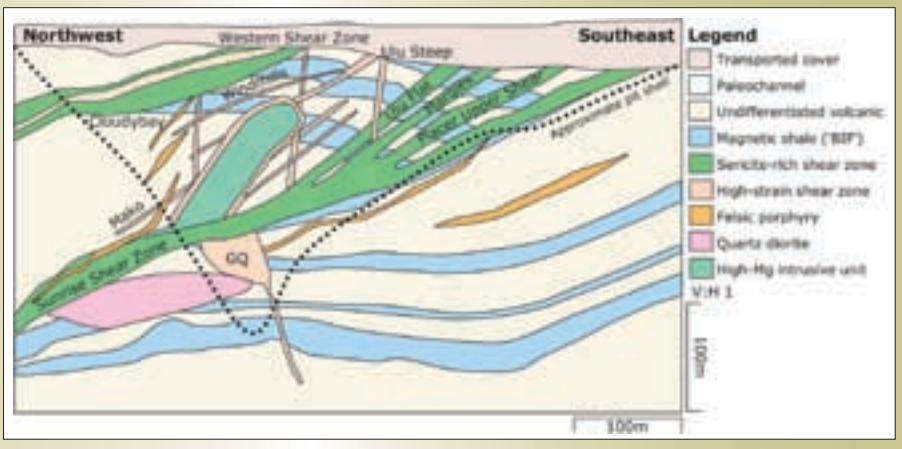

Figure 65: Schematic cross section (location – Figure 64) through Sunrise Dam for the northern region of the deposit (AngloGold Ashanti, 2002).

measurement apparatus and techniques as Evans (1999) and complimented the original 12 samples with a further 116 measurements. Described below are the techniques utilised by these studies to measure physical properties.

Density was determined using the displacement method of Emerson (1990). By comparing the mass of an air-dried sample (m_{dry}) and the same sample displacing water ($m_{displaced}$), the density is given by $m_{dry} / (m_{dry} - m_{displaced})$. This method does not account for porosity in the sample affecting the water displaced mass, so there are some errors associated with the porosity although, for typical crystalline rocks, these errors will be minimal (Emerson, 1990).

Seismic velocity for each sample was determined using a P-wave signal from two ultrasonic transducers, placed at either end of core samples which had been prepared with parallel faces (Rumel and Heerden, 1978). The input source frequency was ~30 kHz, with sample lengths of 50 to 230 mm and core diameters of 35-65 mm.

No external pressure was applied to the samples, and so the results could have slower than true P-wave velocities due to the presence of microfractures in the samples (Dolan et al., 1998).

A compilation of all available hand-specimen measured P-wave velocity and densities for the Wallaby region (Figure 67) indicates that some of the measured seismic velocities are well below those expected for most crystalline rocks (Ji et al., 2002).

The following effects could explain the large variation in seismic velocities:

- Weathering of samples
- Chemical alteration
- Anisotropy of velocities in minerals
- Micro- to small-scale fractures

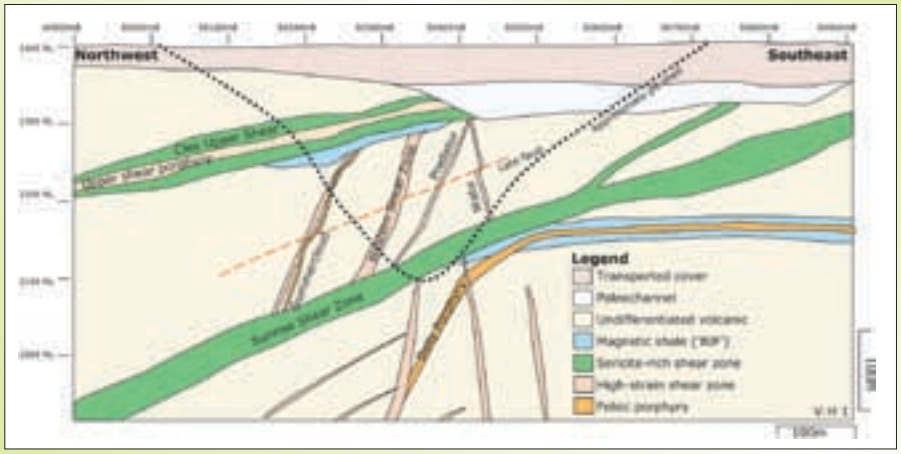

Figure 66: Schematic cross section (location – Figure 64) through Sunrise Dam, for the southern region of the deposit.

Both weathering and chemical alteration effects do not adequately explain this trend. All of the samples were well below the base of weathering and saprolite (around 125 m for this region – Anand and Paine, 2002) indicating that weathering cannot be the source of this velocity decrease. Weathering is also likely to decrease the density of samples (Emerson, 1990), which is not observed. Chemical alteration of the samples also does not explain the velocity trend, as there are no alteration minerals with sufficiently low velocities.

Mineral anisotropy may potentially explain some of the velocities observed. Some minerals, such as muscovite, have considerably slower propagation is one direction. For muscovite oriented with its single cleavage plane perpendicular to the direction of propagation of the seismic energy the velocity is ~4500 ms^{-1}, almost half as slow as the velocity of propagation (8500 ms^{-1}) of the energy parallel to its cleavage plane. Even taking anisotropy into account, however, there are no minerals which are sufficiently slow to explain some of the velocities observed for samples.

The presence of small-scale fractures will also decrease the measured seismic velocity. For the high frequencies utilised for the measurement of seismic velocities, very small fractures will impede the energy travelling through the samples and hence slow the measured seismic velocity are important (Dolan et al., 1998).

The most economically important geological unit at Wallaby is the Wallaby conglomerate. The majority of the densities observed for this unit are tightly clustered, although the seismic velocity is highly variable (Figures 68 and 69). The variations in seismic velocity can be attributed to the effects of small-scale fractures, discussed above, as well as alteration. To understand the physical property changes due to alteration, the median of each of the geological units was taken. The median was taken as, unlike the mean, it does not incorporate anomalous results such as the low seismic velocity due to small-scale fractures, and there are insufficient samples to calculate a modal sample (Fisher, 1970).

A large-scale alteration feature at Wallaby is the actinolite-magnetite-epidote-calcite (AMEC) pipe which lies beneath the deposit. The magnetite within this body results in a distinct magnetic anomaly over the deposit (Salier et al., 2004). The hand-specimen results available for Wallaby (Figure 68) also indicate that this pipe may be very slightly denser and seismically faster (Figure 69) than most of the least altered conglomerate, although measurement errors and an insufficient number of samples mean that this trend is probably undersampled. There are two samples

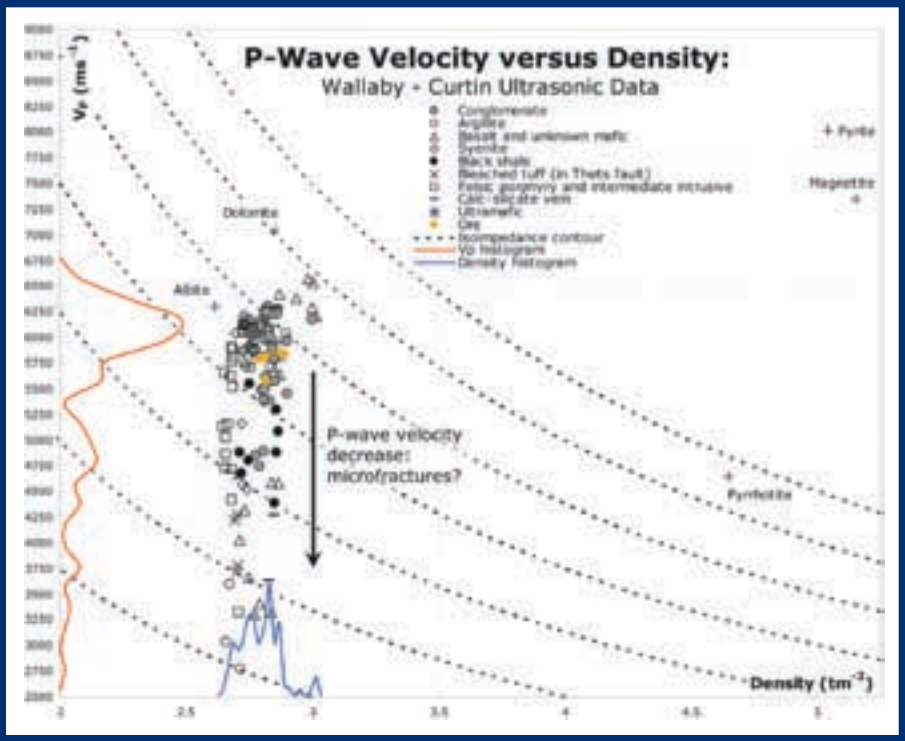

Figure 67: Seismic velocity-density relationship for hand-specimens in the Wallaby region.

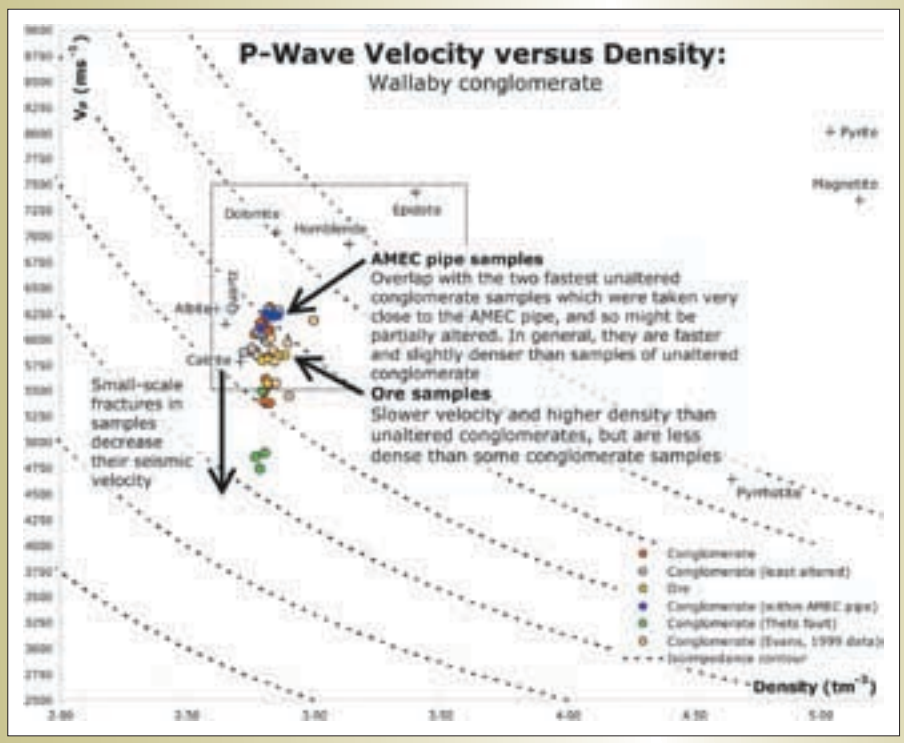

Figure 68: Seismic velocity-density relationship for all hand-specimen samples of the Wallaby conglomerate. Note the differences between the unaltered conglomerate samples, the AMEC pipe samples, and the ore samples. Dashed box denotes position of Figure 69.

of least altered conglomerate which are faster and similarly dense as the AMEC pipe samples, but these samples are positioned close to the AMEC pipe and thus may represent a physical property affinity closer to that of the AMEC pipe. The physical properties are as expected for alteration to an AMEC assemblage, noting that the seismic velocity and density of hornblende is used to approximate those of actinolite due to a lack of measurements of the seismic velocity of actinolite.

Samples of ore hosted in the Wallaby conglomerate indicate that they have a slightly higher density and a lower seismic velocity than the least altered conglomerate (Figure 69). This is in contrast to the downhole density measurements for Wallaby (Section 5.2.1.2), but may result from insufficient sampling of the least altered conglomerate, the ores, or both. The lower seismic velocity is most likely due to a combination of small-scale fractures reducing the measured seismic velocity, and the gold-related alteration.

There are two trends evident for the ore samples. The median ore sample has followed a trend away from the least altered samples, to lower velocities. This trend could be attributed to fracturing of samples. As ores represent some of the most altered regions of a deposit, and contain brittle minerals such as quartz, they possibly contain more fractures. If we examine all of the ore samples, however, there is a definite trend to higher velocities for higher densities, with the exception of a single sample which shows an anomalously low seismic velocity and thus may represent a fractured sample. This second trend does not start at the properties of the unaltered conglomerate due to the velocity decrease from the fracturing of samples.

Some samples had no alteration noted in their original study. These samples probably represent a whole suite of various alteration types. Some of these samples show properties very similar to the least altered conglomerate samples, some have properties similar to the ore samples, and some similar to the AMEC pipe samples. In some cases, these samples show considerably higher densities, for example, one sample from Evans (1999) study has a density of 3.0 tm^{-3}, 0.1 tm^{-3} greater than any other sample. These samples may represent more altered samples, or unmineralised alteration such as epidote alteration, but without alteration data logged for these samples these interpretations cannot be drawn.

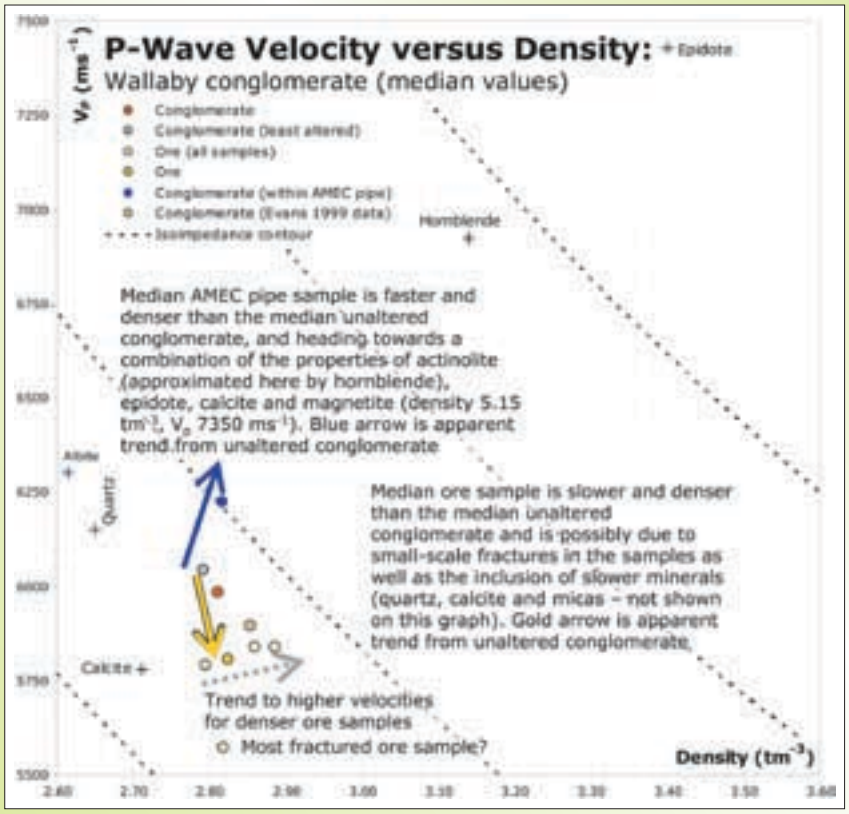

Figure 69: Seismic velocity-density relationship for the median values of all hand-specimen samples of Wallaby conglomerate. Note that this figure is a subset of Figure 68.

5.2.1.1.1 Seismic velocity model of alteration

Salier et al. (2004) proposed a model (Figure 70) for the entire Wallaby deposit, with the following units:

- Regolith
- Gold-related alteration of the conglomerate
- AMEC alteration of the conglomerate
- Syenites which intrude the conglomerate
- Unaltered conglomerate, which has been regionally metamorphosed to include chlorite and calcite.

The available hand-specimen data (Figures 67–69) are sufficient to define the densities and seismic velocities for these materials (Table 7). From these data the acoustic impedance, which is the physical parameter that determines seismic reflections, can be calculated.

By digitising the alteration model (Figure 70) and then attributing the units according to these properties a model of acoustic impedances was produced. This model was discritised into 5 x 5 m cells, with each cell's acoustic impedance derived from the digitising of the alteration model. A vertical reflection coefficient model (Figure 71) was then calculated from the acoustic impedance model by the relationship R_a (reflection coefficient for model cell $a) = \frac{Z_a - Z_b}{Z_a + Z_b}$, where Z_a and Z_b are the acoustic impedances of cells a and cell b, respectively, with cell b directly beneath cell a.

The reflection coefficient model indicates where reflections will occur – for this particular alteration model and the observed physical properties, reflections will occur from all interfaces although they will vary considerably in strength. The strongest reflection will occur from the regolith-bedrock interface. The next strongest reflections are those from the gold lodes and the dipping syenites – with a reflection coefficient of ~0.04, these features have the potential to be imaged, although the ambient seismic noise will dictate the resolvability of these features. The weakest reflections would come from the unaltered country rock and the sides of the AMEC pipe, although with a reflection coefficient of 0.02, this will be a very weak reflection.

A suitably large reflection coefficient is only part of the requirement for a seismic reflection to be imaged. A reflector needs to be at least one-quarter the thickness of the seismic wavelength to image both its top and bottom. Destructive interference of the reflection from the top and the bottom of a unit will reduce the amplitude of any

Unit	Median density (tm^{-3})	Median Vp (ms^{-1})	Acoustic impedance ($tm^{-2}s^{-1}$)
Regolith	2.2	2000	4400
Ore	2.83	5806	16430.98
AMEC pipe	2.82	6225	17554.5
Syenite	2.74	5865	16070.1
Regional chlorite-calcite alteration	2.79	6043	16859.97

Table 7: Densities, seismic velocities and acoustic impedance (the product of density and seismic velocity), derived from hand-specimen measurements (Figure 69).

reflection should it be thinner than this. Typical seismic reflection surveys in the Yilgarn have a majority of their energy occurring at a frequency of 50 to 60 Hz (Goleby et al., 2003); at a crustal velocity of 6000 ms^{-1}, the seismic wavelength will be between 100 and 120 m long. Therefore, to image the top and the bottom of a gold lode, it would need to be at least 30 m thick – none of the lodes in the alteration model are this thick. The complex interference patterns created by a number of thin but close gold lodes, as well as the dipping syenites, will create a zone of moderate reflectivity which may be difficult to interpret in a seismic section. Due to the dip of the syenites and the AMEC pipe, any seismic line over the Wallaby deposit would also need to be much longer than the zone of interest – for the ~1.4 km wide model above, a seismic line of at least 5km in length would be required to ensure correct migration of data at the depths of interest, and to ensure that dipping features were correctly imaged (Goleby et al., 2003).

5.2.1.2 Downhole geophysical results

The downhole geophysical results from Wallaby are derived from a single drillhole, WBAD047. This drillhole was chosen as it is relatively deep (> 400 m), has excellent gold intersections (including 5 m @ 5 gt^{-1}, and two intersections of 2 m @ 12 gt^{-1}), and samples a number of alteration assemblages. The downhole measurements used here are density (logged using the gamma-gamma technique) and P-wave velocity (measured by travel times between transducers on the downhole probe). The hole mainly penetrates the Wallaby conglomerate, but does intersect felsic porphyry. The top ~125 m of the drillhole samples regolith materials. These materials range from transported clay at the top of the hole to saprock, representing the base of oxidation.

Downhole geophysical results are often not comparable with hand-specimen measurements, as they sample different scales of features, are subject to calibration errors, and may have spurious results caused by fracturing or wall collapse (Fallon et al., 1997), with the largest errors generally due to calibration differences (Emerson, 1990). To examine if there are any calibration issues between the hand-specimen and downhole measurements, the frequency histograms of a property, such as density, can be examined (assuming they have sampled similar rocks).

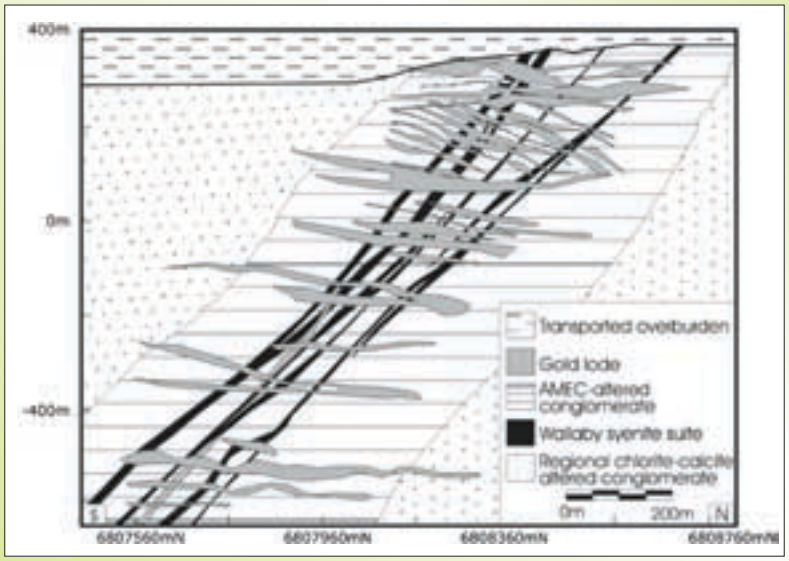

Figure 70: North-south cross-section depicting an alteration model for the Wallaby mine (Salier et al., 2004), along 432330 mE.

Figure 71: Vertical reflection coefficient cross-section, derived from Salier et al. (2004)'s alteration model for Wallaby and the hand-specimen density and seismic velocity measurements. Note that this figure is not a synthetic seismic section. Broadly speaking, a reflection coefficient greater than 0.06 or less than -0.06 will produce a strong reflection (Salisbury et al., 2000); the sign indicates the phase of the reflection, either positive (in phase with the incoming seismic signal) or negative (out of phase with the seismic signal). Shown by the key are simplified reflection strength classes, based on this rough rule of thumb. The model indicates that there will be a particularly strong reflection from the base of the regolith, moderate reflections from the gold lodes and the dipping syenites, and weak reflections from the sides of the AMEC pipe. This is assuming, of course, suitable signal to noise in the seismic survey, and that the frequency content of the incoming seismic signal is suitably high (the longer the wavelength, the thicker that a reflector needs to be in order to be imaged).

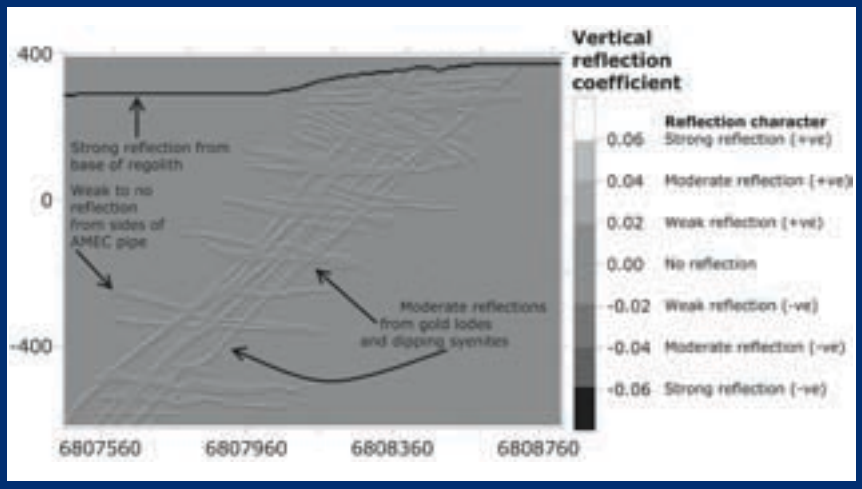

If there are no calibration errors, the distributions should be similar. If there is a range difference between the two distributions, there may be a calibration scale error; likewise, if there is an offset between any measure of central tendency (such as the median or the mode) of the two distributions, then there may be a calibration level error.

By comparing the histograms for the density (Figure 72) and seismic velocity (Figure 73) measured for the hand-specimen measurements to those measured by downhole logging, it is apparent that there is a difference in the centres of the two largest peaks in the histograms. This suggests there is an offset between the properties measured for hand-specimens compared with the downhole measurements. As there are no hand-specimen measurements for this hole, there is no certainty regarding the nature of the errors between these two measurement types. By comparing relative changes between different alteration types measured downhole, the effect of any errors in the measurements are minimised.

To simplify this comparison, we will use box-and-whisker plots, with the 'whiskers' highlighting the minimum and maximum of any property for a given alteration type. The box itself spans the 25th to 75th percentile, with a line marking the median (Figure 74). The median is used as it represents a measured middle value, unlike the average ((Fisher, 1970). This can be important for samples which mainly are low-density, but also feature high-density outliers.

5.2.1.2.1 Density

The density results (Figure 75) indicate that, as expected, there are distinct differences in density between the regolith and the bedrock at Wallaby. There is also a clear trend with overburden (transported clays, gravels and the like) the least dense, and laterite and saprolite (which includes saprock[3]) around 20% denser than the overburden. Laterite has a slightly higher median density but a lower maximum density than saprolite. This is most likely due to saprock, which is the densest of all Wallaby regolith, unsurprising as it represents the least weathered material.

3 Saprock is partially oxidised rock, with saprolite completely oxidised rock (Anand and Paine, 2002). It may be possible to identify the primary lithology of saprock, but generally not saprolite.

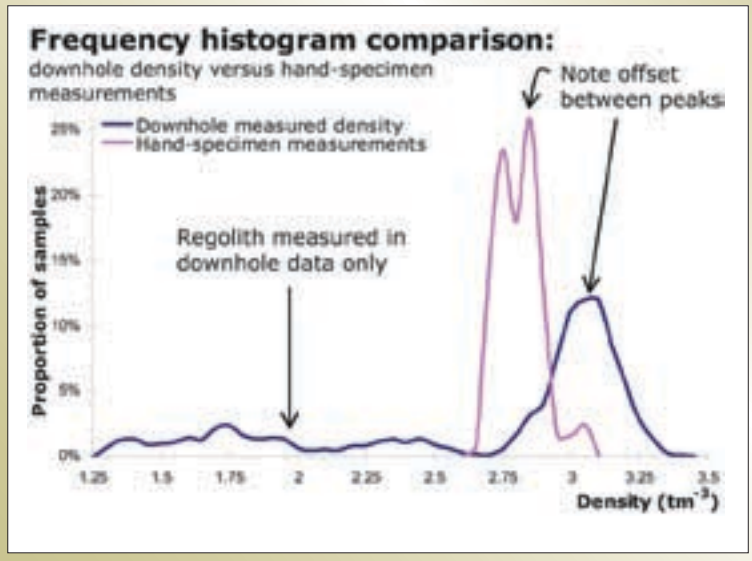

Figure 72: Comparison between the density frequency histogram for the hand-specimen and downhole data. There is an offset between the peaks of the two distributions, indicating that there is at least a calibration level shift between the two datasets.

The felsic porphyry samples are less dense than the majority of the conglomerate samples. Indeed, the only samples of conglomerate with lower density than the felsic porphyry samples is the chlorite altered conglomerate, as this occurs entirely as saprolite. The assorted conglomerate samples, which include sericite-carbonate-fuchsite alteration, are also of comparable density to the felsic porphyry samples, and again this is due to weathering. To remove the effects of weathering, samples were filtered to only include those that occur at greater than 125 m downhole depth (Figure 76), the approximate base of oxidation[4].

4 In the geological logging of WB047AD, 125 m is recorded as the base of oxidation, but saprock is logged below this depth, suggesting that partial oxidation could still be present.

The filtered samples show that there are density differences which we can attribute to alteration, including mineralisation. On average, conglomerates which are altered but unmineralised show higher median densities than mineralised conglomerates. The conglomerate samples associated with the highest gold grades are the sericite-carbonate-fuchsite samples, included in the "conglomerate, assorted" class. This class also shows the lowest median density of all conglomerates. This is in contrast to the hand-specimen results which suggest that there is a very small density increase of ore samples. This result may be due to the limited sampling in the hand-specimen studies. This disagreement between the hand-specimen and downhole results does not affect the Wallaby seismic

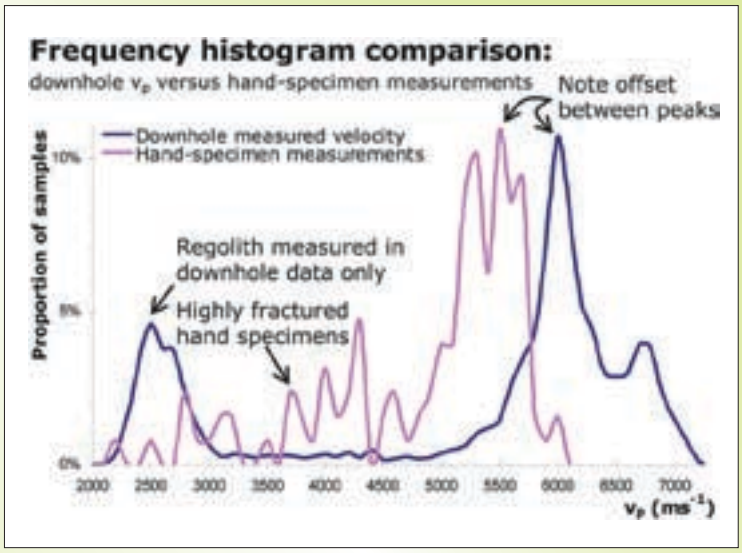

Figure 73: Comparison between the density frequency histogram for the hand-specimen and downhole data. There is an offset between the peaks of the two distributions, indicating that there is at least a calibration level shift between the two datasets.

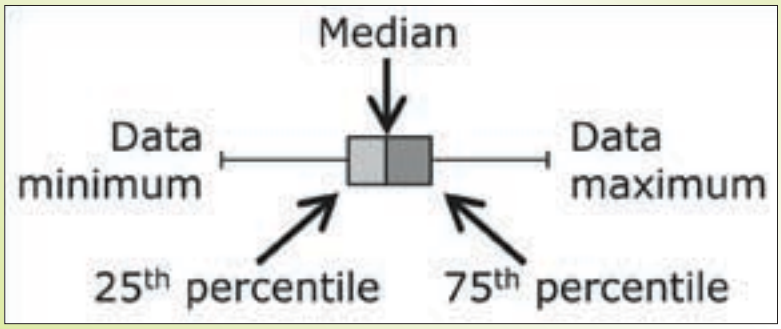

Figure 74: Key to interpreting the box-and-whisker plots used in this section. The 'whiskers' represent the entire data range and the sides of the boxes represent the 25th and 75th percentile respectively. The median of the data is shown by the line separating the two differently shaded portions of the box.

model which was derived from the hand-specimen measurements (Figure 71) as a lower density for ores in this model will only increase the reflectivity of the ores with respect to the AMEC pipe, which is already high.

The epidote-altered samples have the highest median density, which corresponds to the high density result observed for the AMEC pipe samples in the hand-specimen results. The largest range of densities occurs for the chlorite-calcite altered conglomerates; this may be due to partial oxidation, as the least dense samples of this alteration type occur very close to the 125 m downhole depth that was used as a rough guide to the base of oxidation, based on the geological logging of WB047AD.

As was noted for the unfiltered data, the felsic porphyry samples, which are also mineralised in this drillhole, show significantly lower densities than the samples of conglomerate.

5.2.1.2.2 Seismic velocity

As for the density results (Figures 75 and 76), the seismic velocity results for drillhole WB047AD show that there is a distinct contrast between the seismic velocity of the regolith and the bedrock (Figure 77). Samples which include some weathered material, such as the assorted conglomerate, also have some very low velocities. This indicates, as per the results for the seismic response of the hand-specimens, that the regolith-bedrock interface will produce a very strong seismic reflection. As the seismic velocity response of weathering is so significant (involving velocity changes in the order of 300%), the best trends of velocity due to alteration will only be apparent when we filter out most of the weathered samples (Figure 78).

There is less partitioning between the seismic velocities for mineralised versus unmineralised samples than for density, although there are some apparent trends. The densest alteration type (epidote-altered conglomerate) also shows the highest median velocity. The second fastest alteration type (of the conglomerates), the quartz-carbonate-sericite-hematite alteration, is only marginally (2.7%) slower than the epidote alteration. This alteration type is faster than the comparable quartz-sericite-carbonate alteration; the velocity difference between these two types is most likely due to the inclusion of hematite (seismic velocity 6550 ms^{-1}: Salisbury et al., 2000), which will increase the seismic velocity of this alteration assemblage.

Figure 75: A box-and-whiskers plot of downhole-measured density for all materials with N ≥ 30 samples. The "conglomerate, assorted" group includes two different types of predominantly sericite-carbonate-fuchsite alteration. Alteration mineral key is given in Table 2.

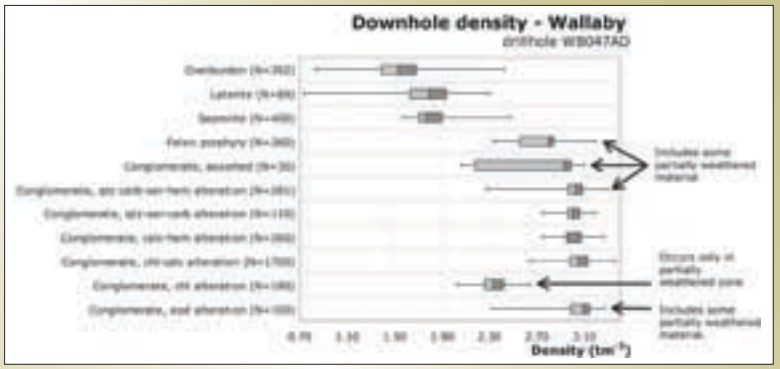

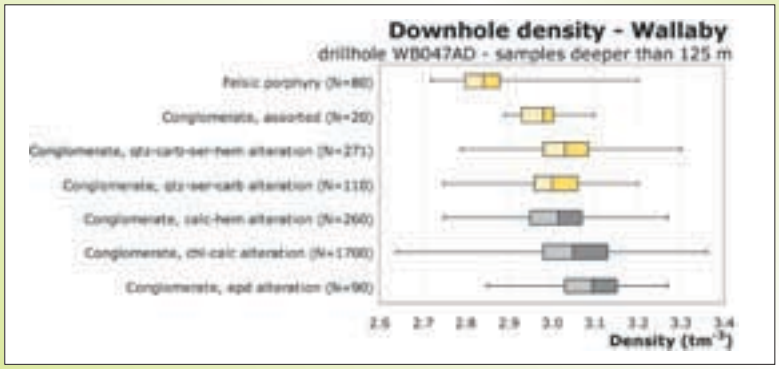

Figure 76: Box-and-whiskers plot depicting the densities, occurring greater than 125 m downhole depth in drillhole WB047AD, of felsic porphyry and various alteration of the Wallaby conglomerate occurring greater than 125 m downhole depth. The gold-coloured boxes are those groups associated with mineralisation. The alteration mineral key is given in Table 2.

The most mineralised conglomerate, the assorted conglomerate type, shows the lowest seismic velocity. As this alteration assemblage is predominately sericite-carbonate-fuchsite, this is unsurprising, as these minerals have low P-wave velocities (Christensen, 1989). The mica sericite in this alteration assemblage may also be oriented such that its cleavage plane is approximately perpendicular to the drillhole; this would result in the slowest apparent seismic velocity if measured downhole. This orientation would be due to the preferential orientation of the micas due to structural controls, such as the orientation of shear zones. Other alteration assemblages that include sericite may have less preferential orientation of the single cleavage plane of the mineral.

5.2.1.3 Summary

- The Wallaby conglomerate is a dense (2.8–3.0 tm^{-3}) and seismically fast unit (5800–6200 ms^{-1}), which is comparable with intermediate to mafic rocks elsewhere in the Yilgarn Craton (such as St Ives, see Section 3.2).
- Hand-specimen measurements show two trends due to alteration in the Wallaby conglomerate: a trendto higher velocities and higher densities due to the AMEC-related alteration, and a trend to higher densities with a very slight increase in seismic velocity, related to mineralisation of the Wallaby conglomerate.
- The gold-lodes and syenites have a small velocity contrast to the AMEC pipe, indicating that they may be imaged as very weak reflections on small-scale seismic sections. The reflections from these units may be particularly complex due to their geometries.
- Downhole geophysical measurements indicate that alteration can increase the densities and seismic velocities of the Wallaby conglomerate, although the gold-related alteration generally is of lower densities than altered but unmineralised conglomerates. Seismically, the mineralised alteration is slower than unmineralised alteration, although the inclusion of small proportions of fast minerals, such as hematite or sulphides, will change this balance as the velocity contrasts are generally small (~2-5%).
- The disparity between the hand-specimen and downhole logged densities for gold-related alteration may result from insufficient sampling – a number of hand-specimen measurements that had no alteration

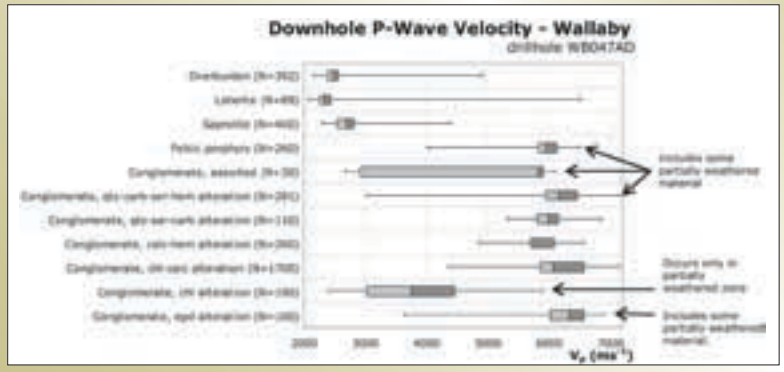

Figure 77: A box-and-whiskers plot of downhole P-wave velocities for all materials in drillhole WB047AD, with >30 samples. The "conglomerate, assorted" group includes two different types of predominantly sericite-carbonate-fuchsite alteration. The alteration mineral key is given in Table 2.

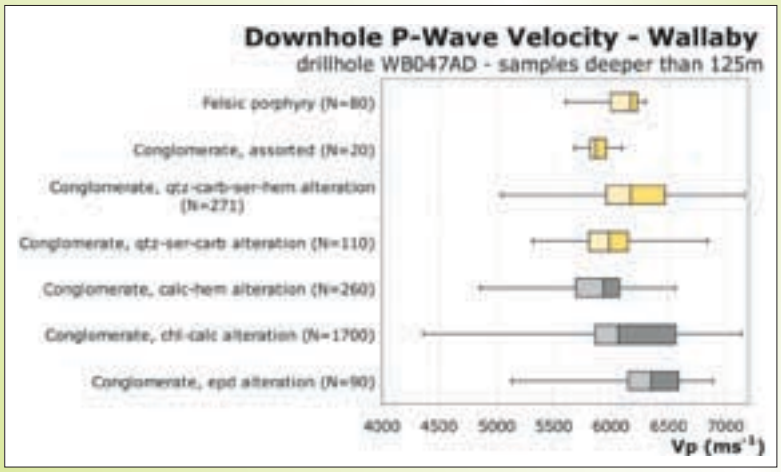

Figure 78: Box-and-whiskers plot depicting the downhole P-wave velocities of materials occurring greater than 125m downhole depth, drillhole WB047AD. The gold-coloured boxes are groups with mineralisation. The alteration mineral key is given in Table 2.

type recorded in the original study are denser than the samples of ore. Furthermore, if the gold-related alteration does have a lower density than the least altered conglomerate (as suggested by the downhole density results), then gold lodes would present a more significant density contrast and hence also an acoustic impedance contrast to the AMEC pipe they lie within. If hand-specimen and downhole measurements were performed for the same hole, then these two datasets could have been combined to increase the sampling as well as the accuracy.

5.2.2 Sunrise Dam

To examine the relationship between the seismic velocity and density and alteration at Sunrise Dam, hand-specimen measurements of samples, obtained from both the open-pit and underground operations at Sunrise Dam, were undertaken at the Geological Survey of Canada (GSC)-Dalhousie High Pressure Laboratory, Halifax. Measurements were performed by Matthew Salisbury (Geological Survey of Canada) and staff. By using a pressure apparatus with jacketed samples (Figure 79) this laboratory is capable of applying pressure to cores taken from hand-specimens, closing any microfractures in the samples. This avoids the problems of anomalously low velocities, as measured for the unconstrained samples from Wallaby (Figures 67–69). Note that the seismic velocity varies with pressure due to the response of the elastic moduli of the sample to pressure (Figure 80), as well as due to the closure of microfractures. Measurements were made to 600 MPa; for this study we use an applied pressure of 200 MPa to compare velocities. 200 MPa measurements are also traditionally used for the laboratory measurements of minerals (Christensen, 1989).

High-pressure velocity measurements are primarily undertaken to understand the seismic velocity at great depths in the Earth (Christensen and Mooney, 1995), but have also been undertaken to define the seismic response of alteration around nickel mines in Canada (Salisbury et al., 2000).

The majority of samples measured at Sunrise Dam plot within a very restricted range (Figure 82). This is because most of the samples measured are either little altered felsic to intermediate volcaniclastic rocks, or felsic to intermediate porphyries. The similar mineralogy of these samples produces relatively similar seismic velocity and density relationships. Contrasting to this is the increase in density with little increase in seismic velocity that is evident for the most altered samples and the magnetic shale samples. This increase may be due to alteration to quartz-pyrite-magnetite, a common mineralised assemblage throughout the Yilgarn Craton (Hagemann and Cassidy, 2001; Neumayr et al., 2003; Walshe et al., 2006).

The change in seismic velocities and densities for moderately altered samples, corresponding to poorly mineralised rocks, is more difficult to determine; to do so we will examine the relationship between density, seismic velocity and alteration for the samples of felsic porphyry (Figure 83) and andesite (Figure 84) separately.

The density of the background chlorite-calcite altered porphyries and those showing minor alteration (background alteration with a very small proportion of

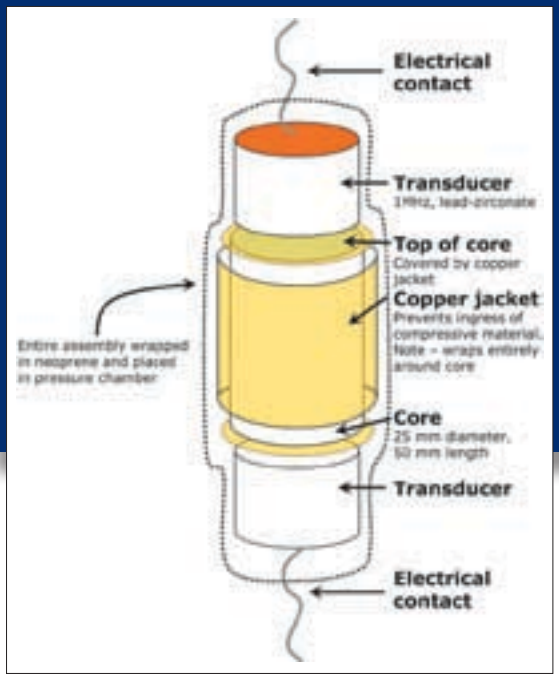

Figure 79: Schematic diagram of the apparatus at the GSC-Dalhousie High Pressure Laboratory. In this configuration, with transducers at either end, Vp can be measured. Measurements are made on jacketed samples, placed within a 7-tonne double-walled vessel. Samples are cores with a diameter 25 mm, and up to 50 mm in length. Pressures up to 1.4 GPa are able to be applied to the ends of the cores, allowing analysis for how confining pressure changes the seismic velocity (Figure 80). The transducers in the apparatus operate at 1 MHz. The obtained accuracy for Vp is 0.5%, and density can be determined to ± 0.005 tm-3. Shear wave velocities are also obtained but not discussed in this report. To measure foliated samples, cores are obtained both parallel and perpendicular to the foliation (Figure 81).

sulphides, and possibly some additional mica such as muscovite) are very restricted, with the density ranging from 2.75 to 2.78 tm^{-3} (Figure 83). The seismic velocity anisotropy of these porphyries is around 8–9%. Typically, a pure sample of mica will have an anisotropy of around 40–50% (Ji et al., 2002), and a velocity range of between ~4.5 and 8.0 kms^{-1}. These values explain the gross velocities of all of the felsic porphyry samples. Of note is that SRD203 is always faster than sample SRD204 which is not explained by preferential orientation of micas. A petrological study of the mineralogical differences between these samples would be the best method to determine the differences between these samples, resulting in the velocity variations observed.

In contrast with the samples of felsic porphyry, there are more density variations for the andesites of low to moderate alteration (Figure 84). Predominately, the lowest densities are observed for samples of the background altered andesite, and the highest density for samples of moderately altered (predominately pyrite, and epidote) andesite.

Figure 80: Variation in P-wave velocity with respect to confining pressure for sample SRD003xy (Figure 81). Two dashed lines are superimposed on the graph, highlighting the two trends in seismic velocity with respect to pressure. The line marked by short dashes is a least-squares best fit for the sample measured at confining pressures up to and including 60 MPa; it shows the increase in velocity due to the closing of microfractures. The line marked by the longer dashes is a least-squares fit for the sample measured at 80 to 600 MPa, and shows the increase in velocity purely due to compaction of the sample. The measured data is a combination of these two trends. Note that the velocity at 0 MPa, that is, measured as per the hand-specimen measurements for Wallaby, would be approximately 6020 ms^{-1}, an error of around 4.6% with respect to the velocity at 200 MPa (6300 ms^{-1}).

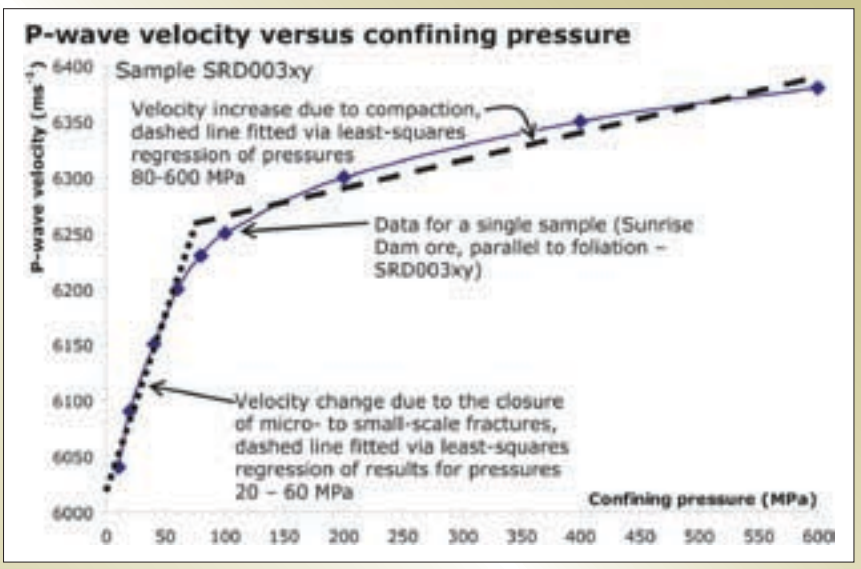

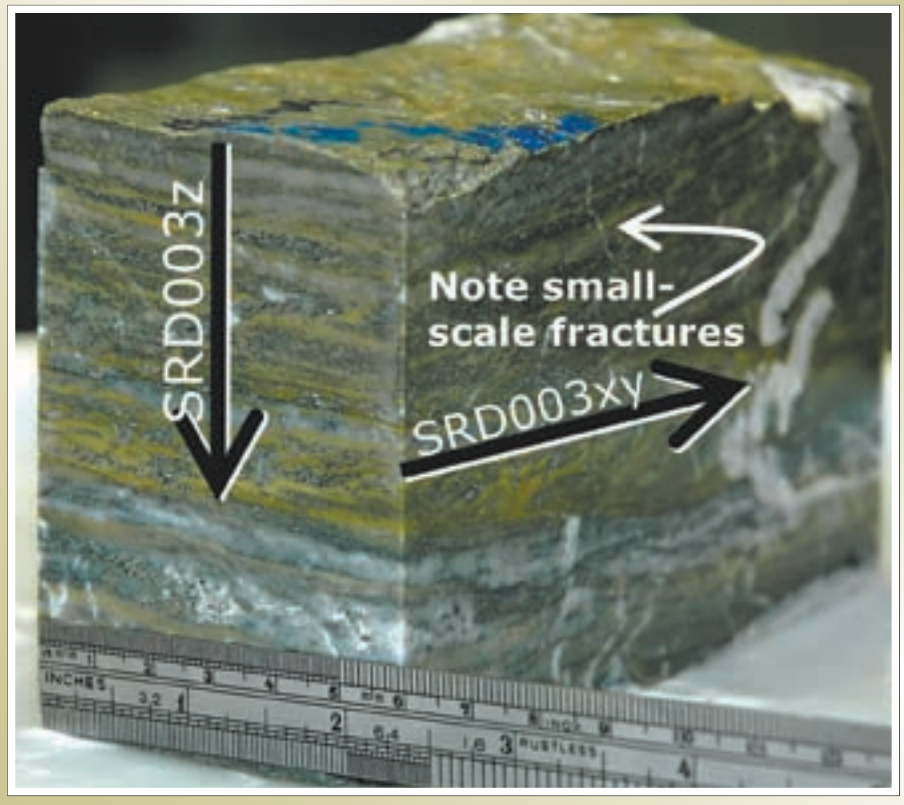

Figure 81: Sample SRD003, showing the orientation and approximate positions of cores extracted from the sample. Sample SRD003xy is obtained by extracting a core along the foliation, and SRD003z is obtained by extracting a core perpendicular to the foliation. This nomenclature (xy and z) is used for all samples which were measured for anisotropy. Care is taken to ensure that the cores accurately represent all the material in the entire sample.

Figure 82: P-wave velocity (measured at 200MPa confining pressure) versus density for all hand-specimens from Sunrise Dam. The limited field (dashed oval) is where the majority of samples measured plot. Note that the moderately altered samples plot within this field. These moderately altered samples measured at Sunrise Dam tended to contain variable amounts of sulphides (mainly pyrite), and the background altered samples tended to have lower amounts of sulphides. The highly altered samples follow a trend highlighted by the orange arrow, which is to higher densities with only a minor change in seismic velocities. The increases and decreases in velocity with no change in density is due to seismic anisotropy – in all cases, the fastest velocities were obtained parallel to the fabric in the rock, and the slowest perpendicular to this fabric.

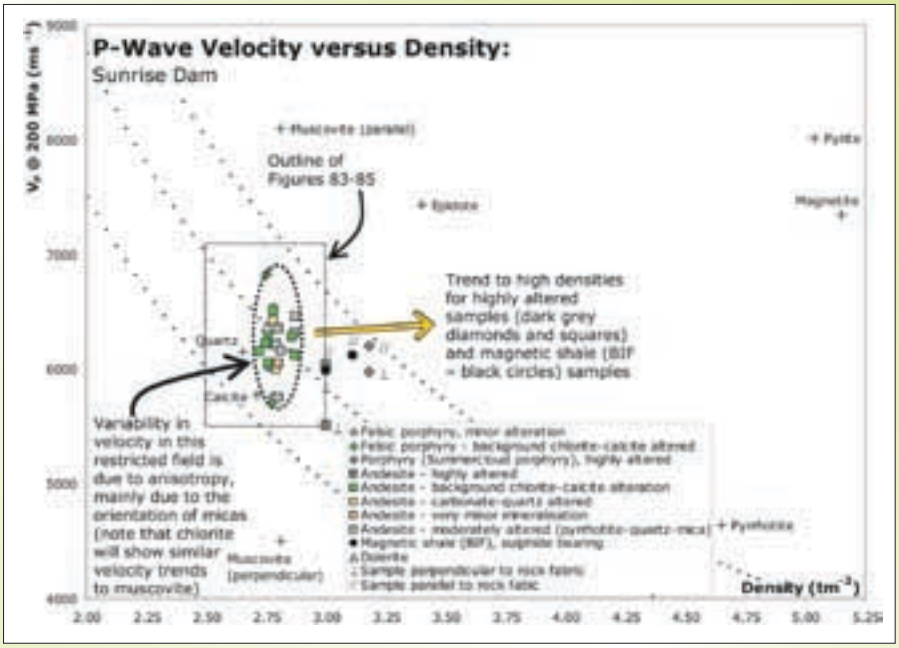

One background altered andesite (SRD215) has a density very similar to the densest moderately altered andesite. Additional sampling would be required to confirm the overlap in densities between these different alteration types. The carbonate-quartz altered samples also may have a density that is slightly higher than the background altered andesite, an anomalous result as both quartz and calcite are lower density than the background altered andesite. The carbonate-quartz alteration is associated with minor sulphides, which could explain the elevated densities.

Seismically, the samples of andesite indicate that this unit is less anisotropic than the felsic porphyry. To understand the seismic velocity trends due to alteration, and to produce a realistic velocity for each alteration type, the average of the density and velocity for each of the rock and alteration types was taken (Figure 85). The average is used as all the measurements of the fabric should be included to provide a realistic velocity for each rock and alteration type.

The average velocities suggest that the moderately altered andesite, which includes additional epidote and pyrite, is slightly faster than the background altered andesite. There are small velocity decreases for carbonate-quartz and andesites with very minor alteration. The minor altered felsic porphyry samples, however, have a higher velocity than the background altered felsic porphyry, suggesting that there are chemical differences between the andesite and felsic porphyry which result in different alteration mineralogy, even at low levels of alteration.

Taking the average of the seismic velocities also provides a measure of the expected background velocity variation. Structural studies at the deposit suggest that the fabric in shear zones is considerably more organised than the fabric of the background rocks (Miller and Nugus, 2006); thus the seismic velocity of the background altered and low level alteration types can be simulated by using the average of each of the alteration types. The seismic response of a shear zone thus depends on its orientation to the incoming seismic energy, and the background can be assumed to be a uniform velocity, with the velocity dependant on the lithology the shear zone intersects. To a first order, a 'stacked' seismic section simulates a section where the seismic energy has only traversed the crust with vertical incidence, and we can use this to produce a simple model of seismic reflections from a shear zone

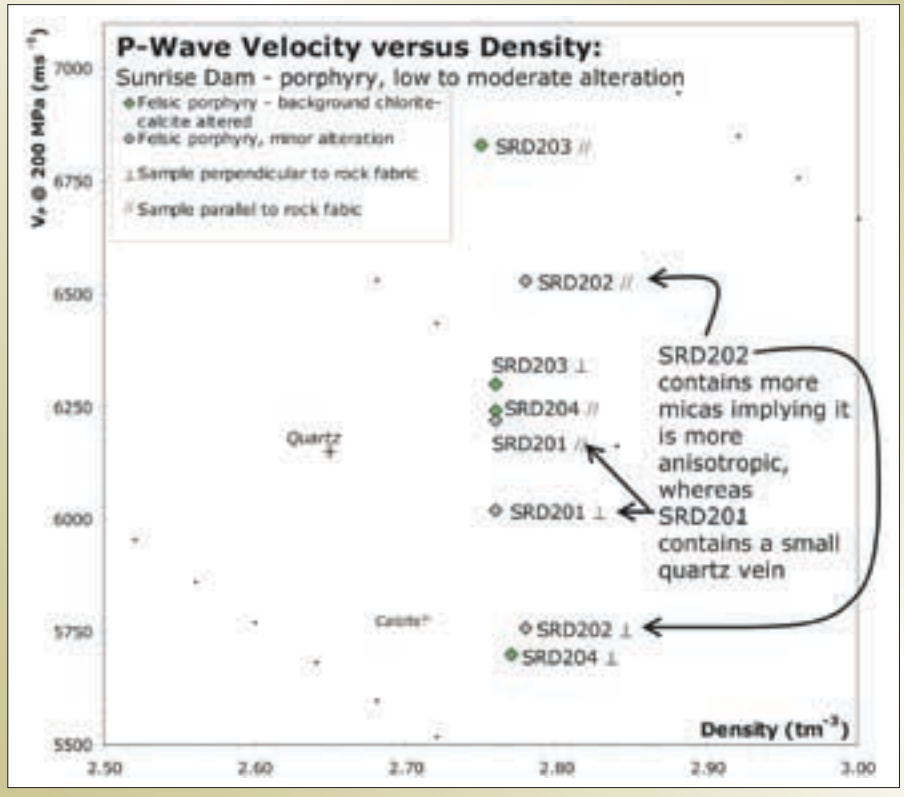

Figure 83: Samples of low to moderately altered felsic porphyries. The large variation in velocity is due to anisotropy of the samples, predominately the result of the regional chlorite alteration. This is a detailed view of the dashed rectangular area in Figure 82.

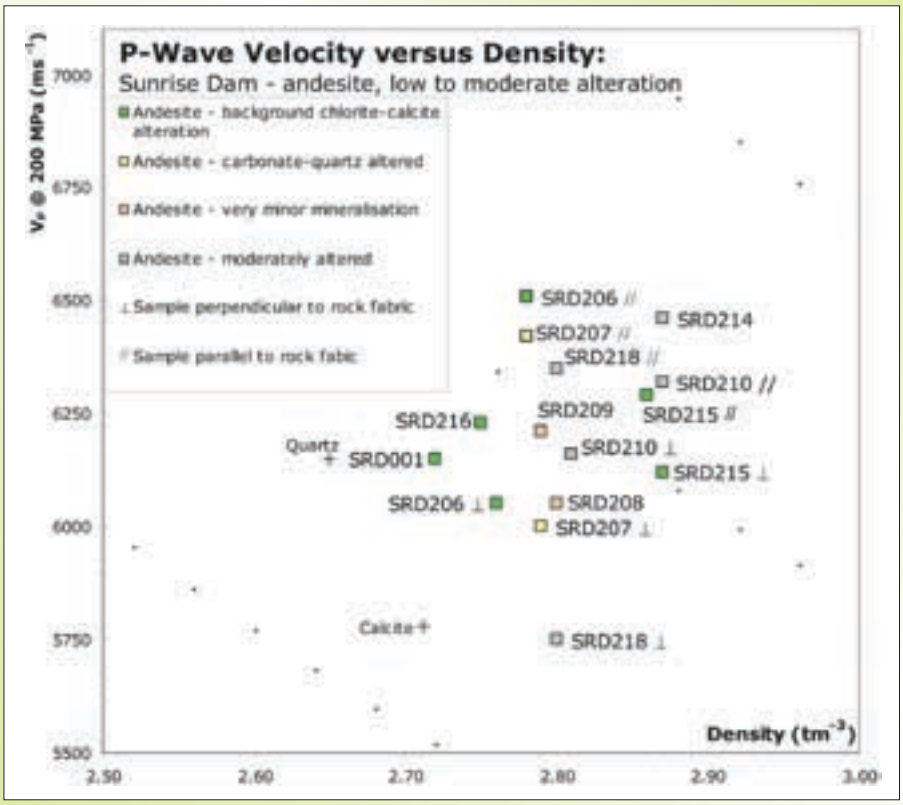

Figure 84: Samples of andesite with low to moderate alteration. These samples show more density variation and less seismic velocity anisotropy than the felsic porphyry samples (Figure 83). Samples, such as SRD210, which show significant density variations for differently oriented samples, indicate that these rocks are highly heterogenous and the cores taken to measure the seismic velocities are sampling different minerals.

Figure 85: Densities and seismic velocities for the averages of each of the samples of felsic porphyry (Figure 83) and andesite (Figure 84). The average was taken (rather than the median, as for Figure 69) to best incorporate the seismic velocity anisotropy.

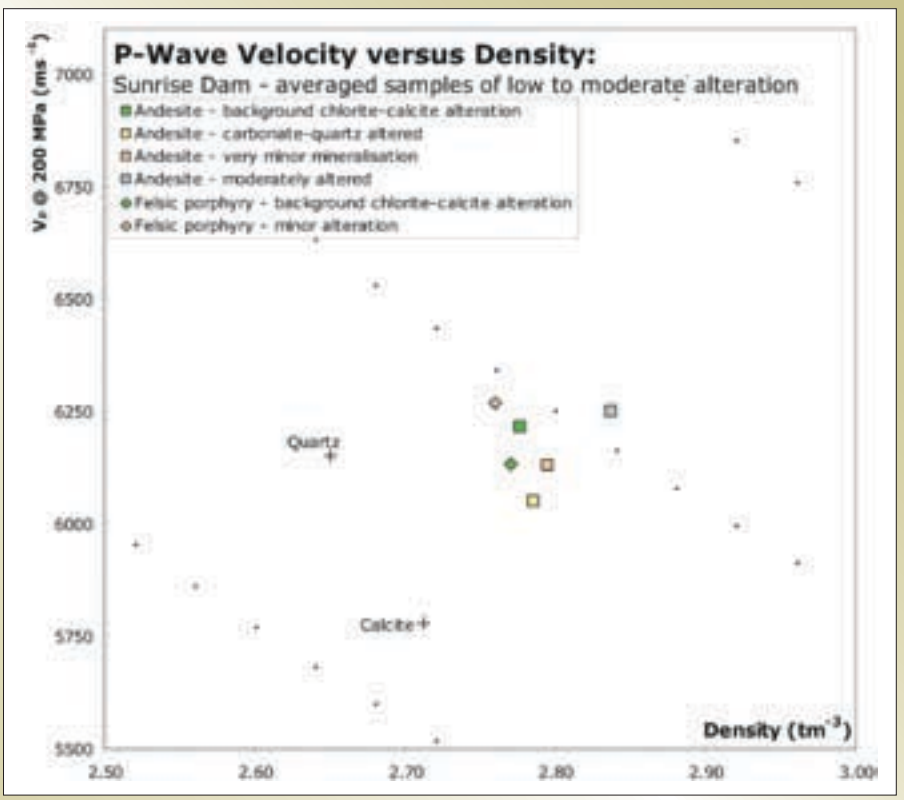

(Figure 86). As the velocity of the shear zone varies with dip (Figure 87), the acoustic impedance (the product of density and seismic velocity) will also vary with dip. Seismic reflections are the result of a contrast in acoustic impedance (Yilmaz and Doherty, 2000), hence a shear zone will change reflectivity as its dip varies (Figure 88). As the majority of the background rocks at Sunrise Dam are more likely to be an andesite, the modelling was also performed for the case of the Sunrise Shear Zone in andesite (Figure 89).

Clearly, the Sunrise Shear Zone has the potential to be highly reflective assuming it is sufficient altered. The most altered sample from Sunrise Dam is the felsic porphyry, and is very dense (3.18 tm-3). If the Sunrise Shear Zone had similar properties to this sample, then there would be a strong reflection produced irrespective of the dip of the shear zone (Figure 88). For the case of the Sunrise Shear Zone consisting of the most altered andesite, the shear would be reflective only for steeper dips (Figure 89). For the typical range of dips of the Sunrise Shear (30–45°), the shear zone would produce a weak to moderate reflection. Predominantly, the reflectivity appears to be controlled by the density of the material within the Sunrise Shear Zone. To further define the reflectivity of this structure additional measurements of both seismic velocity and density are required.

This change in reflectivity with respect to shear-zone dip has implications for the imaging of structures.

Firstly, seismic energy is generally not acquired for vertical incidence only: a number of receivers, offset from the seismic source, are used, effectively producing reflections that are due to a range of angles of incidence. During seismic processing, these offsets are 'stacked' to increase the signal to noise ratio of the seismic survey. These offsets contain considerable information about seismic anisotropy, as well as physical properties – a technique called amplitude variation with offset is often utilised in petroleum seismic surveys to delineate hydrocarbon reserves (Backus, 1987; Burianyk, 2000), and also have been utilised in hard-rock environments (van den Berg et al., 1992). Based on these seismic velocity data from Sunrise Dam, there is the potential to model the AVO response of structures such as the Sunrise Shear Zone, to understand how to better image these mineralising shears in seismic data.

Secondly, there are differences in reflectivity in seismic lines acquired to the north and to the south of the Sunrise Dam deposit (seismic line location Figure 64). The seismic line to the north of Sunrise Dam (AG_S2) shows a number of linear, sub-parallel shears, all dipping at 30 to 45°, which can be interpreted to represent the Sunrise shear and others

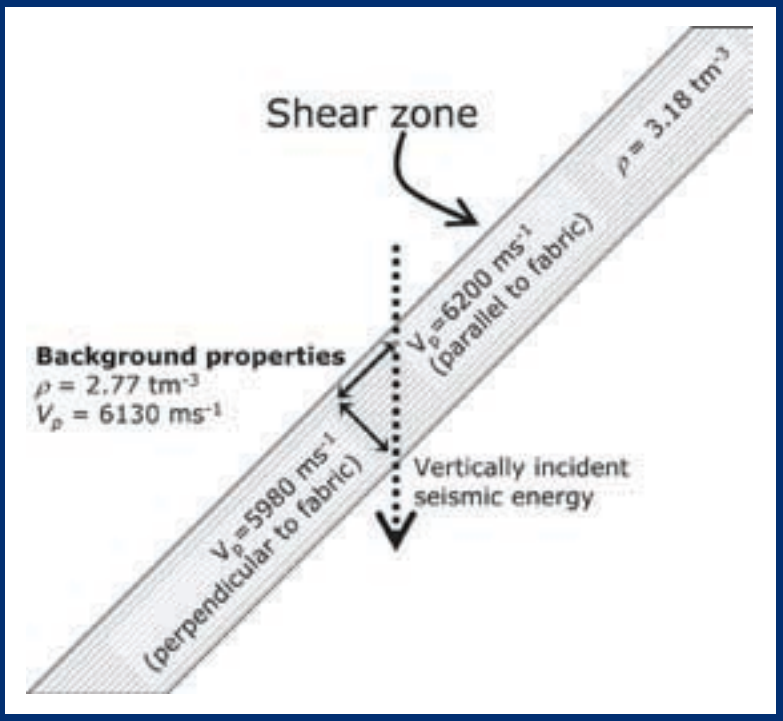

Figure 86: Schematic diagram showing the dip of a shear zone, its seismic velocity anisotropy, and the relationship to the vertically incident seismic energy.Background properties are an average of the background altered felsic porphyry and the properties of the shear zone are from the highly altered felsic porphyry sample taken from the Sunrise Shear Zone. Similar background properties would be obtained using the average of the samples of background altered andesite.

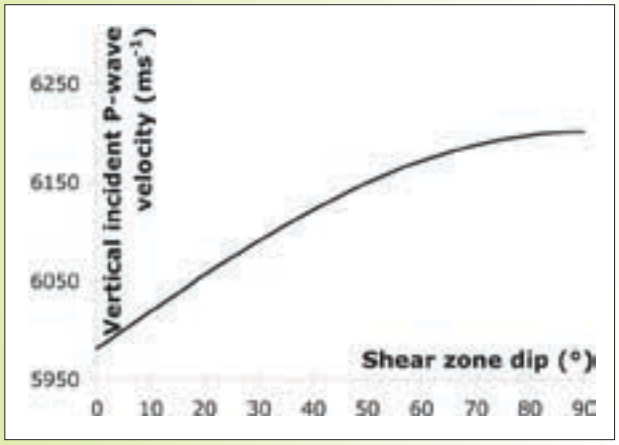

Figure 87: Variation in seismic velocity for a vertically-incident seismic wave. The properties of the shear zone are of the highly altered felsic porphyry sample taken from the Sunrise Shear Zone. The plane of fastest velocity is oriented parallel to the top and bottom of the shear zone, and the plane of slowest velocities is oriented perpendicular to the shear zone's orientation (Figure 86).

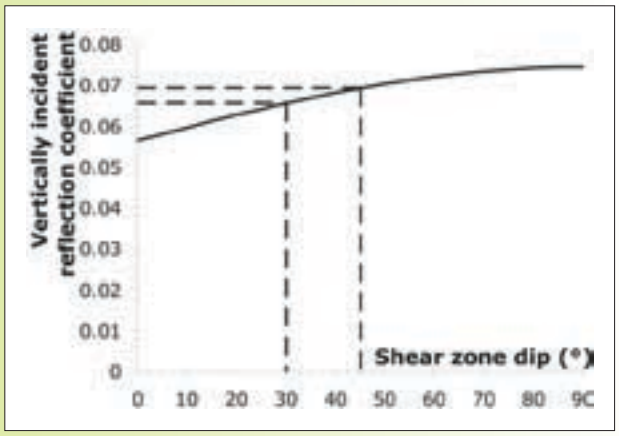

Figure 88: The reflectivity of a shear zone, as a function of dip. Velocity of the shear zone as a function of dip is given above (Figure 87), and the background velocity is that of the average background altered felsic porphyry (Figure 85). The Sunrise Shear Zone dips between 30° and 45°, and the dashed lines are drawn to highlight the reflection coefficient for this range of dips. A reflection coefficient greater than 0.06 will produce a very strong positive reflection.

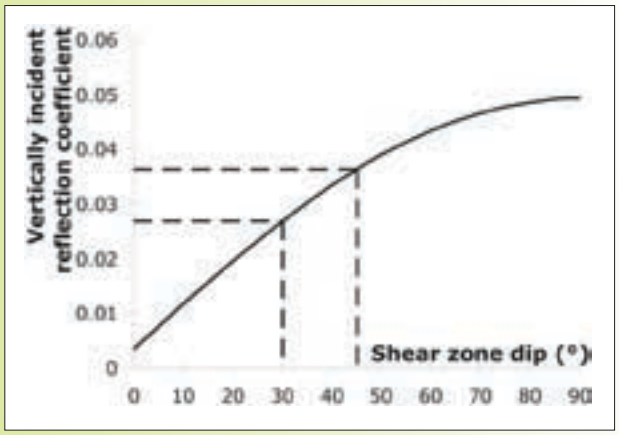

Figure 89: The reflectivity of a shear zone, as a function of dip. In contrast to Figure 88, this depicts the change in reflection coefficient for the Sunrise Shear intersecting the background andesite. The Sunrise Shear Zone dips between 30° and 45°, and the dashed lines are drawn to highlight the reflection coefficient for this range of dips. A reflection coefficient greater than 0.06 will produce a very strong positive reflection.

parallel to it (Figure 90). The other rocks with properties that would produce a reflection are the magnetic shales, which are sub-parallel to the Sunrise Shear Zone. The three seismic lines to the south of the deposit, however, show very variable reflectivity which is difficult to reconcile with known structures in the area (Figure 91).

The westernmost seismic line of the three southern lines (AG_S3) is considerably more crooked than the other seismic lines, which may account for some of the variable reflectivity observed in the southern lines. The differences in reflection character also may be due to the larger number of steep high-strain shears, which are very thin and would be very difficult to image in seismic data: For short seismic lines, dips greater than 60° are almost impossible to image and to correctly migrate (Goleby et al., 2002). The southern portion also contains fewer magnetic shales, which potentially are a reflective unit. Finally, the seismic lines are oriented differently, with the northern line almost entirely across strike, whereas the southern seismic lines are

oblique to strike. This difference may account for some of the changes in reflectivity – the apparent dip of the Sunrise Shear Zone will be shallower for the oblique southern lines. This shallower dip will, for the 2D seismic acquired, result in lower reflectivity (as for the change in dip changing the reflectivity, discussed above).

5.2.2.1 Summary

- High-pressure velocity measurements at Sunrise Dam show that the majority of volcanic rocks (predominately andesitic in composition) and porphyries (predominantly felsic in composition) in this deposit have very similar seismic velocities and densities. For moderate to unaltered samples of either lithology, the variations observed in density are due to anisotropy, primarily due to the preferential alignment of micas in the background alteration at the deposit. This variation, however, is only organised on a local scale and therefore the background rocks can be assumed to be isotropic.
- Seismic velocities of highly altered samples show increased densities when compared with the unaltered lithologies. These samples are generally aligned such that the seismic velocity parallel to the top and bottom of a shear zone will be fast, and the seismic velocity perpendicular to the shear zone will be slow.
- The seismic velocity anisotropy in the shear zones indicates that shear zones may be reflective for some particular dip angles. In particular, a structure such as the Sunrise Shear Zone shearing andesite will only begin to have a weak to moderate reflection at dips of around 30°. The Sunrise Shear Zone will, however, be highly reflective in highly altered porphyries. The reflectivity of the shear zones should increase with increasing dip, although steeper structures will be considerably more difficult to resolve using current seismic reflection techniques.
- The seismic reflection studies at Sunrise Dam indicate that there are more consistent reflections to the north of the deposit when compared to the south. There

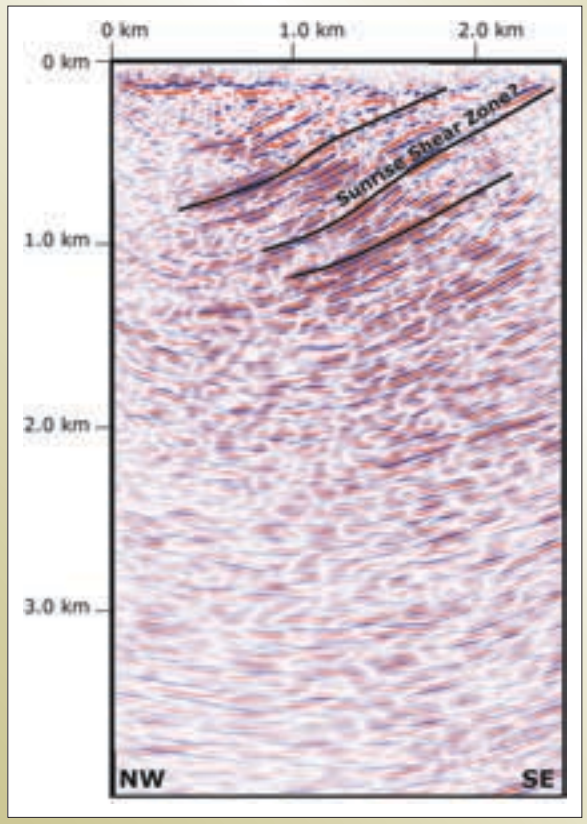

Figure 90: The northern seismic line at Sunrise Dam, looking to the north-east. Highlighted (with black lines) are some possible shears; there are also other reflections which could be interpreted as shear zones. The middle of the three interpreted shear zones corresponds to an extension of the Sunrise Shear Zone. Contrast the consistent reflectivity apparent in this line with the confused reflectivity in the southern lines (Figure 91).

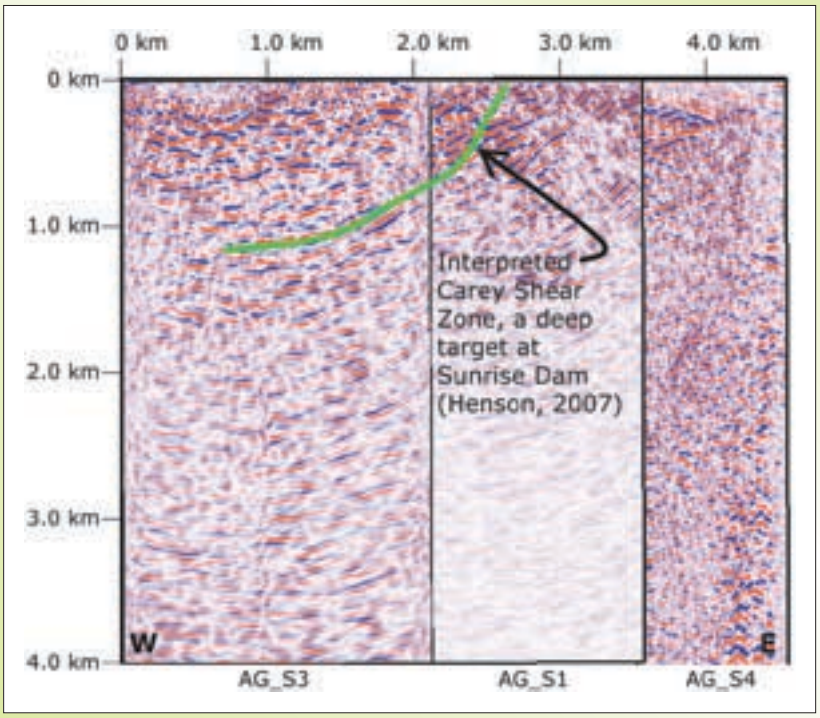

Figure 91: The southern seismic lines at Sunrise Dam, looking to the north-east. The reflectivity in this region is considerably more difficult to interpret, although it has been utilised to extend the deep shear zone the Carey shear beyond the known locations from drilling (Henson, 2007).

are both geological and geophysical reasons for this: geologically, there are more coherent structures which have shallow to moderate dips, and more magnetic shale to the north of the deposit. Geophysically, the northern line is entirely perpendicular to strike at the deposit and is straight; one of the southern lines is crooked, and all are oblique to strike.

- The seismic velocity results obtained for Sunrise Dam contain information required for the modelling of amplitude-variation-with-offset effects due to alteration and anisotropy, a technique utilised in petroleum seismic studies to examine anisotropy and rock properties. The provision of shear-wave velocities will also allow for the modelling of a 3-component (3C) seismic survey, another technique routinely utilised in petroleum seismic. Shear-wave velocities, although acquired (Appendix A8), were not studied for this deposit as they do not direct translate into an understanding of the reflection seismic studies that have been undertaken in the region.
- To fully delineate the density and velocity changes at Sunrise Dam, additional sampling is still required. Potentially, a downhole geophysical survey could be calibrated using high-pressure seismic velocity measurements.

5.3 Conclusions

The use of hand-specimen and downhole geophysical results in the Laverton region allows the following relationships between density, seismic velocity and alteration to be established:

- The Wallaby conglomerate is both dense (2.8–3.0 tm^{-3}) and seismically fast, similar in properties to some mafic rocks in the Yilgarn Craton.
- The AMEC pipe at Wallaby produces an alteration assemblage which increases both the density and the seismic velocity of rocks within the pipe. Other unmineralised alteration also produces a density increase coupled with a slight seismic velocity increase.
- Gold-related alteration at Wallaby produces either a marginal density increase, or a slight density decrease. This trend is not fully resolved due to inadequate sampling, as the hand-specimen and downhole density results are only comparable in relative rather than absolute terms.
- The rock properties at Wallaby suggest that gold lodes and the syenite intrusions have the potential to be imaged as weak reflections in seismic data, assuming the seismic data was of sufficient high frequency to resolve these thin bodies.

- The most seismically reflective units at Sunrise Dam are altered andesite, felsic porphyry and the magnetic shale (BIF). Rocks from the shallowly-dipping shear zones, such as the Sunrise Shear, are anisotropic and these shear zones will change reflectivity with dip. For the typical dip range for these shears (30-45°), they will be imaged as moderate to strong reflections, such as those recorded in the northern seismic line at Sunrise Dam. The seismic data in the southern portion of the deposit, however, is hampered by the geology (with less reflective magnetic shale, and increased steep shears which will not be imaged due to their dip and how thin they are) and the acquisition, with one of the southern seismic lines more crooked than the northern line. Acquisition of oblique lines may also result in reduced reflectivity, with the line showing the most reflectivity also the line which is parallel to strike in the region.
- Sampling of altered products at Sunrise Dam could be augmented by coupling a high accuracy hand-specimen sampling regime with a downhole geophysical survey.

End of Laverton Physical Properties folding near Sunrise Shear Zone

6. SEISMIC AND GRAVITY RESPONSE OVER A MINERALISED REGION

The Victory-Defiance region of the St Ives Gold Mine is an area of substantial gold endowment – in the order of 2.3MOz gold (Prendergast, 2007). The region is underlain by a granite dome (Henson et al., 2005), which is clearly imaged in the mine-scale Victory seismic line (Stolz et al., 2004; also Figure 92). The solid geology of the St Ives camp is also well known; combing the Victory seismic line with the solid geology allows for a robust interpretation of the geology which underlies the Victory-Defiance Region (Figures 93 and 94).

Validation of the geological architecture was conducted using the regional gravity data as a constraint and modelling was performed in MODELVISION, using the densities of unaltered Yilgarn rocks as reported by House et al. (1999). When this was performed, there was a misfit between the seismic interpretation, forward modelling using these unaltered Yilgarn rock densities, and the observed gravity data, which must be due to one or more subsurface physical properties which are different from the properties used for modelling. This could be due to some or all of the following: a misidentification of lithology in the seismic architecture, the physical properties for each lithology were incorrect, and/or that chemical alteration has changed the physical properties.

One possible solution is to revise the architecture to provide a better fit to the available gravity data (Figure 95). Note that this represents only one possible interpretation

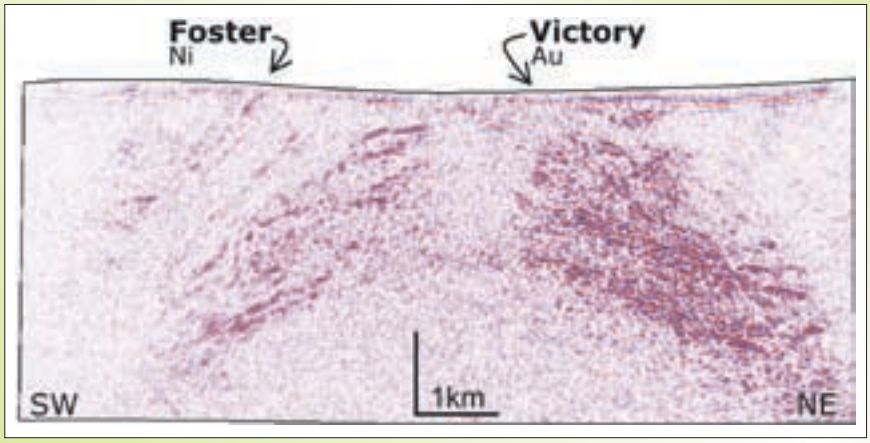

Figure 92: The Victory mine-scale seismic line. The granite dome beneath Victory is well imaged as the zone of bland reflectivity. The position of the Victory mine is denoted by Au, and the position of the Foster nickel mine is denoted by Ni.

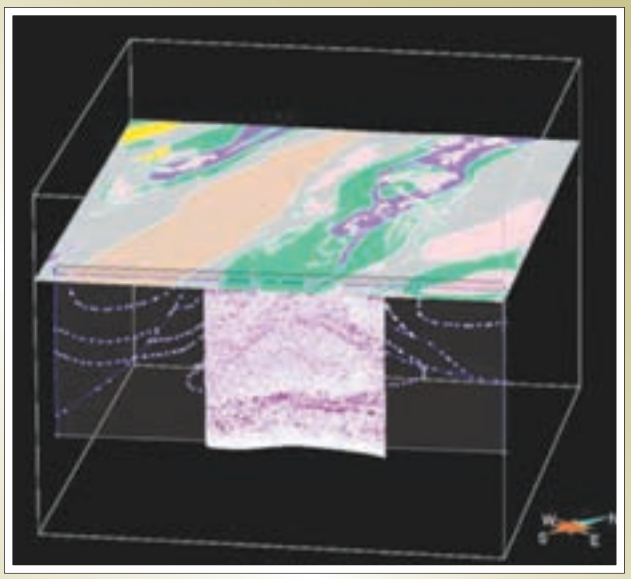

Figure 93: 3D image showing the relationship between the surface solid geology and the architecture, as delineated by the Victory seismic line.

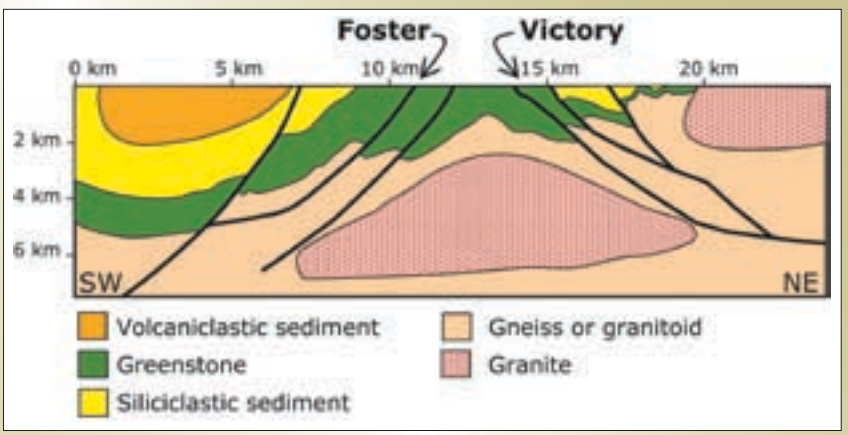

Figure 94: Interpreted geology for the Victory seismic line and surrounding region, derived from the Victory seismic line, regional solid geology and mine-scale drilling.

of the subsurface architecture and property distribution, as potential field data are inherently non-unique (Telford et al., 1990a), with an infinite number of models able to reproduce any observed data.

If we examine the changes to the architecture that allow a better fit of the calculated to the observed gravity data (Figure 95), they have the following form (Figure 96):

- A decrease in density beneath the Victory gold mine
- An increase in density either side of the Victory gold mine
- A decrease in density beneath the Foster nickel mine
- An increase in density to the side of the Foster nickel mine

As stated above, the misfit for the seismic architecture may be due to misidentification of lithologies. Alternatively, the properties used may have been invalid, although, if this were the case then all of the units would have required their properties to be changed, which was clearly not performed. An alternative hypothesis is that the misfit represents the alteration that culminates in the deposition of the 2.3 MOz Victory-Defiance orebodies. The changes in subsurface physical properties around the Victory mine are very similar to those indicated by the geophysical modelling of the listric fault model (Section 4.3). Thus, the observed gravity response for Victory-Defiance may well be the result of alteration; the misfit can be entirely attributed to this alteration rather than an incorrect interpretation of the seismic data. There is also a density decrease underneath the Foster nickel mine, which would not have formed by the exact processes simulated by the listric fault model (see Section 4.3). Generally, serpentinisation is associated with nickel deposits, and serpentinisation of a rock will decrease the density of the rock (Toft et al., 1990).

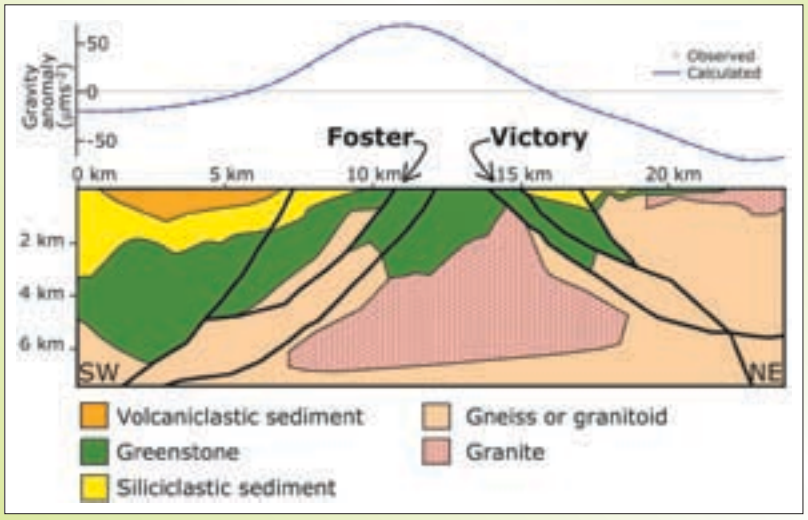

Figure 95: MODELVISION forward-model of the interpretation of the seismic data and solid geology, with the architecture modified from the original seismic interpretation to better fit the available gravity data.

Figure 96: The differences in density between the original seismic interpretation and the model adjusted for reduced misfit between the predicted and observed gravity response. A blue oval indicates a region that has a decrease in density in the revised architecture, and a red oval indicates a region that has an increase in density in the revised architecture. Background architecture is the model after revision by gravity modelling.

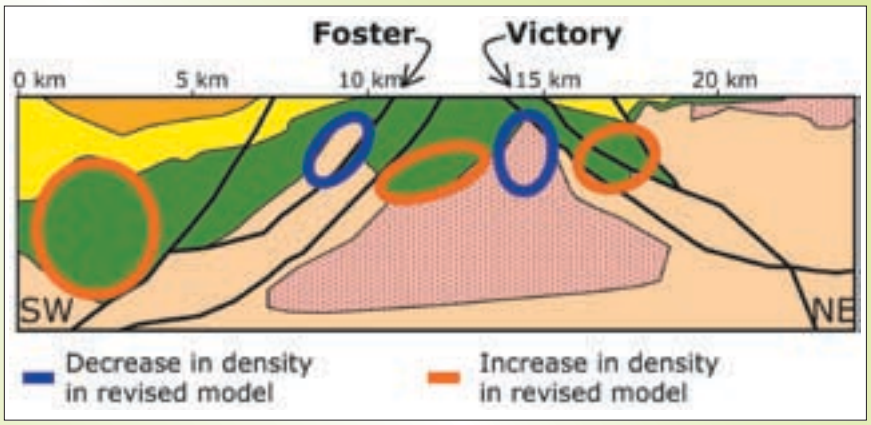

As we have independent controls on the architecture, in the form of an excellent mine-scale seismic line, modifying the architecture to match the forward-modelled gravity data simply serves to hide the signature of alteration. An implication for exploration is that the effects of alteration are significant enough to be detectable in even regional gravity surveys, and the use of multiple datasets (such as seismic and gravity here) are the best ways to detect alteration footprints using geophysical techniques. Note that this study has been performed using regional gravity data, indicating it is possible that even regional gravity data, coupled with seismic data and 3D interpretations of geology, contain the signatures required to target a 2.3 MOz orebody. This target may also be evident if it was buried by several hundred metres.

Veins and alteration, Victory-Defiance region, St Ives

7. SYNTHESIS OF PROJECT RESULTS

The work of Project A3 has involved studying the geophysical response of chemical alteration by using both empirical and synthetic (numerical simulation) approaches. The results of these studies support each other, adding to their validity.

The studies of physical properties (Sections 3.2, 5.2.1 and 5.2.2) all suggest that alteration is a phenomenon that can result in significant physical property contrast. As a physical property contrast is the cause of any geophysical response, the contrasts that are due to alteration are therefore capable of producing a geophysical response. The exact physical property contrast depends on the nature of the host rock and the alteration assemblage produced. Alteration to minerals which have considerably different properties to an unaltered rock, such as sulphides, will produce vast changes in physical properties. Alteration to minerals, such as quartz, more commonly found in the host rocks will produce a smaller response in the physical properties. Alteration can also cause a rock to have physical properties closer to another unaltered rock – in the case of a felsic rock, for example, alteration to a small proportion of sulphide will produce a rock which has a density and magnetic susceptibility that are similar to an unaltered mafic rock. One method, using geophysical inversions, to detect the difference between an altered rock and an unaltered rock of different lithology is discussed below (Section 7.1).

The seismic response of alteration, inferred in Section 2, is given validity by the physical properties of altered rocks, observed in the Laverton region. Anisotropy may result in the enhancement of reflectors within the crust. Sunrise Dam, for example, which has a number thick and coherent shear zones which dip shallowly, has the properties to produce consistent reflections from shear zones. These consistent reflections are well imaged in one of the mine-scale seismic lines at this deposit; interpretation is more difficult in other seismic lines at Sunrise Dam due to the survey design. The physical property studies suggest that there are the properties at other deposits, such as Wallaby, to produce reflections from the alteration system although these are not definitively imaged in the mine-scale seismic data at these deposits.

Numerical simulations of alteration are a powerful method to examine an entire mineral system. As the physical properties, and hence geophysical responses, due to alteration are the result of mineralogical differences, any numerical model which simulates a mineral system, and produces a result in the form of mineralogy, is suitable for forward-modelling for geophysical responses. Forward-modelling of a simple Yilgarn gold system analogue in 2D (Section 4.3) suggests the following as targets, with respect to the unaltered geophysical response of the architecture:

- An increase in gravity response either side of a deposit
- A decrease in gravity response directly above a deposit
- A small magnetic intensity spike directly above a deposit
- An increase in reflectivity along a shear zone which has acted as a fluid conduit to the deposit.

Although these targets were developed from a simple analogue of the Yilgarn gold systems, the gravity response at the Victory-Defiance region of the St Ives Gold Mine (Section 6) appears to follow these trends. In this case, the unaltered architecture that these targets were tested against was a mine-scale seismic line in the region, which allowed the interpretation of an architecture independently of the available potential field data.

The numerical simulation results also produced an alteration response that echo the empirical results. Alteration up to 4 km distance from the gold system at Victory-Defiance produced a density increase comparable with the density increase predicted by the 2D alteration model. The 2D alteration model also correlates with a simple 1D alteration model, produced by using the properties of host rocks from St Ives. Although the 1D alteration model suggests different minerals in the alteration assemblages to the 2D alteration model, the resulting geophysical responses are very similar between the two models.

7.1 Recommendations for future work

The majority of the physical property studies were undertaken on existing datasets from exploration companies. Examining all available physical property data with a view to examining the differences between alteration (an example would be Section 5.2.1) is one method to discover the physical property, and hence geophysical response, changes due to alteration.

Numerical simulations are a new method of targeting. The simulations can be based on the '5 answers' of a mineral system, and therefore provide targets directly from the mineral systems approach. By taking an unaltered architecture from a region, and using a numerical simulation to predict where deposits are likely to form, the expected geophysical responses are a very powerful tool to potentially discover new deposits that are under cover. Numerical simulations can also be tailored to a deposit to then produce mine-scale targets and their probable geophysical responses.

Another method to discover alteration through geophysical techniques is to look at inversion results. In the St Ives Gold Mine case study (Section 3.2), a method was developed to establish probable alteration types based on physical properties. In the case of the St Ives study, these properties were derived from downhole geophysical logging. Geophysical inversions, such as on gravity and magnetics, produce models of physical properties for the subsurface. We would expect that alteration will produce physical properties within this model which would be different from those we would expect for an unaltered rock. Indeed, the method developed at the St Ives Gold Mine has been applied to the geophysical inversion results from the Cobar region, New South Wales (Chopping et al., 2007; note that this report is confidential to Project T11 sponsors until January 2009.). These studies have also been performed by other studies using different techniques (Williams and Dipple, 2006). Williams and Dipple utilise an inversion methodology to infer probable alteration minerals from constrained gravity and magnetic inversions, in contrast to the 'alteration cone' method (Section 3.2) developed within Project A3 which could be applied to even unconstrained inversions.

The ultimate future test of the results from Project A3 is to use the methodology developed here to discover new ore deposits which lie undercover. Ultimately, our only knowledge of regions which have no outcrop is through geophysics; rock properties, one of the major areas of study of this project, is our link from geology to geophysics. The project has demonstrated that alteration can produce geophysical responses which are significant enough to be detected in regional datasets. Understanding these geophysical responses, and how to detect them, is crucial to future exploration success in undercover or poorly explored regions. Application of the detection techniques coupled with new methods of predicting the geophysical responses due to alteration developed within the project provides the tools to assist in exploration of areas which have significant cover.

Sunrise Dam east pit wall

8. REFERENCES

Adam, E., Maillard, B., Arnold, G. & Bonenfant, A. (2002). A petrophysical study of the Bell Allard deposit alteration pipe, Matagami, Quebec. *72nd Annual International Meeting.* Society of Exploration Geophysicists.

Anand, R. R. & Paine, M. (2002). Regolith geology of the Yilgarn Craton, Western Australia: implications for exploration. *Australian Journal of Earth Sciences,* 49(1), pp. 3-162.

AngloGold Ashanti (2002). Schematic cross-sections through the Sunrise Dam deposit, unpublished AngloGold Ashanti data.

Anselmetti, F. S. & Eberli, G. P. (1993). Controls on Seismic Velocity in Carbonates. *Pure and Applied Geophysics,* 141(2-4), pp. 287-323.

Backus, M. M. (1987). Amplitude versus offset: a review. *57th Annual International Meeting: Society of Exploration Geophysicists*, pp. 359-364.

Barnicoat, A. C. (2006). *Exploration Science*. ***pmd*CRC*** Fact Sheet, ***pmd*CRC***, Melbourne. http://www.pmdcrc.com.au/pdfs/brochures_exploration_science_fs.pdf, accessed 2 July 2007.

Barrick Gold Corporation (2006). Barrick Now: Annual Report 2006. 171 p.

Berkhemer, H., Rauen, A., Winter, H., Kern, H., Kontny, A., Lienert, M., Nover, G., Pohl, J., Popp, T., Schult, A., Zinke, J. & Soffel, H. C. (1997). Petrophysical properties of the 9-km-deep crustal section at KTB. *Journal of Geophysical Research – Solid Earth,* 102(B8), pp. 18337-18361.

Berryman, J. G. (1995). Mixture Theories for Rock Properties. In Ahrens, T. J. (Ed.) *Rock Physics and Phase Relations: A Handbook of Physical Constants.* American Geophysical Union. pp. 205-238.

Beske-Diehl, S. & Banerjee, S. K. (1979). An example of magnetic properties as indicators of alteration in ancient oceanic lithosphere – the Othris Ophiolite. *Earth and Planetary Science Letters,* 44(3), pp. 451-462.

Burianyk, M. (2000). Amplitude-Vs-Offset and Seismic Rock Property Analysis: A Primer. *CSEG Recorder,* 25(9), pp. 6-16.

Carmichael, R. S. (1989a). Magnetic Properties of Minerals and Rocks. In Carmichael, R. S. (Ed.) *Practical Handbook of Physical Properties of Rocks and Minerals.* CRC Press. pp. 301-358.

Carmichael, R. S. (1989b). *Practical Handbook of Physical Properties of Rocks and Minerals*. CRC Press, 741 p.

Champion, D. C. & Cassidy, K. F. (2002). Granites in the Leonora-Laverton transect area, north eastern Yilgarn. In Cassidy, K. F. (Ed.) *Geology, geochronology and geophysics of the north eastern Yilgarn Craton, with an emphasis on the Leonora-Laverton transect area.* Geoscience Australia Record 2002/18. pp. 13-35.

Chopping, R., Roy, I. G., and van der Wielen, S. E. (2007). Identifying alteration from geophysical integration. In: Final Report, Project T11: 3D Architecture and Predictive Mineral System Analysis of the Central Lachlan Subprovince and Cobar Basin, NSW. van der Wielen, S. E. and Korsch, R. J. (eds). ***pmd*CRC***, Melbourne, pp. 119-142. **Confidential to Project T11 sponsors until end of January 2009.**

Christensen, N. I. (1989). Seismic Velocities. In Carmichael, R. S. (Ed.) *Practical Handbook of Physical Properties of Rocks and Minerals.* CRC Press. pp. 431-546.

Christensen, N. I. & Mooney, W. D. (1995). Seismic velocity structure and composition of the continental crust: A global view. *Journal of Geophysical Research – Solid Earth,* 100(B6), pp. 9761-9788.

Clark, D. A. (1984). *Magnetic properties of pyrrhotite: applications to geology and geophysics*. M.Sc. thesis, University of Sydney.

Cleverley, J. S., Hornby, P. & Poulet, T. (2006). *pmd**RT: Combined fluid, heat and chemical modelling and its application to Yilgarn geology. In Barnicoat, A. C. & Korsch, R. J. (Eds.) *Predictive Mineral Discovery Cooperative Research Centre – Extended Abstracts from the April 2006 Conference.* Geoscience Australia, Record 2006/07.

Collinson, D. W. (1986). An estimate of the hematite content of sediments by magnetic analysis. *Earth and Planetary Science Letters,* 4(6), pp. 417-421.

Connolly, J. & Kerrick, D. M. (2002). Metamorphic controls on seismic velocity of subducted oceanic crust at 100-250km depth. *Earth and Planetary Science Letters,* 204, pp. 61-74.

Connors, K., Donaldson, J., Morrison, B. & Davy, C. (2003). The Stratigraphy of the Kambalda-St Ives District: workshop notes. Gold Fields unpublished report.

Cox, S. F. & Ruming, K. (2004). The St Ives mesothermal gold system, Western Australia – a case of golden aftershocks? *Journal of Structural Geology,* 26(6-7), pp. 1109-1125.

Dobrin, M. B. (1976). *Introduction to Geophysical Prospecting, 3rd Edition*. McGraw-Hill, New York.

Dohr, G. (1974). *Applied Geophysics*. Halsted/John Wiley and Sons, New York.

Dolan, S. S., Bean, C. J. & Riollet, B. (1998). The broad-band fractal nature of heterogeneity in the upper crust from petrophysical logs. *Geophysical Journal International,* 132(3), pp. 489-507.

Drieberg, S., Walshe, J. L., Halley, S. & Hall, G. (2004). Embedded insights into the Wallaby gold deposit, Western Australia. In Barnicoat, A. C. & Korsch, R. J. (Eds.) *Predictive Mineral Discovery Cooperative Research Centre – extended abstracts from the June 2004 Conference.* Barossa Valley, Geoscience Australia Record 2004/009.

Drummond, B. J., Goleby, B. R., Owen, A. J., Yeates, A. N., Swager, C., Zhang, Y. & Jackson, J. K. (2000). Seismic reflection imaging of mineral systems: Three case histories. *Geophysics,* 65(6), pp. 1852-1861.

Drummond, B. J., Hobbs, B. E. & Goleby, B. R. (2004a). The role of crustal fluids in the tectonic evolution of the Eastern Goldfields Province of the Archaean Yilgarn Craton, Western Australia. *Earth, Planets and Space,* 56, pp. 1163-1169.

Drummond, B. J., Hobbs, B. E., Hobbs, R. W. & Goleby, B. R. (2004b). Crustal fluids in tectonic evolution and mineral systems: evidence from the Yilgarn Craton. In Barnicoat, A. C. & Korsch, R. J. (Eds.) *Predictive Mineral Discovery Cooperative Research Centre – extended abstracts from the June 2004 Conference.* Barossa Valley, Geoscience Australia Record 2004/009. http://www.ga.gov.au/image_cache/GA6868.pdf.

Drummond, B. J., Hobbs, R. W. & Goleby, B. R. (2004c). The effects of out-of-plane seismic energy on reflections in crustal-scale 2D seismic sections. *Tectonophysics,* 1-4, pp. 213-224.

Dunlop, D. J. (1995). Magnetism in rocks. *Journal of Geophysical Research – Solid Earth,* 100(B2), pp. 2161-2174.

Dvorkin, J. & Nur, A. (1998). Time-averaged equation revisited. *Geophysics,* 63(2), pp. 460-464.

Eaton, D. W., Milkereit, B. & Salisbury, M. H. (2003). Seismic methods for deep mineral exploration: Mature technologies adapted to new targets. *The Leading Edge,* 22(6), pp. 580-585.

Emerson, D. W. (1990). Notes on Mass Properties of Rocks – Density, Porosity, Permeability. *Exploration Geophysics,* 21(3&4), pp. 209-216.

Emerson, D. W. (1997). The Galvanic Electrical Resistivities of Archaean Country Rocks in the Kambalda Region. Unpublished Report to WMC Resources.

Evans, B. (1999). Report on results of Seismic Numerical Modelling of the Wallaby Orebody. Department of Exploration Geophysics, Curtin University of Technology. Curtin Report no. EG/CR/99/2. 11 p.

Ewers, G. R. & Evans, N. (2001). MINLOC Mineral Localities Database. In Kilgour, B. (Ed.) Canberra: Geoscience Australia. http://www.ga.gov.au/bin/htsqr?file=/oracle/geomet/geomet2.htsqr&datasetno=3556.

Fallon, G. N., Fullagar, P. K. & Sheard, S. N. (1997). Application of geophysics in metalliferous mines. *Australian Journal of Earth Sciences,* 44(4), pp. 391-409.

Fannin, P. C., Scaife, B. K. P. & Charles, S. W. (1990). An experimental study of the magnetic susceptibility of colloidal suspensions of magnetite as a function of particle volume fraction. *Journal of Physics D: Applied Physics,* 23(12), pp. 1711-1714.

Fisher, R. A. (1970). *Statistical methods for research workers (14th Edition)*. Oliver and Boyd, Edinburgh. 362 p.

Goleby, B. R., Korsch, R. J., Fomin, T., Bell, B., Nicoll, M. G., Drummond, B. J. & Owen, A. J. (2002). Preliminary 3-D geological model of the Kalgoorlie region, Yilgarn Craton, Western Australia, based on deep seismic-reflection and potential-field data. *Australian Journal of Earth Sciences,* 49(6), pp. 917-933.

Goleby, B. R., Blewett, R. S., Groensewald, P. B., Cassidy, K. F., Champion, D. C., Jones, L. E. A., Korsch, R. J., Shevchenko, S. & Apak, S. N. (2003). *The 2001 Northeastern Yilgarn Deep Seismic Reflection Survey*. Geoscience Australia Record 2003/28, 143 p.

Grant, F. S. & West, G. F. (1965). *Interpretation theory in applied geophysics*. McGraw-Hill, New York. 583 p.

Groves, D. I., Goldfarb, R. J., Gebre-Mariam, M., Hagemann, S. G. & Robert, F. (1998). Orogenic gold deposits: a proposed classification in the context of their crustal distribution and relationship to other gold deposit types. *Ore Geology Reviews,* 13**,** pp. 7-27.

Groves, D. I., Goldfarb, R. J., Robert, F. & Hart, C. J. R. (2003). Gold Deposits in Metamorphic Belts: Overview of Current Understanding, Outstanding Problems, Future Research, and Exploration Significance. *Economic Geology,* 98(1)**,** pp. 1-29.

Guéguen, Y. & Palciauskas, V. (1994). *Introduction to the Physics of Rocks*. Princeton University Press, 294 p.

Hagemann, S. G. & Cassidy, K. F. (2001). World class gold camps and deposits in the Eastern Goldfields Province, Yilgarn Craton: diversity in host rocks, structural controls and mineralisation styles. In Hagemann, S. G., Neumayr, P. & Witt, W. K. (Eds.) *World-class gold camps and deposits in the eastern Yilgarn Craton Western Australia, with special emphasis on the Eastern Goldfields Province.* Geological Survey of Western Australia, Record 2001/17. pp. 7-44.

Hargraves, R. B. & Banerjee, S. K. (1973). Theory and Nature of Magnetism in Rocks. *Annual Review of Earth and Planetary Sciences,* 1**,** pp. 269-296.

Harrison, C. (2005). Seismic velocity and density results for the Wallaby-Granny Smith mines. Unpublished data provided to PlacerDome.

Henson, P. A., Blewett, R. S., Champion, D. C., Goleby, B.R., Cassidy, K. F., Drummond, B. J., Korsch, R. J., Brennan, T. and Nicoll, M. (2005). Domes: the characteristic 3D architecture of the world-class lode-Au deposits of the Eastern Yilgarn. In Hancock, H. (ed) *STOMP 2005: Structure, tectonics and ore mineralisation processes, Abstract Volume.* Economic Geology Research Unit, James Cook University.

Henson, P., Blewett, R. S., Champion, D. C., Goleby, B. R. & Czarnota, K. (2006). Towards a unified architecture of the Laverton Region, W.A. In Barnicoat, A. C. & Korsch, R. J. (Eds.) *Predictive Mineral Discovery Cooperative Research Centre: extended abstracts from the April 2006 Conference.* Geoscience Australia Record 2006/07.

Henson, P. A. (2007). Sunrise Dam – deep targets (Carey Shear). ***pmd*CRC** Project report – Project Y4. **pmd*CRC***, Melbourne. https://pmd-twiki.arrc.csiro.au/twiki/pub/Pmdcrc/ProjectY4/Sunrise_Dam_-_deep_targets.pdf.

Herrmann, W., Blake, M., Doyle, M., Huston, D., Kamprad, J., Merry, N. & Pontual, S. (2001). Short Wavelength Infrared (SWIR) Spectral Analysis of Hydrothermal Alteration Zones Associated with Base Metal Sulfide Deposits at Rosebery and Western Tharsis, Tasmania, and Highway-Reward, Queensland. *Economic Geology,* 96(5)**,** pp. 939-955.

Hobbs, R. W., Drummond, B. J. & Goleby, B. R. (2006). The effects of three-dimensional structure on two-dimensional images of the crustal seismic sections and on the interpretation of shear zone morphology. *Geophysical Journal International,* 164(3)**,** pp. 490-500.

House, M., Dentith, M. C., Trench, A., Groves, D. I. & Miller, D. (1999). Structure of the highly mineralised late-Archaean granitoid-greenstone terrain and the underlying crust in the Kambalda-Widgiemooltha area, Western Australia, from the integration of geophysical datasets. *Exploration Geophysics,* 30**,** pp. 50-67.

Huleatt, M. B. & Jaques, A. L. (2005). Australian gold exploration 1976-2003. *Resources Policy,* 30(1)**,** pp. 29-37.

Jaques, A. L., Jaireth, S. & Walshe, J. L. (2002). Mineral systems of Australia: an overview of resources, settings and processes. *Australian Journal of Earth Sciences,* 49(4)**,** pp. 623-660.

Ji, S., Wang, Q. & Xia, B. (2002). *Handbook of Seismic Properties of Minerals, Rocks and Ores*. École Polytechnique de Montréal, 630 p.

Kean, W. F., Day, R., Fuller, M. & Schmidt, V. (1976). The effect of uniaxial compression on the initial susceptibility of rocks as a function of grain size and composition of their constituent titanomagnetites. *Journal of Geophysical Research,* 81(5)**,** pp. 861-872.

Kitware, Inc. (2007). *VTK File Formats*. The VTK User's Guide, Kitware, Inc., New York. http://www.vtk.org/pdf/file-formats.pdf, accessed 28 May 2007.

Konty, A., Friedrich, G., Behr, H. J., Wall, H. D., Horn, E. E., Möller, P. & Zulauf, G. (1997). Formation of ore minerals in metamorphic rocks of the German continental deep drilling site (KTB). *Journal of Geophysical Research – Solid Earth,* 102(B8), pp. 18323-18336.

Leaman, D. E. (1991). Surface gravity and magnetic responses of mineralization, Mt. Isa, northwest Queensland, Australia. *Geophysics,* 56(4), pp. 542-549.

Li, Y. & Oldenburg, D. W. (1996). 3-D inversion of magnetic data. *Geophysics,* 61(2), pp. 394-408.

Li, Y. & Oldenburg, D. W. (1998). 3D inversion of gravity data. *Geophysics,* 63(1), pp. 109-119.

Martin-Hernandez, F. & Hirt, A. M. (2003). The anisotropy of magnetic susceptibility in biotitie, muscovite and chlorite single crystals. *Tectonophysics,* 367(1-2), pp. 13-28.

Mavko, G., Mukerji, T. & Dvorkin, J. (2003). *The Rock Physics Handbook: Tools for Seismic Analysis in Porous Media*. Cambridge University Press, 339 p.

Miller, J. M. & Nugus, M. (2006). The structural evolution of the Sunrise Shear Zone and the overlying Watu and Western Shear Zones, Sunrise Dam gold deposit, Laverton, W.A., ***pmd****CRC* Project Report: Project Y4, ***pmd****CRC* Melbourne, 90p.

Milsom, J. (2003a). *Field Geophysics, Third Edition*. John Wiley & Sons Ltd, 244 p.

Milsom, J. (2003b). Magnetic Method. In *Field Geophysics, Third Edition.* Third Edition ed. John Wiley & Sons, Ltd. pp. 232.

Mooney, H. M. & Bleifuss, R. (1953). Magnetic susceptibility measurements in Minnesota part II: Analysis of field results. *Geophysics,* 18(2), pp. 383-393.

Nelson, P. H. & Johnston, D. (1994). Geophysical and geochemical logs from a copper oxide deposit, Santa Cruz project, Casa Grande, Arizona. *Geophysics,* 59(12), pp. 1827-1838.

Neumayr, P., Hagemann, S. G., Walshe, J. L. & Morrison, R. S. (2003). Camp- to deposit-scale zonation of hydrothermal alteration in the St Ives gold camp, Yilgarn Craton, Western Australia: evidence for two fluid systems? *Proceedings of the Society of Geology Applied to Mineral Deposits Conference.* Athens, Greece.

Neumayr, P., Walshe, J. L., Horn, L., Petersen, K., Deyell, C., Moran, K., Howe, D., Connors, K., Stolz, N., Morrison, R. S. & Hagemann, S. G. (2004). Hydrothermal alteration footprints and gold mineralization in the St Ives gold camp. In Barnicoat, A. C. & Korsch, R. J. (Eds.) *Predictive Mineral Discovery CRC Conference.* Barossa Valley. https://www.ga.gov.au/servlet/BigObjFileManager?bigobjid=GA6780.

Neumayr, P., Walshe, J. L. & Hagemann, S. (2005). Camp- to Deposit-Scale Alteration Footprints in the Kalgoorlie-Kambalda Area. ***pmd****CRC* Project Y3 Final Report.

Neumayr, P., Walshe, J. L. & Henson, P. (2006). Alteration and Fluid Flow at Laverton. In Barnicoat, A. C. & Korsch, R. J. (Eds.) *Predictive Mineral Discovery Cooperative Research Centre – Extended Abstracts from the April 2006 Conference.* Geoscience Australia Record 2006/07.

Newton, P. G., Gibbs, D., Grove, A., Jones, C. M. & Ryall, A. W. (1998). The Sunrise-Cleo gold deposit. In Berkman, D. A. & Mackenzie, D. H. (Eds.) *Geology of Australian and Papua New Guinea Mineral Deposits.* The Australian Institute of Mining and Metallurgy Monograph 22, The Australian Institute of Mining and Metallurgy, Melbourne. pp. 179-186.

O'Reilly, W., Hoffmann, V., Chouker, A. C., Soffel, H. C. & Menyeh, A. (2000). Magnetic properties of synthetic analogues of pyrrhotite ore in the grain size of 1-24μm. *Geophysical Journal International,* 142(3), pp. 669-683.

Olhoeft, G. R. & Johnson, G. R. (1989). Densities of Rocks and Minerals. In Carmichael, R. S. (Ed.) *Practical Handbook of Physical Properties of Rocks and Minerals.* CRC Press. pp. 141-176.

Parasnis, D. S. (1973). *Mining geophysics, revised ed.* Elsevier, Amsterdam. 395 p.

Peters, C. & Thompson, R. (1998). Magnetic identification of selected natural iron oxides and sulphides. *Journal of Magnetism and Magnetic Materials,* 183, pp. 365-374.

Prendergast, K. (2007). Application of lithogeochemistry to exploration in the St Ives goldfield, Western Australia. *Geochemistry: Exploration, Environment, Analysis,* 7(2), pp. 99-108.

Putnis, A. (1975). Observations on coexisting pyrrhotite phases by transmission electron microscopy. *Contributions to Mineralogy and Petrology,* 52(4), pp. 307-313.

Rauen, A., Soffel, H. C. & Winter, H. (2000). Statistical analysis and origin of the magnetic susceptibility of drill cuttings from the 9.1-km-deep KTB drill hole. *Geophysical Journal International,* 142(1), pp. 83-94.

Ramachandra Rao, M. B. (1975). *Outlines of Geophysical Prospecting*. Wesley Press, Mysore, India.

Roache, A. (2005). Comparison of alteration and structure between Conqueror, Belleisle and Maximus: implications for exploration. *MERIWA 358 Report to Goldfields – St Ives.*

Rona, P. A. (1978). Magnetic Signatures of Hydrothermal Alteration and Volcanogenic Mineral Deposits in Oceanic Crust. *Journal of Volcanology and Geothermal Research,* 3(1-2), pp. 219-225.

Rumel, F. & Heerden, W. L. V. (1978). International Society for Rock Mechanics: Commission on Standardization of Laboratory and Field Tests. Suggested Methods for Determing Sound Velocity. *International Journal of Rock Mechanics and Mining Sciences & Geomechanics Abstracts,* 15(2), pp. 53-58.

Ruming, K. J. (2006). *Controls on Lode Gold Mineralisation in the Victory Thrust Complex, St Ives Goldfield, Western Australia*. PhD thesis, School of Environmental and Life Sciences, University of Newcastle, Newcastle. 561 p.

Salier, B. P., Groves, D. I., McNaughton, N. J. & Fletcher, I. R. (2004). The world-class Wallaby gold deposit, Laverton, Western Australia: An orogenic-style overprint on a magmatic-hydrothermal magnetite-calcite alteration pipe? *Mineralium Deposita,* 39, pp. 473-494.

Salisbury, M. H., Milkereit, B., Ascough, G., Adair, R., Matthews, L., Schmitt, D. R., Mwenifumbo, J., Eaton, D. W. & Wu, J. (2000). Physical properties and seismic imaging of massive sulfides. *Geophysics,* 65(6), pp. 1882-1889.

Salisbury, M. H. & Snyder, D. (2004). Seismic Methods. Report to Natural Resources Canada. http://gsc.nrcan.gc.ca/mindep/method/seismic/pdf/methods.seismic.salisbury_snyder.pdf.

Schwarz, E. J. (1991). Magnetic expressions of intrusions including magnetic aureoles. *Tectonophysics,* 192(1-2), pp. 191-200.

Shandley, P. D. & Bacon, L. O. (1966). Analysis for magnetite utilizing magnetic susceptibility. *Geophysics,* 31(2), pp. 398-409.

Sheldon, H. A., Zhang, Y., Blewett, R. S., Barnicoat, A. & Ord, A. (2006). Testing predictive exploration models for the Yilgarn by computer simulation. In Barnicoat, A. C. & Korsch, R. J. (Eds.) *Predictive Mineral Discovery Cooperative Research Centre: extended abstracts from the April 2006 Conference.* Geoscience Australia Record 2006/07.

Shvarov, Y. V. & Bastrakov, E. N. (2003). logK package: UT2K and R2K utilities. Unpublished computer file: Canberra, © 2003-2007 ***pmd*CRC***.

Stacey, F. D. (1962). The Physical Theory of Rock Magnetism. *Advances in Physics,* 12(45), pp. 45-133.

Standing, J. G. (2007). Terrane amalgamation in the Eastern Goldfields Superterrane, Yilgarn Craton: Evidence from tectonostratigraphic studies of the Laverton Greenstone Belt. *Precambrian Research,* in press, doi:10.1016/j.precamres.2007.06.015.

Stolz, E. (2003). Direct detection of gold bearing structures at St Ives, WA – DHEM vs DHMMR. ASEG Conference, Adelaide, February 2003. *Preview*, 102, pp. 77-82.

Stolz, E., Urosevic, M. & Connors, K. (2004). Reflection seismic surveys at St Ives Gold Mine, WA. *17th Geophysical Conference and Exhibition.* Sydney, Australia, Australian Society of Exploration Geophysicists.

Strangway, D. W. (1967). Mineral magnetism, and Magnetic characteristics of rocks. In *Mining Geophysics – Theory, Vol. 2.* Society of Exploration Geophysicists, Tulsa.

Sung, Y.-H., Ciobanu, C. L., Pring, A., Brügger, J., Skinner, W., Cook, N. J. & Nugus, M. (2007). Tellurides from Sunrise Dam gold deposit, Yilgarn Craton, Western Australia: a new occurrence of nagyágite. *Mineralogy and Petrology,* 91(3-4), pp. 249-270.

Swager, C. (1997). Tectono-stratigraphy of late Archaean greenstone terranes in the southern Eastern Goldfields, Western Australia. *Precambrian Research,* 83(1), pp. 11-42.

Telford, W. M., Geldart, L. P. & Sheriff, R. E. (1990a). *Applied Geophysics (Second Edition)*. Cambridge University Press, Cambridge. 790 p.

Telford, W. M., Geldart, L. P. & Sheriff, R. E. (1990b). Seismic Method. In *Applied Geophysics (Second Edition).* Cambridge University Press, Cambridge. pp. 136-283.

Toft, P. B., Arkani-Hamed, J. & Haggerty, S. E. (1990). The effects of serpentinization on density and magnetic susceptibility: a petrophysical model. *Physics of the Earth and Planetary Interiors,* 65(1-2), pp. 137-157.

Urosevic, M., Stolz, N. & Massey, S. (2006). Seismic exploration of complex mineral deposits – Yilgarn Craton. In Denham, D. (Ed.) *Convention handbook: Australian Earth Sciences Convention 2006: GSA 18th Australian Geological Convention & ASEG 18th International Geophysical Convention and Exhibition.* Melbourne Convention and Exhibition Centre.

van den Berg, C. P., Gidiow, R. M., Duweke, W. A., Müller, B. & Smith, G. C. (1992). AVO Analysis in Gold Exploration: A South African Case Study. *62nd Annual International Meeting: Society of Exploration Geophysicists*, pp. 856-859.

Walshe, J. L., Neumayr, P. & Petersen, K. J. (2006). Scale-integrated, architectural and geodynamic controls on alteration and geochemistry of gold systems in the Eastern Goldfields Province, Yilgarn Craton: M358 Project. *MERIWA Final Report 256.*, Minerals and Energy Research Institute of Western Australia, 290p.

Watchorn, R. B. (1998). Kambalda-St Ives gold deposits. In Berkman, D. A. & Mackenzie, D. H. (Eds.) *Geology of Australian and Papua New Guinean Mineral Deposits.* The Australian Institute of Mining and Metallurgy Monograph 22, The Australian Institute of Mining and Metallurgy, Melbourne. pp. 243-254.

Watt, J. P. (1988). Elastic Properties of Polycrystalline Minerals: Comparison of Theory and Experiment. *Physics and Chemistry of Minerals,* 15(6), pp. 579-587.

Werner, S. (1945). *Determinations of the magnetic susceptibilities of ores and rocks from Swedish iron ore deposits*. Swedish Geological Survey, Stockholm. Series C 472, # 39. 79 p.

Whitford, M. D. (2004). *Geophysical properties of the regolith near the Victory gold mine at Kambalda, Western Australia*. BSc (Hons) thesis, Department of Exploration Geophysics, Curtin University of Technology (Report No.: GPH 3/04).

Widess, M. B. (1973). How Thin Is A Thin Bed? *Geophysics,* 38(6), pp. 1176-1180.

Williams, N. C. & Dipple, G. (2006). Mapping sulfide abundances using densities and magnetic susceptibilities. In Denham, D. (Ed.) *Convention handbook: Australian Earth Sciences Convention 2006: GSA 18th Australian Geological Convention & ASEG 18th International Geophysical Convention and Exhibition.* Melbourne Convention and Exhibition Centre.

Wyllie, M. R. J., Gregory, A. R. & Gardner, L. W. (1956). Elastic wave velocities in heterogeneous and porous media. *Geophysics,* 21(1), pp. 41-70.

Yang, K. (2006). Mineralogical Interpretation of HyLogging Data for Drill-holes from the Conqueror Deposit of the St Ives Goldfield, WA. CSIRO Exploration and Mining.

Yilmaz, O. & Doherty, S. M. (2000). *Seismic Data Analysis: Processing, Inversion and Interpretation of Seismic Data*. Society of Exploration Geophysicists, Tulsa. 2027 p.

APPENDICES

A1. Table of mineral properties

Density

Group	Mineral	Notes	Density (average, tm^{-3})	Reference
Amphibole	Ferrohornblende		3.230	http://webmineral.com/data/Ferrohornblende.shtml
Amphibole	Hornblende	$(Ca,Na)_{2-3}(Mg,Fe,Al)_5(Al,Si)_8O_{22}(OH)_2$	3.150	http://www.galleries.com/minerals/silicate/hornblen/hornblen.htm
Amphibole	Hornblende		3.120	Carmichael (1989b)
Amphibole	Hornblende		3.150	Carmichael (1989b)
Amphibole	Magnesiohornblende		3.230	http://webmineral.com/data/Magnesiohornblende.shtml
Andalusite		Al_2SiO_5	3.150	http://www.galleries.com/minerals/silicate/andalusi/andalusi.htm
Anhydrite		$CaSO_4$	3.000	http://www.galleries.com/minerals/sulfates/anhydrit/anhydrit.htm
Anhydrite		$CaSO_4$	2.970	http://webmineral.com/data/Anhydrite.shtml
Aragonite		$CaCO_3$	2.900	http://www.galleries.com/minerals/carbonat/aragonit/aragonit.htm
Aragonite		$CaCO_3$	2.930	http://webmineral.com/data/Aragonite.shtml
Baryte		$BaSO_4$	4.480	http://webmineral.com/data/Barite.shtml
Baryte			4.400	http://en.wikipedia.org/wiki/Barite
Biotite			3.050	Carmichael (1989b)
Biotite			3.090	http://webmineral.com/data/Biotite.shtml
Biotite			3.150	http://www.galleries.com/minerals/silicate/biotite/biotite.htm
Bronzite		$Mg_{0.8}Fe_{0.2}SiO_3$	3.354	Carmichael (1989b)
Bronzite		Synonym hypersthene	3.550	http://webmineral.com/data/Hypersthene.shtml
Calcite		$CaCO_3$	2.710	http://webmineral.com/data/Calcite.shtml
Calcite		$CaCO_3$	2.712	Carmichael (1989b)
Celestine		$SrSO_4$	3.950	http://webmineral.com/data/Celestine.shtml
Chalcopyrite			4.190	http://webmineral.com/data/Chalcopyrite.shtml
Chromite			4.190	http://webmineral.com/data/Chromite.shtml
Coesite			2.930	http://webmineral.com/data/Coesite.shtml
Diamond			3.510	http://webmineral.com/data/Diamond.shtml
Dolomite		$CaMg(CO_3)_2$	2.850	http://webmineral.com/data/Dolomite.shtml
Epidote			3.400	Carmichael (1989b)
Epidote			3.450	http://webmineral.com/data/Epidote.shtml
Epidote			3.400	http://www.galleries.com/minerals/silicate/epidote/epidote.htm
Galena			7.500	http://www.galleries.com/minerals/sulfides/galena/galena.htm

Group	Mineral	Notes	Density (average, tm^{-3})	Reference
Galena			7.400	http://webmineral.com/data/Galena.shtml
Garnet	Almandine		4.190	http://webmineral.com/data/Almandine.shtml
Garnet	Almandine		4.300	http://www.galleries.com/minerals/silicate/almandin/almandin.htm
Garnet	Garnet	$3(Mn_{0.02}Fe_{0.64}Mg_{0.23}Ca_{0.11})O.Al_2O_3.3SiO_2$	4.060	Carmichael (1989b)
Garnet	Garnet	$3(Mn_{0.04}Fe_{0.77}Mg_{0.12}Ca_{0.08})O.Al_2O_3.3SiO_2$	4.060	Carmichael (1989b)
Garnet	Garnet	$3(Mn_{0.06}Fe_{0.74}Mg_{0.13}Ca_{0.07})O.Al_2O_3.3SiO_2$	4.160	Carmichael (1989b)
Garnet	Garnet	$3(Mn_{0.0}Fe_{0.01}Mg_{0.02}Ca_{0.97})O.Al_2O_3.3SiO_2$	3.600	Carmichael (1989b)
Garnet	Garnet	$3(Mn_{0.0}Fe_{0.17}Mg_{0.72}Ca_{0.11})O.Al_2O_3.3SiO_2$	3.670	Carmichael (1989b)
Garnet	Garnet	$3(Mn_{0.0}Fe_{0.63}Mg_{0.29}Ca_{0.08})O.Al_2O_3.3SiO_2$	4.010	Carmichael (1989b)
Garnet	Garnet	$3(Mn_{0.0}Fe_{0.76}Mg_{0.21}Ca_{0.03})O.Al_2O_3.3SiO_2$	4.160	Carmichael (1989b)
Garnet	Garnet	$3(Mn_{0.0}Fe_{0.81}Mg_{0.14}Ca_{0.04})O.Al_2O_3.3SiO_2$	4.183	Carmichael (1989b)
Garnet	Garnet	$3(Mn_{0.54}Fe_{0.46}Mg_{0.0}Ca_{0.0})O.Al_2O_3.3SiO_2$	4.249	Carmichael (1989b)
Garnet	Garnet	$3(Mn_{0.55}Fe_{0.435}Mg_{0.02}Ca_{0.013})O.Al_2O_3.3SiO_2$	4.247	Carmichael (1989b)
Garnet	Grossular	$Ca_3Al_2Si_3O_{12}$	3.570	http://webmineral.com/data/Grossular.shtml
Garnet	Pyrope		3.600	http://www.galleries.com/minerals/silicate/pyrope/pyrope.htm
Garnet	Pyrope		3.740	http://webmineral.com/data/Pyrope.shtml
Gypsum			2.300	http://www.galleries.com/minerals/sulfates/gypsum/gypsum.htm
Gypsum			2.300	http://webmineral.com/data/Gypsum.shtml
Hematite			5.250	http://webmineral.com/data/Hematite.shtml
Ilmenite			4.720	Carmichael (1989b)
K-Feldspar	Microcline	$KAlSi3O_8$	2.560	http://webmineral.com/data/Microcline.shtml
K-Feldspar	Microcline		2.500	http://www.galleries.com/minerals/silicate/microcli/microcli.htm
K-Feldspar	Orthoclase	$KAlSi3O_8$	2.560	http://webmineral.com/data/Orthoclase.shtml
K-Feldspar	Orthoclase	$KAlSi3O_8$	2.545	http://www.galleries.com/minerals/silicate/orthocla/orthocla.htm
K-Feldspar	Sandine		2.545	http://www.galleries.com/minerals/silicate/sanidine/sanidine.htm
K-Feldspar	Sandine		2.520	http://webmineral.com/data/Sanidine.shtml
Limonite			3.132	http://www.simetric.co.uk/si_materials.htm
Magnetite			5.100	http://www.galleries.com/minerals/oxides/magnetit/magnetit.htm
Magnetite			5.150	http://webmineral.com/data/Magnetite.shtml
Majorite		Mj66Py34	4.000	http://webmineral.com/data/Majorite.shtml
Mica	Muscovite	$KAl_3Si_3O_{10}(OH)_2$	2.820	http://webmineral.com/data/Muscovite.shtml
Mica	Muscovite		2.800	http://www.galleries.com/minerals/silicate/muscovit/muscovit.htm
Mica	Phlogopite		2.800	Carmichael (1989b)
Mica	Phlogopite		2.820	Carmichael (1989b)
Monticellite		$CaMgSiO_4$	3.200	http://webmineral.com/data/Monticellite.shtml
Olivine			3.324	Carmichael (1989b)
Olivine	Fayalite		4.390	http://webmineral.com/data/Fayalite.shtml
Olivine	Forsterite		3.270	http://webmineral.com/data/Forsterite.shtml
Olivine	Forsterite		3.220	Carmichael (1989b)
Olivine	Forsterite		3.224	Carmichael (1989b)
Olivine	Forsterite 93%, Fayalite 7%		3.311	Carmichael (1989b)

Group	Mineral	Notes	Density (average, tm^{-3})	Reference
Pentlandite			4.800	http://webmineral.com/data/Pentlandite.shtml
Periclase		MgO	3.780	http://webmineral.com/data/Periclase.shtml
Periclase		MgO	3.600	http://www.galleries.com/minerals/oxides/periclas/periclas.htm
Perovskite		$(Mg,Fe)SiO_3$	4.000	http://www.galleries.com/minerals/oxides/perovski/perovski.htm
Perovskite		$(Mg,Fe)SiO_3$	4.000	http://webmineral.com/data/Perovskite.shtml
Plagioclase	Albite		2.620	http://webmineral.com/data/Albite.shtml
Plagioclase	Albite		2.610	http://www.galleries.com/minerals/silicate/albite/albite.htm
Plagioclase	Anorthite		2.730	http://webmineral.com/data/Anorthite.shtml
Plagioclase	Anorthite		2.760	http://www.galleries.com/minerals/silicate/anorthit/anorthit.htm
Plagioclase	Anorthite:Albite	0.09:0.91	2.610	Carmichael (1989b)
Plagioclase	Anorthite:Albite	0.16:0.84	2.640	Carmichael (1989b)
Plagioclase	Anorthite:Albite	0.24:0.76	2.640	Carmichael (1989b)
Plagioclase	Anorthite:Albite	0.29:0.61	2.640	Carmichael (1989b)
Plagioclase	Anorthite:Albite	0.53:0.47	2.680	Carmichael (1989b)
Plagioclase	Anorthite:Albite	0.56:0.44	2.690	Carmichael (1989b)
Plagioclase	Anorthite:Albite	0.58:0.42	2.680	Carmichael (1989b)
Plagioclase	Perthite	0.054:0.35:0.09 (Or:Ab:An)	2.570	Carmichael (1989b)
Plagioclase	Perthite	0.61:0.36:0.02 (Or:Ab:An)	2.570	Carmichael (1989b)
Plagioclase	Perthite	0.65:0.27:0.04 (Or:Ab:An)	2.570	Carmichael (1989b)
Plagioclase	Perthite	0.67:0.29:0 (Or:Ab:An)	2.540	Carmichael (1989b)
Plagioclase	Perthite	0.74:19:0.02 (Or:Ab:An)	2.570	Carmichael (1989b)
Plagioclase	Perthite	0.75:0.22:0 (Or:Ab:An)	2.540	Carmichael (1989b)
Plagioclase	Perthite	0.79:0.19:0.02 (Or:Ab:An)	2.560	Carmichael (1989b)
Pyrite			5.040	Salisbury et al. (2000)
Pyrite			5.100	Ji et al. (2002)
Pyrite			5.010	http://webmineral.com/data/Pyrite.shtml
Pyrite			5.100	http://www.galleries.com/minerals/sulfides/pyrite/pyrite.htm
Pyroxene	Aegirine	$NaFeSi_2O_6$	3.520	http://webmineral.com/data/Aegirine.shtml
Pyroxene	Aegirine	Uses aegirite, synonym for aegirine	3.500	Carmichael (1989b)
Pyroxene	Aegirine-Augite	Uses aegirite, synonym for aegirine	3.420	Carmichael (1989b)
Pyroxene	Augite		3.320	Carmichael (1989b)
Pyroxene	Augite		3.400	http://webmineral.com/data/Augite.shtml
Pyroxene	Diallage	May refer to amphibole, pyroxene and/or hyperstehene	3.300	Carmichael (1989b) http://www.mindat.org/min-1281.html; Augite or Diopside are suggested by http://www.britannica.com/eb/article-9030257
Pyroxene	Diopside		3.310	Carmichael (1989b)
Pyroxene	Diopside		3.300	http://www.galleries.com/minerals/silicate/diopside/diopside.htm
Pyroxene	Diopside		3.400	http://webmineral.com/data/Diopside.shtml
Pyroxene	Enstatite	$MgSiO_3$	3.200	http://webmineral.com/data/Enstatite.shtml
Pyroxene	Enstatite		3.200	http://www.galleries.com/minerals/silicate/enstatit/enstatit.htm
Pyroxene	Ferrosilite	$FeSiO_3$	3.950	http://webmineral.com/data/Ferrosilite.shtml
Pyroxene	Hedenbergite		3.550	http://webmineral.com/data/Hedenbergite.shtml
Pyroxene	Hedenbergite		3.400	http://www.galleries.com/minerals/silicate/hedenber/hedenber.htm

Group	Mineral	Notes	Density (average, tm^{-3})	Reference
Pyroxene	Jadeite	Pyroxene according to http://www.galleries.com/minerals/silicate/jadeite/jadeite.htm	3.300	http://webmineral.com/data/Jadeite.shtml
Pyroxene	Jadeite		3.300	http://www.galleries.com/minerals/silicate/jadeite/jadeite.htm
Pyroxene	Omphacite		3.340	http://webmineral.com/data/Omphacite.shtml
Pyroxene	Orthopyroxene	Enstatite 0.85 Ferrosilite 0.15	3.335	Carmichael (1989b)
Pyrrhotite			4.650	Salisbury et al. (2000)
Pyrrhotite			4.610	http://webmineral.com/data/Pyrrhotite.shtml
Pyrrhotite			4.600	http://www.galleries.com/minerals/sulfides/pyrrhoti/pyrrhoti.htm
Quartz	Stishovite		4.350	http://webmineral.com/data/Stishovite.shtml
Quartz	Stishovite		4.280	http://www.galleries.com/minerals/oxides/stishovi/stishovi.htm
Quartz			2.649	Carmichael (1989b)
Quartz			2.650	http://www.galleries.com/minerals/silicate/quartz/quartz.htm
Quartz			2.620	http://webmineral.com/data/Quartz.shtml
Ringwoodite			3.900	http://webmineral.com/data/Ringwoodite.shtml
Rutile			4.260	Carmichael (1989b)
Rutile			4.250	http://webmineral.com/data/Rutile.shtml
Rutile			4.200	http://www.galleries.com/minerals/oxides/rutile/rutile.htm
Sillimanite			3.240	http://webmineral.com/data/Sillimanite.shtml
Sillimanite			3.200	http://www.galleries.com/minerals/silicate/silliman/silliman.htm
Sphalerite			4.000	http://www.galleries.com/minerals/sulfides/sphaleri/sphaleri.htm
Sphalerite			4.050	http://webmineral.com/data/Sphalerite.shtml
Spinel		$FeAl_2O_4$	4.280	Carmichael (1989b)
Spinel		$Mg_{0.75}Fe_{0.36}Al_{1.90}O_4$	3.826	Carmichael (1989b)
Spinel		$MgAl_2O_4$	3.640	http://webmineral.com/data/Spinel.shtml
Spinel		$MgAl_2O_4$	3.800	http://www.galleries.com/minerals/oxides/spinel/spinel.htm
Spinel		$MgO.2.6(Al_2O_3)$	3.619	Carmichael (1989b)
Spinel		$MgO.3.5(Al_2O_3)$	3.670	Carmichael (1989b)
Staurolite			3.710	http://webmineral.com/data/Staurolite.shtml
Staurolite			3.750	http://www.galleries.com/minerals/silicate/stauroli/stauroli.htm
Topaz			3.450	http://www.galleries.com/minerals/silicate/topaz/topaz.htm
Topaz			3.550	http://webmineral.com/data/Topaz.shtml
Tourmaline			3.310	http://webmineral.com/data/Buergerite.shtml
Tourmaline			3.150	http://www.galleries.com/minerals/silicate/tourmali.htm
Wadsleyite			3.840	http://webmineral.com/data/Wadsleyite.shtml
Water	Ice		0.920	http://www.elmhurst.edu/~chm/vchembook/122Adensityice.html
Wustite			5.880	http://webmineral.com/data/Wustite.shtml
Zircon			4.700	Carmichael (1989b)
Zircon			4.650	http://webmineral.com/data/Zircon.shtml
Zircon			4.650	http://www.galleries.com/minerals/silicate/zircon/zircon.htm

Table 8: Compilation of the density of minerals from the literature.

Magnetic susceptibility

Mineral	Minimum (SI)	Maximum (SI)	Average (provided)	Average (calculated)	Reference	Notes
Magnetite	1.25	20.10619	6.283185	10.678095	Telford et al. (1990a)	Converted from 10^{-6} emucm^{-3} using 1 emucm^{-3} = 4π SI
	2.5131274	16.33628		9.4247037	Ramachandra Rao (1975)	Converted to SI
			3.769911		Carmichael (1989a)	
	3.769911184	50.26548246		27.01769682	Dohr (1974)	Converted to SI
	3.769911184	10.05309649		6.911503838	Dobrin (1976)	Converted to SI
2% magnetite in epoxy			0.014325663		Kean et al. (1976)	Grain size 1-2 μm, converted to SI
			0.017467255		Kean et al. (1976)	Grain size 4-8 μm, converted to SI
			0.018472565		Kean et al. (1976)	Grain size 37-75 μm, converted to SI
			0.027646015		Kean et al. (1976)	Grain size 75-150 μm, converted to SI
Titanomagnetite, 2%			0.004272566		Kean et al. (1976)	Grain size 1-2 μm, converted to SI
			0.004021239		Kean et al. (1976)	Grain size 5-15 μm, converted to SI
			0.012315043		Kean et al. (1976)	Grain size 75-150 μm, converted to SI
Hematite	0.000502655	0.037699112	0.006911504	0.019100883	Telford et al. (1990a)	
	0.005403539	0.040212386		0.022807963	Ramachandra Rao (1975)	
Ilmenite			1.696460033		Dobrin (1976)	
	1.696460033	3.166725395		2.431592714	Ramachandra Rao (1975)	
	0.314159265	3.769911184		2.042035225	Telford et al. (1990a)	
			1.721596		Carmichael (1989a)	
Limonite			0.002764602		Telford et al. (1990a)	
Pyrrhotite			1.570796327		Dobrin (1976); Ramachandra Rao (1975)	
	0.001256637	6.283185307	1.570796327	3.142220972	Telford et al. (1990a)	
Pyrite	5.02655E-05	0.005277876	0.001633628	0.002664071	Telford et al. (1990a)	
Chalcopyrite			0.000402124		Telford et al. (1990a)	
Siderite			0.005026548		Collinson (1986)	
			0.004875752		Strangway (1967)	
	0.001256637	0.003895575		0.002576106	Telford et al. (1990a)	
Chromite	0.003015929	0.118123884	0.007539822	0.060569906	Telford et al. (1990a)	
Jacobsite			0.025132741		Ramachandra Rao (1975)	
Franklinite			0.452389342		Telford et al. (1990)	
Orthopyroxene			0.001759292		Strangway (1967)	24% FeO, 1% Fe_2O_3
Pyroxene			0.003581416		Collinson (1986)	$FeSiO_2$, calculated from density value by original ref
Biotitie			0.002513274		Collinson (1986)	Calculated from density value by original ref, 19.2% FeO, 7.9% Fe_2O_3
			0.00238761		Strangway (1967)	
			0.00135		Martin-Hernandez and Hirt (2003)	bio1.01
			0.00098		Martin-Hernandez and Hirt (2003)	bio1.02
			0.00102		Martin-Hernandez and Hirt (2003)	bio1.03
			0.00122		Martin-Hernandez and Hirt (2003)	bio1.04
			0.00104		Martin-Hernandez and Hirt (2003)	bio2.01
			0.0011		Martin-Hernandez and Hirt (2003)	bio2.02

Mineral	Minimum (SI)	Maximum (SI)	Average (provided)	Average (calculated)	Reference	Notes
			0.00074		Martin-Hernandez and Hirt (2003)	bio4.01
			0.00113		Martin-Hernandez and Hirt (2003)	bio5.01
			0.0011		Martin-Hernandez and Hirt (2003)	bio6.01
			0.00109		Martin-Hernandez and Hirt (2003)	bio6.02
			0.001		Martin-Hernandez and Hirt (2003)	bio7.02
			0.00114		Martin-Hernandez and Hirt (2003)	bio7.04
				0.001075833	derived from Martin-Hernandez and Hirt (2003)	
Muscovite			0.000402		Martin-Hernandez and Hirt (2003)	mu1.01
			0.000077		Martin-Hernandez and Hirt (2003)	mu2.01
			0.000079		Martin-Hernandez and Hirt (2003)	mu2.02
			0.000065		Martin-Hernandez and Hirt (2003)	mu2.03
			0.000118		Martin-Hernandez and Hirt (2003)	mu3.01
			0.000116		Martin-Hernandez and Hirt (2003)	mu3.02
			0.000115		Martin-Hernandez and Hirt (2003)	mu3.03
			0.000118		Martin-Hernandez and Hirt (2003)	mu4.01
			0.000126		Martin-Hernandez and Hirt (2003)	mu5.01
				0.000135111	derived from Martin-Hernandez and Hirt (2003)	
Chlorite			0.00021		Martin-Hernandez and Hirt (2003)	chl1.01
			0.00022		Martin-Hernandez and Hirt (2003)	chl1.02
			0.00139		Martin-Hernandez and Hirt (2003)	chl2.01
			0.00024		Martin-Hernandez and Hirt (2003)	chl3.01
			0.00041		Martin-Hernandez and Hirt (2003)	chl4.01
			0.00025		Martin-Hernandez and Hirt (2003)	chl5.01
			0.00023		Martin-Hernandez and Hirt (2003)	chl5.02
			0.00096		Martin-Hernandez and Hirt (2003)	chl6.01
				0.00048875	derived from Martin-Hernandez and Hirt (2003)	
Fayalite			0.005516637		Strangway (1967)	Fe2SiO4
Quartz			-1.25664E-05		Telford et al. (1990a)	
Rock salt			-1.25664E-05		Ramachandra Rao (1975)	
Calcite			-7.53982E-06		Telford et al. (1990a)	
Sphalerite			0.000753982		Telford et al. (1990a)	
Galena			-3.24212E-05		Strangway (1967)	
Cuprite			-1.08071E-05		Strangway (1967)	
Hausmannite			0.003279823		Strangway (1967)	Mn3O4
Rhodochrosite			0.004649557		Strangway (1967)	MnCO3
Anhydrite	-1.50796×10^{-5}	-1.3823×10^{-5}		-1.44513×10^{-5}	Ramachandra Rao (1975)	Anhydrite
Rutile			3.76991E-06		Strangway (1967)	
Illite			0.000427257		Collinson (1986)	1.4% FeO, 4.7% Fe_2O_3
Montmorillonite			0.000326726		Collinson (1986)	2.8% FeO, 3% Fe_2O_3
Nontronite			0.001759292		Collinson (1986)	Fe-rich montmorillonite, 0.2% FeO, 28% Fe_2O_3

Table 9: Compilation of magnetic susceptibility of minerals from the literature.

Seismic velocity

Group	Mineral	Formula Notes	v_p min	v_p max	v_p avg	P-wave anisotropy	$v_{s(1)}$ min	$v_{s(1)}$ max	$v_{s(1)}$ avg	$v_{s(2)}$ avg	Reference
Amphibole	Hornblende	$(Ca,Na)_{2-3}(Mg,Fe,Al)_5(Al,Si)_8O_{22}(OH)_2$	6000	7900	6950	23.80%	3400	4300	3850	3600	Ji et al. (2002)
Amphibole	Hornblende				6810				3720		Christensen (1989)
Amphibole	Hornblende				7040				3810		Christensen (1989)
Andalusite		Al_2SiO_5	8600	11000	9800	21.70%	5400	6300	5950	5450	Ji et al. (2002)
Anhydrite		$CaSO_4$	5100	7900	6500	35.30%	3000	4300	3650	2650	Ji et al. (2002)
Aragonite		$CaCO_3$	5200	7400	6300	30.30%	3500	4300	3900	3400	Ji et al. (2002)
Baryte		$BaSO_4$	4000	4900	4450	18.00%	2100	2800	2450	2050	Ji et al. (2002)
Biotite					5260				2870		Christensen (1989)
Bronzite		$Mg_{0.8}Fe_{0.2}SiO_3$			7780				4720		Christensen (1989)
Calcite		$CaCO_3$	5600	7700	6650	27.60%	2900	4700	3800	3150	Ji et al. (2002)
Calcite					5780				3330		Christensen (1989)
Celestine		$SrSO_4$	5000	5700	5350	11.60%	2100	2800	2450	2200	Ji et al. (2002)
Chalcopyrite					5100				2440		Eaton et al. (2003)
Chromite			7900	8400	8150	5.40%	4400	4800	4600	4500	Ji et al. (2002)
Coesite			6800	10200	8500	34.00%	4200	6100	5150	4050	Ji et al. (2002)
Diamond			17500	18600	18050	5.70%	12100	12800	12450	12250	Ji et al. (2002)
Dolomite		$CaMg(CO_3)_2$	6300	8700	7500	27.90%	3600	5300	4450	3650	Ji et al. (2002)
Dolomite		CaMg(CO3)2			7036		0	0	0		Anselmetti and Eberli (1993)
Epidote					7430		0	0	4240		Christensen (1989)
Epidote			6700	8400	7550	19.90%	3500	5000	4250	4000	Ji et al. (2002)
Galena			3400	4100	3750	16.10%	1700	2600	2150	2000	Ji et al. (2002)
Garnet	Almandine	$Alm_{74}Py_{20}Gr_3Sp_3$	8500	8600	8550	0.90%	4700	4800	4750	4750	Ji et al. (2002)
Garnet	Garnet	$3(Mn_{0.02}Fe_{0.64}Mg_{0.23}Ca_{0.11})O.Al_2O_3.3SiO_2$			8450				4850		Christensen (1989)
Garnet	Garnet	$3(Mn_{0.04}Fe_{0.77}Mg_{0.12}Ca_{0.08})O.Al_2O_3.3SiO_2$			8040				4540		Christensen (1989)
Garnet	Garnet	$3(Mn_{0.06}Fe_{0.74}Mg_{0.13}Ca_{0.07})O.Al_2O_3.3SiO_2$			8220				4610		Christensen (1989)
Garnet	Garnet	$3(Mn_{0.0}Fe_{0.01}Mg_{0.02}Ca_{0.97})O.Al_2O_3.3SiO_2$			8720				5070		Christensen (1989)
Garnet	Garnet	$3(Mn_{0.0}Fe_{0.17}Mg_{0.72}Ca_{0.11})O.Al_2O_3.3SiO_2$			8550				4860		Christensen (1989)
Garnet	Garnet	$3(Mn_{0.0}Fe_{0.63}Mg_{0.29}Ca_{0.08})O.Al_2O_3.3SiO_2$			8170				4710		Christensen (1989)
Garnet	Garnet	$3(Mn_{0.0}Fe_{0.76}Mg_{0.21}Ca_{0.03})O.Al_2O_3.3SiO_2$			8530				4760		Christensen (1989)
Garnet	Garnet	$3(Mn_{0.0}Fe_{0.81}Mg_{0.14}Ca_{0.04})O.Al_2O_3.3SiO_2$			8520				4770		Christensen (1989)
Garnet	Garnet	$3(Mn_{0.54}Fe_{0.46}Mg_{0.0}Ca_{0.0})O.Al_2O_3.3SiO_2$			8480				4760		Christensen (1989)
Garnet	Garnet	$3(Mn_{0.55}Fe_{0.435}Mg_{0.02}Ca_{0.013})O.Al_2O_3.3SiO_2$			8470				4770		Christensen (1989)
Garnet	Grossular	$Ca_3Al_2Si_3O_{12}$	9400	9200	9300	2.20%	5400	5600	5500	5500	Ji et al. (2002)
Garnet	Pyrope				9100	0.20%	0	0	5100	5100	Ji et al. (2002)
Gypsum			4600	6700	5650	30.60%	2200	3600	2900	2300	Ji et al. (2002)
Hematite					6550						Salisbury et al. (2000)
K-Feldspar		$KAlSi3O_8$	5100	8100	6600	37.40%	2800	4800	3800	2950	Ji et al. (2002)
Magnetite			7300	7400	7350	2.30%	4100	4300	4200	4200	Ji et al. (2002)

Group	Mineral	Formula Notes	v_p min	v_p max	v_p avg	P-wave anisotropy	$v_{s(1)}$ min	$v_{s(1)}$ max	$v_{s(1)}$ avg	$v_{s(2)}$ avg	Reference
Majorite		Mj66Py34	8900	9000	8950	1.80%	4900	5400	5150	4950	Ji et al. (2002)
Mica	Muscovite	$KAl_3Si_3O_{10}(OH)_2$	4500	8100	6300	44.20%	2500	5000	3750	2950	Ji et al. (2002)
Mica	Phlogopite				5550				2880		Christensen (1989)
Mica	Phlogopite				5440				2990		Christensen (1989)
Monticellite		$CaMgSiO_4$	6900	8300	7600	16.70%	4300	4500	4400	4050	Ji et al. (2002)
Olivine	Fayalite		6200	7800	7000	20.80%	3300	4200	3750	3100	Ji et al. (2002)
Olivine	Forsterite				8990						Calculated by linear mixing
Olivine	Forsterite				8590				5030		Christensen (1989)
Olivine	Forsterite				8570				5020		Christensen (1989)
Olivine	Forsterite 0.93, Fayalite 0.07		7700	10000	8850	22.90%	4900	5600	5250	4650	Ji et al. (2002)
Olivine	Forsterite 0.93, Fayalite 0.08				8420				4890		Christensen (1989)
Olivine					8480				4930		Christensen (1989)
Pentlandite					4645				2960		
Periclase		MgO	9100	10200	9650	10.20%	5800	6600	6200	5950	Ji et al. (2002)
Perovskite		$(Mg,Fe)SiO_3$	10500	11300	10900	8.90%	6600	7000	6800	6650	Ji et al. (2002)
Plagioclase	Albite	Albite	5200	7400	6300	30.90%	3000	4400	3700	3000	Ji et al. (2002)
Plagioclase	Anorthite:Albite	0.09:0.91			6070				3400		Christensen (1989)
Plagioclase	Anorthite:Albite	0.16:0.84			6220				3230		Christensen (1989)
Plagioclase	Anorthite:Albite	0.24:0.76			6220				3340		Christensen (1989)
Plagioclase	Anorthite:Albite	0.29:0.61			6300				3440		Christensen (1989)
Plagioclase	Anorthite:Albite	0.53:0.47			6570				3530		Christensen (1989)
Plagioclase	Anorthite:Albite	0.56:0.44			6620				3360		Christensen (1989)
Plagioclase	Anorthite:Albite	0.58:0.42			6700				3550		Christensen (1989)
Plagioclase	Anorthite:Albite	0.53:0.47	5700	7800	6750	27.40%	3400	4700	4050	3150	Ji et al. (2002)
Plagioclase	Anorthite		5900	8600	7250	31.80%	3600	5000	4300	3350	Ji et al. (2002)
Plagioclase	Perthite	0.054:0.35:0.09 (Or:Ab:An)			5880				3050		Christensen (1989)
Plagioclase	Perthite	0.61:0.36:0.02 (Or:Ab:An)			5650				3190		Christensen (1989)
Plagioclase	Perthite	0.65:0.27:0.04 (Or:Ab:An)			5740				3130		Christensen (1989)
Plagioclase	Perthite	0.67:0.29:0 (Or:Ab:An)			5580				3040		Christensen (1989)
Plagioclase	Perthite	0.74:19:0.02 (Or:Ab:An)			5790				3110		Christensen (1989)
Plagioclase	Perthite	0.75:0.22:0 (Or:Ab:An)			5560				3060		Christensen (1989)
Plagioclase	Perthite	0.79:0.19:0.02 (Or:Ab:An)			5910				3250		Christensen (1989)
Pyrite					8012.5				4950		Salisbury et al. (2000)
Pyrite			7500	8500	8000	27.40%	3400	4700	4050	3150	Ji et al. (2002)
Pyroxene	Aegirine	$NaFeSi_2O_6$	6700	8400	7550	20.40%	3700	4500	4100	3900	Ji et al. (2002)
Pyroxene	Aegirite				7320				4090		Christensen (1989)
Pyroxene	Aegirite-Augite				7320				4090		Christensen (1989)
Pyroxene	Augite				7220				4180		Christensen (1989)

Group	Mineral	Formula Notes	v_p min	v_p max	v_p avg	P-wave anisotropy	$v_{s(1)}$ min	$v_{s(1)}$ max	$v_{s(1)}$ avg	$v_{s(2)}$ avg	Reference
Pyroxene	Augite		6500	8500	7500	23.30%	3900	4700	4300	4050	Ji et al. (2002)
Pyroxene	Diallage				7030				4260		Christensen (1989)
Pyroxene	Diopside				7700				4380		Christensen (1989)
Pyroxene	Diopside		7000	9400	8200	25.80%	4300	5000	4650	4400	Ji et al. (2002)
Pyroxene	Enstatite		7500	8400	7950	11.30%	4900	5100	5000	4700	Ji et al. (2002)
Pyroxene	Ferrosilite		5800	7000	6400	17.10%	3600	3800	3700	3500	Ji et al. (2002)
Pyroxene	Hedenbergite		6900	8600	7750	19.40%	4000	4700	4350	3950	Ji et al. (2002)
Pyroxene	Jadeite		7900	9500	8700	16.80%	4900	5700	5300	4850	Ji et al. (2002)
Pyroxene	Omphacite	Di 30%, Jd 58% (mol)	7600	9400	8500	18.60%	4800	5400	5100	4800	Ji et al. (2002)
Pyroxene	Orthopyroxene	0.85:0.15			7850				4760		Christensen (1989)
Pyrrhotite					4645				2720		Salisbury et al. (2000)
Quartz	Stishovite	SiO_2	10300	13400	11850	23.60%	7600	8400	8000	6500	Ji et al. (2002)
Quartz					6050				4090		Christensen (1989)
Quartz			5300	7000	6150	24.30%	3700	5100	4400	4000	Ji et al. (2002)
Ringwoodite			9600	9900	9750	3.50%	5700	5900	5800	5700	Ji et al. (2002)
Rutile					9260		0	0	5140	0	Christensen (1989)
Rutile			7900	10600	9250	25.10%	5400	6700	6050	4350	Ji et al. (2002)
Sillimanite			8500	10900	9700	22.70%	5000	6300	5650	5350	Ji et al. (2002)
Sphalerite			5000	5600	5300	13.50%	2600	3300	2950	2750	Ji et al. (2002)
Spinel		$FeAl_2O_4$			8670				4420		Christensen (1989)
Spinel		$Mg_{0.75}Fe_{0.36}Al_{1.90}O_4$			9250				5010		Christensen (1989)
Spinel		$MgAl_2O_4$	8900	10600	9750	16.30%	5200	6600	5900	5400	Ji et al. (2002)
Spinel		$MgO.2.6(Al_2O_3)$			9930				5660		Christensen (1989)
Spinel		$MgO.3.5(Al_2O_3)$			9930				5660		Christensen (1989)
Staurolite			6200	9500	7850	34.50%	4300	5000	4650	3300	Ji et al. (2002)
Topaz			8900	10000	9450	11.60%	5600	6100	6350	5600	Ji et al. (2002)
Tourmaline			7300	9900	8600	26.20%	4600	5900	5250	5000	Ji et al. (2002)
Wadsleyite			8900	10500	9700	15.60%	5500	6500	6000	5500	Ji et al. (2002)
Water		Ice	3400	4000	3700	14.50%	1800	2200	2000	1200	Ji et al. (2002)
Wustite			6500	6600	6550	0.90%	2800	2900	2850	2850	Ji et al. (2002)
Zircon					8060				3970		Christensen (1989)
Zircon			7400	8900	8150	17.10%	3800	5000	4400	3500	Ji et al. (2002)

Table 10: Compilation of seismic velocities (P- and S-wave velocities) and anisotropy from the literature.

Combined properties

Group	Mineral	Formula notes	Density (tm^{-3})	Susceptibility (SI)	v_p (ms^{-1})	v_s (ms^{-1})
Amphibole	Hornblende		3.140		6930	3725
Andalusite			3.150		9800	5700
Anhydrite			2.985		6500	3150
Aragonite			2.915		6300	3650
Baryte			4.440		4450	2250
Bronzite			3.354		7780	4720
Calcite			2.712		5780	3330
Celestine			3.950		5350	2325
Chalcopyrite			4.190		5100	2440
Chromite			4.790		8150	4550
Coesite			2.930		8500	4600
Diamond			3.510		18050	12350
Dolomite			2.850		7500	4050
Epidote			3.400		7430	4240
Galena			7.450		3750	2075
Garnet	Almandine	$Alm_{74}Py_{20}Gr_3Sp_3$	4.245		8550	4750
Garnet	Garnet	$3(Mn_{0.02}Fe_{0.64}Mg_{0.23}Ca_{0.11})O.Al_2O_3.3SiO_2$	4.060		8450	4850
Garnet	Garnet	$3(Mn_{0.04}Fe_{0.77}Mg_{0.12}Ca_{0.08})O.Al_2O_3.3SiO_2$	4.060		8040	4540
Garnet	Garnet	$3(Mn_{0.06}Fe_{0.74}Mg_{0.13}Ca_{0.07})O.Al_2O_3.3SiO_2$	4.160		8220	4610
Garnet	Garnet	$3(Mn_{0.0}Fe_{0.01}Mg_{0.02}Ca_{0.97})O.Al_2O_3.3SiO_2$	3.600		8720	5070
Garnet	Garnet	$3(Mn_{0.0}Fe_{0.17}Mg_{0.72}Ca_{0.11})O.Al_2O_3.3SiO_2$	3.670		8550	4860
Garnet	Garnet	$3(Mn_{0.0}Fe_{0.63}Mg_{0.29}Ca_{0.08})O.Al_2O_3.3SiO_2$	4.010		8170	4710
Garnet	Garnet	$3(Mn_{0.0}Fe_{0.76}Mg_{0.21}Ca_{0.03})O.Al_2O_3.3SiO_2$	4.160		8530	4760
Garnet	Garnet	$3(Mn_{0.0}Fe_{0.81}Mg_{0.14}Ca_{0.04})O.Al_2O_3.3SiO_2$	4.183		8520	4770
Garnet	Garnet	$3(Mn_{0.54}Fe_{0.46}Mg_{0.0}Ca_{0.0})O.Al_2O_3.3SiO_2$	4.249		8480	4760
Garnet	Garnet	$3(Mn_{0.55}Fe_{0.435}Mg_{0.02}Ca_{0.013})O.Al_2O_3.3SiO_2$	4.247		8470	4770
Garnet	Grossular	$Ca_3Al_2Si_3O_{12}$	3.570		9300	5500
Garnet	Pyrope		3.670		9100	5100
Gypsum			2.300		5650	2600
Hematite			5.250	0.0069	6550	
Ilmenite			4.720	1.69		
Limonite			3.132	0.00276		
K-Feldspar			2.540		6600	3375
Magnetite			5.125	6.28	7350	4200
Majorite			4.000		8950	5050
Mica	Biotite		3.050	0.00108	5260	2870
Mica	Muscovite (avg.)		2.810	0.00108	6300	3350
Mica	Muscovite (parallel)		2.810	0.00108	8100	3750
Mica	Muscovite (perp.)		2.810	0.00108	4500	2950

Group	Mineral	Formula notes	Density (tm^{-3})	Susceptibility (SI)	v_p (ms^{-1})	v_s (ms^{-1})
Mica	Phlogopite		2.810	0.00108	5495	2935
Monticellite			3.200		7600	4225
Olivine	Fayalite		4.390		7000	
Olivine	Forsterite		3.222		8580	
Olivine	Forsterite-Fayalite	Fo 0.93, Fa 0.07	3.311		8420	
Pentlandite			4.800		4645	2960
Periclase			3.670		9650	6075
Perovskite		$(Mg,Fe)SiO_3$	4.000		10900	6725
Plagioclase	Albite	Albite	2.615		6300	3350
Plagioclase	Anorthite		2.745		7250	3825
Plagioclase	Anorthite:Albite	0.09:0.91	2.610		6070	3400
Plagioclase	Anorthite:Albite	0.16:0.84	2.640		6220	3230
Plagioclase	Anorthite:Albite	0.24:0.76	2.640		6220	3340
Plagioclase	Anorthite:Albite	0.29:0.61	2.640		6300	3440
Plagioclase	Anorthite:Albite	0.53:0.47	2.680		6570	3530
Plagioclase	Anorthite:Albite	0.53:0.47	2.680		6750	3600
Plagioclase	Anorthite:Albite	0.56:0.44	2.690		6620	3360
Plagioclase	Anorthite:Albite	0.58:0.42	2.680		6700	3550
Plagioclase	Perthite	0.54:0.35:0.09 (Or:Ab:An)	2.570		5880	3050
Plagioclase	Perthite	0.61:0.36:0.02 (Or:Ab:An)	2.570		5650	3190
Plagioclase	Perthite	0.65:0.27:0.04 (Or:Ab:An)	2.570		5740	3130
Plagioclase	Perthite	0.67:0.29:0 (Or:Ab:An)	2.540		5580	3040
Plagioclase	Perthite	0.74:19:0.02 (Or:Ab:An)	2.570		5790	3110
Plagioclase	Perthite	0.75:0.22:0 (Or:Ab:An)	2.540		5560	3060
Plagioclase	Perthite	0.79:0.19:0.02 (Or:Ab:An)	2.560		5910	3250
Pyrite			5.040	0.015	8000	4950
Pyroxene	Aegirine	$NaFeSi_2O_6$	3.500		7320	4090
Pyroxene	Aegirite-Augite		3.420		7320	4090
Pyroxene	Augite		3.320		7220	4180
Pyroxene	Diallage		3.300		7030	4260
Pyroxene	Diopside		3.310		7700	4380
Pyroxene	Enstatite		3.200		7950	4850
Pyroxene	Ferrosilite		3.950		6400	3600
Pyroxene	Hedenbergite		3.475		7750	4150
Pyroxene	Jadeite		3.300		8700	5075
Pyroxene	Omphacite	Di 30%, Jd 58% (mol)	3.340		8500	4950
Pyroxene	Orthopyroxene	Enstatite 0.85, Ferrosillite 0.15	3.335		7850	4760
Pyrrhotite	Nonmagnetic		4.620	0.02		
Pyrrhotite			4.620	1.5	4645	2720
Quartz	Stishovite		4.315		11850	7250
Quartz			2.650	0.001	6150	4200

Group	Mineral	Formula notes	Density (tm^{-3})	Susceptibility (SI)	v_p (ms^{-1})	v_s (ms^{-1})
Ringwoodite			3.900		9750	5750
Rutile			4.260		9260	5140
Sillimanite			3.220		9700	5500
Sphalerite			4.025		5300	2850
Spinel		$FeAl_2O_4$	4.280		8670	4420
Spinel		$Mg_{0.75}Fe_{0.36}Al_{1.90}O_4$	3.826		9250	5010
Spinel		$MgAl_2O_4$	3.720		9750	5900
Spinel		$MgO.2.6(Al_2O_{3)}$	3.619		9930	5660
Spinel		$MgO.3.5(Al_2O_{3)}$	3.670		9930	5660
Staurolite			3.730		7850	3975
Topaz			3.500		9450	5975
Tourmaline			3.230		8600	5125
Wadsleyite			3.840		9700	5750
Water	Ice		0.920		3700	1600
Wustite			5.880		6550	2850
Zircon			4.700		8060	3970

Table 11: Representative density, magnetic susceptibility and seismic velocity for minerals compiled from Tables 8 through 10.

A2. property_calcs.py

The property_calcs.py script, and a complete set of documentation, is available from https://pmd-twiki.arrc.csiro.au/twiki/bin/view/Pmdcrc/ProjectA3property_calcs_v2_0 and on the compact disc which accompanies this report.

Requirements

Python version: python 2.4.1, modules sys, csv and math.

Constants

Name	Description
`prop_vp`	Calculate Vp
`prop_vs`	Calculate Vs
`prop_vpvs`	Calculate Vp/Vs
`prop_all`	All seismic properties
`linear_averaage`	Calculate property or properties using linear averaging.
`from_density`	Calculate property or properties directly from the chemistry of the subject.
`log_log_average`	Calculated property (or properties) using a linear fit in *log (property 1) – log (property 2)* space.
`werner_1945`	Calculate magnetic susceptibility via the method of Werner (1945).
`mooney_bleifuss_1953`	Calculate magnetic susceptibility via the method of Mooney and Bleifuss (1953).
`grant_west_1965`	Calculate magnetic susceptibility via the method of Grant and West (1965).
`parasnis_1973`	Calculate magnetic susceptibility via the method of Parasnis (1973).
`time_average`	Calculate seismic velocity using the time-averaged method (Mavko et al., 2003).
`connolly_vrh`	Calculate seismic velocity using the Voigt-Reuss-Hill implementation of Connolly and Kerrick (2002). N.B. not yet implemented.
`csy_volume_key`	Chemical system file, import return value for the molar volume.
`csy_mass_key`	Chemical system file, import return value for the molar mass.

Methods

Pre- and post-conditions are listed on the full documentation for this script, located at https://pmd-twiki.arrc.csiro.au/twiki/bin/view/Pmdcrc/ProjectA3property_calcs_v2_0 or on the CD-ROM accompanying this report.

```
calculate_density(mineralogytype, density_db, molar_mass_db, molar_volume_db)

calculate_linear_average_density(mineralogy, density_db)

calculate_mass_from_chemistry(molar_mineralogy, molar_mass_db)

calculate_volume_from_chemistry(molar_mineralogy, molar_volume_db)

calculate_magsus(mineralogy, type, magsus_db)

calculate_magsus_linear_linear(mineralogy, magsus_db)

calculate_magsus_log_log(mineralogy, magsus_db)

calculate_magsus_werner_1945(mineralogy, magsus_db)

calculate_magsus_mooney_bleifuss_1953(mineralogy, magsus_db)

calculate_magsus_grant_west_1965(mineralogy, magsus_db)

calculate_magsus_parasnis_1973(mineralogy, magsus_db)

calculate_seismic_velocity(mineralogy, type, properties, vp_database, vs_database, vrh_database)

seismo_linear_average(mineralogy, seismo_database)

seismo_time_average(mineralogy, seismo_database)

import_single_property_db(db_name, DelimType)

csy_reader(filename)

scale_mineralogy(mineralogy)
```

Notes

- `Mineralogy` is stored as a dictionary of `mineral_proportions`, keyed by `mineral_name`.
- Property databases (e.g. `vp_database, magsus_db, density_db`) are imported using `import_single_property_db`, which imports a single CSV file. `DelimType` is the DelimType object from the `csv` class, used to specify the delimiter between the mineral_name and the `mineral_property`.
- CSY file requires a small modification to the original UT2K format – mineral names need to be enclosed in quotes if they contain a space.
- `Property_calcs.py` contains some rudimentary testing methods. To test the script, run the command "`python property_calcs.py`" within the directory that `property_calcs.py` resides.

Possible improvements

- Obtain fundamental properties from online databases. In this case, a new method needs to be written to extract required mineral properties as appropriate, and place them into a dictionary with the same structure as `import_single_property_db`.
- Implement other methods of calculating seismic velocities, e.g. Voigt-Reuss-Hill.
- Implement methods to calculate other properties such as conductivity.
- Implement methods to deal with porous media.

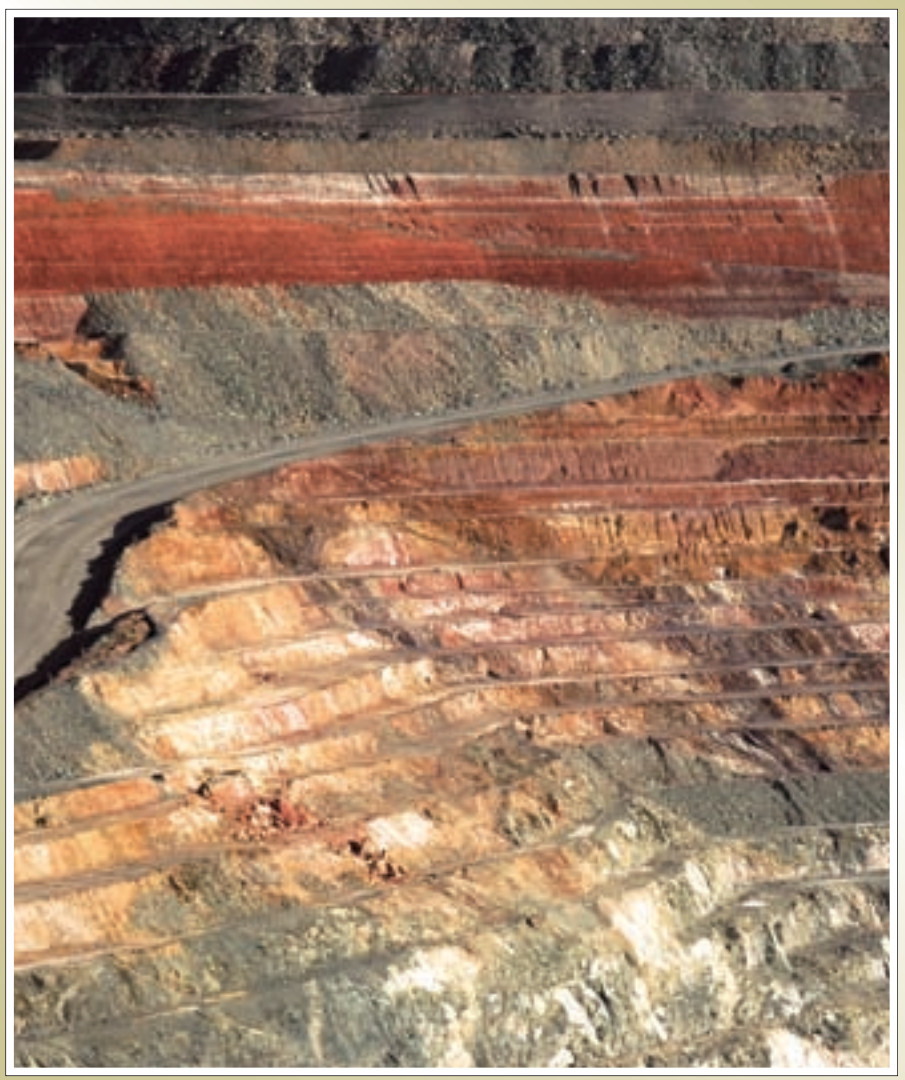

South pit wall, Sunrise Dam

A3. Monte Carlo estimation of alteration properties

The following is the procedure used to estimate the physical properties of an arbitrary alteration assemblage.

An alteration assemblage, as we define it, is a list of alteration end members, for example, quartz-pyrite-calcite-pyrrhotite contains the diagnostic mineral quartz, and the other minerals pyrite, calcite and pyrrhotite.

Without further information to constrain the relative proportions of the minerals, we assume the following:

- the diagnostic mineral is at most twice as abundant as the next most occurring mineral
- the minerals occur with decreasing probabilities as they are ordered in the alteration assemblage

For our quartz-pyrite-calcite-pyrrhotite example, this means that quartz is approximately twice as abundant pyrite, which is more abundant than calcite, which in turn is more abundant than pyrrhotite.

We can, of course, change the relative proportions to any other scheme. Another example might be that quartz is twice as abundant as any other mineral in the assemblage, and all other proportions are relative to the amount of quartz.

Once we have information regarding the proportions of each mineral in the assemblage, we perform the following algorithm (depicted using our example quartz-pyrite-calcite-pyrrhotite assemblage, but can be generalised to an arbitrary assemblage):

- Generate a random number between 1 and 10 000. This is the amount of quartz.
- Generate a random number between 1 and half the amount of quartz. This is the amount of pyrite.
- Generate a random number between 1 and the amount of pyrite. This is the amount of calcite.
- Generate a random number between 1 and the amount of calcite. This is the amount of pyrrhotite.
- Sum the amounts of each mineral.
- Divide each amount of mineral by the total amount of minerals. These numbers are the volume proportions of each mineral.
- Calculate the properties of the alteration assemblage (for this scenario) using a method such as linear averaging (Section 4.1).
- Repeat the calculation for a number of scenarios (for example, 10 000 repetitions). Use some statistical measure of the centre of the populations to provide the properties for the alteration assemblage. For this report, we use the median properties. The median is chosen as it represents the midpoint between all possible alteration assemblages, unlike the mode, as well as representing a property combination actually calculated, unlike the mean (Fisher, 1970).

Using this algorithm leads to a distribution of possible properties, created according to our assumptions of proportions of minerals within the alteration assemblage (Figure 97). The method also establishes an estimate of the likely properties (the median properties) for any arbitrary alteration assemblage.

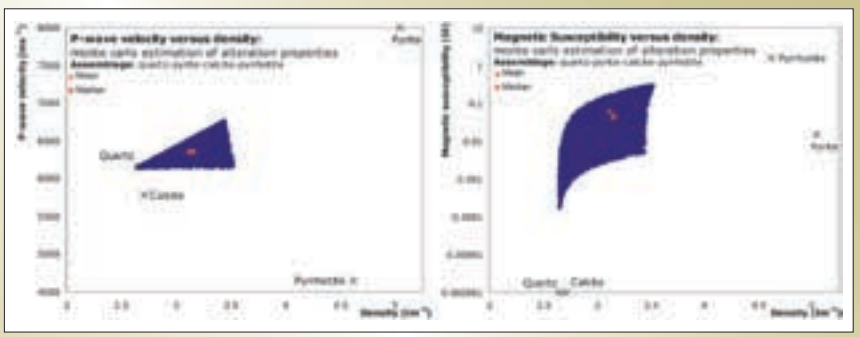

Figure 97: Seismic velocity-density and magnetic susceptibility-density distributions for the Monte Carlo property estimation of the alteration assemblage quartz-calcite-pyrite-pyrrhotite. 10 000 iterations were performed to produce these distributions; the extent of the populations of properties most likely encompasses the entire range of properties for this assemblage. Mean and median properties are shown on the plots – for this report, the properties of an arbitrary alteration assemblage is taken to be the median of each property after estimation using this Monte Carlo method.

A4. Plots of the distribution of individual minerals in the Listric Fault Model

Unaltered model

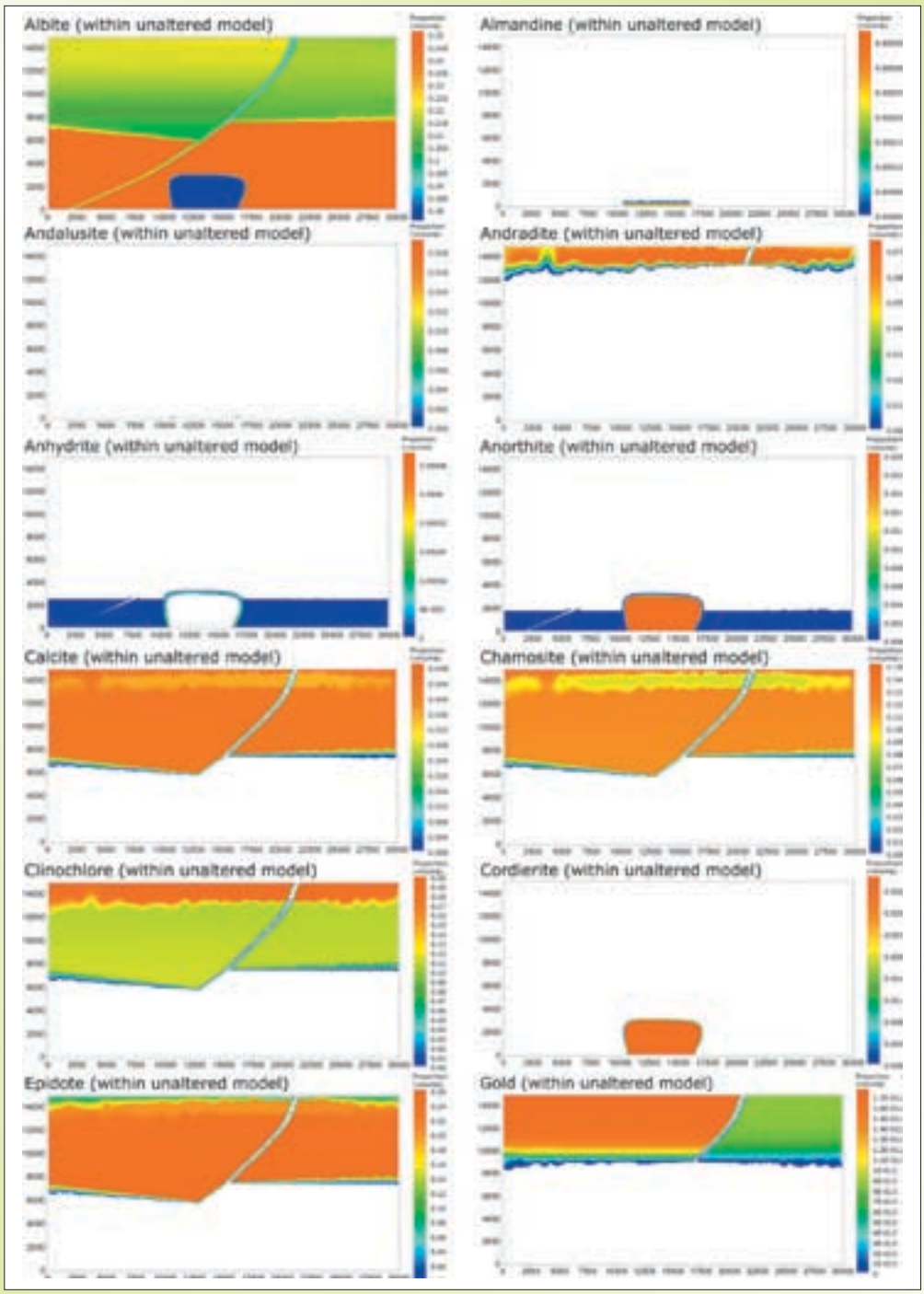

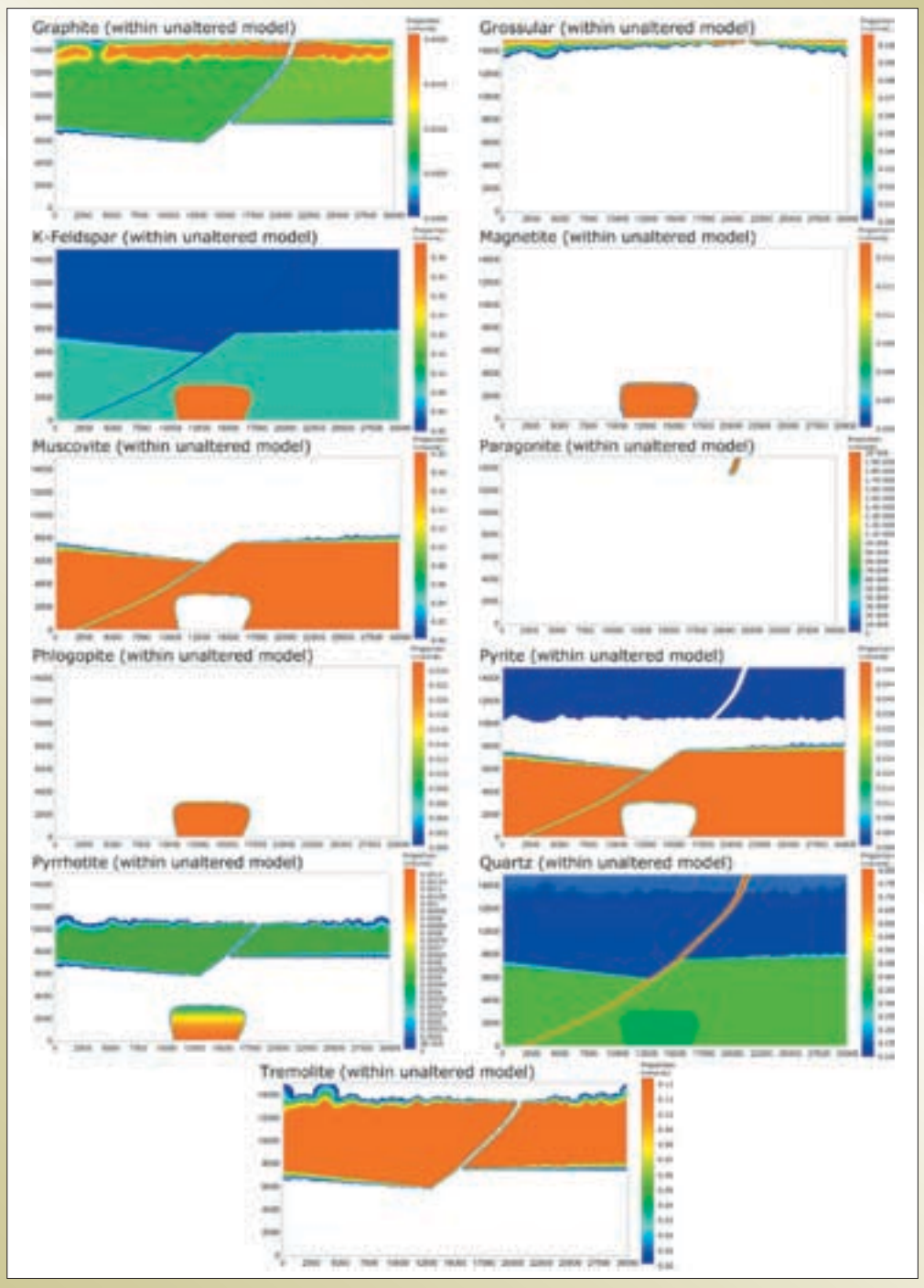
Graphite (within unaltered model)
Grossular (within unaltered model)
K-Feldspar (within unaltered model)
Magnetite (within unaltered model)
Muscovite (within unaltered model)
Paragonite (within unaltered model)
Phlogopite (within unaltered model)
Pyrite (within unaltered model)
Pyrrhotite (within unaltered model)
Quartz (within unaltered model)
Tremolite (within unaltered model)

Altered model

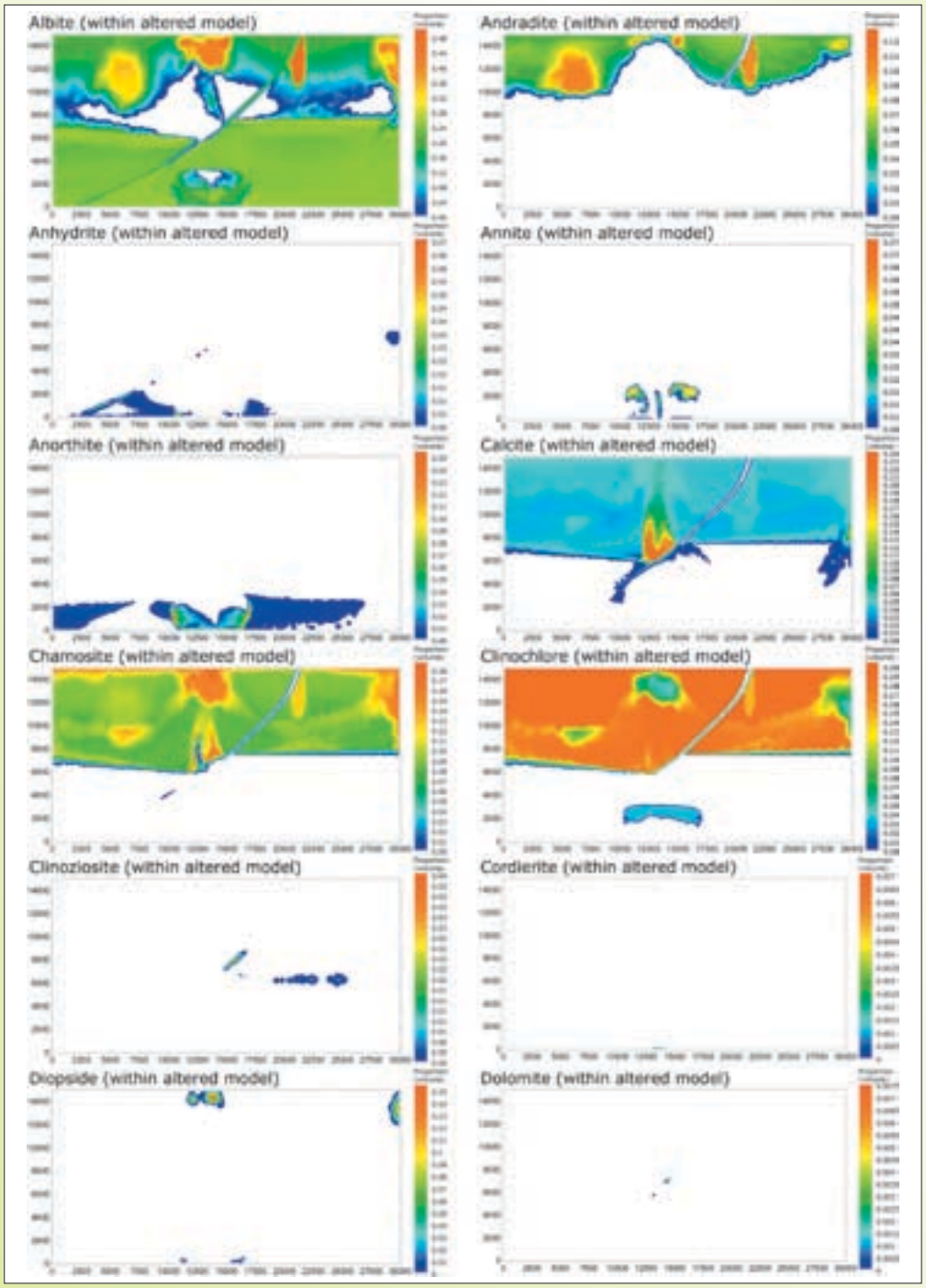

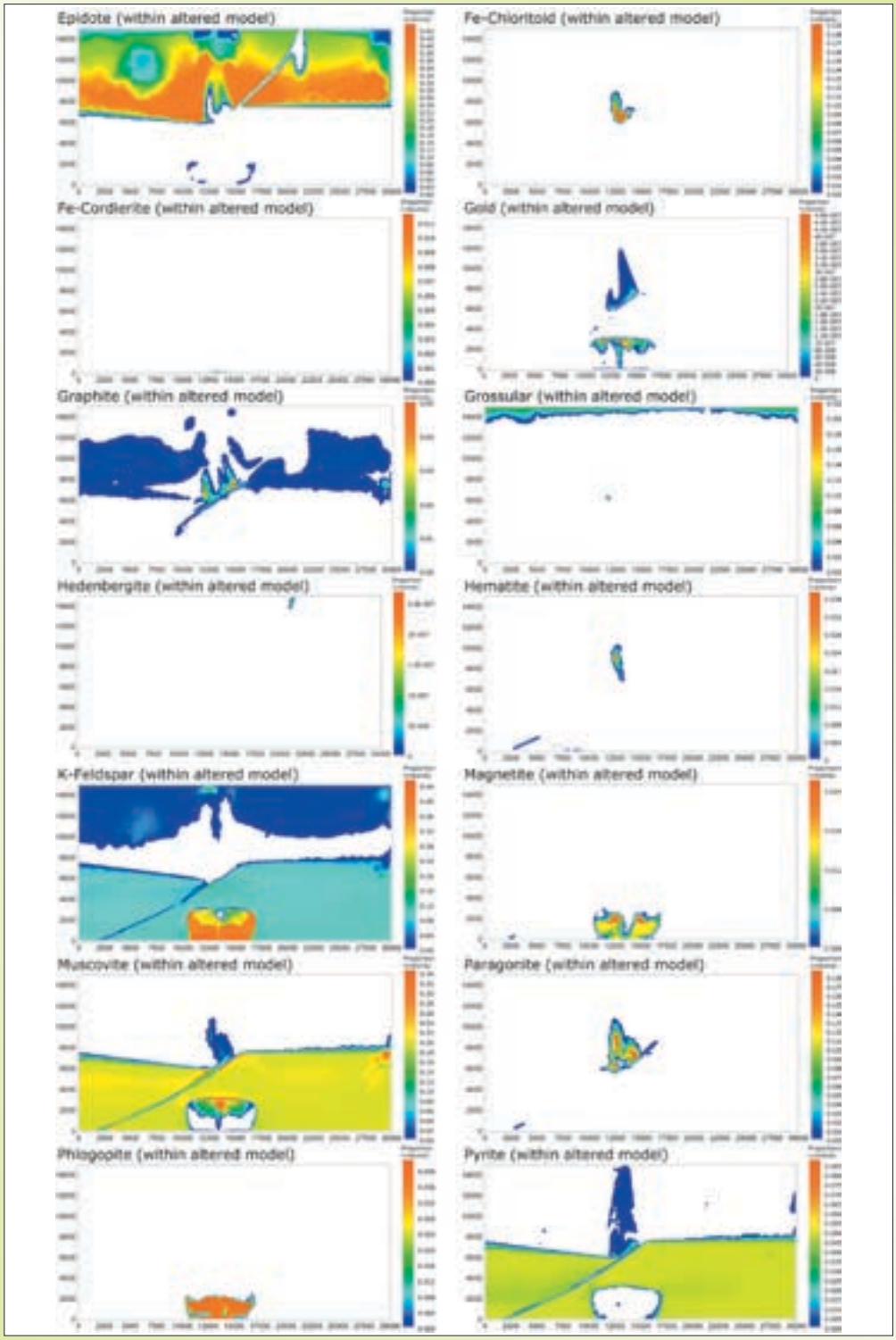
Epidote (within altered model)
Fe-Chloritoid (within altered model)
Fe-Cordierite (within altered model)
Gold (within altered model)
Graphite (within altered model)
Grossular (within altered model)
Hedenbergite (within altered model)
Hematite (within altered model)
K-Feldspar (within altered model)
Magnetite (within altered model)
Muscovite (within altered model)
Paragonite (within altered model)
Phlogopite (within altered model)
Pyrite (within altered model)

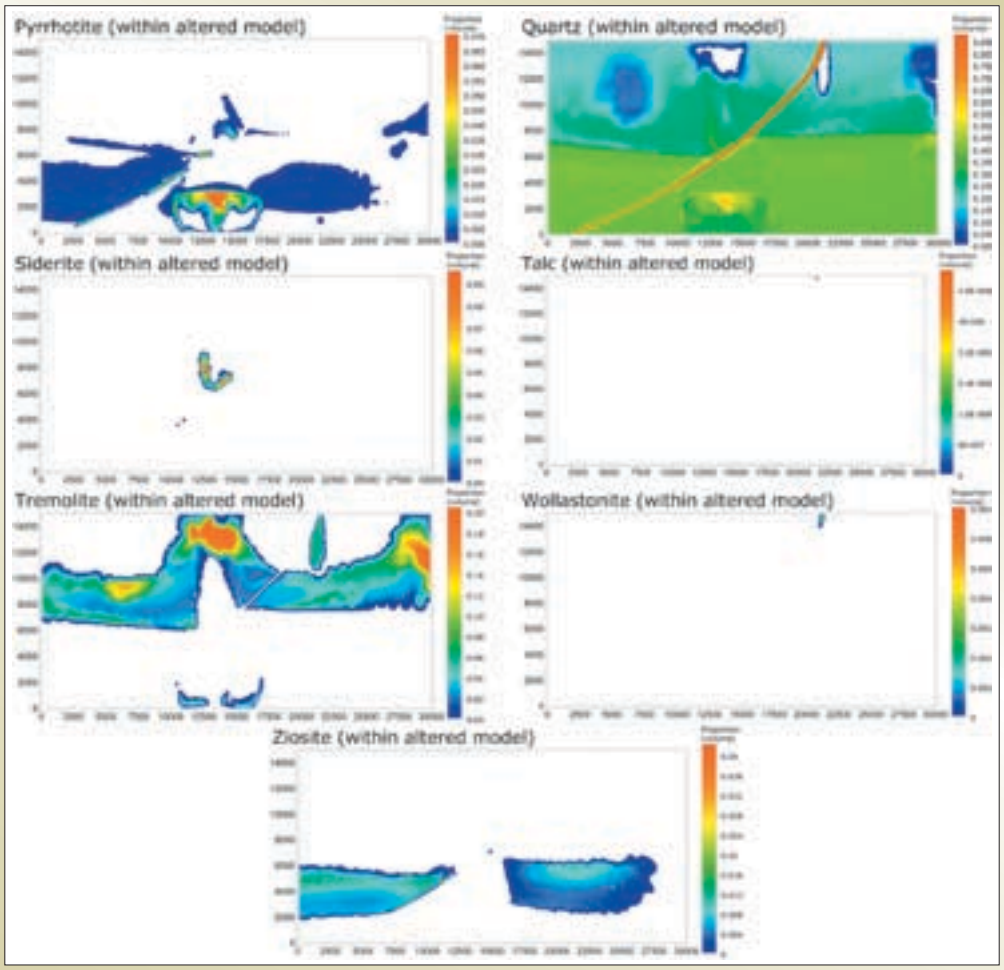
Pyrrhotite (within altered model)
Quartz (within altered model)
Siderite (within altered model)
Talc (within altered model)
Tremolite (within altered model)
Wollastonite (within altered model)
Ziosite (within altered model)

Change in mineralogy

Change in mineralogy is defined as the difference in mineralogy between the altered and unaltered model (*difference = altered – unaltered*).

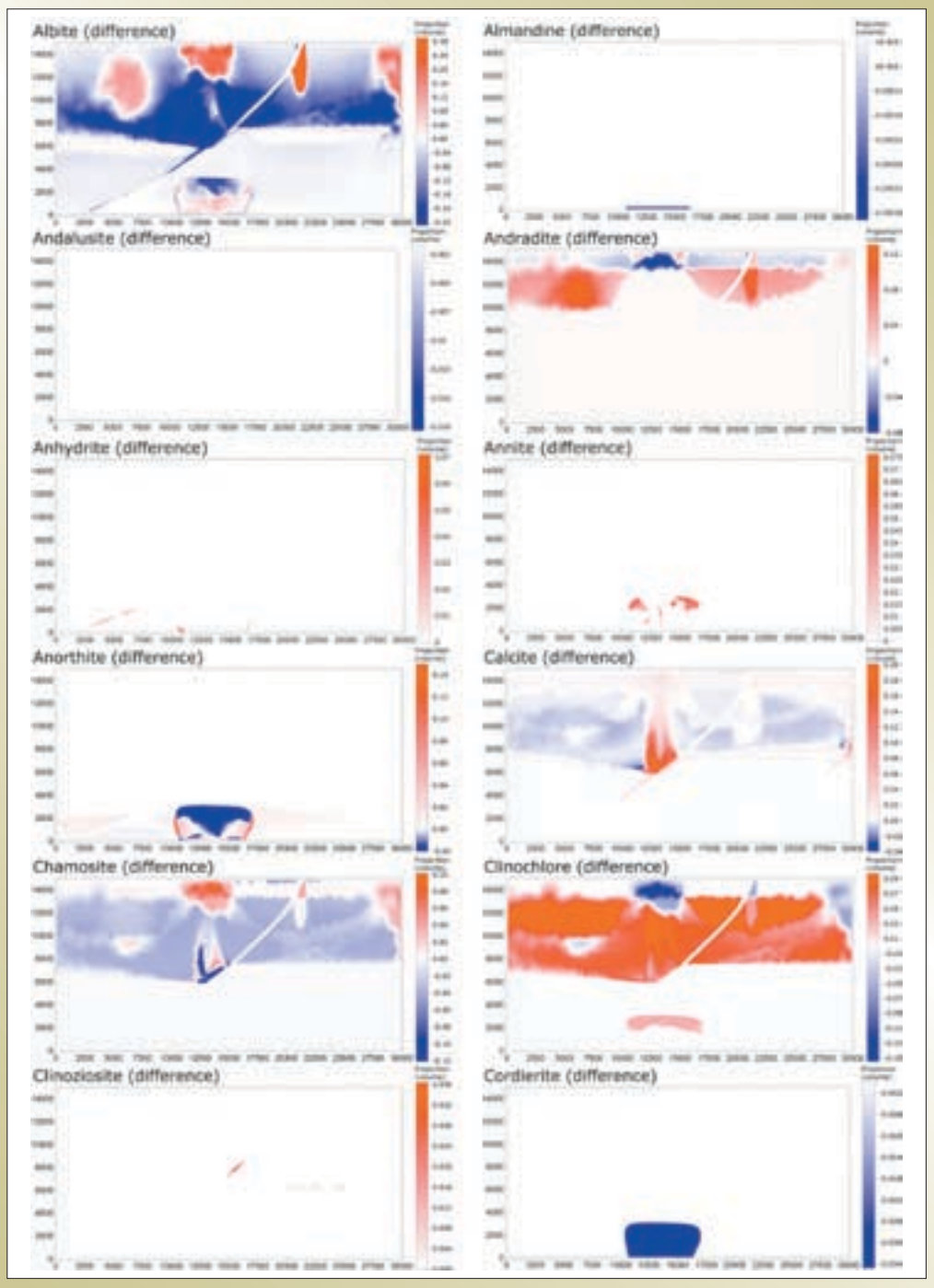

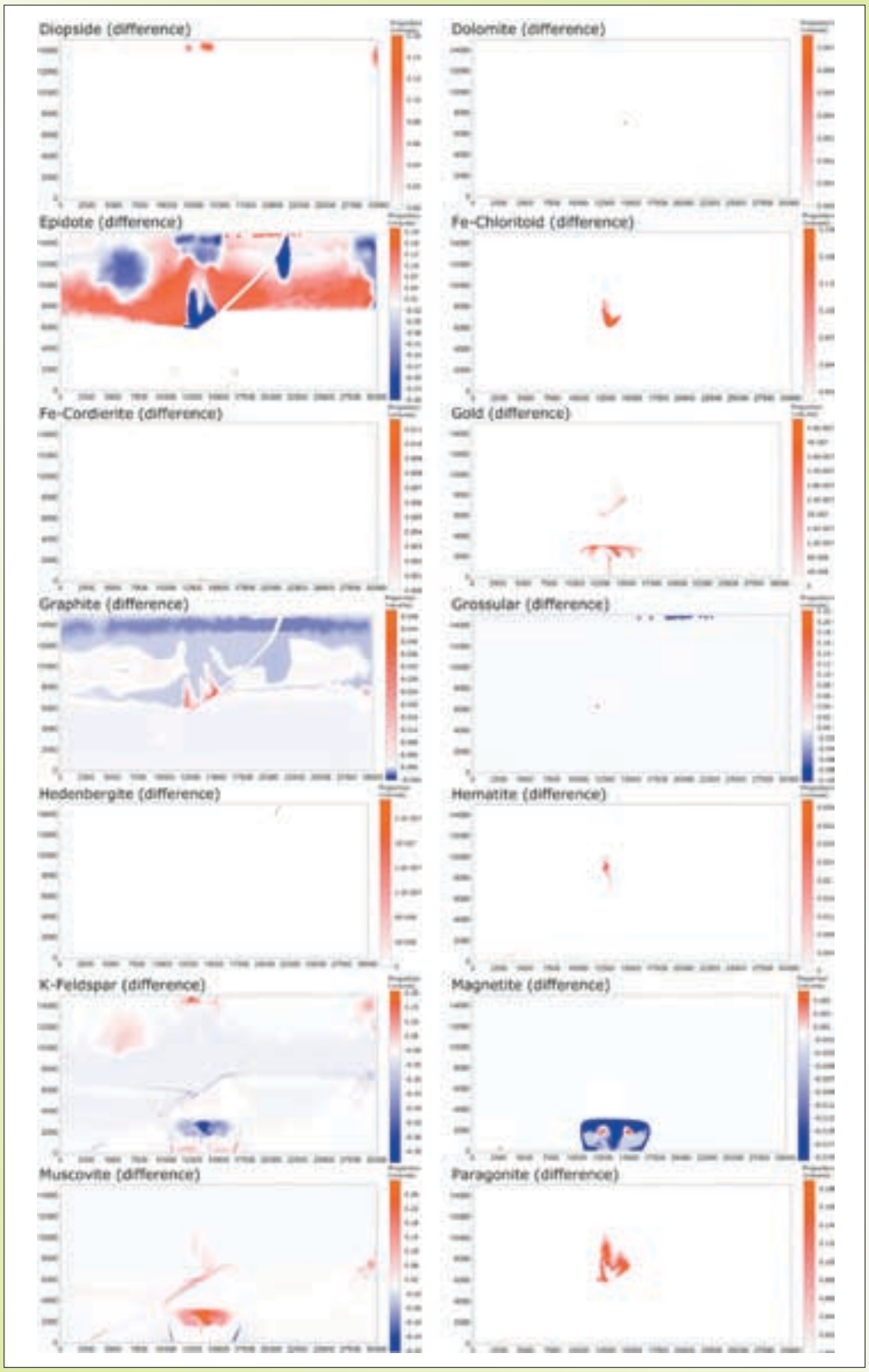
Diopside (difference)
Dolomite (difference)
Epidote (difference)
Fe-Chloritoid (difference)
Fe-Cordierite (difference)
Gold (difference)
Graphite (difference)
Grossular (difference)
Hedenbergite (difference)
Hematite (difference)
K-Feldspar (difference)
Magnetite (difference)
Muscovite (difference)
Paragonite (difference)

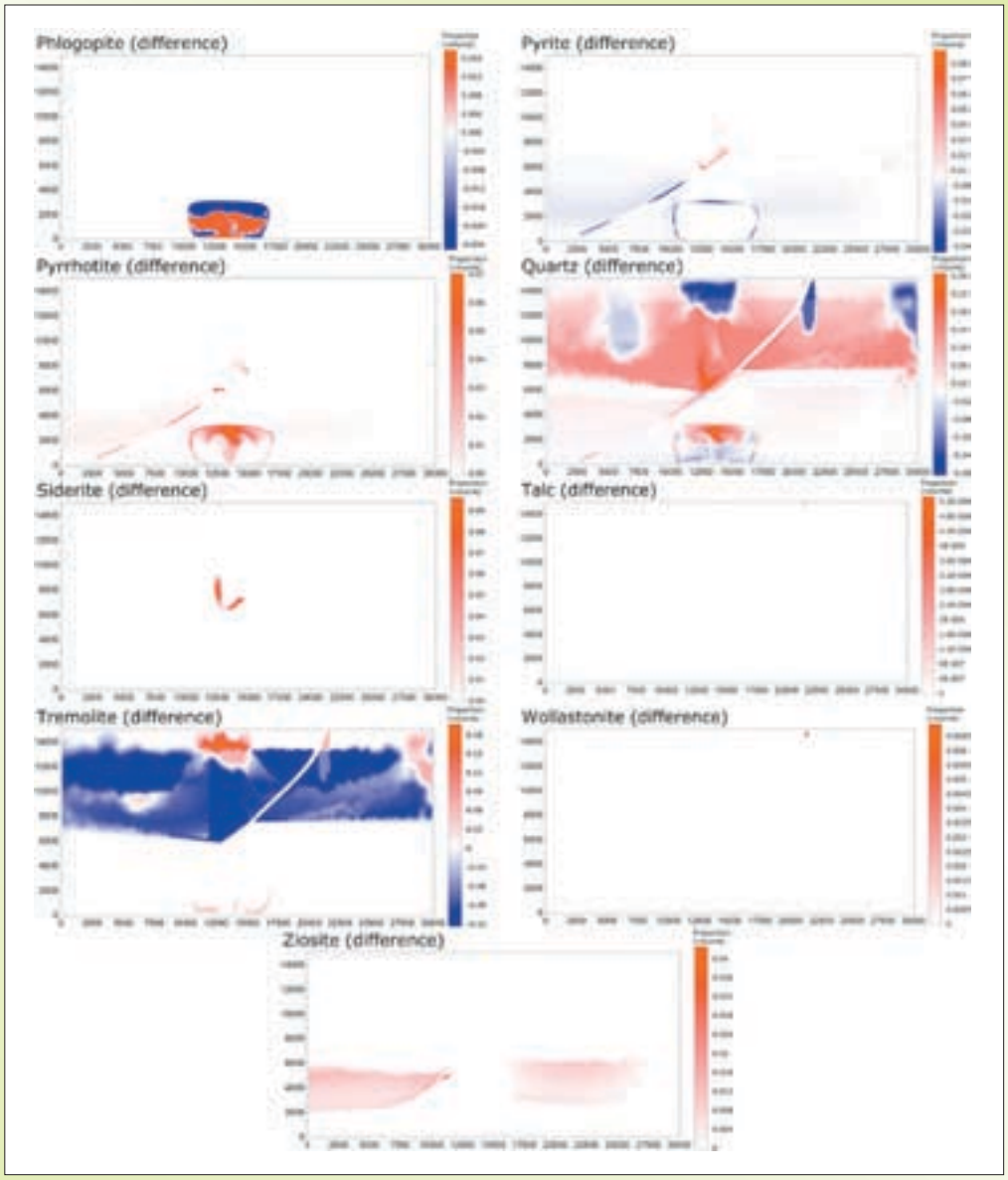
Phlogopite (difference)
Pyrite (difference)
Pyrrhotite (difference)
Quartz (difference)
Siderite (difference)
Talc (difference)
Tremolite (difference)
Wollastonite (difference)
Zoisite (difference)

A5. add_phys_props.py

The `add_phys_props.py` script allows the creation of physical property distributions from the outputs of the ***pmd**CRC* reactive transport code, pmd*RT.

This Appendix refers to `add_phys_props.py`, version 2.0, available from https://pmd-twiki.arrc.csiro.au/twiki/bin/view/Pmdcrc/ProjectA3pmdRTModelPredictions, as well as on the compact disc that accompanies this report.

Mineral physical properties, as used for this report, are those defined in https://pmd-twiki.arrc.csiro.au/twiki/bin/view/Pmdcrc/ProjectA3MineralPhysicalProperties, as well as Appendix A1 of this report.

Notes

`add_phys_props.py` requires the following:

- `property_calcs.py`
  See Appendix A2 for more details of this script
- `[chemical_system_file].csy`
  Chemical system file
  See notes in Appendix A2 for more details on specific requirements of this file.
- `[property_databases].csv`
  Delimited files, containing fundamental mineral properties, e.g. mineral seismic velocities. Imported using methods from `property_calcs.py` (Appendix A2).
- `[input file/files].vtk`
  *pmd**RT output mesh/meshes, containing mineralogy stored at the nodes of the mesh. Add_phys_props.py assumes that vtk v3 file format is used (Kitware, Inc., 2007).
  To provide meaningful filenames, `add_phys_props.py` obtains information about the timestep that the input vtk file represents, from the header of the SOLID_VOLUME scalar.
- Python version 2.4.1 or greater, and the modules `sys` and `csv`

Running add_phys_props.py

- Ensure the input vtk file or files are within the same directory as `add_phys_props.py`, which also requires access to the files as noted above.
- Script is run using the command:
  `python add_phys_props.py output_type [input_vtk_file.vtk]`

  Output type is one, two, or all of:
  - `csv`
    Produce an output distribution of physical properties as a CSV file.
  - `vtk`
    Produce an output vtk file that is the original vtk file, appended with each physical property specified at the nodes.
  - `ts`
    Produce an output distribution of physical properties as a Gocad TSurf file.

  If `input_vtk_file.vtk` isn't specified (as it is optional), the software will prompt you to provide the name of the input vtk file, including the extension.
  To run the script for multiple files, the Windows command line `FOR %f IN (*.vtk) DO python add_phys_props.py %f` can be used, or an appropriate looping command for the platform that you are running `add_phys_props.py` on.

Possible improvements

- Import chemical system file using the ChemicalSystem object directly from pmd*RT.
- Obtain physical properties for minerals from an online database.
- Use the vtk object from pmd*RT.
- Change all calculation methods to work directly within pmd*RT, rather than post-processing datafiles.

A6. Creating pseudo-3D property distributions from 2D distributions

This workflow uses Gocad to create pseudo-3D property distributions for use with the GRAV3D (Li and Oldenburg, 1998) and MAG3D (Li and Oldenburg, 1996) forward-modelling components.

Procedure

- Import the appropriate property distribution as a surface, as created by `add_phys_props.py` (Appendix A5).
- Convert density to a density_contrast. For simplicity, apply a property script to density, and take 2.67 away from the density. This produces a density contrast that would produce Bouguer gravity data.
- Copy the surface to the left, and mirror it (apply property script --> X = X * -1;). Ensure that properties are copied.
- Copy the left surface to the right (copying properties as well), and move it over to the right (apply property script --> X = X + 60000;).
  N.B. 60000 is used as we need to move the surface across the width of two cross sections, and the RT models used for this study were 30km wide.
- We now have a set of front surfaces. These are positioned at Y = -75000 (apply property script --> Y = -75000;). Create a PointsSet from the three front surfaces (centre, left and right), and copy this PointsSet to make a back series of points.
- This back series of points is moved to the back (apply property script --> Y = Y * -1;), and then a PointsSet of all the data points is created from the front and back data points.
- Create regions of various erosion levels on the PointsSet.
- Create PointsSets for these erosion levels (PointsSet mode --> New --> From Object Region, select the full data points PointsSet and the appropriate region). Make sure that **copy properties** is turned **on** (under Advanced options).
- Create a voxet which encompasses a PointsSet for a given level of erosion (Voxet mode --> New --> From Objects Box, select the eroded PointsSet). Create the voxet so that it has 50 x 50m cells in the (X/Y)Z direction, and two cells in the XY direction. For our example, our model is 90km (wide) x 150km (deep) x 7.5km (tall), which would give us the number of cells as 1801 x 2 x 151 cells.
- Paint the appropriate properties to the voxet. (Voxet mode --> Property --> Paint --> With PointsSet, select the appropriate PointsSet, repeat for both density and magsus).
- Initialise the properties (Voxet mode --> Interpolation --> Initialize properties (multi-grid). Repeat for both density and magsus.
- Interpolate the properties (Voxet mode --> Interpolation --> Interpolate properties). Repeat for both density and magsus.

Simulating regolith

- To create a model blanketed by a constant density and magsus material (simulating regolith), create a PointsSet with a constant density, and at the appropriate place in space, e.g. vertical extents of 7500 to 7600m, density of 2, magsus of 0.001 SI, and points at all four corners (which are, in XY space:
  -30000, -75000;
  60000, -75000;
  -30000, 75000;
  60000, 75000;)
- Create a voxet from this PointsSet, with the same XZ and XY cell sizes as used for the property voxet above (e.g. for 100m thick regolith, the number of cells would be 1801 x 2 x 2, as it is only 100m tall, but just as wide and deep as the property voxet).
- Paint this with the density and magsus properties of the PointsSet, initialise and interpolate the properties (as per main procedure), except using the regolith PointsSet).
- Create a voxet which encompasses the appropriate property and regolith voxets (Voxet mode --> New --> From Objects Box --> select both voxets; remember to add the number of cells required in Z, so for our example, this voxet would have 1801 x 2 x 153 cells).
- Transfer the properties from nearby grid cells (Voxet mode --> Property --> Transfer property --> From Nearby Grid Cell or Node. Client voxet is the combined voxet; server is the property voxet, then the regolith voxet). Select the property voxet and transfer the density and magsus properties, then select the regolith voxet and transfer its density and magsus.

Creating UBC property distributions

- With Mira-links (a commercial package from Mira Geoscience) enabled, use the Mira links menu to create a mesh for the voxet, then create a density and magnetic susceptibility distribution.
- We now need to make an observation file. The method described above has created a section where the original data is best observed along an XY traverse, starting at 0, 0, and ending at 30000, 0. We make an observation file in the following format:

```
# of stations
x1 y1 z1
x2 y2 z2
x3 y3 z3
... ... ...
xn yn zn
```

  Note that Z for the observations will be at the top of the profile (for ground gravity stations) – this is half the cell width beyond the top of your highest point. For example, a model of height 7500m has the top of the topmost cell at 7525m.

- We also need to make a separate observations file for the magnetic susceptibility. The file format for this needs to be:

```
mag_field_inclination mag_field_declination
mag_field_intensity anomaly_projection_
inclination anomaly_projection_
declination idir (0 = multicomponent;
1 = single component)
```

```
# of stations
x1 y1 z1
x2 y2 z2
x3 y3 z3
... ... ...
xn yn zn
```

  An example, for Kalgoorlie, with stations every 50m in x, and the top of the model at z = 7525 would be (magnetic parameters derived from the AGRF[5], for June 1, 2007):

```
-64.802 1.164 57946
-64.802 1.164 1
601
0 0 7525
50 0 7525
100 0 7525
... ... ...
30000 0 7525
```

  Note that the Z is 7525, suggesting that this is ground magnetics. We could also simulate various aeromagnetic flight heights by using an appropriate Z (e.g. 100m flight height would have the Z_{obs} of 7625).

- Once we have a set of property models (density to reference model and magnetic susceptibility), and observations files, we can compute the forward models using GRAV3D and MAG3D:

```
gzfor3d mesh.msh grav_obs.loc model.den
magfor3d mesh.msh mag_obs.loc model.sus
```

  which will produce, respectively, `gzfor3d.grv` and `magfor3d.mag` files, which are our simulated profiles.

5 Australian Geomagnetic Reference Field, http://www.ga.gov.au/oracle/geomag/agrfform.jsp

A7. Density and magnetic susceptibility models

Density unaltered

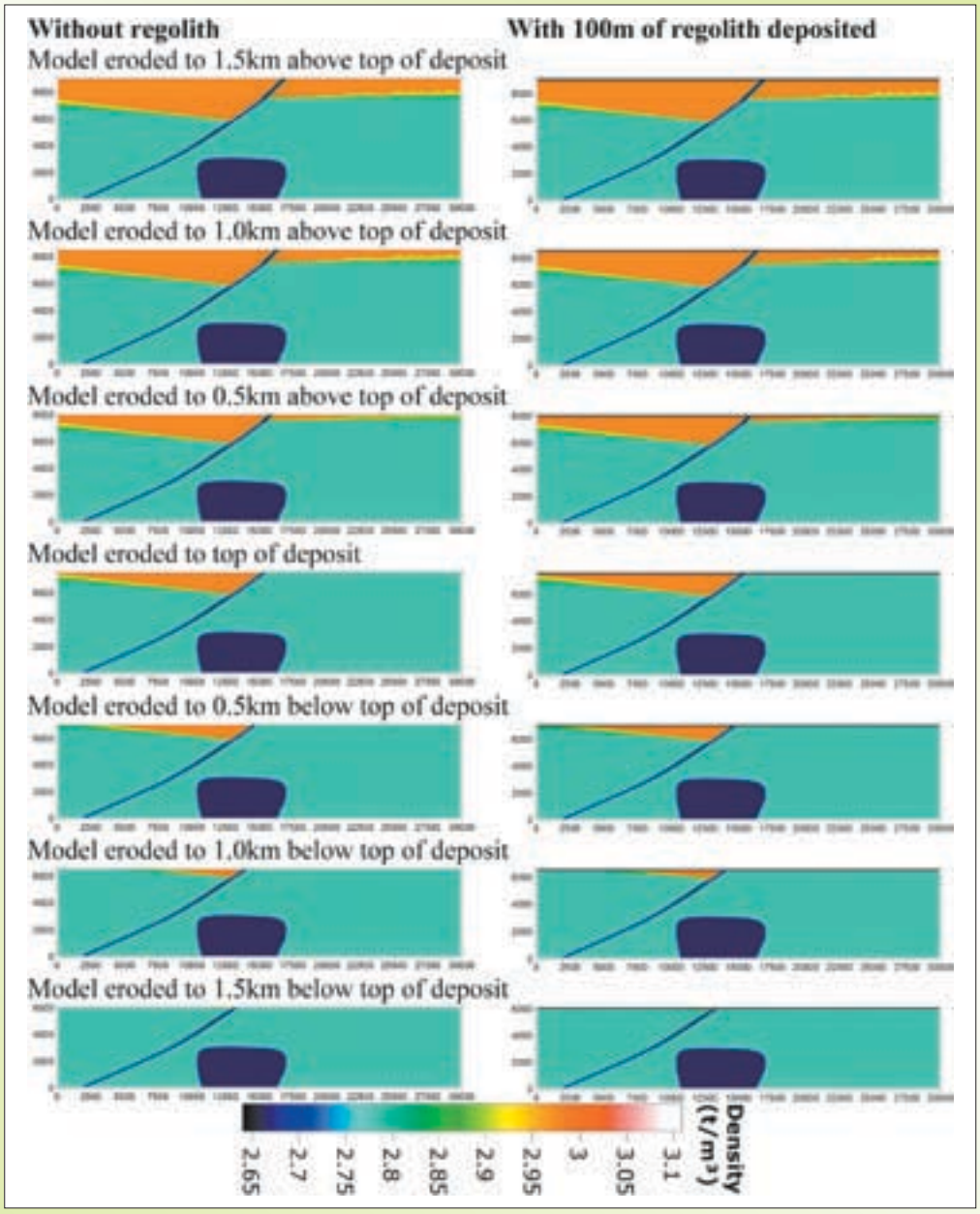

Density altered

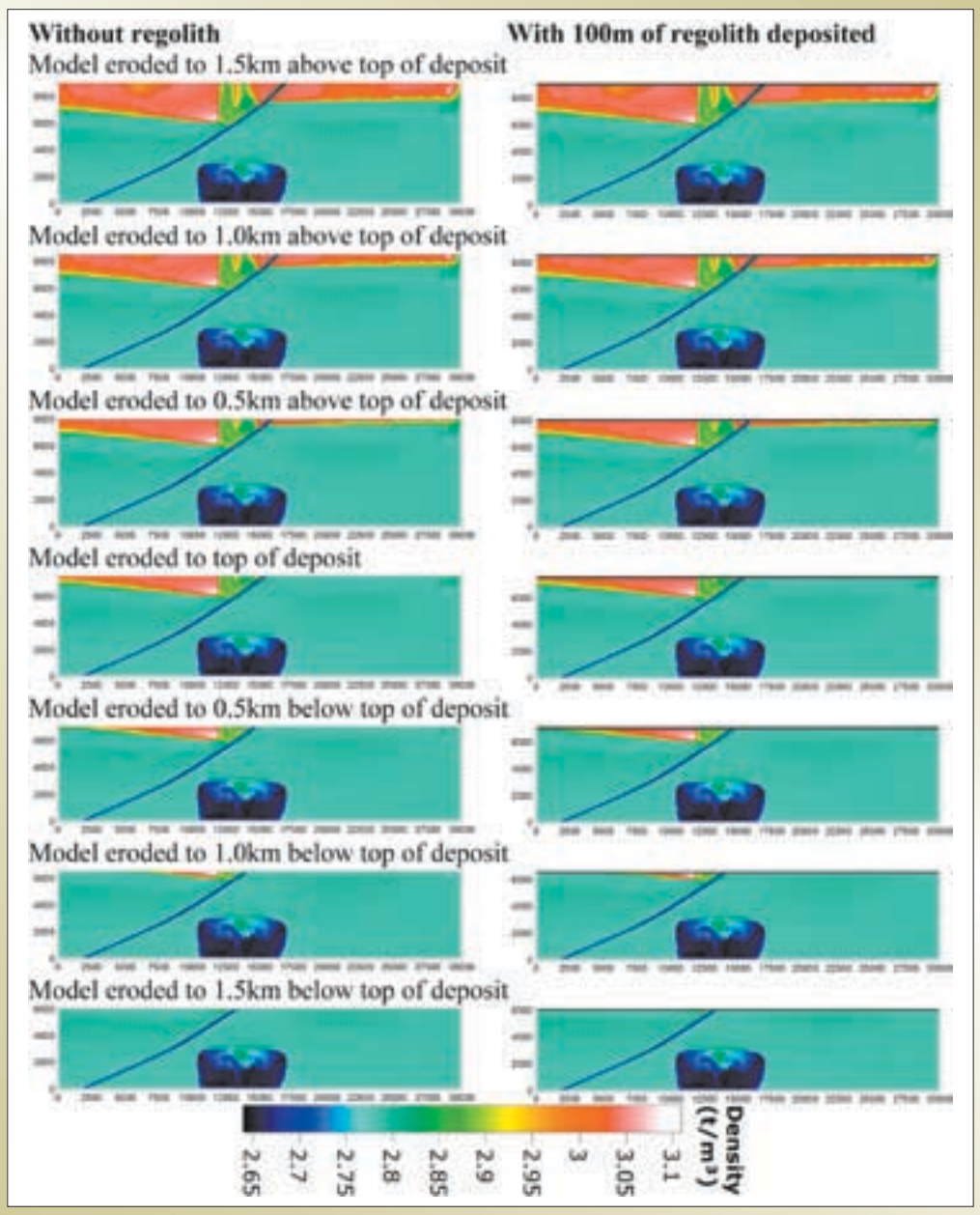

Magnetic susceptibility unaltered

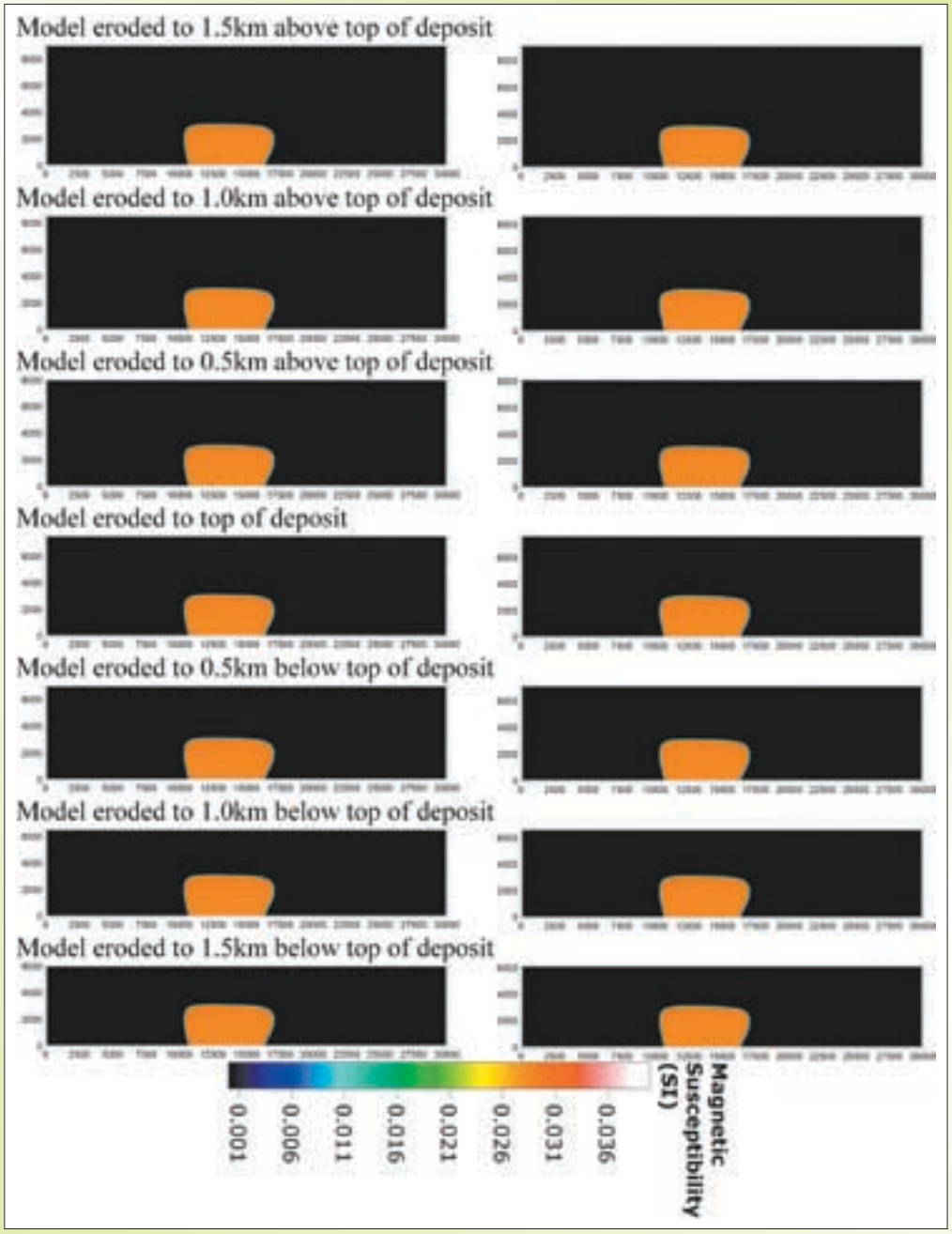

Magnetic susceptibility altered

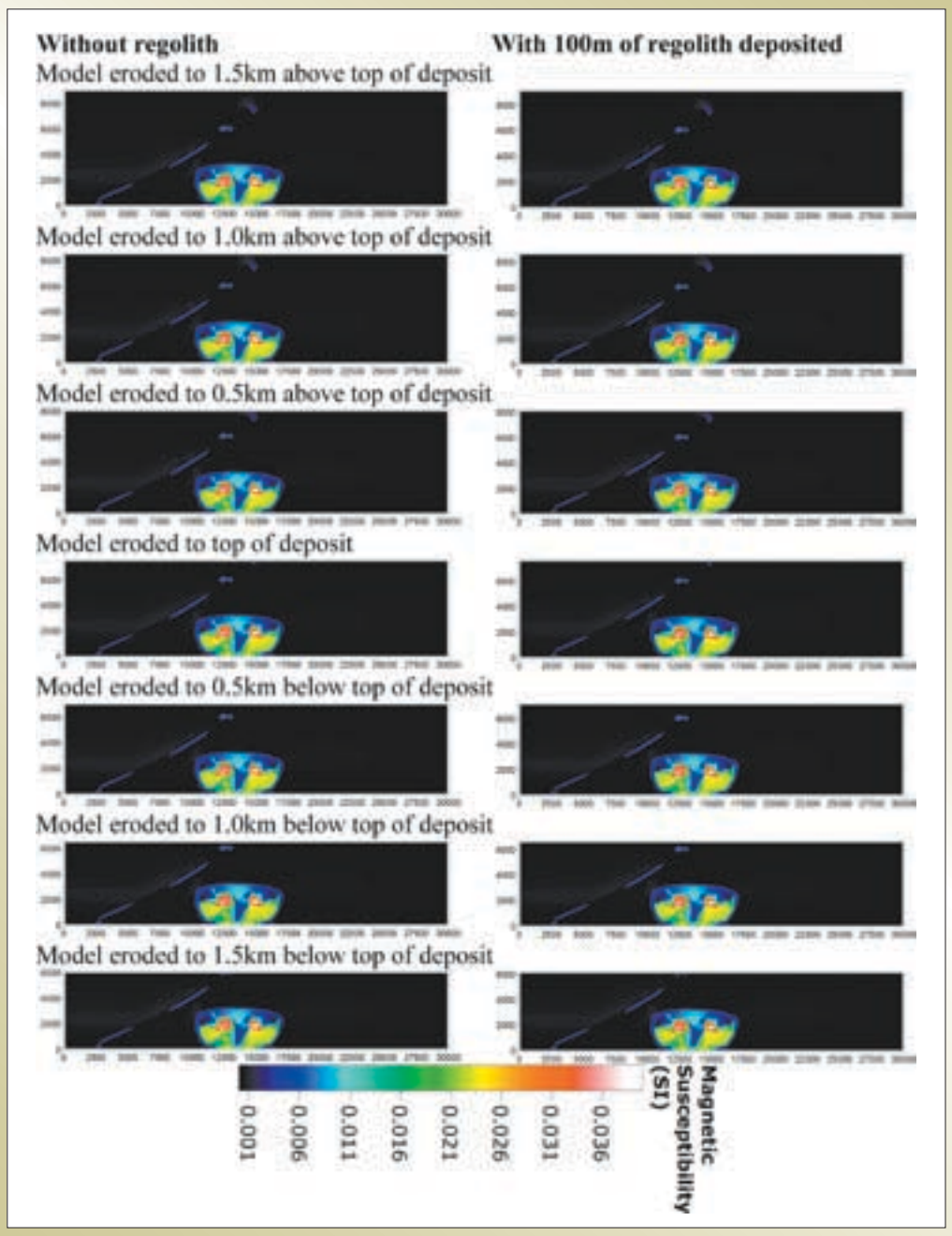

A8. Hand-specimen measurements of density and seismic velocity for Sunrise Dam

P-wave velocity results

Sample	Propagation Direction	Density (tm^{-3})	10	20	40	60	80	100	200	400	600	Lithology	Unit	Remarks
SRD002		2.75		6.20	6.23	6.26	6.28	6.30	6.37	6.44	6.48	Dolerite		
SRD003z	nB	3.00	5.51	5.55	5.62	5.68	5.76	5.76	5.82	5.88	5.92	Altered ore		andesite protolith, banded, highly altered
SRD003xy	pB	3.00	6.04	6.09	6.15	6.20	6.23	6.25	6.30	6.35	6.38	Altered ore		andesite protolith, banded, highly altered
SRD005z	nB	3.11	5.79	5.88	5.92	5.93	5.94	5.95	5.99	6.04	6.07	Banded iron formation		altered; qtz, sulphide-bearing
SRD005xy	pB	3.18	5.90	5.94	5.99	6.01	6.04	6.06	6.12	6.17	6.18	Banded iron formation		altered; qtz, sulphide-bearing
SRD007		2.71	5.70	5.74	5.79	5.83	5.86	5.88	5.98	6.11	6.20	Porphyry		
SRD007		2.71		6.05	6.08	6.11	6.13	6.15	6.20	6.24	6.27	Porphyry		Summercloud fm
SRD201xy	pB	2.76	5.85	6.04	6.10	6.13	6.15	6.17	6.22	6.27	6.28	Porphyry	Dolly	Altered, near base of Sunrise shear zone
SRD201z	nB	2.76		5.71	5.88	5.93	5.96	5.98	6.02	6.07	6.08	Porphyry	Dolly	Altered, near base of Sunrise shear zone
SRD202xy	pF	2.78	6.28	6.37	6.41	6.44	6.46	6.48	6.53	6.58	6.60	Porphyry	Dolly	Altered, near base of Sunrise shear zone
SRD202z	nF	2.78	5.40	5.52	5.62	5.66	5.69	5.71	5.76	5.84	5.89	Porphyry	Dolly	Altered, near base of Sunrise shear zone
SRD203xy	pB	2.75		6.58	6.63	6.68	6.72	6.76	6.83	6.88	6.90	Porphyry	Dolly	"least altered" background, chlorite alteration
SRD203z	nB	2.76		6.08	6.13	6.17	6.20	6.22	6.30	6.35	6.37	Porphyry	Dolly	"least altered" background, chlorite alteration
SRD204xy	pB	2.76			6.13	6.15	6.17	6.18	6.24	6.29	6.31	Porphyry	Dolly	"least altered" background, chlorite alteration; some foliation
SRD204z	nB	2.77	5.52	5.55	5.59	5.61	5.63	5.65	5.70	5.74	5.76	Porphyry	Dolly	"least altered" background, chlorite alteration; some foliation
SRD206xy	pB	2.78		6.34	6.39	6.42	6.44	6.45	6.51	6.56	6.59	Andesite		background sericite-chlorite alteration; near Watu shear zone
SRD206z	nB	2.76		5.90	5.93	5.96	5.98	6.00	6.05	6.10	6.14	Andesite		background sericite-chlorite alteration; near Watu shear zone
SRD207xy	pF	2.78		6.15	6.26	6.30	6.33	6.35	6.42	6.46	6.49	Andesite		carbonate/qtz altered; near Margee's/Watu shear zone
SRD207z	nF	2.79	5.76	5.81	5.85	5.89	5.91	5.93	6.00	6.07	6.11	Andesite		carbonate/qtz altered; near Margee's/Watu shear zone
SRD208		2.80		5.88	5.85	5.95	5.98	6.00	6.05	6.11	6.15	Andesite		moderate grade; massive
SRD209		2.79			5.91	5.97	6.01	6.05	6.21	6.37	6.40	Andesite	Astro Lode	relatively unaltered
SRD210xy	pB	2.87			6.17	6.20	6.22	6.25	6.32	6.37	6.40	Andesite	Astro Lode	altered
SRD210z	nB	2.81		6.02	6.05	6.08	6.10	6.11	6.16	6.21	6.23	Andesite	Astro Lode	altered
SRD214		2.87		6.23	6.29	6.33	6.36	6.38	6.46	6.52	6.55	Andesite	Lower Cosmo Lode	altered
SRD215xy	pF	2.86		6.11	6.15	6.19	6.22	6.24	6.29	6.33	6.35	Andesite	Lower Cosmo Lode	background alteration
SRD215z	nF	2.87	5.83	5.92	5.98	6.02	6.04	6.06	6.12	6.18	6.19	Andesite	Lower Cosmo Lode	background alteration
SRD216		2.75		6.10	6.13	6.15	6.17	6.18	6.23	6.28	6.30	Andesite	Watu Shear Zone	background alteration
SRD218xy	pB	2.80	6.06	6.12	6.19	6.23	6.26	6.29	6.35	6.42	6.48	Andesite	Watu Shear Zone	altered
SRD218z	nB	2.80	5.47	5.53	5.58	5.62	5.64	5.67	5.75	5.83	5.88	Andesite	Watu Shear Zone	altered

Table 12: P-wave velocities for hand-specimens from Sunrise Dam. Samples were measured at the Geological Survey of Canada (GSC)-Dalhousie High Pressure Laboratory, Halifax, Nova Scotia. Propagation direction indicates the orientation of the sample: nB and nF are perpendicular to the fabric in the rock, and pB and pF are parallel to the fabric in the rock.

S-wave velocity results

Sample	Propagation Direction	Vibration Direction	Density (tm^{-3})	10	20	40	60	80	100	200	400	600	Lithology	Unit	Remarks
SRD001			2.72	3.60	3.63	3.65	3.66	3.67	3.67	3.69	3.71	3.72	Andesite		chloritized
SRD002			2.75	3.51	3.55	3.59	3.61	3.63	3.64	3.66	3.68	3.69	Dolerite		
SRD003z	nB	pB	3.00	3.54	3.56	3.59	3.60	3.61	3.62	3.65	3.69	3.73	Altered ore		andesite protolith, banded, highly altered
SRD003xy	pB	pB	3.00	3.79	3.82	3.86	3.88	3.90	3.91	3.95	3.99	4.01	Altered ore		andesite protolith, banded, highly altered
SRD003xy	pB	nB	3.00		3.49	3.51	3.52	3.53	3.54	3.57	3.61	3.63	Altered ore		andesite protolith, banded, highly altered
SRD005z	nB	pB	3.11	3.78	3.79	3.80	3.81	3.82	3.82	3.84	3.86	3.87	Banded iron formation		altered; qtz, sulphide-bearing
SRD005xy	pB	pB	3.18	3.77	3.78	3.80	3.82	3.83	3.83	3.86	3.88	3.89	Banded iron formation		altered; qtz, sulphide-bearing
SRD005xy	pB	nB	3.18	3.75	3.76	3.78	3.79	3.80	3.81	3.85	3.88	3.91	Banded iron formation		altered; qtz, sulphide-bearing
SRD007			2.71	3.50	3.51	3.54	3.56	3.58	3.60	3.64	3.68	3.71	Porphyry		
SRD007			2.71	3.66	3.68	3.70	3.71	3.71	3.72	3.74	3.75	3.77	Porphyry		Summercloud fm
SRD201xy	pB	pB	2.76		3.80	3.82	3.84	3.85	3.87	3.89	3.91	3.93	Porphyry	Dolly	Altered, near base of Sunrise shear zone
SRD201xy	pB	nB	2.76	3.71	3.72	3.74	3.76	3.77	3.78	3.81	3.85	3.87	Porphyry	Dolly	Altered, near base of Sunrise shear zone
SRD201z	nB	pB	2.76	3.75	3.81	3.87	3.89	3.90	3.91	3.94	3.98	4.00	Porphyry	Dolly	Altered, near base of Sunrise shear zone
SRD202xy	pF	pF	2.78	3.77	3.78	3.80	3.82	3.84	3.85	3.88	3.91	3.92	Porphyry	Dolly	Altered, near base of Sunrise shear zone
SRD202xy	pF	nF	2.78	3.40	3.42	3.45	3.48	3.50	3.52	3.55	3.58	3.59	Porphyry	Dolly	Altered, near base of Sunrise shear zone
SRD202z	nF	pF	2.78	3.42	3.44	3.46	3.48	3.49	3.49	3.52	3.55	3.58	Porphyry	Dolly	Altered, near base of Sunrise shear zone
SRD203xy	pB	pB	2.75			3.66	3.67	3.68	3.69	3.71	3.73	3.74	Porphyry	Dolly	"least altered" background, chlorite alteration
SRD203xy	pB	nB	2.75	3.62	3.64	3.67	3.68	3.69	3.69	3.70	3.71	3.72	Porphyry	Dolly	"least altered" background, chlorite alteration
SRD203z	nB	pB	2.76			3.52	3.54	3.56	3.57	3.60	3.63	3.65	Porphyry	Dolly	"least altered" background, chlorite alteration
SRD204xy	pB	pB	2.76		3.67	3.69	3.70	3.70	3.71	3.74	3.78	3.79	Porphyry	Dolly	"least altered" background, chlorite alteration; some foliation
SRD204xy	pB	nB	2.76	3.44	3.46	3.49	3.51	3.53	3.56	3.62	3.68	3.69	Porphyry	Dolly	"least altered" background, chlorite alteration; some foliation
SRD204z	nB	pB	2.77		3.30	3.35	3.38	3.41	3.42	3.46	3.50	3.52	Porphyry	Dolly	"least altered" background, chlorite alteration; some foliation
SRD206xy	pB	pB	2.78		3.62	3.64	3.67	3.68	3.69	3.73	3.76	3.77	Andesite		background sericite-chlorite alteration; near Watu shear zone
SRD206xy	pB	nB	2.78				3.70	3.72	3.73	3.75	3.77	3.78	Andesite		background sericite-chlorite alteration; near Watu shear zone
SRD206z	nB	pB	2.76	3.51	3.53	3.56	3.59	3.60	3.61	3.63	3.66	3.68	Andesite		background sericite-chlorite alteration; near Watu shear zone
SRD207xy	pF	pF	2.78		3.70	3.72	3.73	3.74	3.74	3.76	3.78	3.79	Andesite		carbonate/qtz altered; near Margee's/Watu shear zone
SRD207xy	pF	nF	2.78		3.55	3.59	3.62	3.63	3.65	3.69	3.71	3.73	Andesite		carbonate/qtz altered; near Margee's/Watu shear zone
SRD207z	nF	pF	2.79	3.53	3.56	3.60	3.62	3.63	3.64	3.67	3.70	3.71	Andesite		carbonate/qtz altered; near Margee's/Watu shear zone
SRD208			2.80	3.51	3.56	3.59	3.61	3.63	3.64	3.68	3.72	3.74	Andesite		moderate grade; massive

Sample	Propagation Direction	Vibration Direction	Density (tm^{-3})	10	20	40	60	80	100	200	400	600	Lithology	Unit	Remarks
SRD209			2.79		3.64	3.66	3.67	3.68	3.69	3.72	3.73	3.74	Andesite	Astro Lode	relatively unaltered
SRD210xy	pB	pB	2.87			3.65	3.67	3.70	3.72	3.78	3.81	3.82	Andesite	Astro Lode	altered
SRD210xy	pB	nB	2.87		3.62	3.68	3.73	3.77	3.79	3.83	3.85	3.87	Andesite	Astro Lode	altered
SRD210z	nB	pB	2.81	3.57	3.63	3.65	3.66	3.67	3.67	3.69	3.70	3.71	Andesite	Astro Lode	altered
SRD214			2.87		3.75	3.77	3.79	3.80	3.81	3.85	3.87	3.88	Andesite	Lower Cosmo Lode	altered
SRD215xy	pF	pF	2.86		3.67	3.69	3.71	3.71	3.72	3.73	3.74	3.75	Andesite	Lower Cosmo Lode	background alteration
SRD215xy	pF	nF	2.86				3.54	3.55	3.55	3.58	3.60	3.62	Andesite	Lower Cosmo Lode	background alteration
SRD215z	nF	pF	2.87		3.61	3.63	3.65	3.65	3.66	3.68	3.70	3.71	Andesite	Lower Cosmo Lode	background alteration
SRD216			2.75		3.55	3.58	3.59	3.60	3.61	3.62	3.63	3.65	Andesite	Watu Shear Zone	background alteration
SRD218xy	pB	pB	2.83			3.73	3.75	3.76	3.77	3.80	3.83	3.84	Andesite	Watu Shear Zone	altered
SRD218xy	pB	nB	2.83			3.84	3.87	3.88	3.88	3.90	3.91	3.92	Andesite	Watu Shear Zone	altered
SRD218z	nB	pB	2.80				3.55	3.56	3.57	3.60	3.63	3.65	Andesite	Watu Shear Zone	altered

Table 13: S-wave velocities for hand-specimens from Sunrise Dam (not examined in this report, but included for completeness). Samples were measured at the Geological Survey of Canada (GSC)-Dalhousie High Pressure Laboratory, Halifax, Nova Scotia. Propagation and vibration direction indicates the orientation of the sample: nB and nF are perpendicular to the fabric in the rock, and pB and pF are parallel to the fabric in the rock. Vibration direction is included as shear waves are polarised and thus require propagation parallel to and perpendicular to the fabric in the rock.

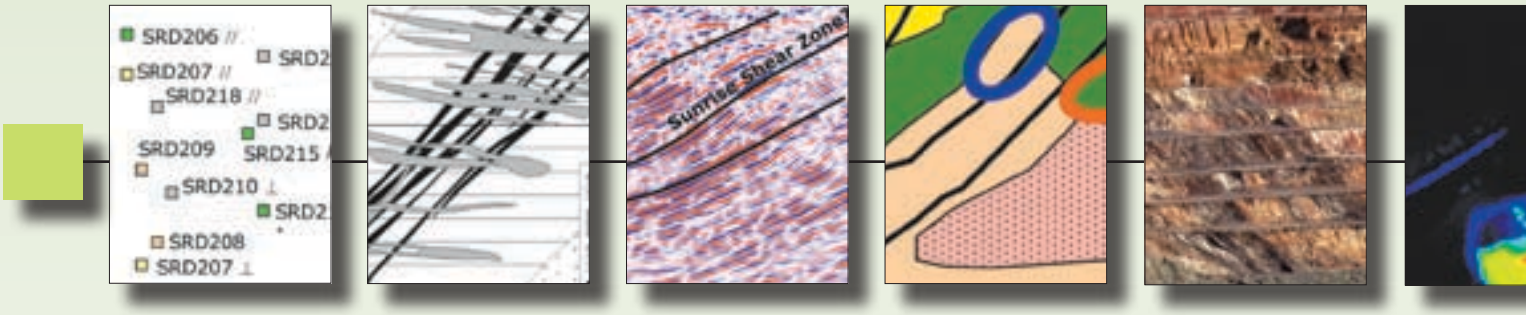
SRD206 //
SRD207 //
SRD218 //
SRD209
SRD215
SRD210 ⊥
SRD208
SRD207 ⊥
Sunrise Shear Zone